UNIVERSITA' DEGLI STUDI DI MILANO-BICOCCA

Mathematical, Physical and Natural Science Faculty

PhD Dissertation

Materials Science

Cycle XXVIII

DESIGN AND SYNTHESIS OF SMALL-MOLECULES FOR NIR-OPERATING LIGHT SENSING AND EMITTING DEVICES

PhD thesis of:
Nunzio Francesco Buccheri
Matr. N.:709312

Supervisor:
Dr. Luca Beverina

Coordinator:
Prof. Giampaolo Brivio

March 2016

“You have to think about one shot.

One shot is what it's all about.

The deer has to be taken with one shot.

I try to tell people that - they don't listen.

Do you ever think about Vietnam?”

Robert De Niro as Mike Vronsky

“The Deer Hunter”

1978

Table of contents

Chapter 1: Introduction

1.1 Organic Electronics

The incipit of the white paper from the Chemical Science and Society Summit held in San Francisco in 2012, states[1]:

"*We live in an electronic world*."

This simple sentence is the perfect description of the time we are living in. After the World War II the human community has experienced a tumultuous growth. The economic growth has been tightly related to the technological development. The most representative achievement of this era is undoubtedly the computer. We passed from room-dimensions, electro-mechanic devices, such as *Colossus* or Turing's machine *Bombe*, which helped the Allies to win the war decrypting the German *Enigma* machines secrete messages, to completely digital lightweight modern laptops or smartphones. The electronics, shrinking the dimensions of the systems, became a mass product and pervasive and ubiquitous in our lives. In our present time is hard to imagine to work or to travel or even to spend our spare time without using a computer to do an internet research, to make an Excel calculation or to check a map on a portable device if we are far from home. To have an idea on the enormous impact of electronics on the economy worldwide, one can check the numbers of the CES 2015 (Consumer Electronics Show), the biggest technology exhibition in the world, that takes place in Las Vegas, Nevada, every January. In this event, 3631 exhibiting companies were present, as long as 375 start-ups and 82% of the Fortune top-100 companies were represented. Totally, more than 170000 attendees were registered[2,3]. In such event, interest of companies is not only focused on computers in itself but encompass 20 categories of products and services[3]:

• 3D Printing

- Accessories
- Audio
- Automotive Electronics
- Communications Infrastructure
- Computer Hardware/Software/Services
- Content Creation & Distribution
- Digital Imagining/Photography
- Electronic Gaming
- Fitness and Sports
- Health and Biotech
- Internet Services
- Online Media
- Robotics
- Sensors
- Smart Home
- Startups
- Video
- Wearables
- Wireless Devices & Services

All these categories represent opportunities to develop business and new technologies. In this sense, electronics has been one of the biggest inheritances of the XX century and the biggest challenge for the XXI.

The above-mentioned 2012 white paper introduces a resume of a new perspective and a new endeavor in the field. It states:

"Economic, health, and national security rely on and are positively impacted by electronic technology. However, the resources and methodologies used to manufacture electronic devices raise urgent questions about the negative environmental impacts of the manufacture, use, and disposal of electronic devices. The use of organic materials to build electronic devices may offer a more eco-friendly -- and affordable -- approach to growing our electronic world."

The research toward new materials is prompted by new needs and new problems that emerged after the big spreading of consumer electronic devices in every segment of the world's population. Rapid changes in technology, falling prices, and planned obsolescence have resulted in a fast growing surplus of electronic waste around the globe. Huge slum settlements appeared in the "peripheries of the world", Africa, south-east Asia, south America, around dumps, were electronic waste are preponderant. The presence of harmful materials like lead, cadmium, americium, beryllium, and hexavalent chromium or precious metals (gold, platinum, indium) in such waste stimulates the implementation of new recycling systems and the use of novel materials to substitute the existing ones. The *Basel Convention on the Control of Transboundary Movements of Hazardous Wastes and Their Disposal*, usually known as the Basel Convention, is an

international treaty that was designed to reduce the movements of hazardous waste (the category electronic waste are ascribed) between nations, and specifically to prevent transfer of hazardous waste from developed to less developed countries. The Convention is also intended to minimize the amount and toxicity of wastes generated, to ensure their treatment as closely as possible to the source of generation, and to assist less developed countries in the recycling[4]. The vast majority of the Nations ratified it but still one of the most important challenges is to act at the top of the production pyramid, rendering the materials used in electronics eco-friendly.

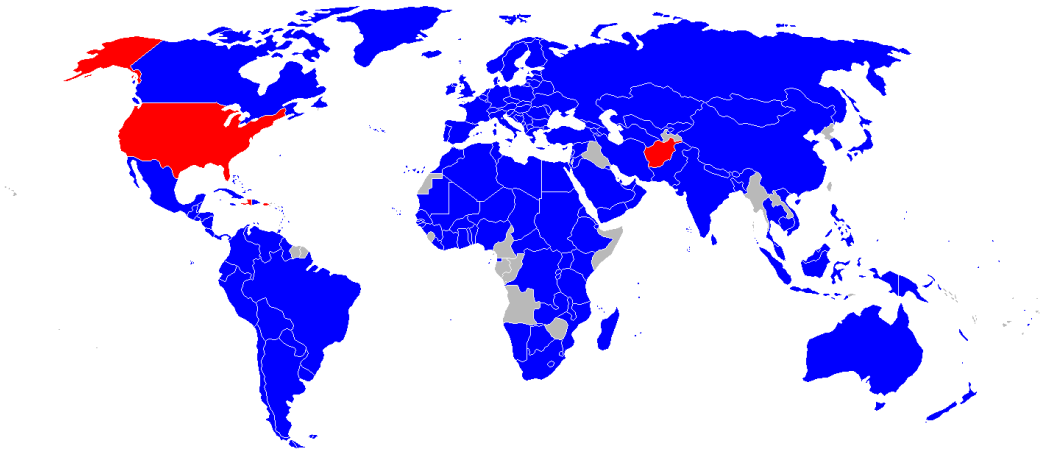

Figure 1.1: countries that signed the Basel Convention. In red are highlighted the countries that have not ratified it yet. Noticeably, the USA congress have not ratified it, unless the country is one of the biggest consumers of electronics (and producers of hazardous waste on the planet)

The environment issue is not the only task the electronic industry has to face: the pursuit of better performances, new features and new application fuels the research on new materials capable to overcome the state of the art and to introduce new challenge and perspectives in the field.

In this frame, a new approach to the electronics emerged in the past two decades: the use of organic molecules as active materials for electronics. The definition of “organic” compound directly derives from classical culture of Vitalism, in which western alchemist believed for centuries, spreading the idea of a “vis vitalis”, a “soul”, capable to generate certain types of molecules. Only after the rising of the modern atomic theory, this believing was abandoned but the formal distinction between “organic” and “inorganic” still resist. For such historical reasons chemists define organic compounds as primarily composed of carbon. In material science, from a functional point of view, they can be divided into small molecules (molecular weight < of 1000 u.m.a) and polymers. The application of organic materials in electronics opened a completely different and innovative industrial field: organic electronics. It represents the branch of materials science concerning the design, the synthesis, the application and the implementation in real devices of organic molecules or polymers, which show properties suitable for electronics, such as conductivity at ambient temperature and semiconducting behavior.

Figure 1.2: Polyera Corp.’s Wove Band, firs example of completely printable and flexible electronic device based on organic semiconductor technology. The inventor A. Facchetti won the American Chemical Society's National Award for Creative Invention[5].

1.2 Organic semiconductors

As a general definition, an organic semiconductor is an organic material that acts as a semiconductor. This apparently tautological statement classifies such compounds by the conductivity, which has to be between that of insulators and that of metals. In a more quantitative way, organic semiconductors are classified as "*intrinsic wide band gap semiconductors*" (band gap above 1.4 eV) compared to "insulators" (band gap above 3 eV). They also show negligibly low intrinsic charge carrier density at room temperature in the dark[6]. Single molecules, oligomers, and polymers can be semiconductive. Exploiting this property, a large number of devices can be produced using organic active materials, from thin-film transistors to light emitting diodes and light harvesting systems such solar cells or photodetectors[7,8,9,10]. The history of such systems spans over three centuries. In middle 19th century the first trials by Letheby to oxidize aniline resulted in the discovery of polyaniline but we have to wait until the second part of '900 to have the first demonstration of conductivity of organic compounds such as perylene-iodine complex or TCNQ-TTF ensembles. The Nobel Prize 2000 in Chemistry stating[11]

"for the discovery and development of conductive polymers"

was awarded to Heeger, Mc Diarmind and Shirakawa for their studies on conductivity of iodine-doped polyacetylene polymers was the definitive confirmation of the extreme importance of this class of materials for the development of technology. From the chemical structure point of view, organic semiconductors (both polymers and small molecules) can be divided in two main families: p-type semiconductors and n-type semiconductors. The first category represents hole-transporting materials, so normally electron-rich systems. The latter represents electron-transporting materials, which are intrinsically electron-poor. Historically, much effort has been put to develop p-type materials and their performances have rapidly grown. Relatively less attention has been

devoted to the development of electron-transporting materials and the scientific panorama, in this sense, is dominated by fullerene derivatives, such as PCBM[12]. An attempt to fill this scientific gap is presented in the device chapter of this work. The library of materials organic chemistry achieved until now is vast: polymeric backbones such as poly(3-hexylthiophene), poly(phenylen-vynilene), poly(triarylamine) or polyfluorene or molecular materials such as phthalocyanines, rubrene, perylene-diimides or dianhydrides or diketopyrrolopyrroles are among the large number of structures that modern organic chemistry offers to us. A non-exhaustive list is reported in the figure:

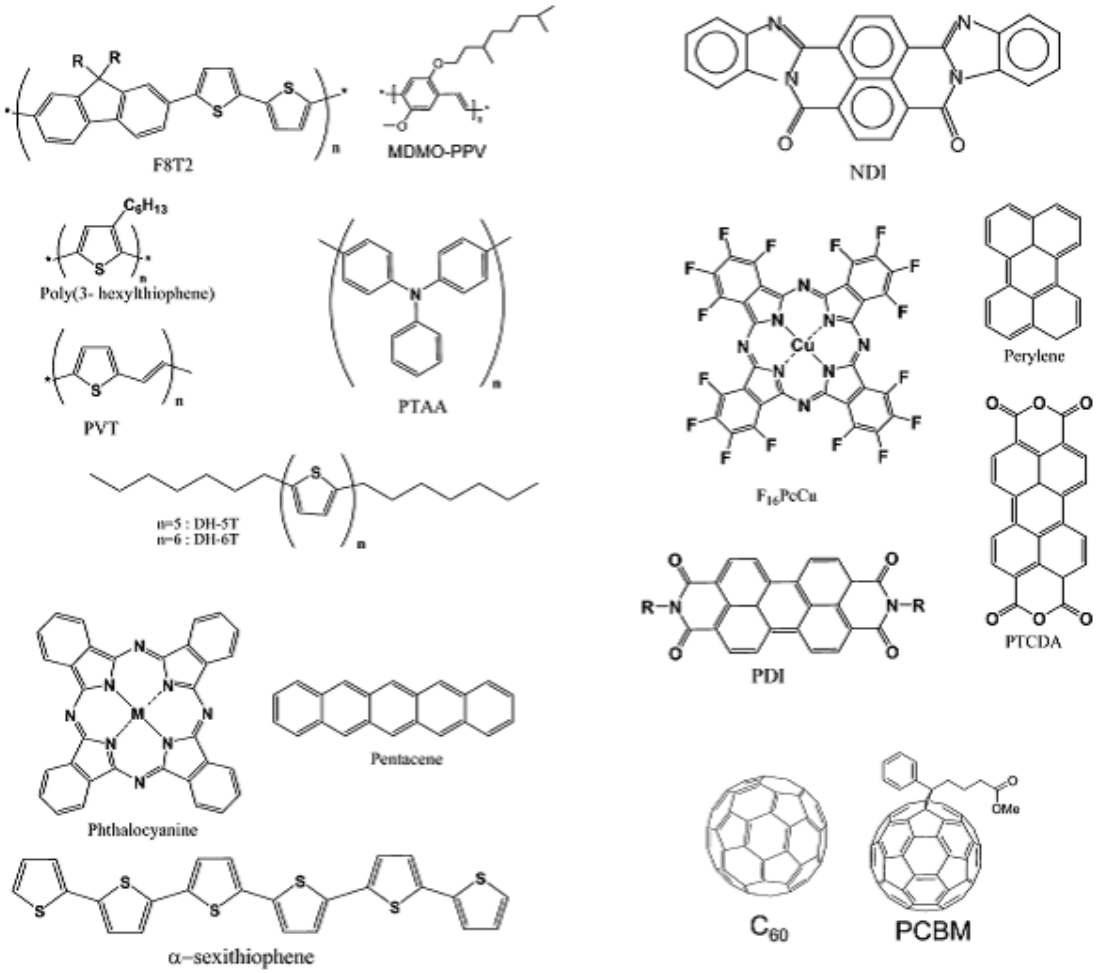

Figure 1.3: selection of representative organic semiconductor structures, donor p-type compounds on the left and acceptor, n-type derivatives on the right, reproduced from[6].

In order to explain the electric behavior of organic semiconductors it is fundamental to consider the intrinsic nature of carbon atom. Organic systems have been considered insulators for long time so a change of paradigm is necessary to understand them. For the carbon atom, it is useful to define the concept of hybridization. It is the linear combination of atomic orbitals. It generates new hybrid orbitals (with different energies and shapes than the original atomic orbitals) suitable for the pairing of electrons to form chemical bonds in valence bond theory. Carbon has four valence orbitals (2s, 2px, 2py, and 2pz) that can be linearly combined to form three types of hybrid orbitals: sp^1 sp^2 sp^3. By overlapping of these new orbitals, it is possible to generate covalent bonds. In this way σ bonds are formed, describing the basic carbon backbone of the molecules. By overlapping of lateral p orbitals double and triple bonds form, generating the molecule's π system that is the most important factor for semiconductor behavior in organic systems. Orbitals are regions of the space described solving the Schrödinger equation, where there is a non-zero probability to find the electron. They can be treated as waves, so they can sum in a constructive or a disruptive manner. They are helpful to describe bonds in organic compound, since the bonds are built from the overlap of separate atoms.

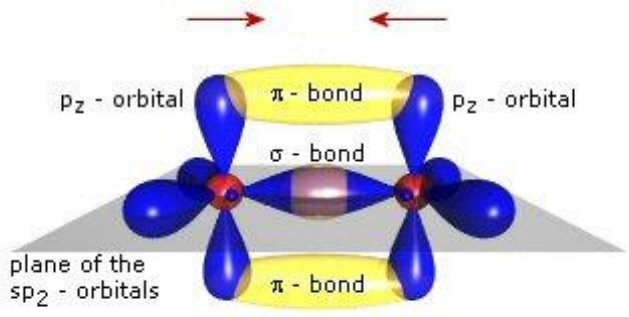

Figure 1.4: simplified drawing of the interaction between hybrid carbon orbitals. The sigma bond lies on the Sp^2 plane while the pz lobes overlap to form the π backbone, responsible for the conductivity[13].

The spatial overlap is high in σ-bond and smaller in π-bonds; the binding energy of π-bonds is smaller and the electrons part of the π system are delocalized along the carbon atoms chain. A molecule in which single and double (or triple) bonds alternate along the chain is called conjugated system. The mobile π electrons form a high electronic density region showing high polarizability, that is the basis for conduction.

The delocalization of the electrons needs a step further to be explained and to be integrated into a more general theory. The molecular orbital theory is a method for determining molecular structure in which electrons are not assigned to individual bonds between atoms, but are treated as moving under the influence of the nuclei in the whole molecule. For many-atoms systems, the Schrödinger equation becomes complex and approximations in the Hamiltonian are required. In the theory, it is assumed that the j-th molecular orbital wave function Ψj can be written as a linear combination of atomic orbitals χi according to:

$$\Psi_j = \sum_{i=1}^{N} c_{ij}\, \chi_i$$

where N is the number of carbon atoms in the molecule, cij are linear coefficients. For N carbon atoms N molecular orbitals are defined. In the ground state, the molecular orbitals of the lowest energies are filled with two electrons of opposite spin (Pauli principle). The filled orbital that present the highest energy is called HOMO (Highest Occupied Molecular Orbital). The first empty orbital above it is defined as LUMO (Lowest Unoccupied Molecular Orbital). This scheme is the core of a more general chemical theory that is able to explain molecular reactivity in a semi-empirical way: the FMO theory (Frontier Molecular Orbitals). When a certain number of molecules are confined in a small volume as in the case of crystals, the arrays of molecules present overlapping of the molecular orbitals among them. This interaction results in a further splitting of the

energies and, for a number of molecules N large enough, in a band-like structure similar to valence and conduction band of inorganic semiconductors[14]. Another strategy to enhance the semiconducting properties of a conjugated system is doping: it is possible to change the energy levels by introducing a small quantity of an electron rich or poor dopant[15].

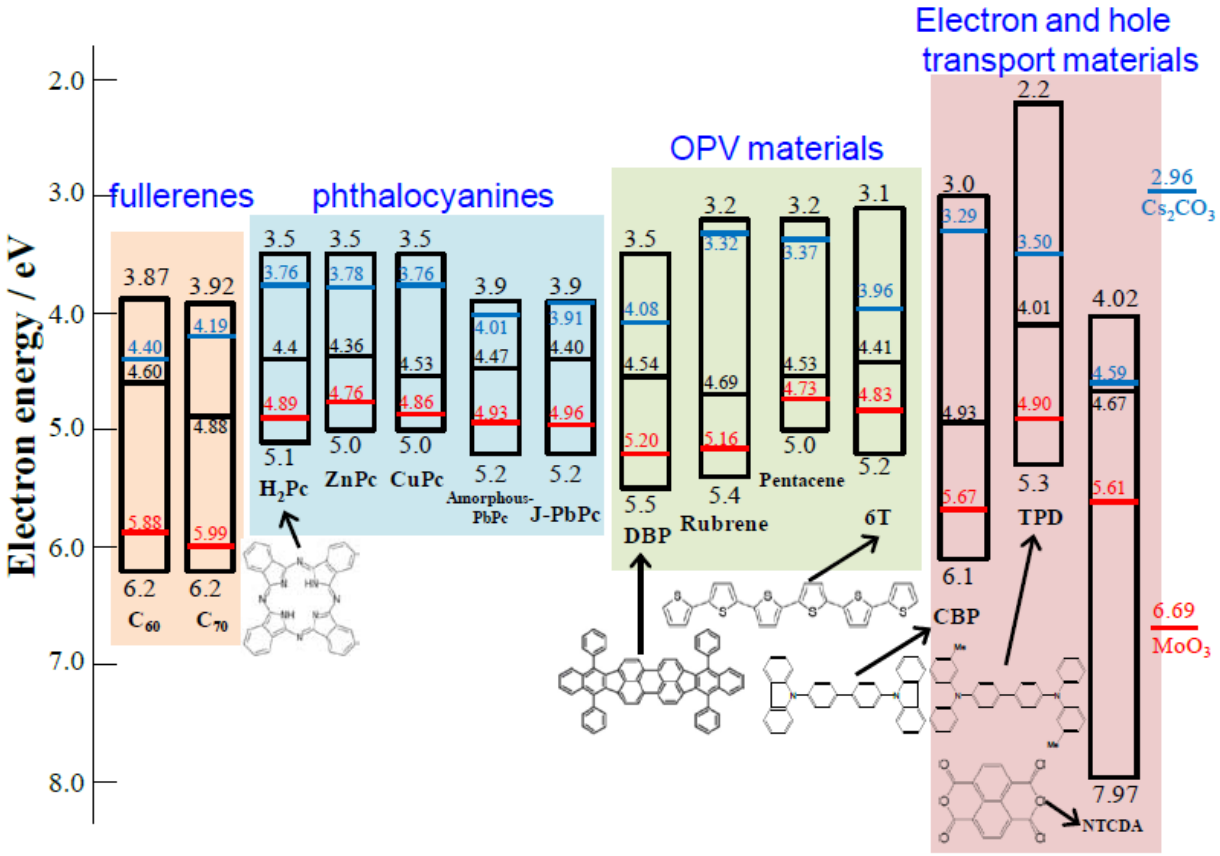

Figure 1.5: Representation of the band-like structure originating from the π backbone of PPV (para-Phenylen-Vynilene)[16].

In the past decades, organic small molecules played a decisive role for the advance of electronics and some application, such as OLEDs, have reached the market and the mass diffusion. As said above the opportunities are many and diverse. This thesis focuses on a

particular one: the interaction between organic structures with light. Going more in depth, it focuses on the near-infrared light. Some applications of NIR-technology, such as night vision goggles or amplifiers have been developed for military uses (WWII, Vietnam War…). My personal belief is that Science is a creative force, not a disruptive one and a product of the good part of human soul. For that, it should support the worldwide Pacifism. The work, from now, will be centered on NIR-active organic molecules and represents the author's infinitesimal tentative to help Science going in this direction.

1.3 Lowering the Band Gap: towards NIR-active compounds

The infrared region spans from roughly 300 GHz (1 mm) to 400 THz (750 nm) and can be divided into three parts: near-infrared, mid-infrared, and far-infrared. The near-infrared (NIR) region typically falls in the spectrum from 120 to 400 THz (2500 to 750 nm). Materials that absorb, emit or reflect light of such wavelength are considered NIR materials and they are gaining importance both in academic and industrial field. The research in this field is prompted by military and civilian uses. Military applications include target acquisition, surveillance, night vision, homing, and tracking. Non-military uses include thermal efficiency analysis, remote temperature sensing, short-range wireless communication, spectroscopy and weather forecasting. Academy invests a great deal of effort on understanding NIR materials behavior and their application in many field such as energy production and conversion, communication, bio-imaging, sensing, and advanced optoelectronics. Spectacular applications have been found in biomedicine: as the NIR light penetrates deeper into the tissues, NIR compounds can be

used as fluorescent tags for cells or as local heat generators in photothermal therapy. NIR absorbers are of great importance in solar energy conversion, since nearly 50% of the solar energy falls in the NIR region of the spectrum. They could be used as heat shield to block the heat or as optical filters to shield the NIR rays in smart windows technology[17].

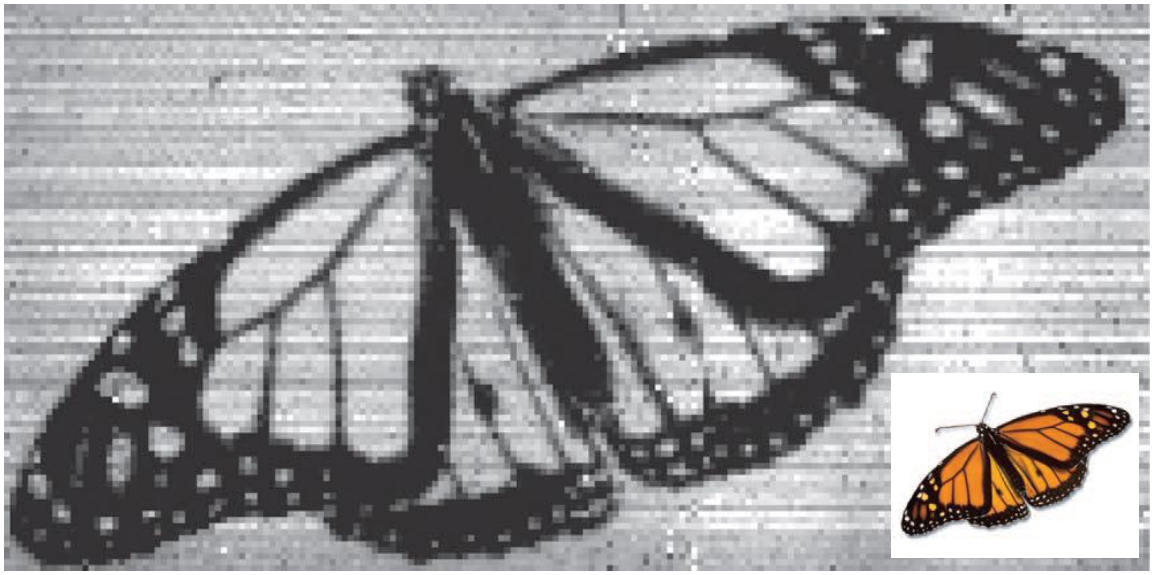

Figure 1.6: infrared shadow-cast at 1310 nm of a monarch butterfly, adapted from reference[18]. In this case, the NIR imager exploits quantum dots as active material. The use of organic molecules to "mimic" the eye behavior is a still ongoing and fascinating research field.

1.4 Effect of conjugation length on the energy gap

One can divide NIR compounds into two groups: inorganic materials, including metal oxides and semiconductor nanocrystals, and organic materials, including metal complexes, ionic dyes, extended p-conjugated chromophores, and donor–acceptor

charge transfer chromophores. For organic molecules, what determines the optical and electronic properties is the energy gap between the highest occupied molecular orbital (HOMO) and the lowest unoccupied molecular orbital (LUMO), called HOMO-LUMO gap (HLG). Narrowing the band gap leads to a red shift of both absorption and emission bands[19]. So tuning of the HLG is the key factor in NIR active organic molecules. One should consider various factors to optimize such parameter: the conjugation length, the bond length alternation, and donor–acceptor charge transfer.

In a typical p-conjugated system, the energy gap originates from the bond length alternation between the double and single bond or a so-called Peierls gap[20]. The bond length alternation (BLA) is a geometrical parameter calculated as the difference between the lengths of a single bond and the adjacent multiple (double or triple) bond in π-delocalized systems. the smaller the bond length alternation is, the lower the energy gap of a conjugated compound will be. Therefore, minimizing the bond length alternation is an important step towards the reduction of the energy gap of conjugated molecules. Polyenes $(CH)_n$ and polyarylenes are the two principal categories of π-delocalized systems. In the case of polyene, the electron can delocalize along the chain while in the case of polyarylene, resonance energy plays an important role. There is a competition for p electrons between confinement within the rings and delocalization along the chain, so the HLG is dependent on the resonance energy in aromatic systems. As a result, the energy gap of aromatic molecules is normally larger than that of polyene molecules. Another difference between polyene and polyarylene systems is the nondegenerate ground state. In the case of polyarylene the molecules can be described with two mesomeric limit forms: aromatic and quinoid[21]. In most cases, the latter has a smaller HLG due to the lower BLA (increasing in double bond character). Increasing the quinoid character of the molecule's ground state is a way to design IR-active molecules.

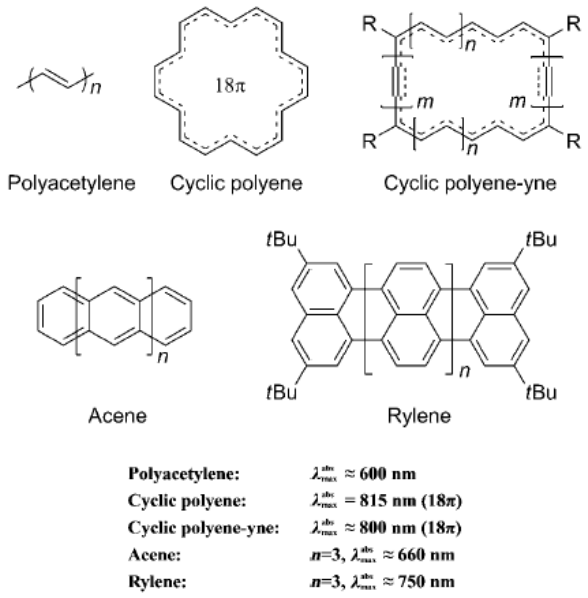

Figure 1.7: different strategies to lower the band gap, adapted from[17].

Another effective strategy to lower the HLG in conjugated molecules is to introduce an electron donor (D) and electron acceptor (A) moieties in the structure. D-A chromophores show two resonance forms, which give rise to an increased double bond character between the D and A units, thus reducing the bond length alternation, resulting in a decrease of the Peierls gap. The energy levels hybridization in such systems raise the HOMO of the donor and lower the LUMO of the acceptor, further decreasing the HLG, according to the representation:

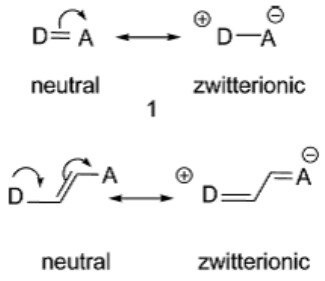

Figure 1.8: schematic representation of the mesomeric charged forms of a model D-A conjugated system. Adapted from [21].

1.5 Advantages of Organic Semiconductors: Solution-Processing

The standard process of fabrication of electronic devices based on inorganic thin-films involves the thermal evaporation of the materials (metals or silicon) performed under ultra-high vacuum chambers. Such systems are steel domes in which a metal crucible (normally tungsten) is placed between two electrodes. Turbomolecular or diffusive pumps are used to reach a vacuum level between 10^{-6} and 10^{-8} Pa inside the chambers. The materials to evaporate are placed on the crucibles and the current, heating up the crucible by ohmic effect, promotes the melting and then the evaporation of the material. The substrate, glass or plastic, lies on the upper part of the dome and the stream of evaporated material condense on it forming the thin film. It is clear that such technique is inherently expensive from the energy and the materials point of view: the system has to be completely isolated and a big amount of energy is required to maintain the vacuum. To evacuate even a small size chamber, a lot of time is required (sometimes hours) and the great part of the evaporated material that forms the so-called evaporation cone condenses on the dome's walls and is wasted. One could think about losing grams of gold in this way and the costs associated to this. Moreover, the metal particles of the stream hit the substrate at high temperature (hundreds of Celsius) and can damage plastic substrates or previously deposed thin films. The vacuum deposition technique is, so, hardly compatible with application in plastic electronics that needs the implementation of high-throughput systems such as roll-to-roll printing for large areas.

In this frame, the research on soluble semiconducting systems open the way to an array of techniques derived from the industry of printing and coatings. Solution-processing materials allow the possibility to print devices on a large scale, with negligible loss of material even on flexible plastics.

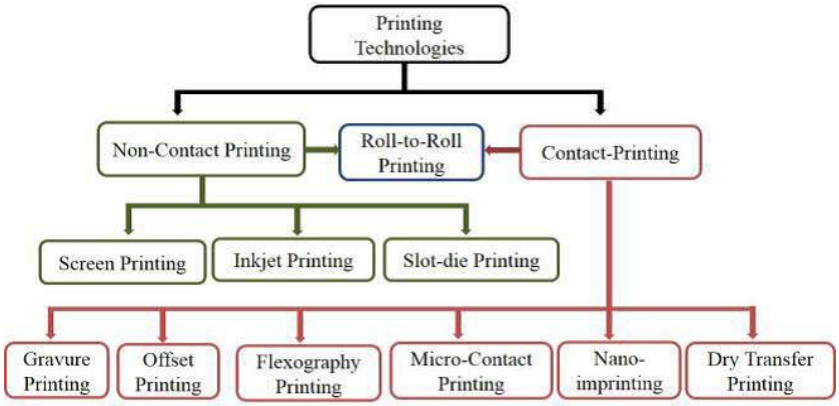

Figure1.9: The tree chart represents the common classification of printing technologies, adapted from[22].

The most widely used techniques for printing of electronics over large area flexible substrates have been extensively reviewed[22,23]. A brief classification of them is the following:

Screen Printing: is one of the most used techniques nowadays for electronics and it consists in a rotary or flatbed equipped with a stencil mask and the ink is poured and squeegeed onto it. It is indicated for fine patterning but not for large area application.

Inkjet Printing: droplets of a solution or a colloid is deposed on the substrate by means of a nozzle with a micrometric size head. The reproducibility of the printing is strongly dependent from the ink formulation and the viscosity, boiling point and surface tension of the solution.

Slot Dye Coating: it is a non-contact technique in which the ink, contained into a pressurized reservoir, is homogeneously deposed on the moving substrate. The speed of the substrate and the solution flow rate are crucial to determine the thickness. It is indicated for large area applications but not for fine patterning.

Gravure Printing: it is the standard technique used in the publishing industry and it is designed for large area printing. It a basic configuration two rotating cylinders, one, patterned, wetted with ink and one equipped with the substrate are placed face to face. A doctor blade removes the excess of ink to obtain the desired printing pattern.

Spray Coating: it is the standard method to apply paints in the automotive industry. A pressurized gas flow atomizes the ink at the opening of the nozzle. The generated droplet flow hit the substrate and dries. It is a high-throughput large area technique but it is not easily applicable for micrometric patterning.

Flexo printing: it is conceptually similar to gravure printing. The main difference is the presence of an anilox cylinder, patterned with micro cavities on the surface, which is in contact with the ink-wetted cylinder. The anilox transfers the ink over rotating printing plates that can be made of rubber or photopolymers. Then the ink is transferred on the substrate. Directly derived from the packaging industry, this technique is also suitable for large area application in electronics.

The ultimate and hardest task to reach a high-throughput system to produce devices over virtually every plastic substrate is to implement the described printing techniques into a roll-to-roll flow process. This possibility to create printed structures kilometers long would lead to a drastic decrease of the cost of the final products. One can think about substituting the standard bulk silicon solar cells with printed ones, so concretely helping remote and poor areas of the planet to access to a basic service as energy.

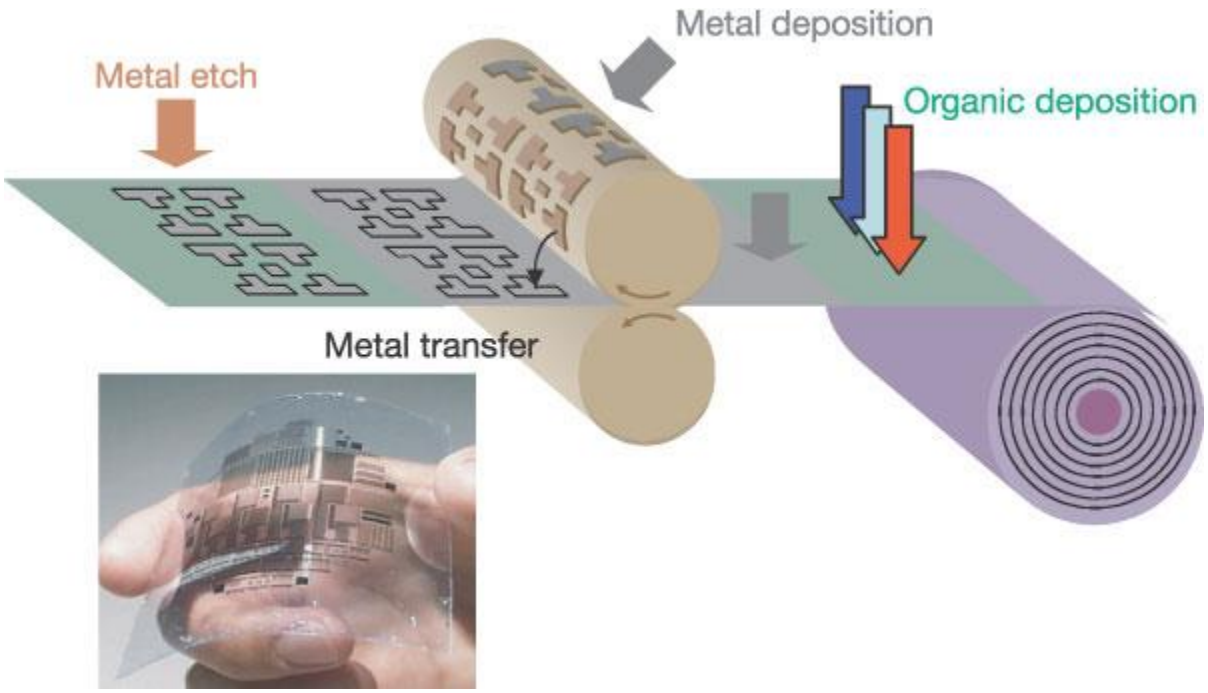

Figura1.10: schematic representation of the potential of the implementation of continuous and low cost roll-to-roll techniques for thin-film electronics. It is worthy to notice that after organics are deposed, metal electrodes are printed and shaped by dry etching. In this vision, no metal evaporation is needed, speeding up the entire process. Adapted from[24].

Finally, it has to be mentioned that in the laboratory scale, the most used technique to deposit an organic thin film over a substrate is undoubtedly by spin-coating. This procedure involves a rotor where the substrate is placed on and kept in place by vacuum suction. The solution to spin is dripped onto the substrate and smeared over it by action of the centrifugal force. The thickness is mainly dependent on the rotor speed. Spin coating is straightforward and does not require expensive equipment. It is the perfect solution for experimental laboratories but the large waste of material makes it not suitable for large-scale industrial plants.

1.6 Scope and organization of the thesis

This thesis is written from an organic chemist's point of view and it is divided in two main parts: the first part is centered on the explorative synthesis and the improvement of some organic structures chosen into the literature to match the requirements of the applications they are intended for. More specifically, the structures presented had to fulfill the following features:

- Good solubility in a large variety of the organic solvent commonly used in a chemistry laboratory or in a device preparation laboratory or industrial scale up. This characteristic is extremely important for the preparation of inks presenting the correct concentration and viscosity to be useful in solution-deposition processes. As reported above, the deposition of active layers from solution enables the use of a great array of techniques and different devices geometries, while decreasing the process time and cost by avoiding strictly controlled conditions such as ultra-high vacuum.
- The structures intended for light-harvesting applications have to show efficient absorption (high molar extinction coefficient) as long as low batochromic or ipsocromic shifts of the bands due to different solvents, in order to be able to strictly control the absorption range during the device fabrication process. In particular, the derivatives have to present absorption bands in the near-infrared part of the electromagnetic spectrum. The NIR is particularly interesting for applications in biology, photovoltaics and telecommunication and, now, less investigated from an engineer point of view compared to the visible or the ultraviolet portions.
- The molecules designed for light-emitting applications should present stable emission in the NIR region, both in diluted solution and in polymeric matrices. The

fluorescence quantum yield has to be as high as possible to allow good efficiencies of the final devices.

- Good thermal stability. It is an important feature for an organic compound to be resilient to thermal treatments. Thermal annealing processes or curing at high temperature are standard procedures in the device fabrication and decomposition of the active layer or uncontrolled crystallization have to be avoided.
- Low aggregation behavior and good compatibility with host matrices. The derivatives could be dispersed into a polymeric matrix and segregation processes could be detrimental for the performances.

The molecules that showed the most interesting characteristics were chosen and tested in devices. The second part of the manuscript reports three applications of a selection of the organic structures previously synthesized and characterized:

- Application of a diketopyrrolopyrrole-derivative as near-infrared emitter in a host-guest configuration for organic light emitting diodes. The optimization of the devices and the testing of thin-films were accomplished in collaboration with the photo-physics lab of Professor Sergio Brovelli of University of Milano Bicocca and the group of Dr. Umberto Giovannella of Politecnico di Milano.
- Application of a perfluorinated subphthalocyanine dimer as an acceptor and dual light-harvesting material in organic photodetectors based on bulk-heterojunction active layer geometry. The acceptor was coupled to a NIR-absorbing donor, making the devices sensitive completely in the infrared region. The fabrication, optimization and characterization of the devices were done in collaboration with the Istituto Italiano di Tecnologia of Milano (IIT) and Università degli studi di Padova (EPR measurements).

- Application of chelates of europium and ytterbium as emissive materials in luminescent solar concentrators. A quantitative evaluation of the re-absorption losses was performed in collaboration with the group of photo-physics of professor Meinardi. The diketopyrrolopyrrole derivative and the subphthalocyanine dimer were also applied in such systems in order to evaluate the feasibility and the performances of green and blue LSC suitable for building integration.

Such classes of devices and applications could appear not correlated each other at a first glance. The idea this work is based on is to explore in an extensive way the scientific space regarding the NIR-active organic compounds. With this idea clear in mind, the fields involved in the investigation should be as wide as possible and the applications all-embracing to set a general trend and benchmarks for further improvements of the research.

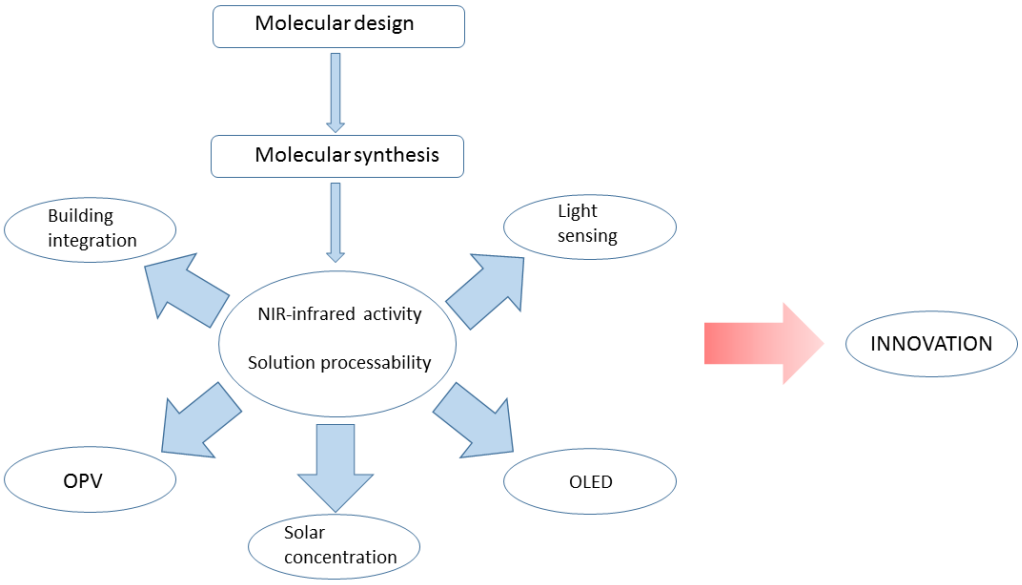

1.7 Bibliography

1. Organic Electronics for a Better Tomorrow: Innovation, Accessibility, Sustainability A White Paper from the Chemical Sciences and Society Summit (CS3) San Francisco, California, United States September 2012
2. https://www.cesweb.org/Why-CES/CES-by-the-Numbers
3. Attendee Audit Summary International Ces® January 6-9, 2015 Las Vegas, Nevada
4. http://www.basel.int
5. http://www.polyera.com/blog.html
6. Serap Gunes, Helmut Neugebauer and Niyazi Serdar Sariciftci, Chem. Rev. 2007, 107, 1324-1338
7. F Garnier, R Hajlaoui, A Yassar, P Srivastava, Science, 265: 1684-1686, 1994
8. C W Tang, S A Van Slyke, Appl Phys Lett, 51: 913-915, 1987
9. N S Sariciftci, L Smilowitz, A J Heeger, F Wudl, Science, 258: 1474-1476, 1992
10. Efficient, high-bandwidth organic multilayer photodetectors Peumans, P. and Bulović, V. and Forrest, S. R., Applied Physics Letters, 76, 3855-3857 (2000)
11. MLA style: "The Nobel Prize in Chemistry 2000". Nobelprize.org. Nobel Media AB 2014. Web. 20 Jan 2016. <http://www.nobelprize.org/nobel_prizes/chemistry/laureates/2000/
12. John E. Anthony, Antonio Facchetti , Martin Heeney, Seth R. Marder , and Xiaowei Zhan, Adv. Mater. 2010, 22, 3876–3892
13. www.iapp.de
14. H. Usta, A. Facchetti, T. J. Marks, “n-Channel Semiconductor Materials Design for Organic Complementary Circuits”, Accounts of Chemical Research,Vol. 44, No. 7, 2011, 501–510
15. J. Drechsel, B. Mannig, F. Kozlowski, D. Gebeyehu, A. Werner, M. Koch, K. Leo, M. Pfeiffer, High efficiency organic solar cells based on single or multiple PIN structures, Thin Solid Films 451 –452 (2004) 515–517

16. Masahiro Hiramoto, Masayuki Kubo, Yusuke Shinmura, Norihiro Ishiyama, Toshihiko Kaji, Kazuya Sakai, Toshinobu Ohno and Masanobu Izaki, Bandgap Science for Organic Solar Cells, Electronics 2014, 3, 351-380
17. Gang Qian and Zhi Yuan Wang, Chem. Asian J. 2010, 5, 1006 – 1029
18. Tobias Rauch, Michaela Boberl, Sandro F. Tedde, Jens Furst, Maksym V. Kovalenko, Gunter Hesser, Uli Lemmer, Wolfgang Heiss and Oliver Hayden, Near-infrared imaging with quantum-dot sensitized organic photodiodes, Nature Photonics 3, 332 - 336 (2009)
19. U. Salzner, J. B. Lagowski, P. G. Pickup, R. A. Poirier, Synth. Met. 1998, 96, 177 –189.
20. R. E. Peierls, Quantum Theory of Solids, Oxford University Press, London, 1956.
21. L. Beverina, G.A. Pagani, "π-Conjugated Zwitterions as Paradigm", Accounts of Chemical Research, Vol. 47, No. 2, 2014, 319–329
22. Khan Et Al.: Technologies For Printing Sensors And Electronics: A Review Ieee Sensors Journal, Vol. 15, No. 6, June 2015
23. Søndergaard, Roar R., Markus Hösel, and Frederik C. Krebs. "Roll-to-Roll fabrication of large area functional organic materials." Journal of Polymer Science Part B: Polymer Physics 51.1 (2013): 16-34.
24. Forrest, Stephen R. "The path to ubiquitous and low-cost organic electronic appliances on plastic." Nature 428.6986 (2004): 911-918.

Chapter 2: NIR Organic Functional Materials

2.1 Organic small Molecules: from dyes and pigments to functional materials

According to Markets&Markets forecasts, dated 2013, the global trade volume of dyes and pigments should grow by a 3.6% from 2013 to 2018 reaching 11 million of metric tons by that year[1]. The Asia-Pacific market plays a key role on driving this market, due to the thriving economic growth they are experiencing (actually, in the months this thesis is written, China is experiencing a sort of economic sudden stop, with a growth rate approaching "only" six percent. This deeply affects the global growth and the forecast could change). Such market involves many industrial fields, and thousands of workers:

- Textiles
- Leather
- Paper
- Paints & Coatings
- Plastics
- Constructions
- Paper & Specialty
- Printing Inks

A clear trend in the past ten-fifteen year has been the progressive migration of manufacturing capacity from the industrially more developed western countries to the low cost developing countries[2]. The 2007-2008 crisis accelerated this process, leading to an alarming industrial desertification in the USA and Europe. If USA recovered somehow the pre-crisis production levels (Keynesian politics are not debated in this work), Europe is far from a real stability. One of the possible strategies to face this problem is to focus on high-technology products of high value added: Europe has the expertise to invest in

this sense, even in the Horizon 2020 framework[3]. Regarding the dyes and pigments industry, the most promising perspective is represented by new functional materials, materials that are not used only for staining purposes but are exploited for a well-defined task. Organic dyes and pigments are attractive in this sense: their properties directly derive from the inherent conjugated structure, that can be used, as said, to transport charge. The tools that organic chemistry provides allow the functionalization of these systems in a straightforward way, allowing the fine tuning of the properties, such as absorption and emission range and HOMO-LUMO gap. This enables the possibility of customized synthesis, adapted to solve every specific industrial problem. Applications of such concept find spectacular examples in the field of organic solar cells, organic sensors, organic thin-film transistor or organic light emitting diodes[4]. The challenge is, hence, to develop new materials for specific functions and improve the procedures to obtain them, both from cost and time point of view.

2.2 Organic NIR active compounds

As said, there is a great interest on developing new "functional" organic dyes and one of the most promising fields is the exploiting of NIR radiation. One of the main problems is that the literature on this kind of compounds, and on the applications of it, is scarce compared to other spectral regions, such as ultraviolet or visible[5,6]. Nonetheless, many different classes of compounds have been demonstrated to be active in the NIR, due to the extent of the conjugated core and the efficient delocalization of electrons along the

π-backbone. This part of the text reports a brief presentation of the most widely used categories of NIR compounds.

Acenes and Rylenes derivatives. Acenes are structurally obtained by annulation of benzene rings. The enlargement of the aromatic core lowers the band gap and lead to a bathocromic shift of the absorption and the emission. Rylene dyes are directly based on the perylene moiety that is, conceptually, a naphthalene dimer, with bonds between the 1 and 1’ positions and between the 8 and 8’ positions of adjacent naphthalene units, so they are considered they are oligo(peri -naphthalene)s. Probably the most studied of rylene systems are rylene bis-imides, in which two six membered dicarboxylic imides are fused at the peri-position of the rylene. The intrinsic chemical stability and the ease of functionalization at the imidic nitrogen and at the bay positions, as long as the good charge transport properties made such derivatives very popular in organic electronics[7].

The scheme in figure 2.1 shows the common strategy adopted to push the band gap to lower value. The general structure is maintained, while naphthalene units are successively added to enlarge the aromatic core.

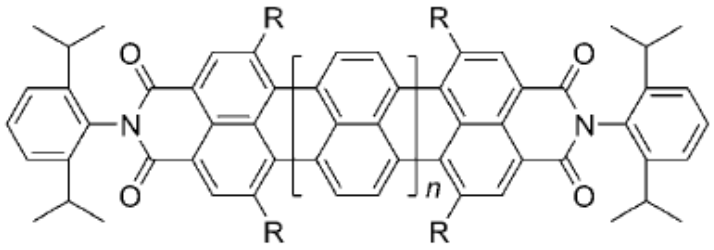

1, *n* = 0, R = H, $\lambda_{max}^{abs} \approx 590$ nm
2, *n* = 1, R = H, $\lambda_{max}^{abs} = 664$ nm
3, *n* = 2, R = H, $\lambda_{max}^{abs} = 762$ nm
4, *n* = 2, R = 4-*t*-butylphenoxy, $\lambda_{max}^{abs} = 781$ nm
5, *n* = 3, R = 4-*t*-octylphenoxy, $\lambda_{max}^{abs} = 877$ nm
6, *n* = 4, R = 4-*t*-octylphenoxy, $\lambda_{max}^{abs} = 953$ nm

Figure 2.1: series of rylene derivatives viewed as a progressive sum of naphthalene units. Adapted from[6].

The effectiveness of this strategy towards NIR chromofores is demonstrated, just to mention an example, by the work of Mullen et al.[8], that produced rylenes with six repeating units (hexarylene) that showed intense absorption at 953 nm.

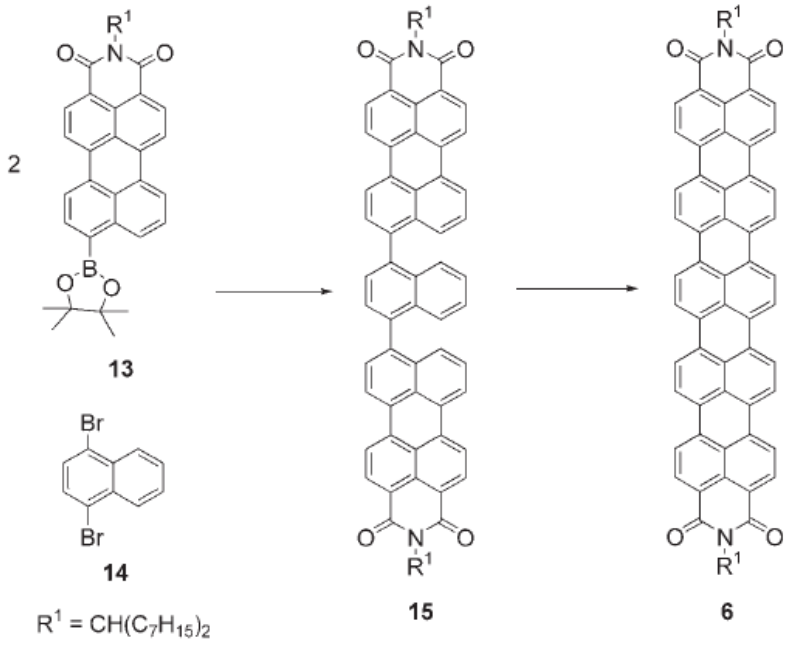

Figure 2.1: strategy used to achieve hexarylen-bisimide followed by Mullen et al. (adapted from[8]). It is worthy to note that the iminic nitrogens have to be functionalized with two branched very long alkyl chains to impart enough solubility to the derivative. The extended aromatic core experience strong π-stacking.

2.2.2 Polymethine dyes. Polymethyne s differ from polyenes because of the presence of a donor and an acceptor group at the opposite side of the conjugated chain. Examples of this class are merocyanines ($X=NR_2$, $Y=O$)[6].

A subcategory of polymethine dyes are the charged analogues cyanines. They belong to an industrially important large family of compound. Cyanines are known since more than one century and, because of their intense absorption in the Visible-NIR region, they found applications in many different field such as photography, lasers and, more recently, bio-labelling[9,10].

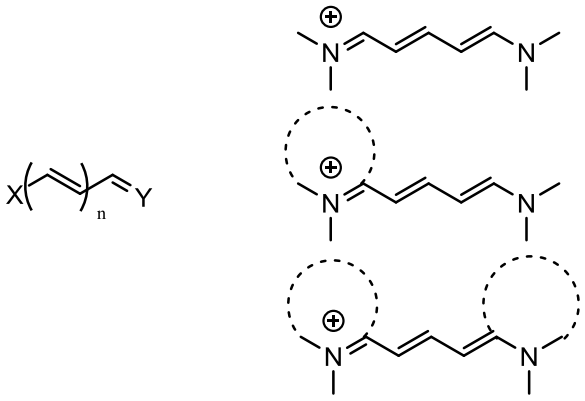

Figure 2.3: left, general representation of a polymethinic structure. X and Y can be N or O atoms. On the right representation of the different cyaninic structures, from top to bottom streptocyanines, hemicyanines and closed cyanines.

Energy gap of cyanines can be easily toned by modification of either the end groups or extending the methynic chain. As said in the introduction, extending the conjugated backbone leads to a red shift of both the absorption and emission bands. Interestingly, it has been demonstrated that each vinylene group causes a batochromic shift of about 100 nm[11].

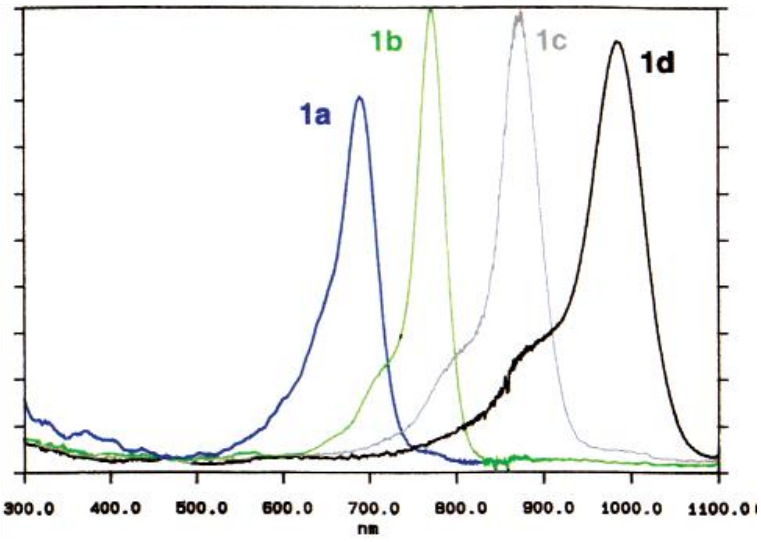

Figure 2.4: comparison of UV-Vis spectra of guaiazulene-based cyanines with chain length of 0,1,2,3 (respectively 1a, b, c and d). The batochromic shift is roughly 100 nm, pushing the absorption close to 1000 nm. Adapted from[11].

Although the conjugated chain extension is an effective way to obtain NIR-active cyanines, it usually leads to a decreasing of photo- and thermal stability. Moreover, cyaninic structures are fluorescent but the quantum yield tends to lower while increasing the chain length. The chain extension introduces a flexibility factor and ease of photo-isomerization, making the fluorescent quantum yield rarely higher than 15%[6]. These conditions represent a major drawback for practical applications. One of the strategy to improve the stability and to rise the fluorescence efficiency of such kind of systems is to stiffen the structure either introducing a rigid ring in the polymethinic chain or to annulate the structure. In this sense, squaraine dyes and boron rigid complexes, such as BODIPY or functionalized DPP, are considered cyaninic derivatives and will be discussed in a separate section later in the text.

Squaraines. In the vast galaxy of cyanine-like structures, squaraines are among the most studied and reviewed[12]. The optical properties are closed to the cationic polymethine dyes and show intense and sharp absorption in the Vis-NIR region and are emissive in that range[13]. For these characteristics they have been implemented in organic photovoltaics, non-linear optics, photodynamic therapy and bio labeling[15,16,17]. From the chemical structure point of view squaraines can be viewed as the condensation product of squaric acid with two equivalents of an electron rich moiety. They can be represented by three resonance forms. The main difference with the canonical cyanine structure is that sqaraines are zwitterions, thus electrically neutral (a positive e and a negative charge coexist on the same structure, without need of a counterion).

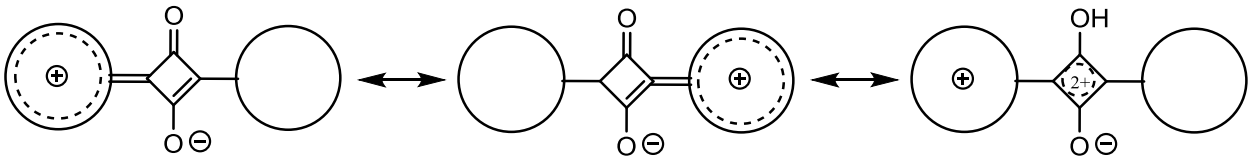

Figure 2.5: general scheme of mesomeric forms of squaraines.

The squaric acid core in the central position of the structure, being a four-membered tensioned ring, rigidifies the conjugated backbone, planarizing the structure. Such a conformation has two main advantages: the conjugation is efficient along the entire structure and the conformational changes in the excited state is reduced, avoiding non-radiative de-excitation. For this reason, normally squaraines show low Stokes shift. The mentioned characteristics have to be considered for application for squaraines both as light-harvesting and light emitting materials. The planar, extended conjugated core is the basis of the tendency to aggregate of such compounds.

For that, absorption bands tend to broaden in the solid state[13]. From the synthesis point of view, beside a great diversity in the structures, squaraines are straightforward to obtain and virtually every activated arene, π-excessive heterocycle or anhydrobase could react with squaric acid (in the reality, who worked with these systems knows the difference between paper chemistry and the real one). The following scheme show a non-exhaustive series of structurally diverse squaraine achieved so far.

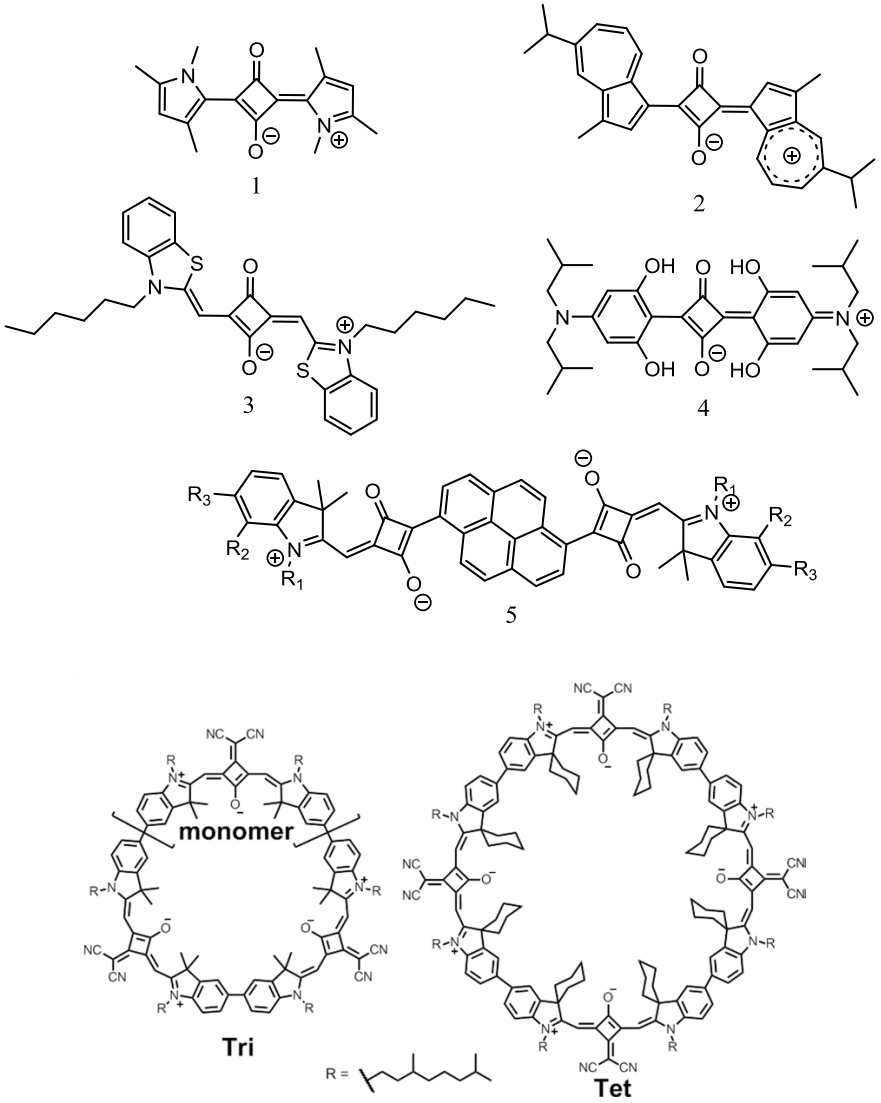

Figure2.6: squaraines obtained by condensation of 1) heteroaromatic π-excessive ring[12], 2) electron rich arene[18], 3) heteroaromatic anhydrobase[19], 4) amino- resorcinic derivatives[20], 5) π-extended NIR bis-squaraines[21]. The bottom figure reports a new entry tri- and tetrameric cyclic squaraines, with activity in the NIR region (adapted from[22]).

A general strategy to push absorption and emission of squaraines toward NIR is to use strong electron donors or to extend the conjugated skeleton (or both). The use of stylbenoid structures has been demonstrated to be an effective way to achieve longer wavelength absorption and reversible electrochemistry[23].

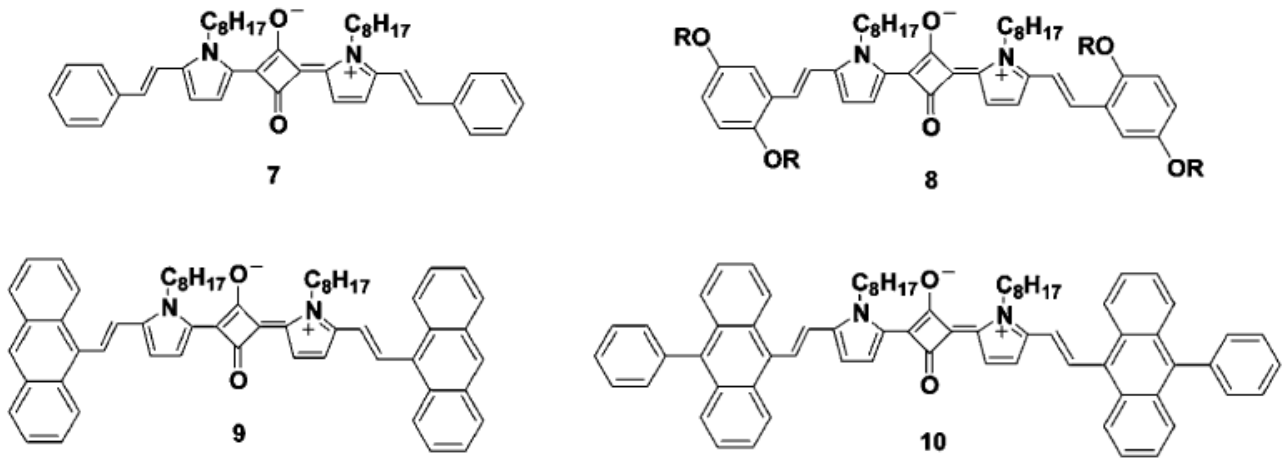

Figure 2.7: π-extended squaraines active in the NIR region. Adapted from[24].

If the application of squaraines is as light harvesting systems in organic photovoltaic, beside the NIR absorption, one can think about rendering the dye panchromatic. Panchromaticity is the phenomenon of the absorption of light at different wavelength, exploiting the sun spectrum as broadly as possible. This behavior can be achieved by direct functionalization of the squaraine core with acceptor groups directly attached to the cyclobutenic moiety. This introduces a new strong transition moment perpendicular to the principal one, resulting in a new band in the absorption spectrum, normally in the visible range.

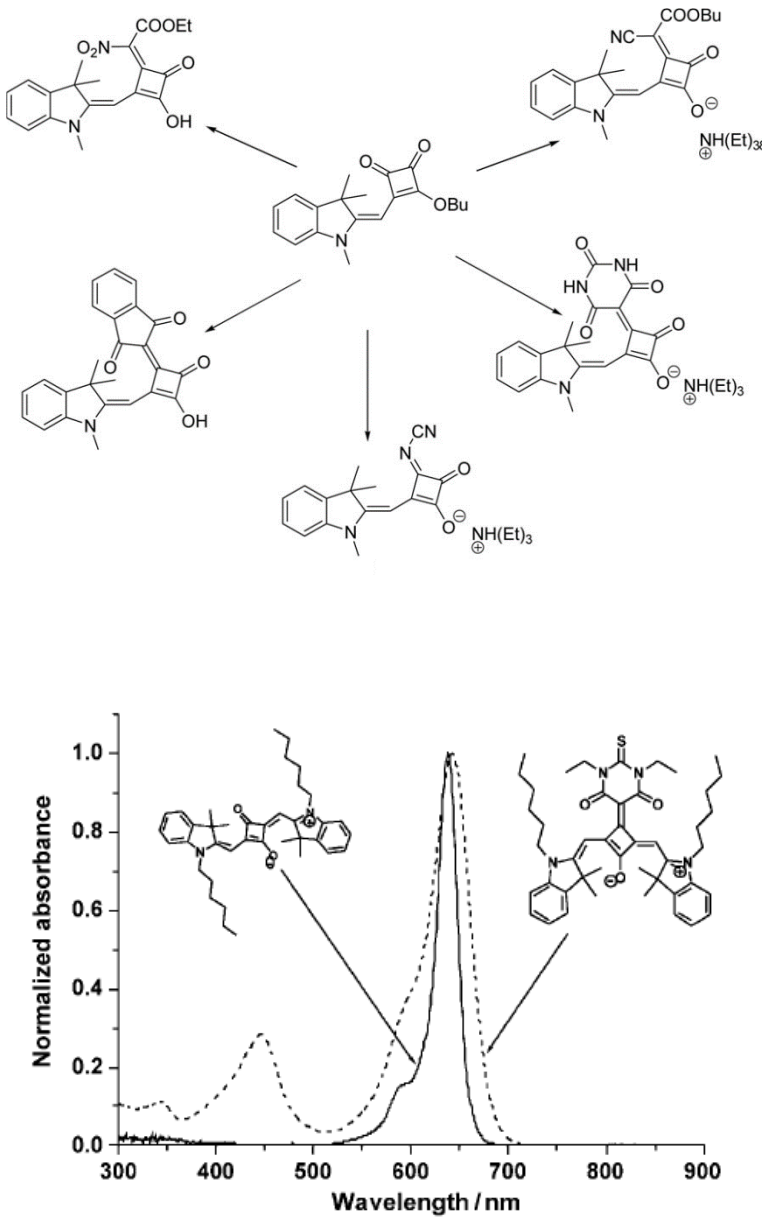

Figure 2.8: strategy to panchromatic light-harvesting squaraines. The top scheme represents some different functionalities compatible with the squaraine core. The bottom spectra refer to two analogue systems. The appearance on a new band at lower wavelength is evident. Adapted from[12,25].

All the strategies described have been attempted in this work in order to achieve efficient NIR light harvesting sqaraines and the details will be discussed in the results dedicated section.

Cyanine-like boron complexes. One of the strategy to improve performance of polymethine dyes is the complexation with boron. The resulting stiffening of the structure dramatically increase the fluorescence quantum yield, limiting non radiative de-excitation. So this kind of materials can be efficiently implemented as luminescent systems in light emitting devices such as OLEDs or solar concentrators. They gained a lot of popularity in recent years and it is interesting, for this work purposes, to analyze their properties. The literature based on a systematic structural analysis of such compounds is scarce and one of the few review works was done by Frath et al. in 2014[26]. The forefather of this class of molecules is 4,4'-difluoro-4-bora- 3a,4a-diaza-s-indacene (BODIPY), that present the following general structure:

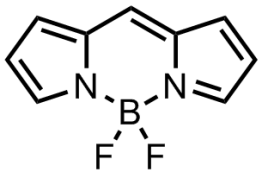

Methynic-bridged BODIPY dyes show narrow absorption and emission band, very high molar absorption coefficients and an environment-independent fluorescence quantum yields, often approaching 100%. Also remarkably they show reversible redox activity, making them attractive materials for electronics. An important drawback of BODIPY dyes is the weak emission in the solid state that limits optoelectronic applications. This weak emission is due to re-absorption, resulting from small Stokes shift (the separation between the absorption band and the emission band). In order to overcome these problems, many classes of compounds containing B(III) have been synthesized so far. In

general, they present a cyanine or merocyanine core rigidified by introducing a boron center locked by N-N, N-O, N-C, C-C, C-O or O-O chelating moieties.

One of the atoms involved in the chelation are negatively charged and two additional anions (usually F or Ar) on the boron center ensure neutrality of the resulting dyes. The fourth heteroatom stabilizes the boron center completing the valence shell, filling the unoccupied p orbital of boron (dative bond). The role of the B(III) center is to to stabilize the ligand by coordination and to planarize the π-system, thereby enhancing conjugation and charge transfer along the main molecular axis. These features induce well-defined and sharp absorption and emission bands as long as high quantum yields.

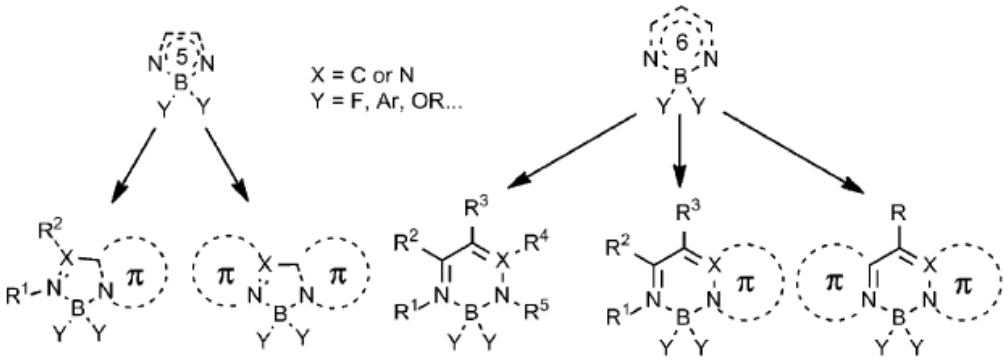

Figure 2.9: classification of five- and six-membered N-N organic boron complexes. Adapted from reference[26].

The boron complexes dyes can be classified by the number of atom of the resulting heterocycle. For the scope of this work, only N-N chelation modes will be presented. Figure 2.9 shows the five main chelation modes identified for such systems. For the purposes of this work, it is worthwhile to focus on the N-N bis-cyclic structures (last right in figure 2.9). In general, they present a large conjugated backbone, thus pronounced electronic delocalization and are highly fluorescent both in the visible and red- near infrared part of the spectrum. This category includes, quinolone indole and azaindole

BPh_2 complexes, naphthyridine and pyridomethene BF_2 complexes, indolocarbazole based complexes as well as azaboron diquinomethene complexes that strongly emits in the visible 78. Derivatives of diketopyrrolopyrroles (DPP) and azapirrolopyrroles (both BF_2 and BPh_2) complexes are of particular interest for their electronic characteristic and the strong NIR emission. The last representatives of such class of materials are DPP-Cyanine boron complexes, which are fundamental for this work and it can be interesting to describe them more in depth.

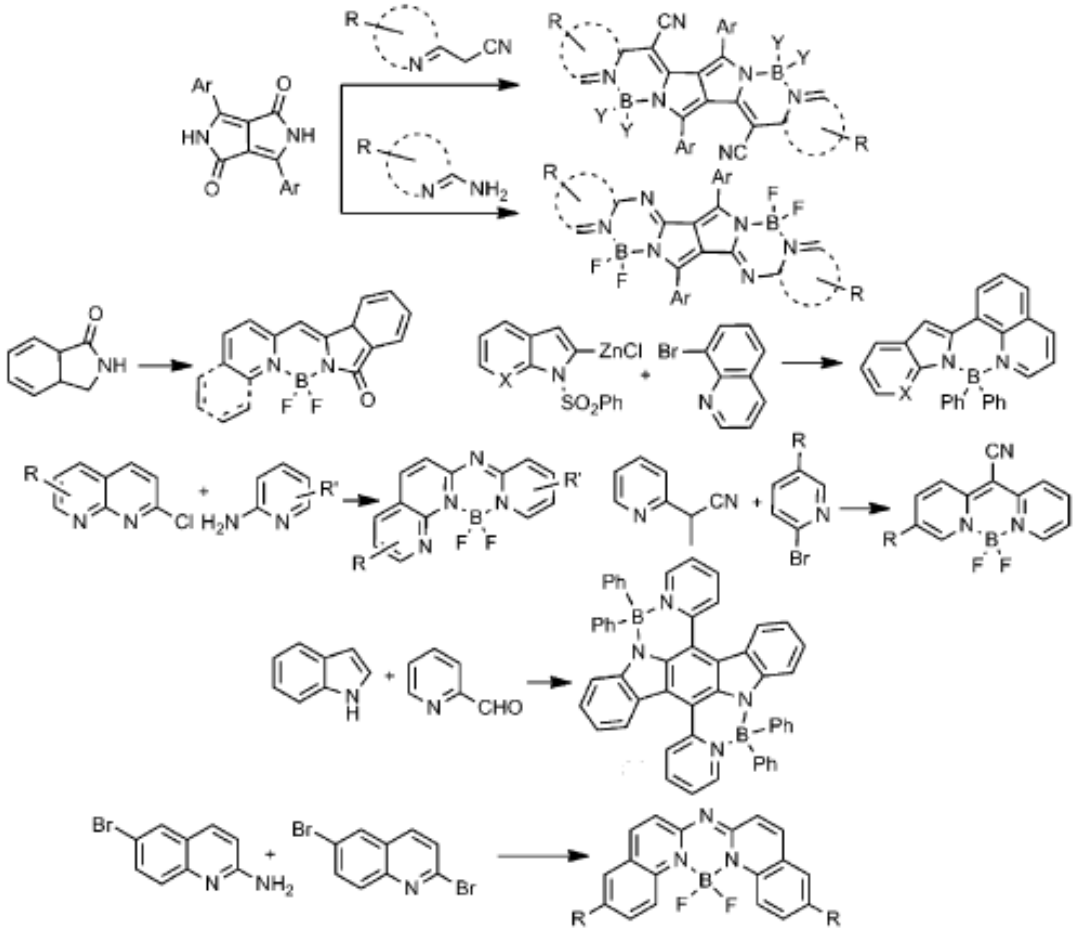

Figure 2.10.: summarizing scheme reporting six-membered N-N chelating boron(III) complexes as classified by Frath et al[26]. Interestingly, the scheme reports the aromatic precursors too, highlighting the relatively ease of synthesis of such materials, compared to larger, more challenging, π systems.

In 2007 Daltrozzo et al. reported the synthesis of diketopyrrolopyrrole (DPP) derivatives binuclear boron complexes for the first time[27]. From a structural point of view, they contain a pyrrolopyrole core that is the central element of a cyanine-like chromophore, condensed with two aromatic acetonitrile groups (HAA). The structure is stiffened by complexation with two BF_2 or BPh_2 centers.

Going back to the history, DPP pigments were first synthesized in 1974 in small amounts through Reformatsky reaction in the laboratories of the former Ciba-Geigy (now Novartis, after merging with Sandoz in 1996)[28]. Extensive work to optimize the synthesis lead to the first product on the market in 1986. After the expiration of the patent in 2004, several competing products were placed in the market, in particular the most important representative, CI Pigment Red 254, sold by European and Asian companies, providing a sharp drop of DPP prices. Because of their high resistance to heat, light, and solvents, they rapidly became important in paints and coating dyes. In recent years DPP have attracted the attention of the chemistry community as promising candidates for organic electronics and bio-imaging applications[29,30].

Several modifications are possible in the peripheral aromatic moieties or on the lattamic nitrogen and π-extended and polymeric structures are known[31]. Due to the intrinsic chemical inertia of the electron poor pyrrolopyrrole core, only few examples of chemical modification of the carbonyls are possible. Activation with Lawesson's reagent to produce more reactive thiocabonyls has been reported as well as activation with $POCl_3$ and subsequent reaction with anilines[28].

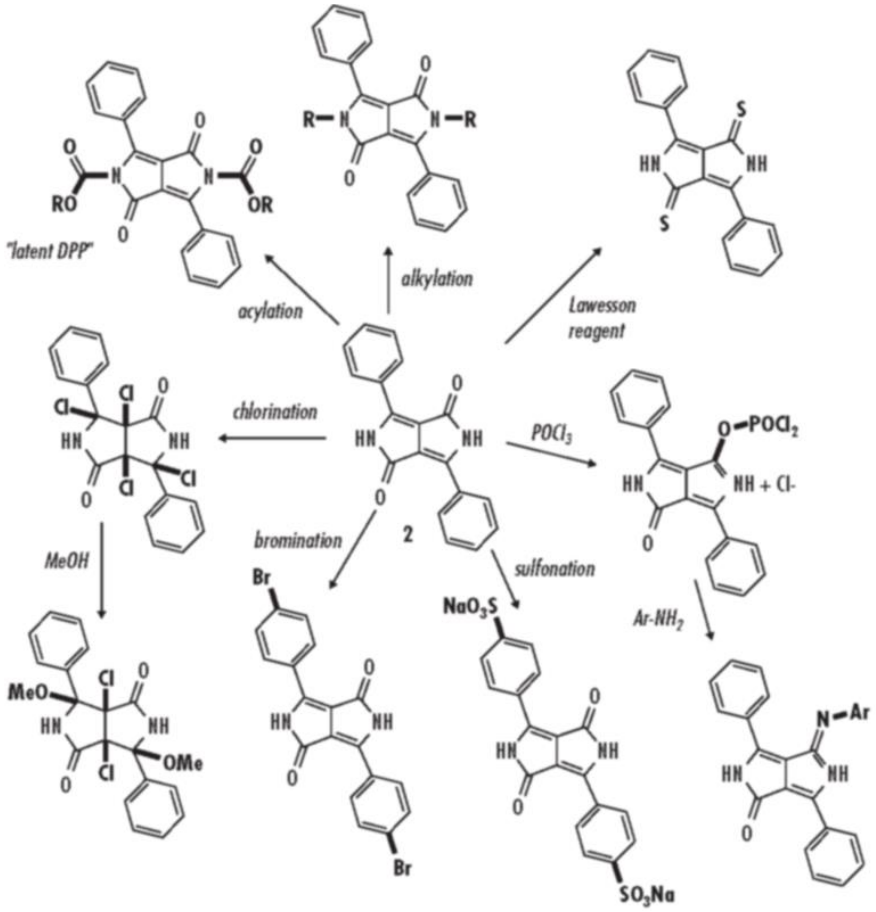

Figure2.11: several functionalizations are possible starting from the diaryl-DPP building block. Noteworthy, carbonyl functionalization is challenging and only few examples are reported in literature. Adapted from reference[28].

One-pot condensation with HAAs via activation with $POCl_3$ has proven to be a convenient and straightforward method to obtain DPP-Cyanine. The products of this reaction are in the form of hydrogen chelates. They present very strong and narrow absorption in the NIR. No fluorescence is present due to the torsional degrees of freedom of the heteroaromatic acetonitrile group that leads to thermal depopulation of the excited state (confirmed by fluorescence observed at 70 K frozen solution).

The stiffening of the structure is achieved by complexation with either BF_2 or BPh_2 groups[32]. The obtained fluorophores present an extended planar structure, which shows strong fluorescence and high quantum yields.

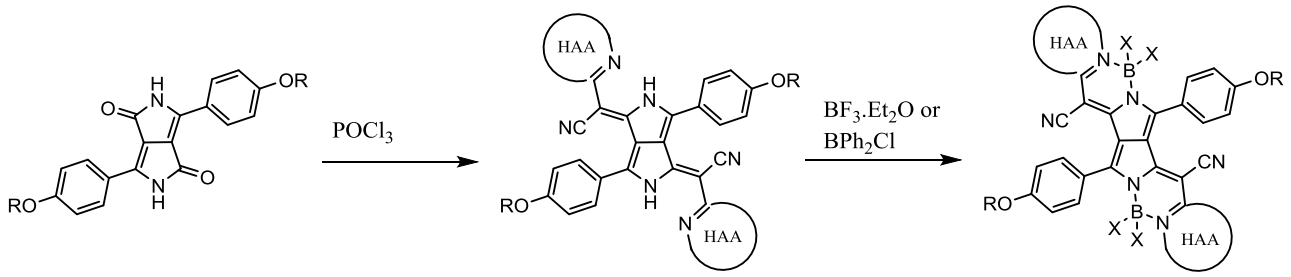

Figure 2.12: synthetic pathway to DPP-cyanines as reported by Daltrozzo et al. R= alkyl chain, X= F or Ph.

The structure has been elucidated by X-Ray diffraction of single crystals. The chromophoric system is nearly planar and the side aromatic rings are twisted out of the plane. This observation suggest that the conjugation is lower on the minor axis and only the functionalization of the HAAs residues can significantly affect the chromophore properties.

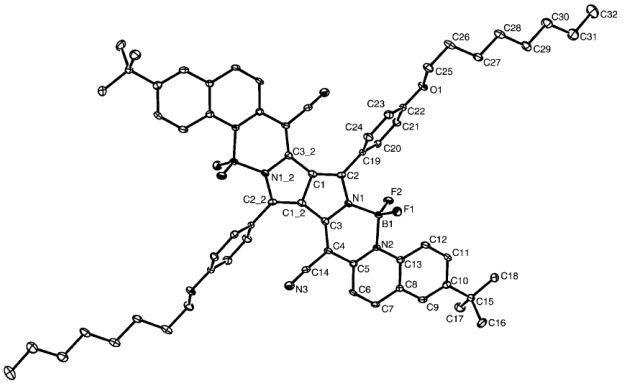

Figure2.13: x-ray diffraction analysis reported by Daltrozzo et al. The image clearly shows that the pheripheral phenoxy group are twisted with respect to the molecule main plane, giving us an important information on how to proceed in the synthesis. Reprinted from[32].

DPP-cyanines show peculiar spectroscopic characteristics. Single core systems cover the spectral absorption region from 684 to 864 nm, with negligible absorption in the visible, and the emission goes from 708 to 881 nm, matching the first “NIR window”. Surprising, they present remarkably high fluorescence quantum yields ranging from 32 to 64%. These favorable characteristics, together with the high photostability and low solvatochromic effect demonstrated in Daltrozzo and coworkers pioneer work, render this class of materials of particular interest for optoelectronic application.

2.2.5 Macrocyclic derivatives: phthalocyanines and core-contracted homologues. Macrocyclic dyes represent one of the most structurally diverse class of photoactive molecules. IUPAC defines a macrocycle as "a cyclic macromolecule or a macromolecular cyclic portion of a molecule”. Porphyrin and the synthetic analogues phthalocyanine are two of the most studied example of macrocyclic ring systems. Heme, chlorophyll and vitamin B12 are examples of conjugated macrocycles widely present in nature. Phthalocyanine class represents around 25% of all artificial organic pigments on the market. They are used in the textile industry as direct dyes for cotton or in the paper industry. One of the most successful application of phthalocyanines (together with cyanine and azo dyes) is in the compact disc fabrication, were a thin layer of dye is used as data-storage medium[33].

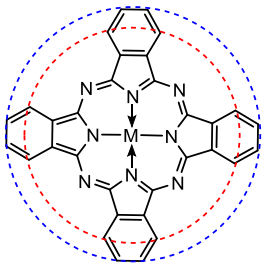

Figure 2.14: general structure of a metal-phthalocyanine. The functionalization sites are highlighted in blue for peripheral positions and red for bay positions.

Chemical industry of dyes and pigments invests a great deal of effort on developing new macrocycles. A more academic field of research is the synthesis of contracted porphyrinoids. Although they are not strictly NIR compound, their description will be useful for the present work. Contracted three-membered analogues of phorphyrines and phthalocyanines can be ascribed to the following categories: subporphyrins (SubPs), benzosubporphyrins (BzSubPs), subporphyrazines (SubPzs), and subphthalocyanines (SubPcs). The latter contains three isoindole units and it will be discussed in depth. Contracted pophyrinoid compounds present peculiar characteristics. They are only known as boron (III) derivatives. Boron halides, with general formula BX_3 (X= Cl, Br), are the only templating agents used so far. The most relevant feature regards the electronic and structural properties: they possess a 14 π-electron aromatic core but, nonetheless, adopt a nonplanar cone-shaped conformation. Therefore, they represent one of the few examples of nonplanar aromatic rings and, not surprisingly, they are characterized by peculiar chemical, spectral and electronic features[34].

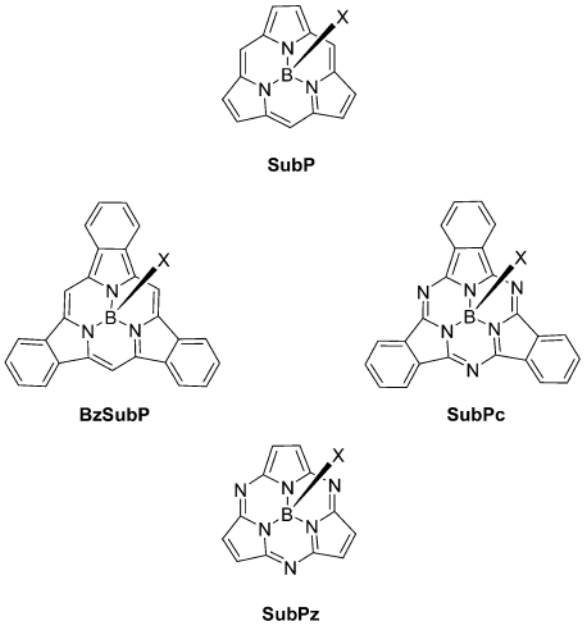

Figure 2.15: different types of contracted macrocycles. Reprinted from[34]. Interestingly, even expanded core systems, called superphthalocyanine, were synthesized, showing the ability to host bulky metal atoms such as uranium.

Among the contracted porphyrinoids, subphthalocyanines are the most investigated and known. They were serendipitously discovered in 1972 by Meller and Ossko, as they were trying to obtain boron Pc[35]. The condensation reaction of phthalonitrile in the presence of boron trichloride in chloronaphthalene at 200 °C did not lead to the expected cyclotetramerization product. Instead, they observed the formation of a purple compound whose analysis was consistent with the formation of chloro-SubPc.

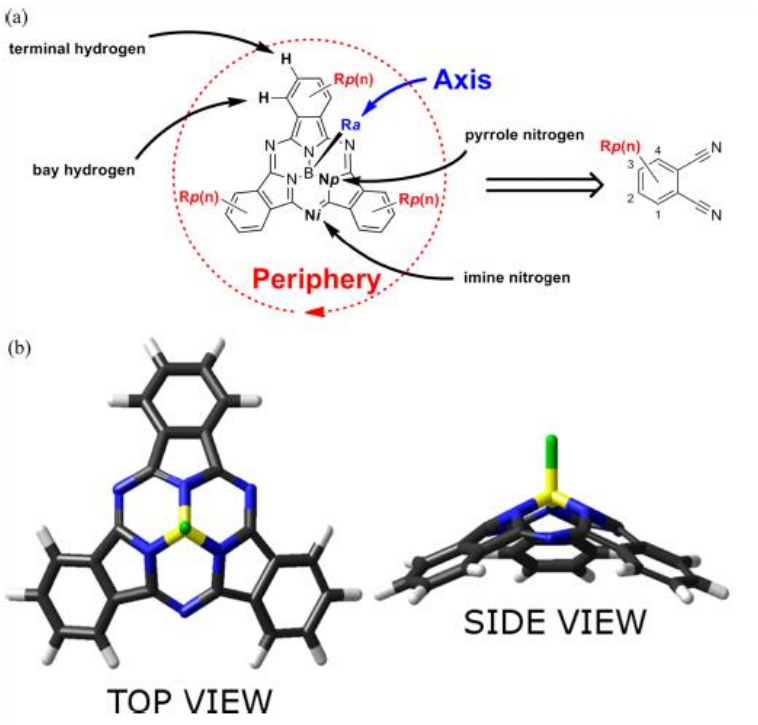

Figure 2.16: a) detailed description of SubPc structure. Rp(n) represents type and number of substituents on the periphery, Ra on the axis. B) simulation showing on the cone shape of the subPc core. Adapted from[36].

In these compounds, three isoindole subunits are bound together by three aza-bridges. For that, the core is an aromatic 14 π-electron heteroannulene. The chemistry of SubPcs developed over the last two decades due to the intensive effort of academic groups all around the world such as Kobayashi[37], Bender[38], and Torres[39] groups.

This class of compounds started to have an impact on many technological fields as active materials in artificial photosynthetic systems, photodetectors, OLED, organic solar cells and bio-imaging[34,36]. The SubPc framework construction has evolved in the time after the pioneering attempt of Meller and Ossko. The standard procedure is the cyclotrimerization reaction of a phthalonitrile derivative in the presence of a boron-based Lewis acid. Unlike phthalocyanines, attempts to synthesize SubPcs without boron or with a different central metal have not been successful so far. Moreover, only one-pot statistic condensation can be carried out to synthesize the core, and a stepwise synthesis of SubPcs, which would provide higher structural flexibility, still remains a challenge. The standard boron reagents, which have been employed so far in the synthesis of SubPcs, are BCl_3 and BBr_3. They generate the corresponding chloro- and bromo-boron SubPc when reacted with a phthalonitrile. BCl_3 is slightly less reactive than BBr_3 even though gives rise to the more stable chloroboron SubPc, due to the higher stability of the B−Cl bond with respect to the B−Br bond.

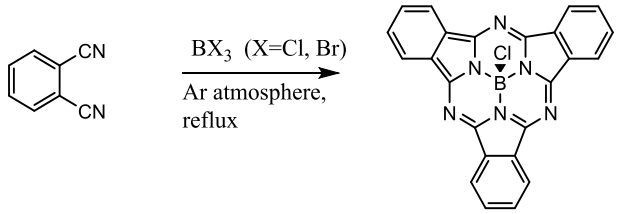

Figure 2.17: synthesis of subPc using boron trihalides as templating agent.

Both quantum-mechanical studies and experimental analyses have been exploited to elucidate the formation mechanism of subPcs in a benchmarking paper[40]. A computational study shows that the postulated elementary reaction steps leading to the formation of the SubPc-precursor macrocycle are indeed exothermic or at least

kinetically allowed. The results of extensive quantum-chemical energetic, structural, and charge distribution computations show that a catalytic effect of boron trichloride is essential to explain that molecular chlorine is liberated in the formation of chloroboron SubPc in a concerted process. The mechanistic study of chloroboron SubPc formation from phthalonitrile and BCl_3 in aromatic solvents, such as p-xylene or toluene, suggests the formation of the initial phthalonitrile-BCl_3 adduct produces (1Z)-3-chloro-N-(dichloroboryl)-1H-isoindol-1-imine. Such species is both nucleophilic and electrophilic and is the actual active species. This fact has been confirmed by isolation (Torres and co-workers) of the hydrolyzed product, without traces of starting phthalonitrile, that is quantitatively converted in the very first step of the reaction.

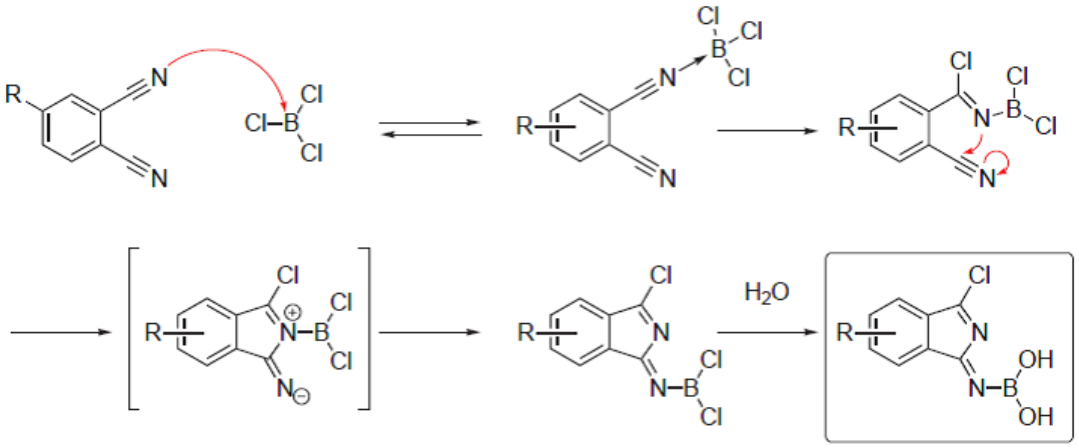

Figure 2.18: Formation of the hydrolysis products 4 from intermediate 3 generated in the reaction between phthalonitrile and boron trichloride. Adapted from[40].

As successive addition of three molecules of isoindoleimine derivative leads to the formation of the open-chain SubPc. It is of particular importance for the three pyrrolic nitrogen atoms to be coordinated to a central boron atom since this spatial arrangement

assures the proximity between the meso nitrogen atom and the iminic carbon atom for the ring-closing step. There must be a boron atom acting as the template in order for the cyclization to proceed at this stage.

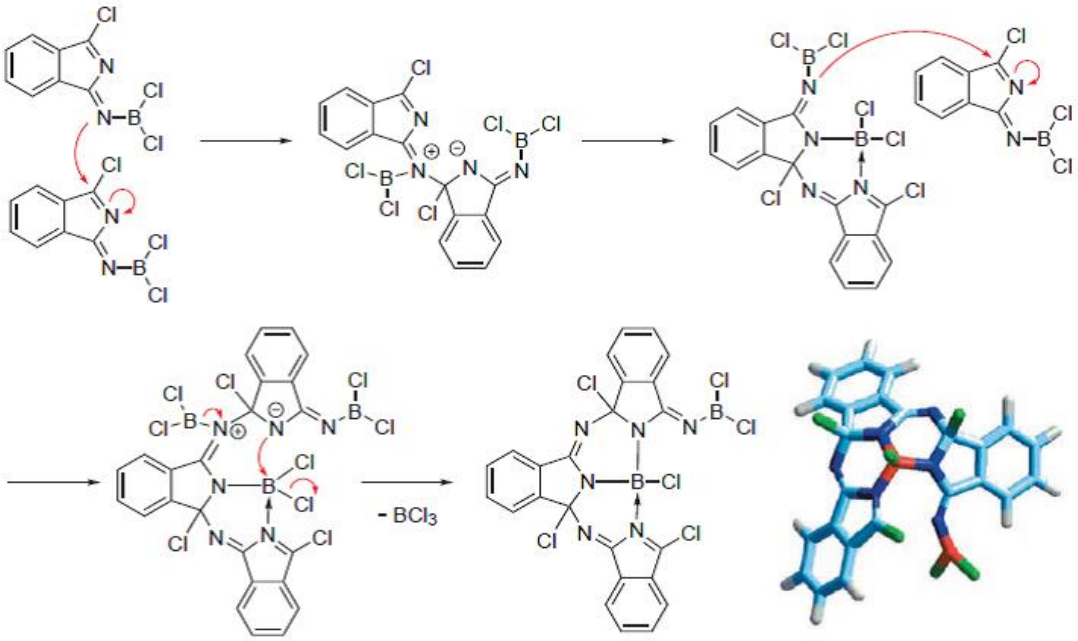

Figure 2.19: Progressive assembly of the subphthalocyanine macrocycle and 3D structure. Adapted from[40].

The last step is a reductive process that take place in presence of Lewis acids species into the reaction medium (and not by the central boron atom in itself). In this last process, molecular chlorine is liberated.

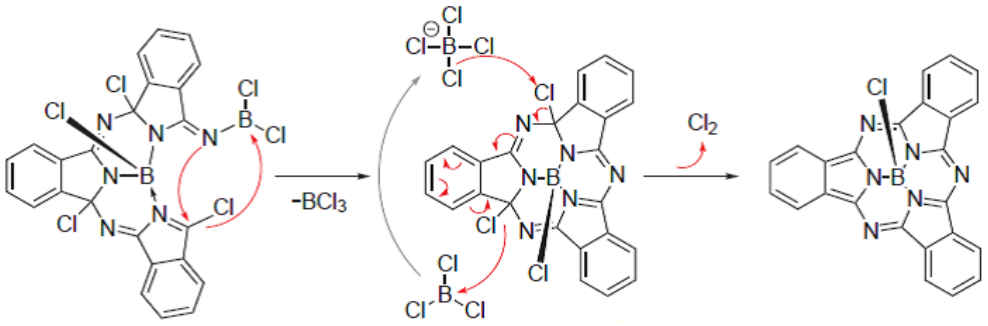

Figure 2.20: final ring closure of the SubPc precursor, and reduction to SubPc. Adapted from[40].

Reactivity of SubPc can be classified in three main families of reactions: axial reactivity, peripheral reactivity and ring expansion. Only the first two class are discussed herein for sake of brevity. Axial substitution is the replacement of the original halogen atom directly linked to the boron center with a different molecular fragment, by means of a covalent bond. Despite this wide use, the axial substitution approach has various limitations that arise from the relatively poor reactivity of the SubPc boron atom. The 3D cavity formed by the three isoindole groups and the axial ligand offers steric and electronic protection to the tetracoordinated boron atom, whose vacant p orbital is occupied by formation of a dative bond with one of the nitrogen atoms in the macrocycle. As a result, the reaction with nucleophiles typically requires high temperatures[34]. The most successful way to activate the boron center, proposed by Torres et al.[41] is the substitution with triflates. The reaction consists in a first step in which the irreversible generation of an activated SubPcB-triflate intermediate by reaction with AgOTf or Me_3SiOTf reagents takes place. In a second step, the nucleophile is added and the reaction is completed within a few hours in mild conditions.

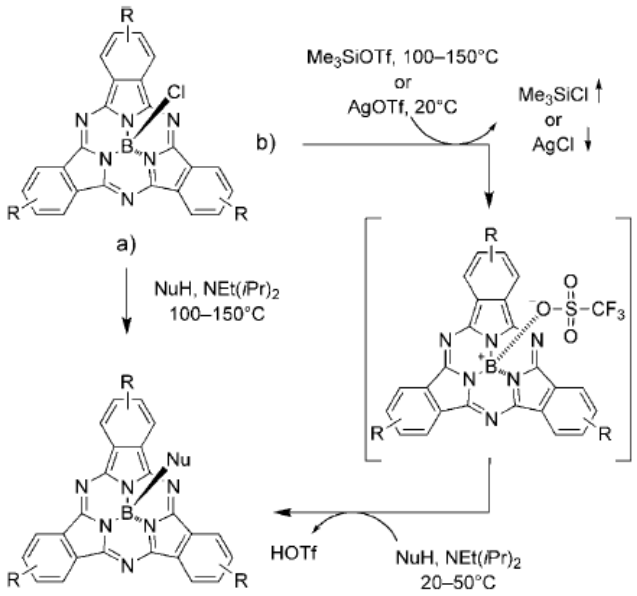

Figure 2.21: substitution reaction by a) direct substitution with a nucleophile and b) triflate path. Reprinted from[41].

The peripheral reactivity is the introduction of different substituent on the benzene ring of the isoindolic moiety. In this case the boron-axial ligand bond is not involved. SubPc are relatively unstable compared to Pc, due to the intrinsic constrain of the three membered macrocycle, thus the chemical manipulation should be carefully selected to prevent ring opening. Direct use of strong nucleophiles should be avoided because they normally lead to ring opening. The harsh condition used in the SubPc synthesis also limit the kind of functional groups that can be introduced in the phthalonitrile precursors, the most typical being halogen atoms, nitro groups, alkyl groups, thioethers. Amines, alkyl ethers or double and triple bonds are reactive towards the Lewis acid, so they are normally introduced after the macrocycle formation. Metal-catalyzed cross coupling is a widely explored methodology to introduce functional groups directly to the isoindole moiety or on the aromatic apical group. Suzuki, Sonogashira and Stille reactions are used to form C-C bonds and to couple SubPc with other photoactive units. Buchwald-Hartwig protocol has been successfully used to introduce amino groups and efficiently shift absorption maximum of SubPc toward NIR[42].

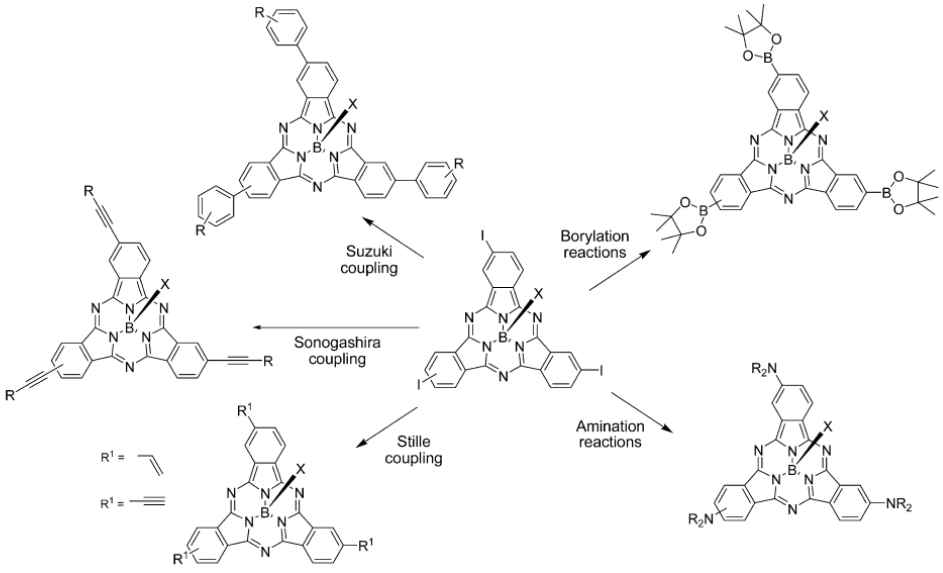

Scheme 2.22: triiodo-subPc is the perfect example of key intermediate for peripheral functionalization. Cross coupling procedures allow a vast array of synthetic pathways. Reprinted from[34].

The last sub-class of macrocycle it is worthy to mention here are subphthalocyanines fused dimers. In 1991 Kobayashi claimed the synthesis of the first example of dimer of an aromatic macrocycle containing boron, a bridged, fused subphthalocyanine[43]. The first systematic study on synthesis and structure characteristic was published only in 2002 in two independent works of Kobayashi and Torres[44,45]. Topoisomers *anti*-94 and *syn*-94 were synthesized by crossover condensation of tetrafluorophthalonitrile and 1,2,4,5-benzenetetracarbonitrile in a 10:1 ratio, and in the presence of 3 equivalents of BCl_3, separated and independently characterized. Trimer formation was also reported during the synthesis. The ^{1}HNMR spectrum of these species shows the central benzene ring protons signals shifted at very low fields, the "fingerprint" of the dimer formation. The absorption main band (Q band) is red-shifted of tenths of nanometers with respect to the corresponding single-core subphthalocyanine and it is situated in the first part of the NIR region (700nm). This demonstrates the structures are fully conjugated and represent one of the few examples of extended, π-conjugated non-planar structures. The properties off such derivatives will be discussed in the device chapter.

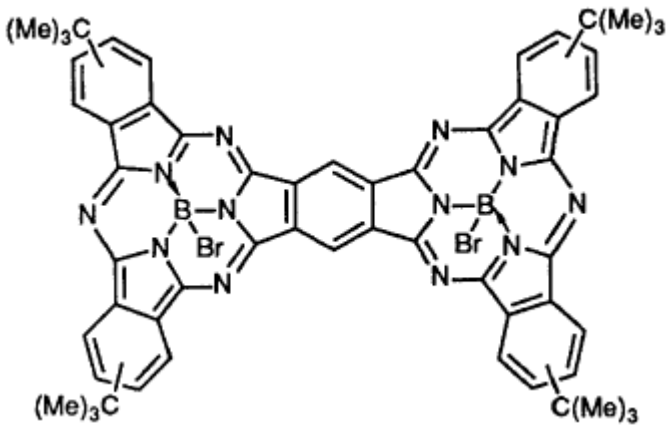

Figure 2.23: dimers of subphthalocyanine as firstly reported by Kobayashi. Adapted from[43].

Luminescent materials: lanthanides complexes. Another class of technological relevant molecules are complexes of lanthanides. Although they are structurally different from the highly conjugated, purely organic chromophores presented above in the present text, it is important to introduce and briefly review them in the analysis. Such class of compounds are widely used as luminescent materials and their emission properties in the infrared region are relevant for the discussion.

As stated in a recent review by Bunzli[46] "*Presently, phosphors and luminescent materials for lighting, telecommunications, displays, security inks and marking, as well as for probes in biosciences represent one third of the total value of the lanthanides used worldwide".* One can immediately recognize the importance of invest in the research on such materials. Focusing on the structure and reactivity of lanthanides complexes, one can note that they are based on the properties of *f*-orbitals. The general electronic configuration is [4]f^n and the filling of 4*f* orbitals determines the similarity in the chemistry. All lanthanides present stable 3+ oxidation states, whose chemistry is defined by the ionic radius, that decreases along the series (lanthanides contraction). The peculiar configuration of *f*-orbitals (shielded and highly localized) origins a large number of energy levels and, thus, possible electronic transitions. For this reason, the emission range of trivalent lanthanide ions spans from the visible part of the electromagnetic spectrum, for Sm, Eu, Tb and Dy, to the near-infrared portion for Er, Yb and Nd. The unique electronic and photophysical characteristic make these materials suitable for a large number of technological application. Focusing on NIR emitting lanthanides, the most cited ones are Nd(III) showing emission bands at 860, 1060 and 1350 nm, Er(III), emitting at 1540 nm ad Yb(III), emitting at around 1000 nm. The latter is of particular interest because of the emission matches the crystalline silicon energy gap.

Noteworthy, other lanthanides present useful NIR emission bands, such as Pr(III) (900-1100 nm), Sm(III) (900-1200 nm), Ho(III) (980-1500, 1900 nm) and Tm(III) (780, 1450 nm)[46].

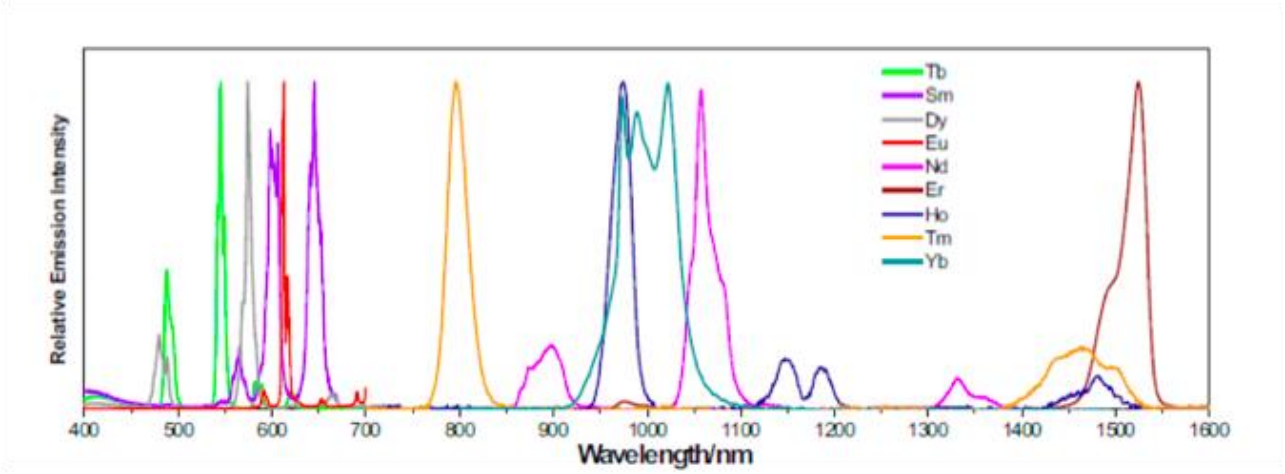

Figure 2.24: emission lines of lanthanides, covering all the NIR range. From www.pitt.edu.

The possible optical transitions in lanthanides are $f \leftrightarrow d$ transitions, charge transfer transitions (such as ligand to metal charge transfer LMCT) and $f \leftrightarrow f$ transitions. The latter are responsible for the emission bands of lanthanides. Although f-f transitions give well defined and sharp bands, due to the low ligand effect and the shielding of f-orbitals, they are forbidden by the *Laporte's parity transition rule*. For that, the absorption band present very low absorption molar coefficients, resulting in weak emission.

An effective solution to enhance the absorption capability of lanthanides is to exploit the so-called antenna effect, firstly proposed by Weissman in 1942[47]. The metal ion is surrounded by ligands with high absorptivity and excitation transfer capability. Organic chromophores are usually used for this scope. The mechanism involved is an excitation transfer from the excited state of the organic ligand (S_1) to an emissive triplet state of the metal (S_3), by inter system crossing (ISC).

The emission of the lanthanide is “sensitized” and red shifted in this way. A more detailed treatment will be described in the device section. A wide range of ligand and co-ligands is present in the literature. Mono-, bi- and poly-dentate ligands are possible and, although lanthanides are oxophiles, nitrogen-based ligands are very common, such as bipyridinic derivatives[48].

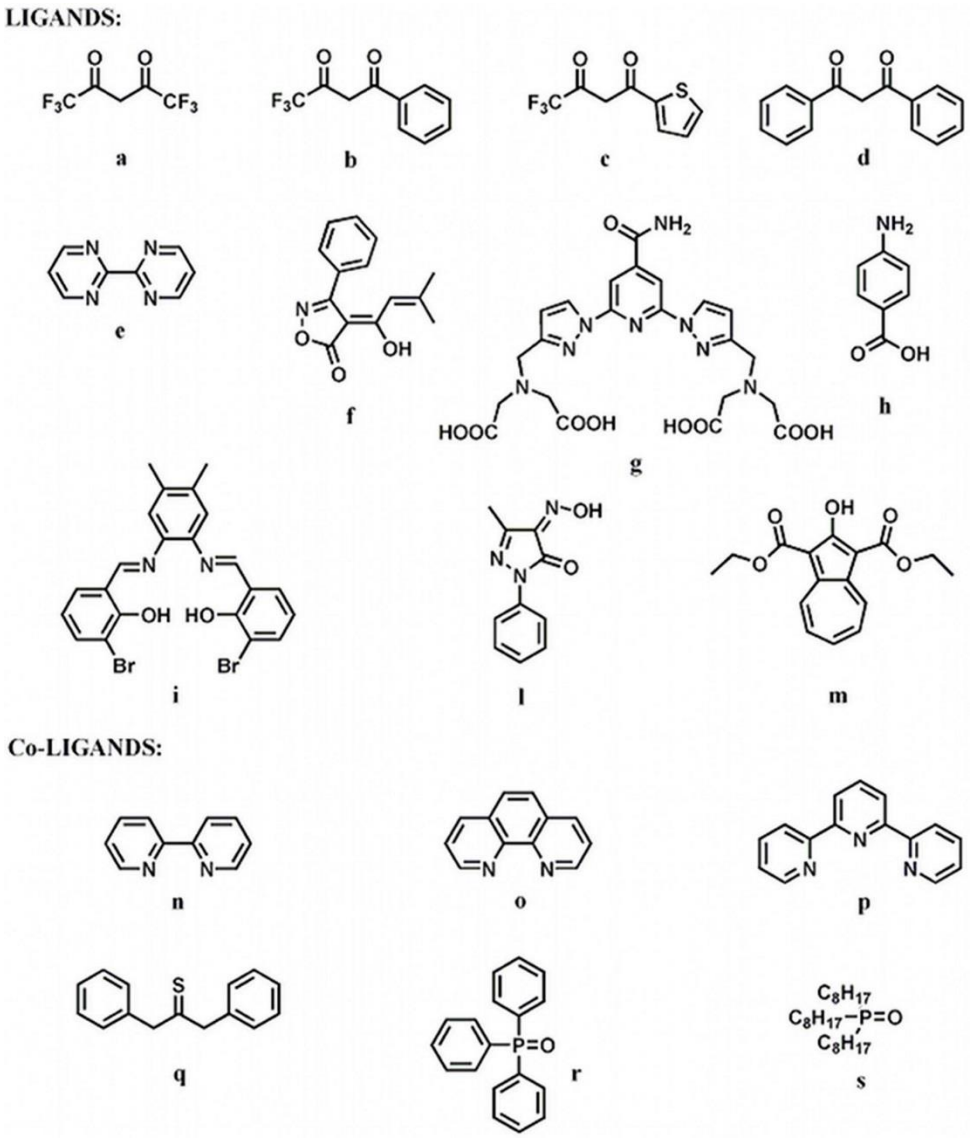

Figure 2.25: Ligands and co-ligands commonly used in lanthanides complexes. A,b,c and d are exemples of oxygen-based ligands, β-diketonates. Very common co-ligands are nitrogenbased bipyridines (n), phenantrolines (o) and ter-pyridines (p), as long as aromatic and alkylic phosphine oxides. Adapted from[48].

As said, NIR emitting lanthanides are well known in the literature and they have been extensively reviewed[49]. It has to be considered that one of the most important drawbacks in using organic system to sensitize NIR luminescence is the presence of C-H and C=C bonds that can quench the infrared emitted light[50]. The need to overcome this problem and to enhance higher values of luminescence quantum yield prompted the research towards innovative organic ligands for lanthanides.

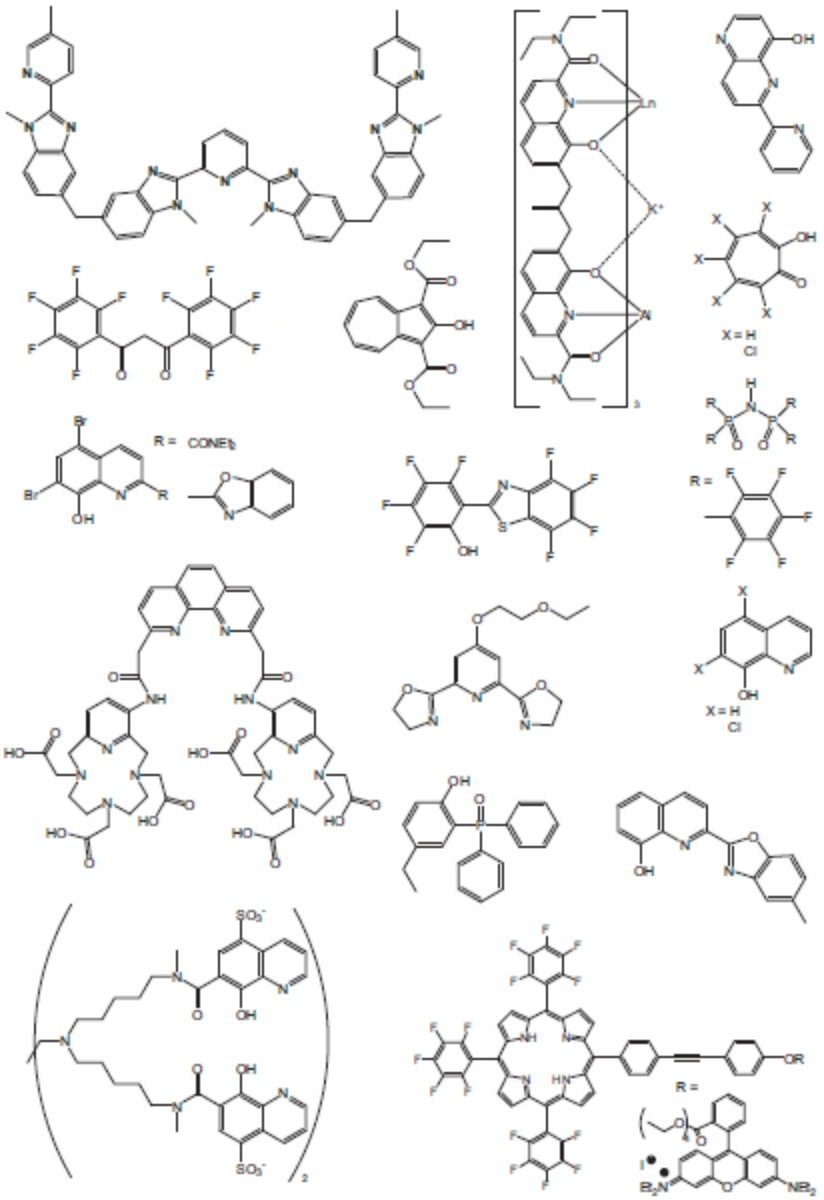

Figure 2.26: examples of organic ligands used in highly NIR-luminescent lanthanide complexes. Adapted from[46].

2.3 Results and discussion: design, synthesis and characterization of the molecules

The first part of this chapter represents an attempt to present and review some classes of organic and organo-metallic structures that found applications in the vast and diverse panorama of organic electronics. Among the uncountable different structures that modern organic chemistry allows, the doctorate work herein presented focused on:

- boron-containing cyaninic structures
- squaraines
- boron-containing macrocycles (subphthalocyanines)
- chelates of lanthanides

The chemical design was aimed at producing molecules able to fulfill the requests mentioned in the introduction: have an efficient emission and/or absorption in the NIR, be soluble enough to allow solution-processed devices production, be chemically and thermally stable, introduce an element of novelty in the structure or in the preparation. In this section an array of structures, selected among the various trials done during the thesis, is presented and the synthesis, the prominent features and the characterizations done so far are discussed in detail. The possible applications of every system are also discussed, as long as the possible improvements or research strategies to overcome the weakness points or to complete the characterizations. As said, the attempt was to explore a wide range of structure to enrich the knowledge of the properties of near-infrared active compounds and their applications. For an easy reading, every reaction scheme is identified with a letter (A-M) and every product is identified by a number and a letter referring to the scheme.

2.3.1 Light harvesting systems: squaraines

The introduction presented the important class of squaraine dyes, trying to make the reader familiar with the structural features and the most important characteristics. One of the remarkable features of squaraines is the structural flexibility, since a large number of electron-rich moieties are able to react with squaric acid (or squaric esters). The reaction conditions are well established in the skills patrimony of Beverina's group, where the work was done. Along with the electron-rich moiety, the solvent plays a fundamental role in the formation of squarines. The standard conditions report the use of a 1:1 mixture of toluene (b.p. 110 °C) and n-butanol (b.p. 118°C). The alcohol gives esterification on the squaric acid at the working temperature, activating the system. Given that it is a condensation reaction, two equivalents of water are generated. To push the reaction toward the products the water is generally eliminated by azeotropical distillation (Dean-Stark apparatus) or by chemical reaction with a dehydrating agent, such as tri-butyl ortoformate.

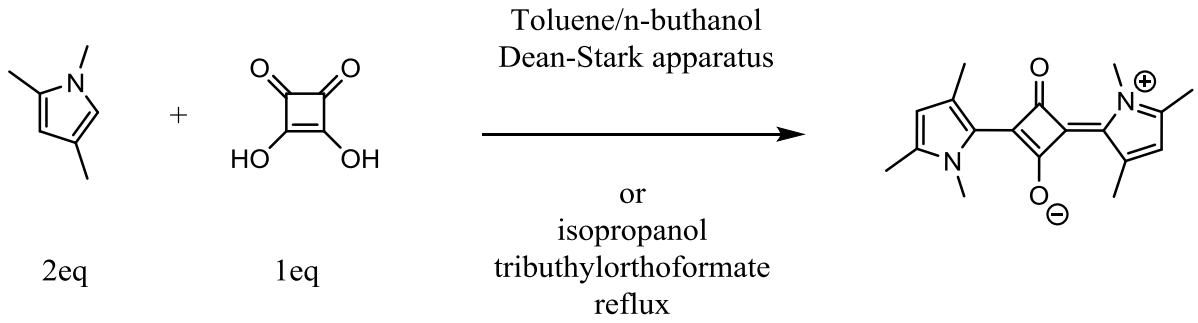

Figure 2.2.1: example of squaraine dyes synthesis.

Squaraines are efficient light harvesters and can find a use in organic photovoltaics or light sensing devices. The explorative synthesis carried out during the doctorate work exploited some of the methodologies described to push the absorption of the squaraines derivatives toward the NIR: building up of extended conjugated cores, functionalization of the central core, stiffening of the structure with H-bonds. The general scheme reporting the structures investigated is reported below and all the synthesis and attempts are described as long as the optical characterizations.

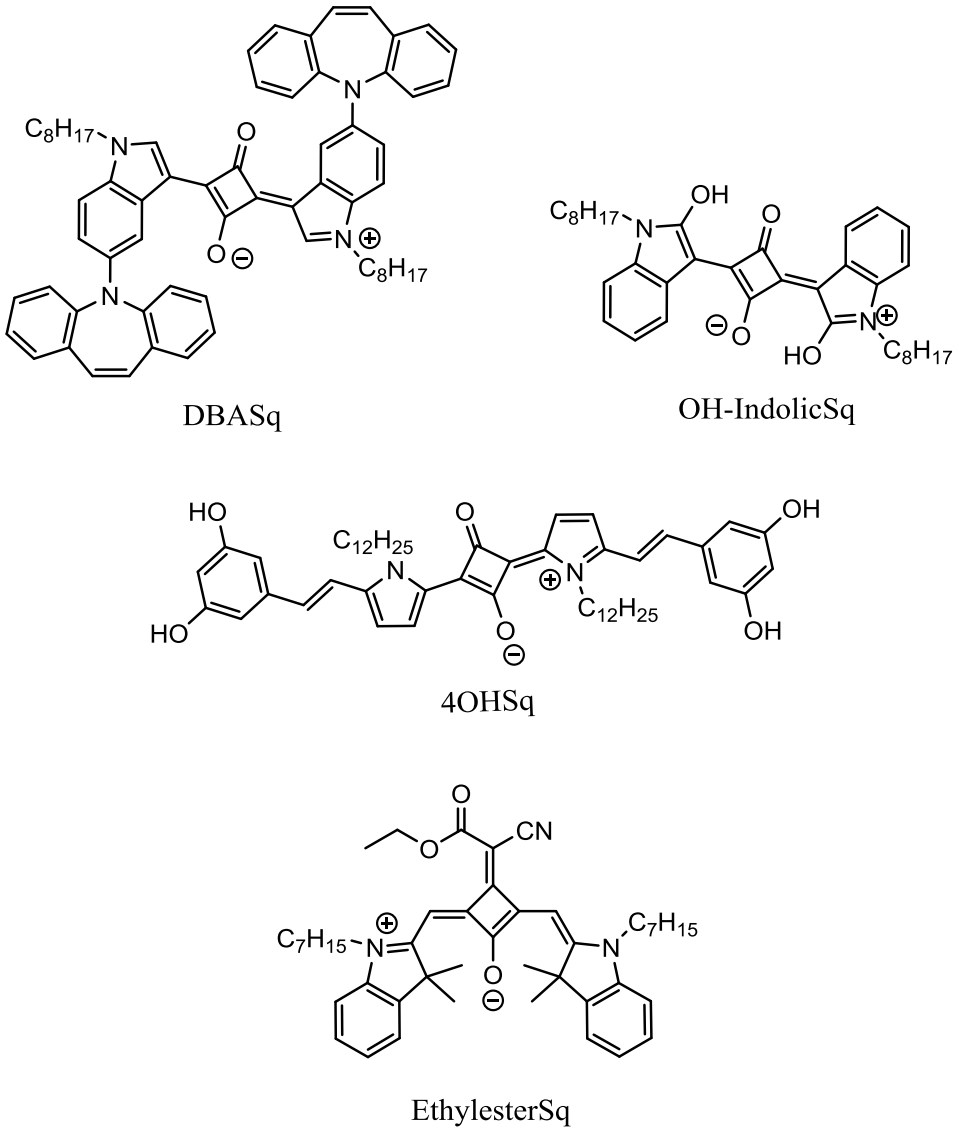

Figure 2.2.2: structures of squaraines presented in this work.

Indolic squaraines:

The first synthetic route attempted started from the molecular design of the indolic squaraine, whose properties in the field of organic electronics were investigated in a 2013 paper by Sassi et al. as donor material for OPV[51]. In that case, the indole was end-capped with a diphenylhydrazonic functionality, recording an absorption maximum at 589 nm. To push the absorption of such class of materials toward the NIR, two possible strategies are to enhance the donor capacity of the electron-rich moiety of the squaraine or to stiffen the central core of the structure by means of hydrogen bonds. To corroborate the first method, a dibenzoazepine residual was coupled to the indole, following the subsequent procedure:

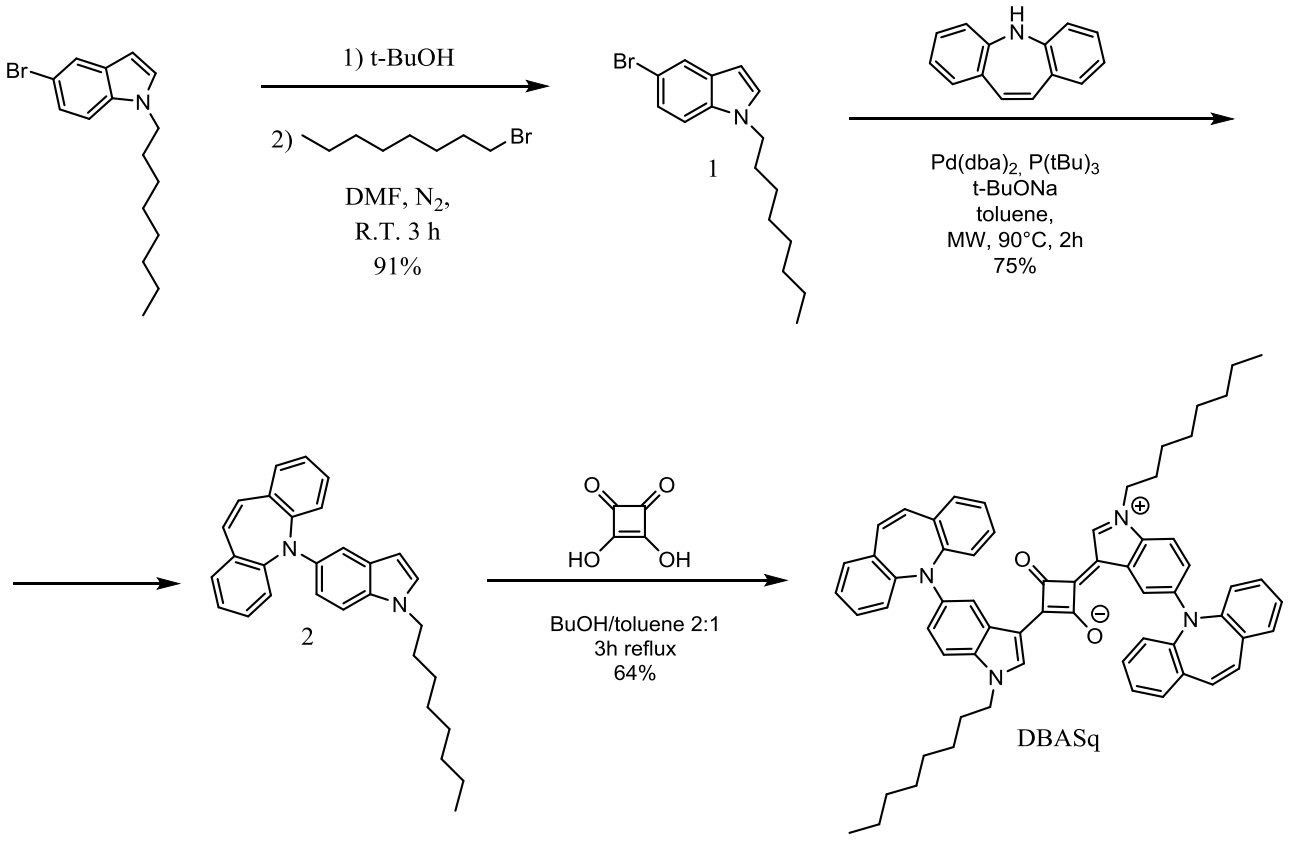

Scheme 2A: synthesis of dibenzoazepine squaraine.

The dibenzoazepine group has been demonstrated to be a stronger donor with respect to other aromatic donor moieties in a study by Turrisi et al. The comparison was done on a perylene monoimide dye, functionalized with different amines. Dibenzoazepine showed enhanced donor capabilities with respect to diphenylamine, carbazole, dialkylamine, and indolizine[52]. The same approach was then implemented on a squaraine structure.

The three steps synthesis started from the N-alkylation of bromoindole with a linear octil-chain, to impart enough solubility to the π-extended final compound. Alkylated bromoindole 1 was thus subjected to Buchwald-Hartwig palladium-catalyzed amination reaction to introduce the dibenzoazepine capping, following a microwave-enhanced protocol. The product 2 was then condensed with squaric acid under azeotropic removal of the formed water to give the product DBAsq.

The UV-Vis characterization of the derivative was performed over a diluted solution in CH_2Cl_2. The introduction of dibenzoazepine actually red shifts the main absorption band of the squaraine to 599 nm, with respect to the hydrazonic analogue.

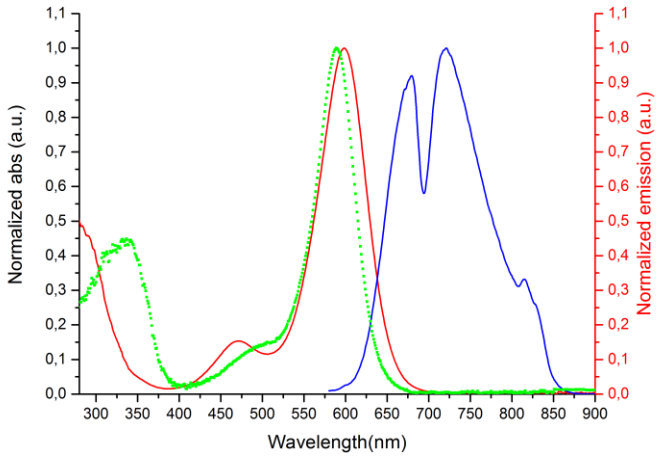

Figure 2.2.3: absorption spectra of reference hydrazonic squaraine (green line) and DBAsq (red line) and emission of DBAsq (blue line).

The product retains the high-energy band ascribed to the localized transitions of the electron-rich substituent. The emission is structured in two main bands, likely due to an instrumental artifact caused by the lamp change, peaked at 680 nm and 721 nm, with a third, less intense peak at 815 nm, clearly within the NIR region.

The derivative was also electrochemically characterized. The trace of a 10^{-5} M solution in CH_2Cl_2 with tetrabutylammonium tetrafluoborate as the supporting electrolyte was recorded. The first oxidation peak onset is placed at 484 mV with a maximum at 632 mV. The reduction semi-wave shows an onset at -1260 mV with a maximum value at -1420 mV. The calculated FMO energy value are 4.47 eV for the HOMO and 2.74 eV for the LUMO, giving a value of the HOMO-LUMO gap of 1.73 eV.

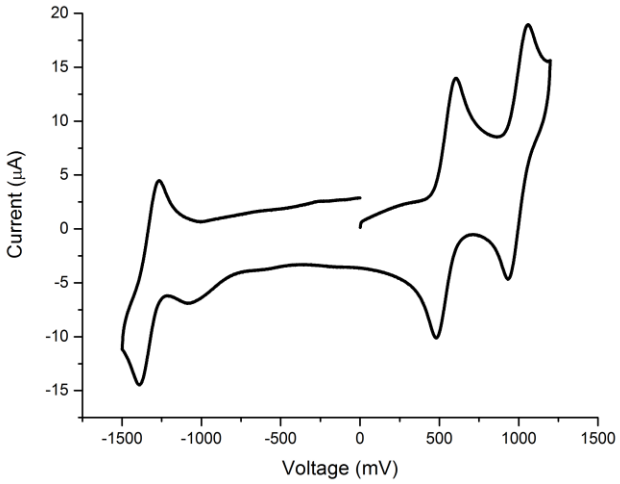

Figura 2.2.4: cyclic voltammetry trace of DBAsq.

The second approach tested to obtain NIR-active indolic squaraine was the core-stiffening exploiting intramolecular H-bonds. This approach was extensively studied by Forrest and demonstrated to be effective in the planarization of the structures, leading to red shift both in absorption and emission[53,54]. The H-bonds between the -OH groups

of the catecholic residuals and the central oxigens on the cyclobutene, planarizing the structure, render the conjugation more effective.

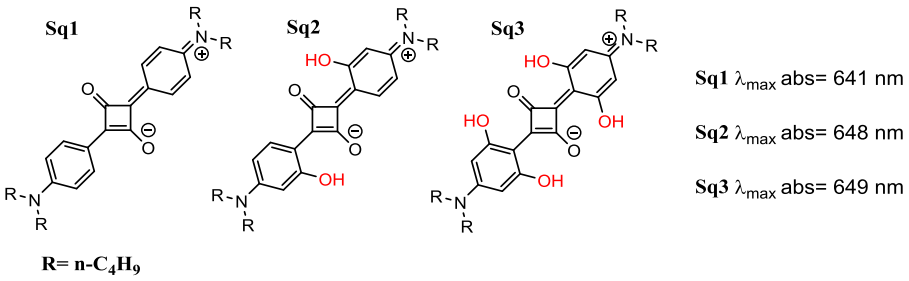

Figure: 2.2.5 structures and absorption maxima of aniline squaraines presented in[54].

In the case presented herein, the -OH groups are directly placed on the indolic donor. The synthesis, reported in scheme 2B, consists in a N-alkylation of 2-oxyindole and subsequent condensation with squaric acid under azeotropic distillation. The particularity of this reaction is the use of an excess of concentrated H_2SO_4.

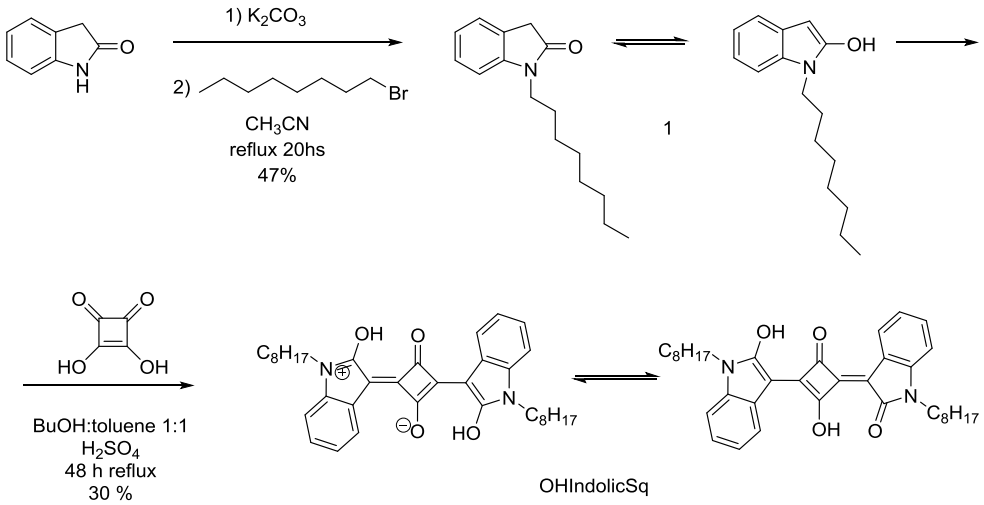

Scheme 2B: synthesis of OHindolicSq.

The oxyndole presents tautomeric equilibrium between the lactamic form and the hydroxylic form, with a net prevalence of the former. It does not condense with squaric

acid in “classic” squaraine formation conditions, even after 24 hours at reflux. The presence of the strong acid shifts the equilibrium towards the enolic form, that is the actual species that gives condensation with squaric acid, through acid catalyzed enolization. To the best of author’s knowledge, this reaction represents the first synthesis of a squaraine dye carried out in such strong acidic conditions. The nature of this compound was investigated by UV-Vis analysis, showing an unexpected behavior. As a comparison, an analogue 2-methylindolic squaraine was synthesized: the absence of intramolecular H-bond in this case, should lead to a less efficient conjugation and a blue-shift of the absorption with respect to a planar structure. Actually, the absorption of OHindolicSq resulted slightly blue shifted with respect to the methylindolic squaraine (557 nm vs 559 nm). This could be ascribed to the tautomerism that such structure shows: the lattamic tautomer present less donating capability toward the squarilium core, shifting the absorption at higher energies. However, a certain grade of intramolecular H-bond is demonstrated by the absorption peak structure that shows a vibronic structure likely due to such interactions.

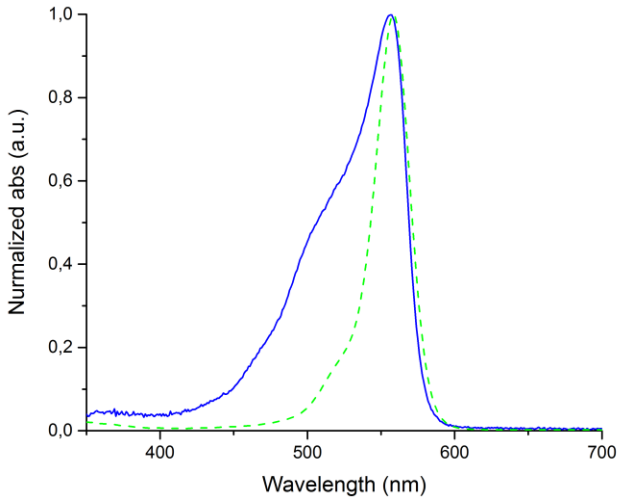

Figure 2.2.6: absorption trace of OHindolicSq compared to the methylindolic one (recorded in $CHCl^3$, 10^{-4} M).

The squaraine was electrochemically characterized in diluted solution (10^{-5} M) solution in CH_2Cl_2 with tetrabutylammonium tetrafluoborate as the supporting electrolyte. The oxidation peak onset is placed at 151 mV with a maximum at 320 mV. The reduction semi-wave shows an onset at -1173 mV with a maximum value at -1428 mV. (HOMO-LUMO of 1.32eV, 1.83 for the methylic derivative).

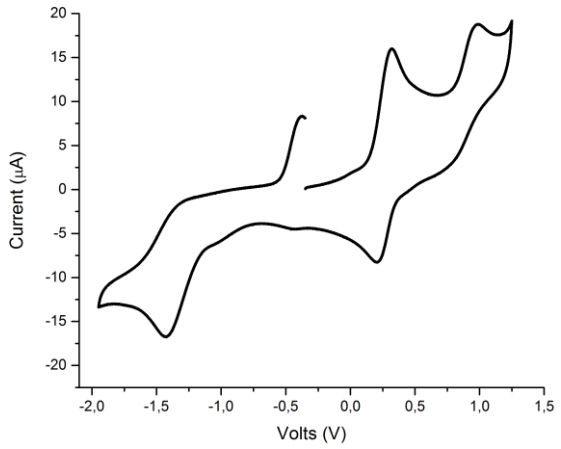

Figure 2.2.7: cyclic voltammetry trace of OHindolicSq.

A sample of squaraine was recrystallized from CH_3CN/Toluene 1:1 giving single crystals that were analyzed by x-ray diffraction, confirming the nature of the target compound and demonstrating that in the crystal, the dominant tautomer is the enolic one.

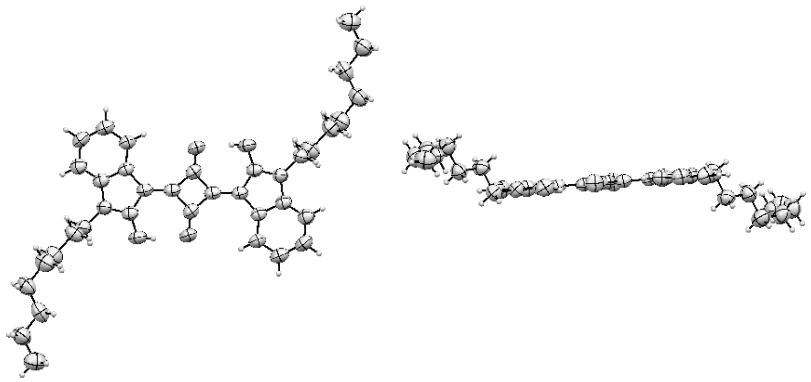

Figure 2.2.8: side view of OHindolicSq as reported from x-Ray diffraction (probability ellipsoids).

Core-extended squaraines:

The conjugated core expansion is another effective strategy to lower the band gap of squaraines. In this sub-section, a new π-extended squaraine is reported. The peculiarity of such structure is the presence of four cleavable methoxy-residues in the peripheral phenyl rings. The cleavage of such residuals, as long as the long alkylic chains on the pyrroles, was designed to offer the possibility of a selective packing in the solid state. The hydroxylic group can provide H-bonds, while the C_{12} chains can interact by means of Van Der Waals forces. Such characteristic can provide a suitable feature to be exploited to obtain ordered thin films for organic electronic devices. Also NIR-active J-aggregates could be achieved with this strategy, since J-aggregates in π-extended squaraines have already been demonstrated[55,56].

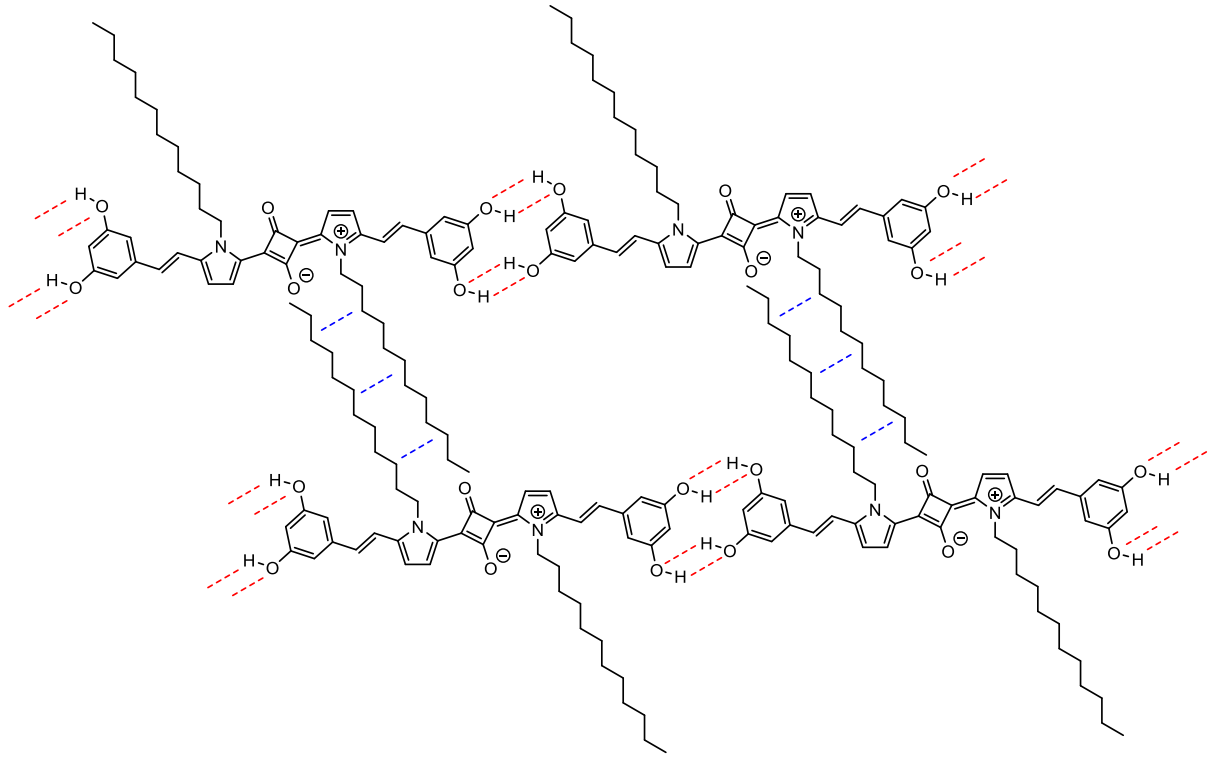

Figure 2.2.9: representation of the possible aggregation mode of the squaraine presented. The blue dotted lines represent Van der Walls interactions, while red ones the net of H-bonds.

The convergent synthesis, reported in scheme 2C, started from the building up of the heteroaromatic stylbenoid electron rich moiety. Commercially available 3,5-metoxy benzaldehyde was transformed in the corresponded phosphonate 2 by means of a reduction to benzylic alcohol 1 with an excess of $NaBH_4$ and subsequent Arbuzov reaction with iodine in triethylphosphite. The pyrrole carboxyaldehyde was alkylated following a standard procedure with dodecyl-bromide, deprotonating the pyrrole with NaH to achieve the compound 3. The subsequent Horner-Hemmons coupling was performed, using potassium tert-butylate as a base, to obtain the stylbenoid structure 4.

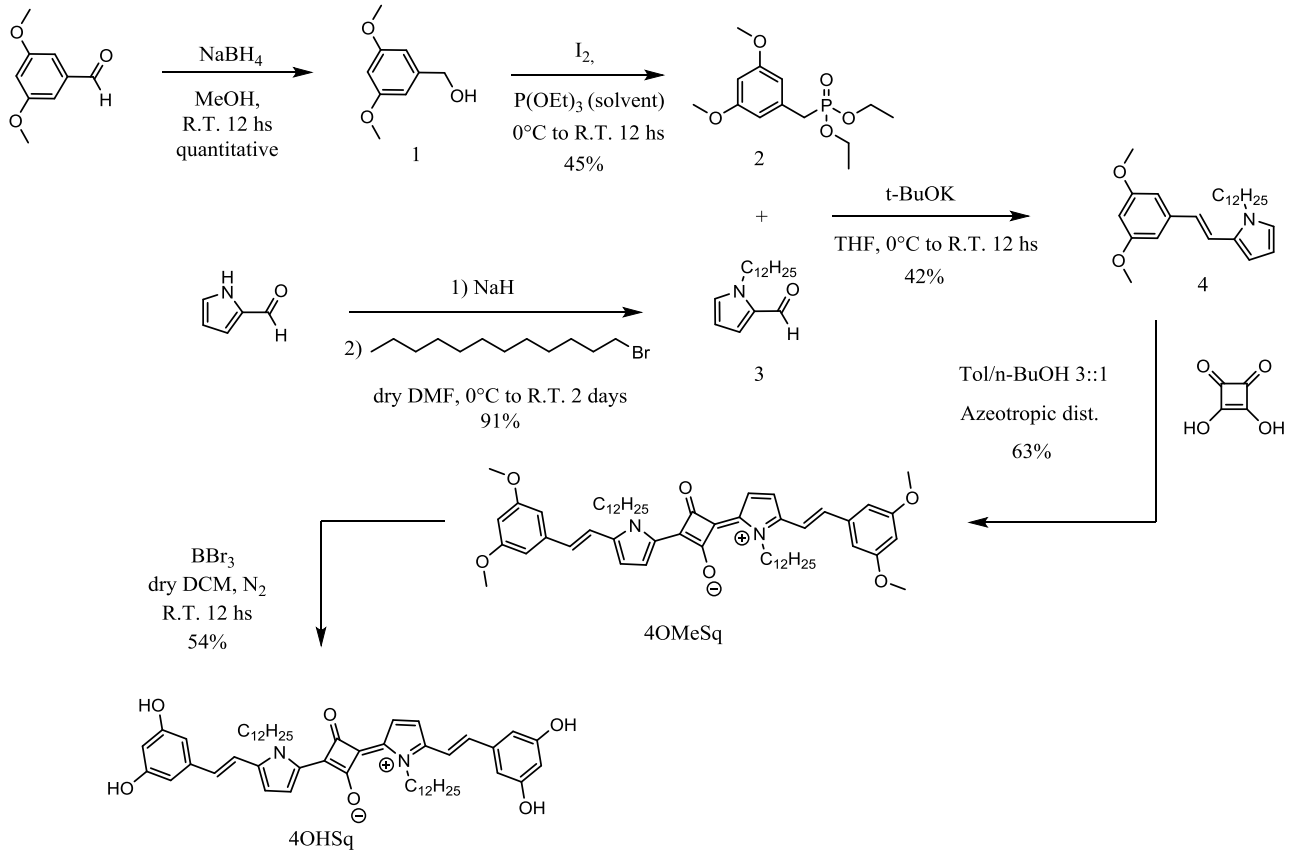

Scheme 2C: synthesis of 4OHSq

Noticeably, structure 4 presents two possible points of condensation for squaric acid: the 2-position of pyrrole and the 4-position of the phenyl residues. The hypothesis is that for such derivatives, the condensation would undergo on the π-excessive pyrrole if the reagent ratio 4/squaric acid is 2:1. If the ratio would be 1:1 or even with an excess of squaric acid, the double-headed compound 4 could form polysquaraine, a class of materials interesting for NIR-related applications[24]. In the present case, two equivalents of 4 were condensed with squaric acid, giving the squaraine named 4MeSq in surprisingly high yield (63%). A de-protection reaction was performed on a small scale to achieve the compound 4OHSq. The reaction was performed in DCM at reflux, using a strong Lewis acid, BBr_3, as deprotecting agent. The light blue product showed amphiphilic behavior during the work-up and strong aggregation. The reaction was monitored by UV-Vis and the spectrum recorded in diluted solution showed a broad main peak centered at 683 nm and a second peak, with lower ε, centered at 728 nm. This second peak is probably due to J-aggregate formation, that would confirm the presence of strong intermolecular interactions likely due to a H-bond net among the peripheral -OH groups.

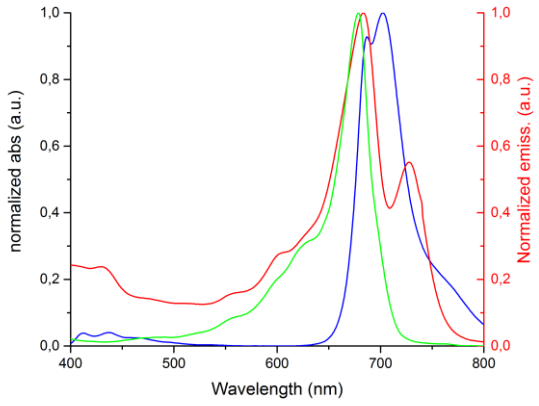

Figure 2.2.10: Uv-Vis spectra of precursor 4MeSq green line, 4OHsq, red line and emission of 4OHsq, blue line, recorded in chloroform, ~10^{-4} M.

Fluorescence spectra of the derivative was also recorded. Upon excitation at 683 nm, the trace showed a structured pathway, with two main bands centered at 687 and 702 nm and a shoulder at lower energies, at around 760 nm probably due to J-aggregate emission. No further characterization was carried on due to the small amount of product. As the preliminary results showed are encouraging, some further analysis are planned: a NMR spectrum recorded at high temperature could be useful to de-aggregate the supramolecular formations to obtain more insights on the structure and, with a scale-up of the reaction, analysis of thin film behavior could be performed.

Core functionalized squaraines:

One of the possibility to exploit the structural flexibility of squaraines to impart new properties is the core-functionalization. It was mentioned in the introduction that active methylenes, bearing electron-withdrawing groups, can be placed on the squaraine core by condensation on one of the carbonyls of a squaric ester precursor. In the synthesis herein reported (scheme 2D) a hydrolizable group have been introduced on the core. This functionality adds the possibility, after hydrolysis, to obtain a carboxylic group that can be exploited as a grafting point over metal surfaces or oxides. A natural application could be the sensitization of TiO_2 in dye-sensitized solar cells, enabling the harvesting of the low energy portion of the solar spectrum, were standard visible-active dyes do not operate. Moreover, the residual visible absorption peak proper of core-substituted squaraines can further enhance the light-harvesting. A similar approach was proposed by Beverina et al.[57]. placing the anchoring group on the indolenine moiety in a non-symmetric squaraine fashion.

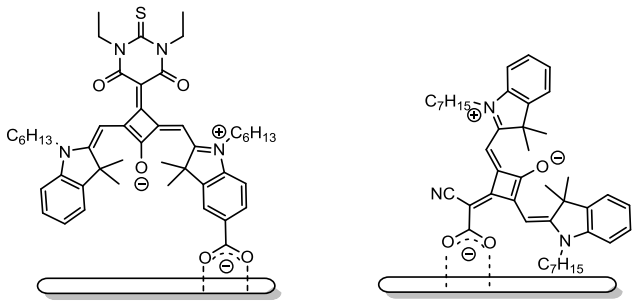

Figure 2.2.11: representations of the anchoring modes of the squaraine reported in ref.[57] and the core-substituted one.

Placing the anchoring group directly on the core avoids multistep asymmetric squaraine synthesis and could provide a better charge transfer due to the presence of two donor moieties directly attached to the acceptor one.

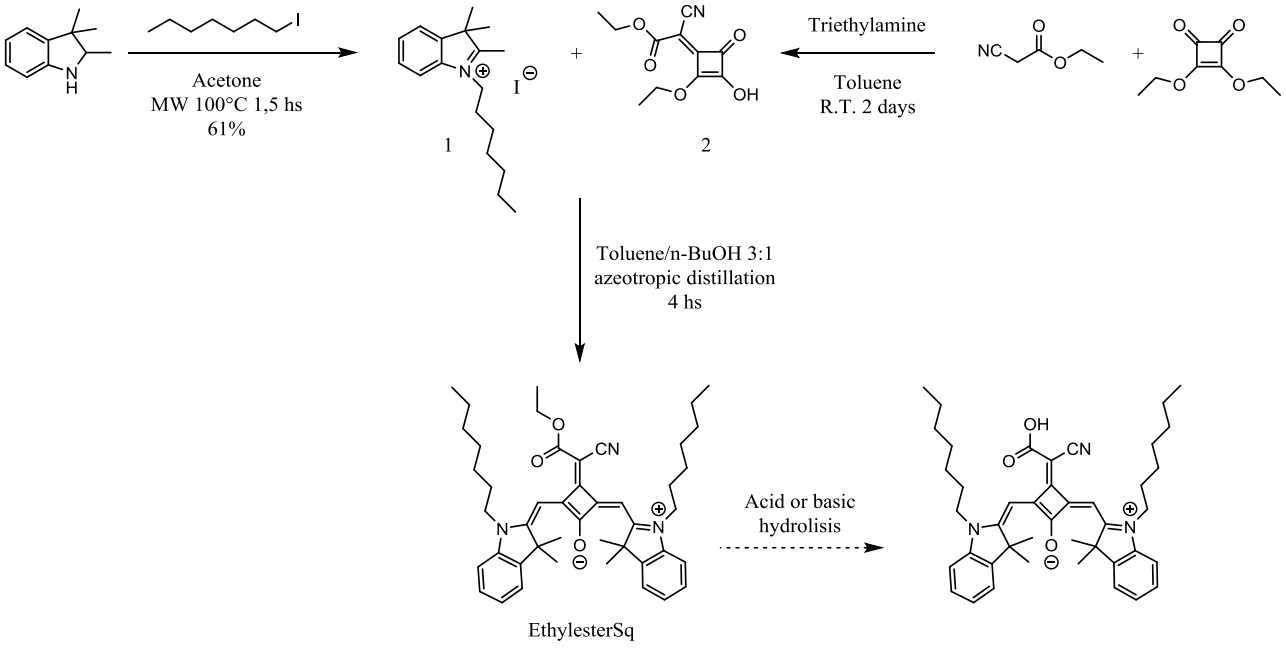

Scheme 2D: synthesis of EthylesterSq and hydrolysis trials of it.

The synthesis started from the alkylation of 2,3,3-trimethylindole with iodoheptane performed in microwave oven that lead to compound 1. Ethyl cyanoacetate was then condensed with an equivalent of ethyl squarate in the presence of trimethylamine as a

base, to give the core-substituted derivative 2. The final condensation between derivatives 1 and 2 was performed following the standard protocol in 3:1 mixture toluene/n.buthanol and azeotropic removal of water. The squaraine named EthylesterSq was spectroscopically characterized, showing a main absorption peak centered at 688 nm typical of squarainic dyes plus the additional band centered at 400 nm due to the insertion of the ethyl cyanoacetate on the cyclobutenic core. The emission showed a well-defined peak centered at 710 nm.

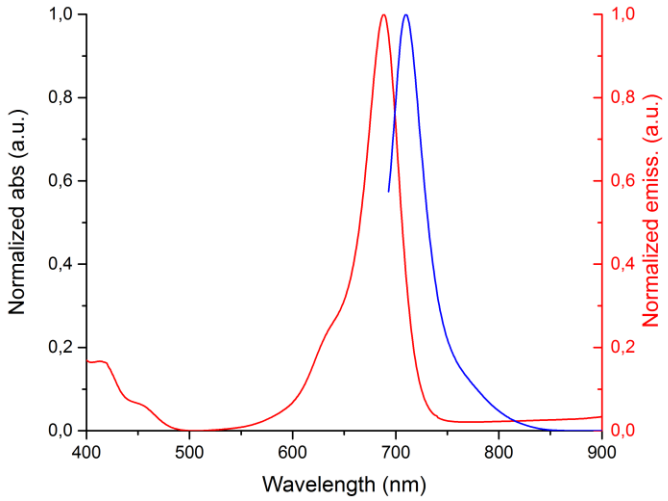

Figure 2.2.12: absorption and emission traces of EthylesterSq in chloroform, 10-4 M.

Various hydrolysis conditions, both acidic and basic, were attempted to obtain the free carboxylic acid functionality, giving no reaction or decomposition of the reagent (see de experimental part for the conditions). Since all the attempts were unfruitful, a possible strategy is to substitute the ethylester group with a more easily hydrolizable one such as a tert-butilic residual. Trials in this sense are ongoing.

2.3.2 Light harvesting systems: axial substituted subphthalocyanines

Subphthalocyanines are a relatively new entry among the compounds suitable for organic electronics. In the introduction the two main functionalization pathways, axial and peripheral, were described. One of the most interesting manipulation of these systems, from the synthesis point of view, is the creation of panchromatic dyes by linking of different chromophores together in the same structure. In this sense, both peripheral and axial couplings are reported in the literature for phthalocyanines and subphthalocyanines[34]. However, there is only one case in which a macrocyclic structure was axially coupled with a squaraine. In 2009, a paper of Silvestri et al.[58] described the synthesis and the properties of an ensamble phthalocyanine-squaraine-phthalocyanine, intended for light-harvesting applications, that demonstrated pancromaticity, with coverage of the solar spectrum from 250 to 850 nm.

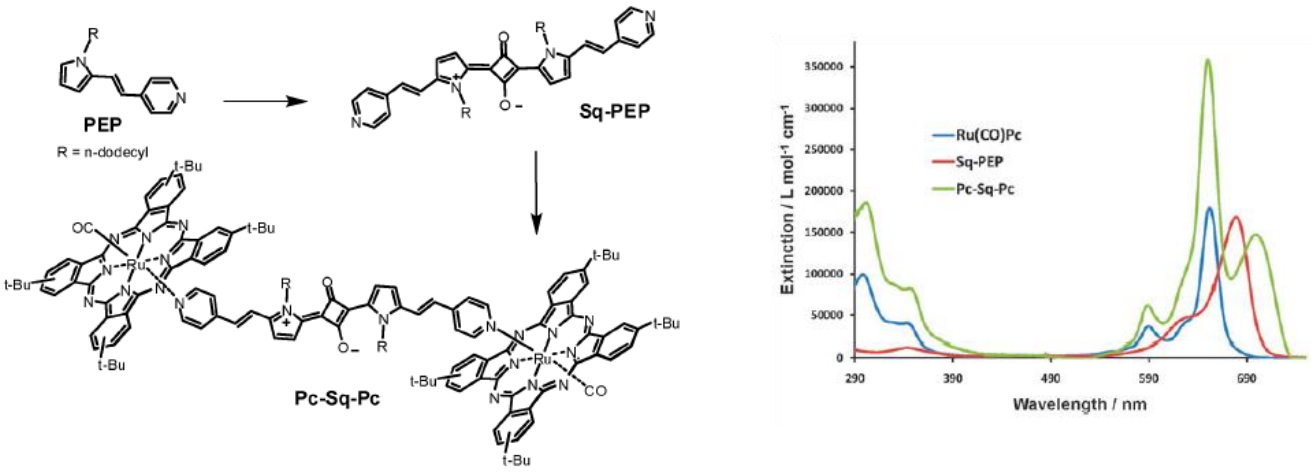

Figure 2.2.13: panchromatic PC-Sq ensemble reported by Silvestri et al. Adapted from[58].

In such case, the supramolecular structure is achieved by coordinative bonds between the pyridic nitrogens of the squaraine and the ruthenium centers of the phthalocyanine.

So far, no squaraine ensembles with subphthalocyanines are known. In this part of the discussion it is reported the synthesis and a preliminar characterization of the first compound with such characteristic. The synthetic route is reported in the following scheme:

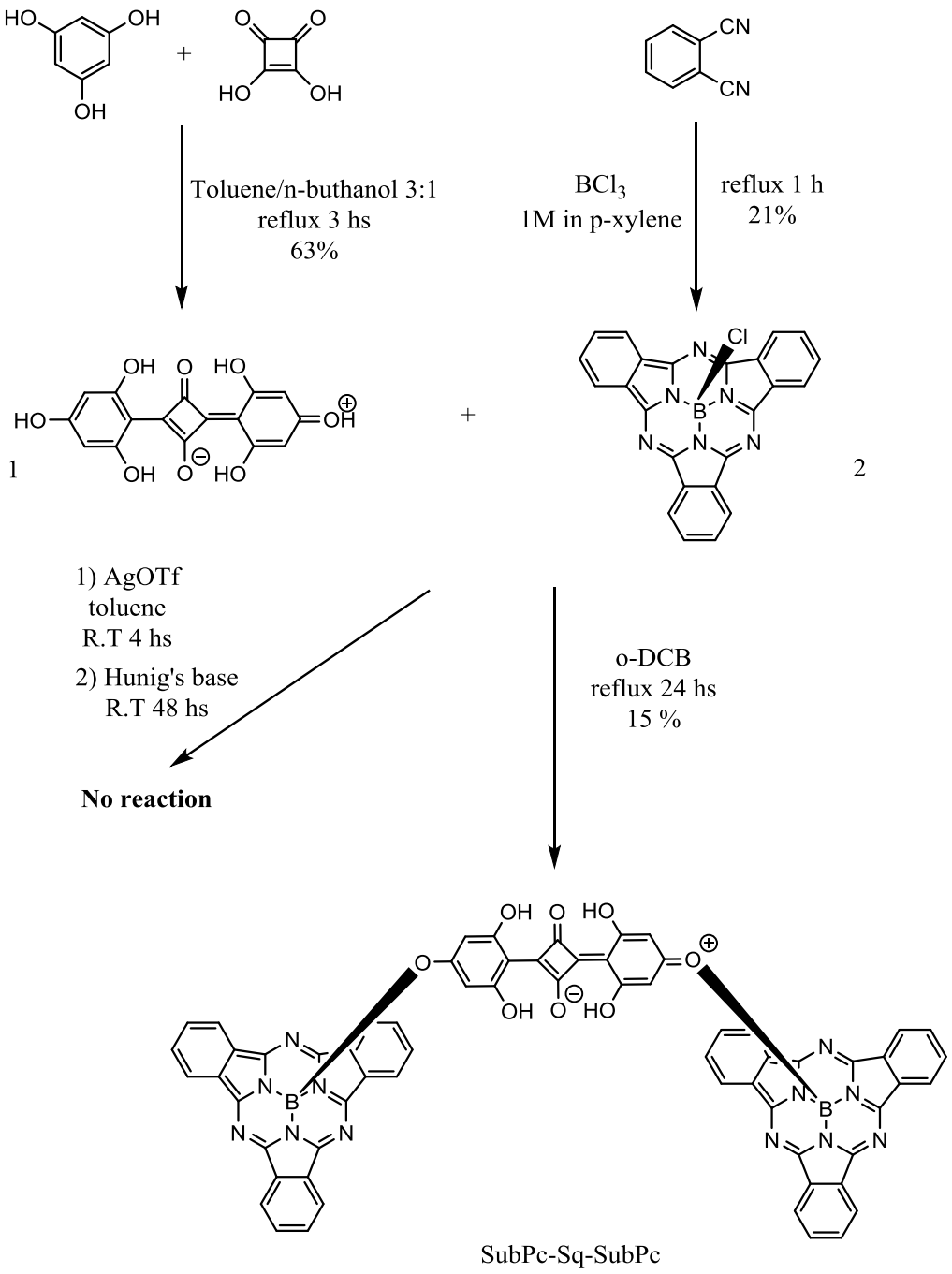

Scheme 2E: synthesis of ensemble SubPc-Sq.

The core-planarized squaraine 1 was synthesized by condensation of commercially available phloroglucinol with squaric acid under azeotropic distillation of water. The literature procedure[59] was followed to obtain the chloro-subphthalocyanine 2. A solution of boron trichloride in p-xylene was syringed directly onto the phthalonitrile as a solid and heated up. A high boiling point solvent like xylene is necessary for the reaction to undergo. Subsequently, a first attempt of axial substitution of subphthalocyanine to end-cap the squaraine was done following the triflate pathway. The activated SubPc triflate was formed using AgOTf (this kind of reactions are confirmed by the formation insoluble AgCl on the flask walls). After addition of the squaraine and the base, no sign of reaction appeared, even after 48 hs at room temperature. The temperature was likely the key parameter in this case.

Hence, a second reaction was carried on using more drastic conditions, refluxing the two compounds in o-dichlorobenzene (b.p. 180°C) for 24 hs. The Subpc-Sq-Subpc ensamble was collected after column chromatography on silica.

Due to the scarce solubility of the derivative the compound nature was confirmed only by MALDI-TOF (Matrix Assisted Laser Desorption Ionization-Time of Flight). MALDI is a soft ionization technique in which the sample is embedded in a matrix (usually organic) that is evaporated by means of a laser beam. The sample is indirectly ionized, preventing rapid destruction. It is normally used for fragile, high molecular weight structures such as biomolecules or drugs. The analysis showed the presence of the molecular ion peak at 1118,3 m/z. Furthermore, the exact mass analysis confirmed this result. The adapted reports are shown in the experimental section.

Uv-visible spectra analysis was performed to investigate the nature of the SQ-Subpc ensemble. Comparing the absorption of the single components, squaraine (564 nm) and subphthalocyanine (563 nm), with the ensemble one, one can notice that two overlapped bands appear at 585 and 568 nm. The bands are broadened, separated and slightly red shifted with respect to the separated components.

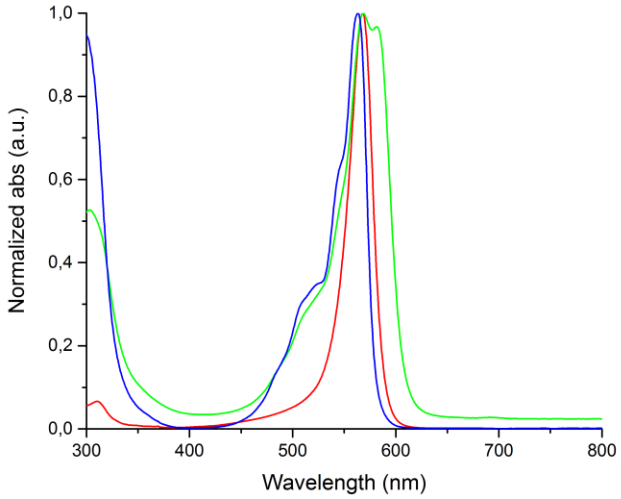

Figure 2.2.14: absorption spectra of phloroglucynol squaraine (blue line), subphthalocyanine (red line) and ensemble Subpc-Sq (green line), recorded in chloroform in diluted solution.

Due to the very close absorption maxima of the two chromophores, the assignment of the bands in the ensemble is not intuitive. A clear identification of the bands can give insights on the electronic distribution in the compound and which moiety is subjected to the larger red shift. This information can also play an important role in further improvements of the structure towards molecular design. To achieve this goal, a qualitative analysis of the variation of the relative peaks intensity in the ensemble was performed. The Uv-Vis spectra in various solvents were recorded in order to evaluate

possible shifts of the bands due to solvents effects. It was noticed that pyridine completely quenched the lower energy band of the ensemble.

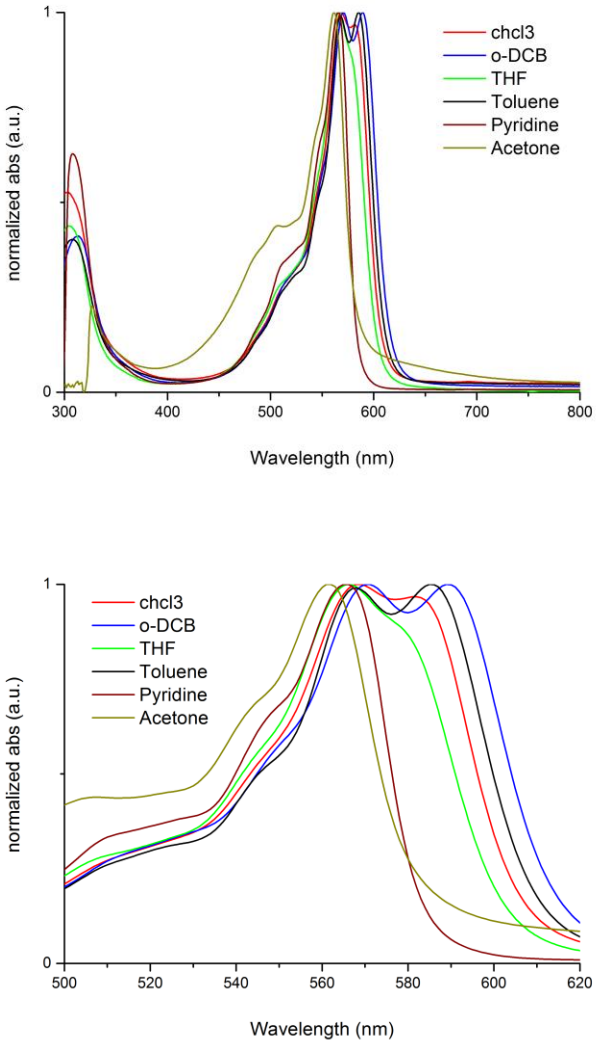

Figure 2.2.15: spectra of the ensemble in an array of solvents (peaks zoomed in the bottom image).

The consequent deduction was that pyridine reacted with the core of the squaraine, interrupting the conjugation. The compound loses his color, or, in from a spectroscopic

point of view, the absorption coefficient decreases drastically. A description and an application of this phenomenon was recently confirmed by Galliani et al.[60], showing that this process is reversible.

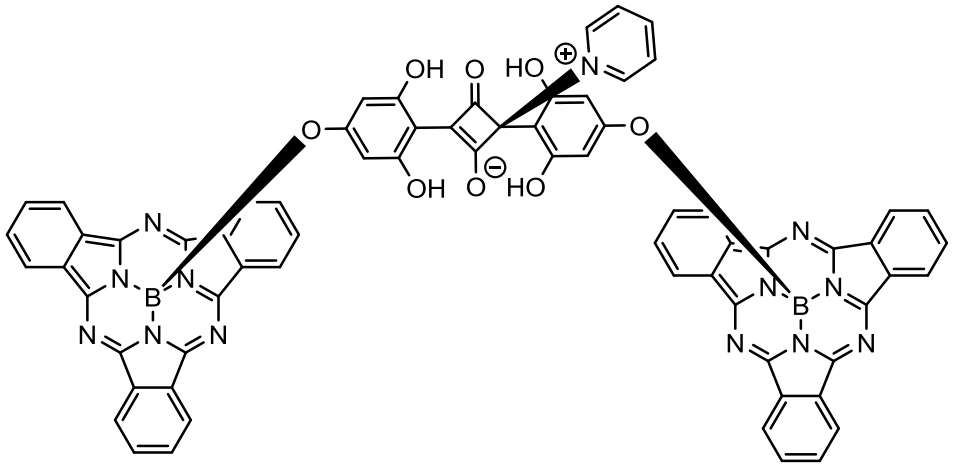

Figure2.2.16: possible quenched species upon addition of pyridine on the squaraine core.

A qualitative test aimed to confirm this hypotesis was thus performed in a UV cuvette scale. A pipette drop of pyridine was added to a diluted solution in toluene of Subpc-sq-Subpc compound and the spectra were recorded at 5 minute intervals. The correspondent decreasing of the squaraine's band over time was observed. After 20 minutes, addition of diluted acid (1% H_2SO_4), a recover of the absorption of such band was noticed.

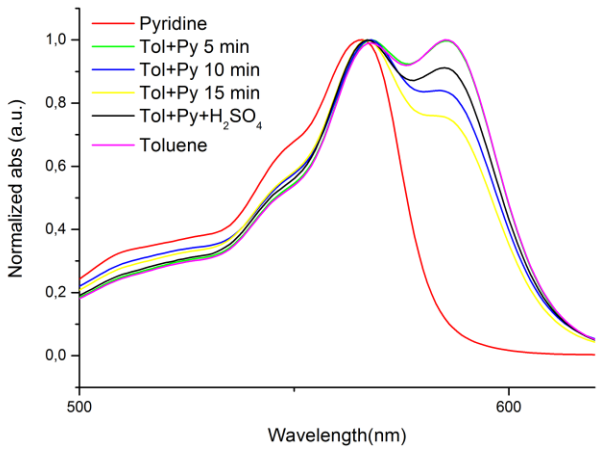

Figure 2.2.17: spectra of the ensemble recorded at various in the time to evidence the band quenching. The black line shows the (partial) recovering of absorbance after acid addition.

The synthesis and the preliminary characterization of the described compound give a series of interesting information: the spectroscopic properties change upon linking of the chromophores, in particular the squaraine core has the largest red shifting effect (21 nm). The Soret band of the subphthalocianine and the double band at lower energies cover a broad part of the solar spectrum, making the dye panchromatic and adapted for light-harvesting applications. The capability of the squarilyum core to give reversible addition of bases could be useful for color-switching indicators. Moreover, the presented structure represents the first example of squaraine-bridged macrocycle linked by covalent bonds, that are potentially more robust than the coordinative ones present in the literature and indicated for applications involving thermal treating (evaporation, annealing). Finally, the identification of the squaraine band is important to define the future direction to improve such system: the linking has no effect on the subphthaocyanine but strongly impact on the squaraine absorption. Extending the squaraine core to reach the NIR region is the natural prosecution of this study.

2.3.3 Light harvesting systems: peripheral substituted subphthalocyanines

In the previous section, the axial functionalization of a subphthalocyanine with a chromophore has been reported. The "axial" chemistry is pretty rich and a great number of possible ensembles are possible. More trick, and, of course, challenging, is the introduction of π-extended systems on the periphery of subphthalocyanines. As said, the axial substitution does not realty affect the optical and electronic properties of the macrocycle in itself, due to the presence of a node on the ground state molecular orbital. The only way to change the band gap is, for that, peripheral substitution. It has been shown that placing strong donors on the isoindole units is a useful strategy to move towards red and NIR-active subphthalocyanines. Archetypical substituents described so far are alkyl- and aryl-thiols and diarilamines[61,62]. 5,5-alkylthio-phthalonitriles generate subphthalocyanines absorbing above 600 nm, while the introduction of diphenylamine by Buchwald-Hartwig amination on a tri-iodo subphthalocyanine pushes the absorption maximum to around 650 nm, rendering the dye panchromatic (bands panning from 300 to 650 nm).

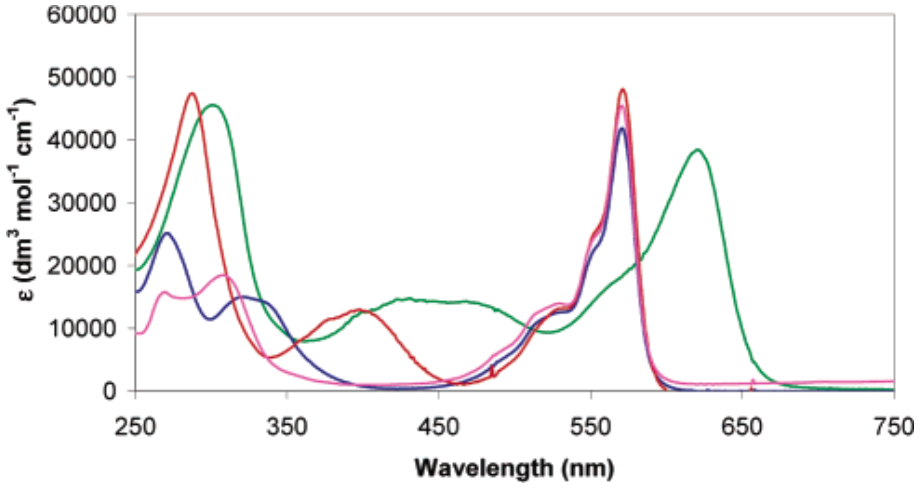

Figure: 2.2.18: absorption shift of subpc substituted with a strong electron-donating group (diphenylamine). Reprinted from[62].

The strategy proposed in this part of the discussion is the introduction of thiophene fragments on the main backbone of the macrocycle. Oligo-thiophenes derivatives have been widely investigated as materials for organic electronics. However, only a paper from Mauldin et al.[63] reported a systematic study of thiophene on subphthalocyanines and only in axial position. To investigate oligothiophene-subphthalocyanine, the literature strategy to obtain triiodo-subphthalocyanine was followed.

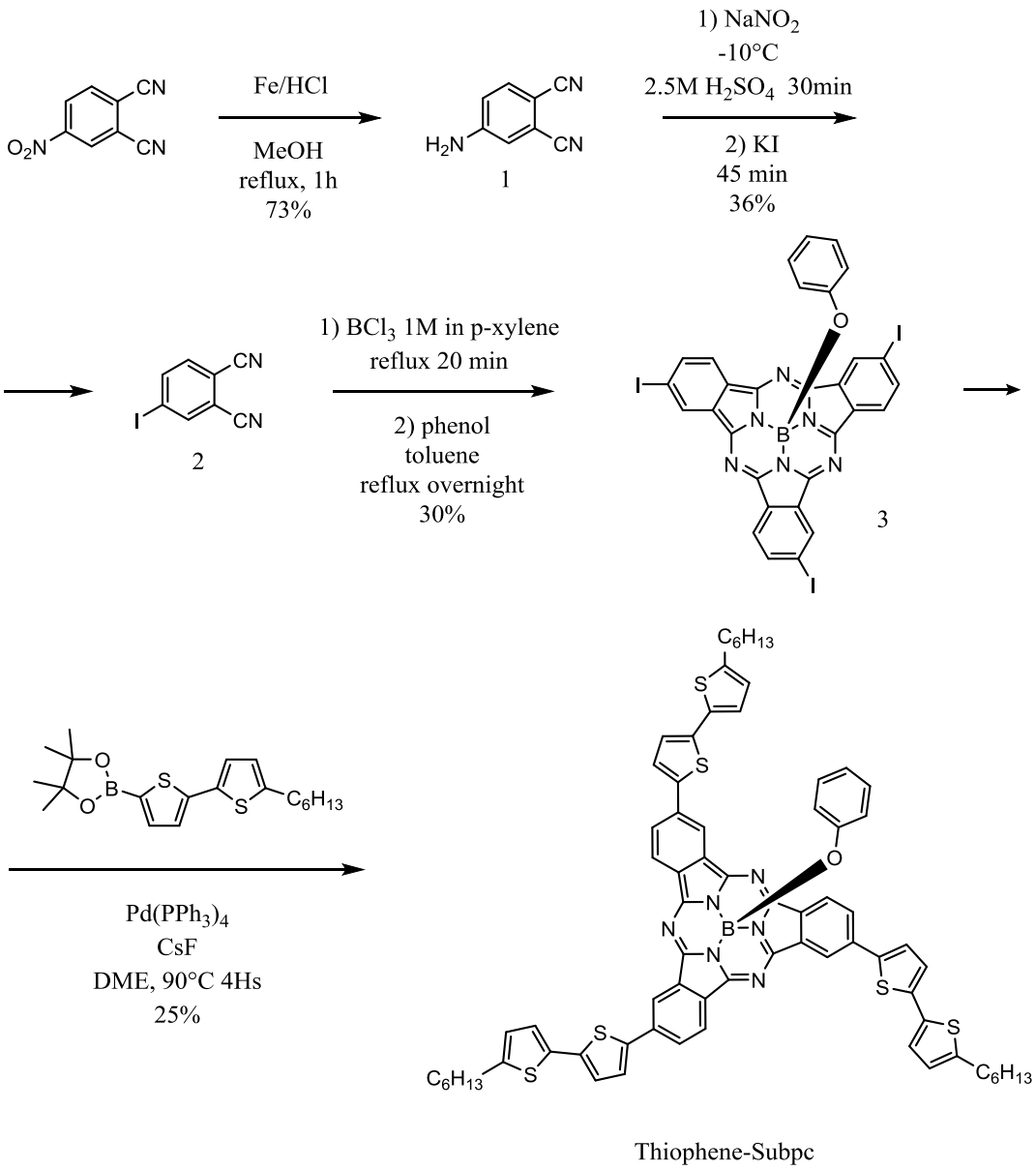

Scheme 2F: synthesis of Thiophenic-SubPc.

Commercially available 4-nitro phthalonitrile was reduced to 4-amino phthalonitrile by reduction with iron in concentrated HCl. This derivative was converted into the iodine-analogue by formation of aryldiazonium salt and quenching with a source of iodide (KI). The iodo-derivative was then reacted with BCl_3 in p-xylene to give the axial-chlorine subphthalocyanine, that was directly converted into the phenol-substituted derivative, refluxing the crude in the presence of phenol. The final compound thiophene-subpc was obtained by Suzuky coupling between commercially available pinacol-boronic ester of 5'-hexyl bithiophene and the triiodo-subphthalocyanine. The reaction used palladium tetra-triphenylphosphine as catalyst and cesium fluoride as a base in DME at 90°C (scheme 2F).

Furthermore, a dodecylthiole-functionalized subphthalocyanine was synthesized. In a four-steps procedure, commercially available 5,5-dichloro phthalic acid was converted into the corresponding phthalonitrile trhough cyclization to phthalanhydride, conversion to phthalimide, basic hydrolysis with ammonia to obtain the corresponding phthalamide and final reduction to phthalonitrile. The nitrile was functionalized with two equivalents of dodecylthiole by aromatic nucleophile substitution to give compound 5G. The thiolic derivative was finally converted into the final dye by a two-steps procedure: cyclization with BCl_3 to give the axial-chlorine derivative and final substitution with phenol in toluene at reflux (scheme2G).

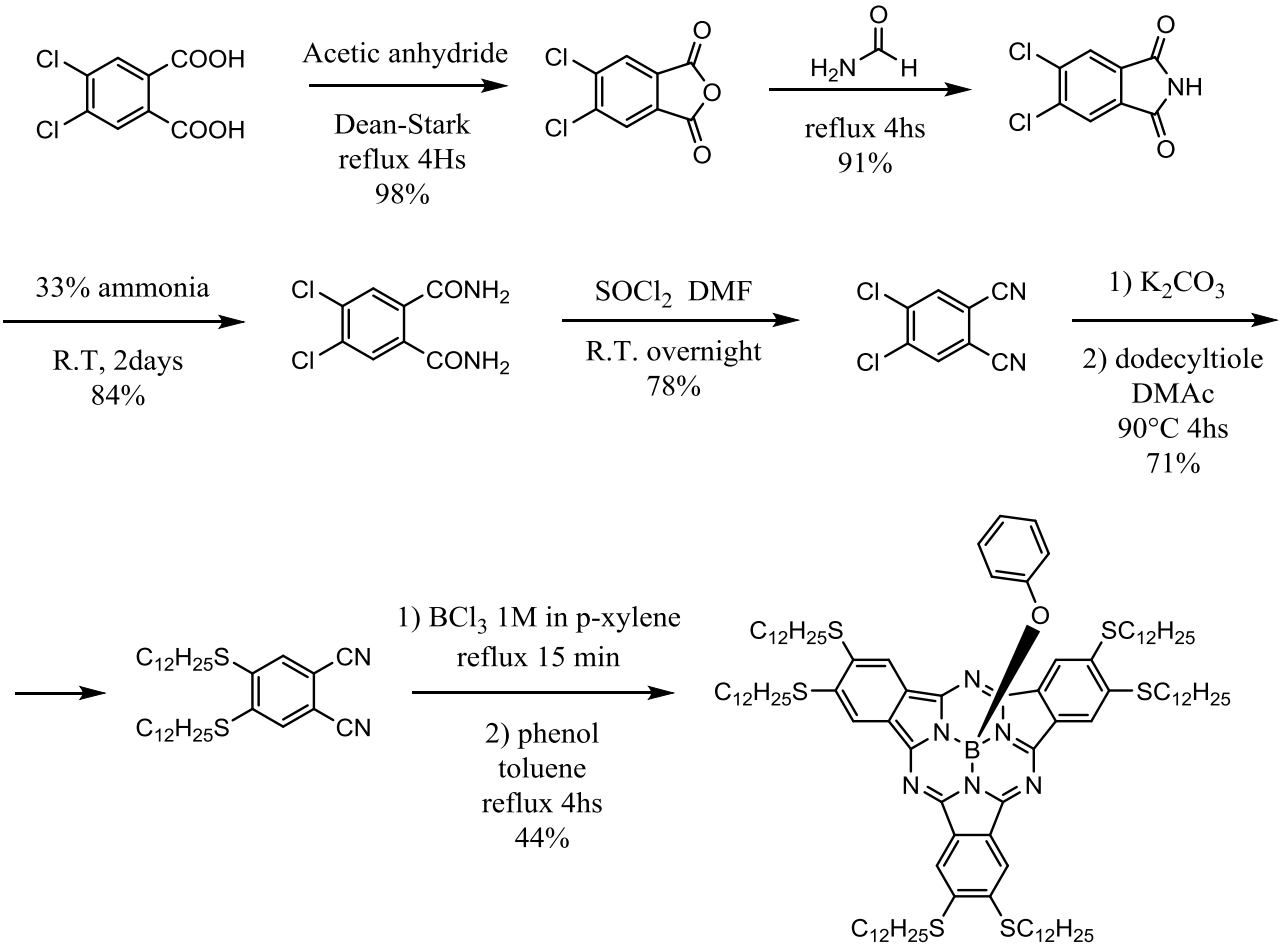

Scheme 2G: synthesis of thiolic-subpc.

The nature of the two above described compounds was confirmed by NMR and the optical properties were investigated by UV-Vis and fluorescence spectroscopy. It is interesting to make a comparison between the thiolic-subphthalocyanine and the thiophenic one, using the triiodo-derivative as a comparison and as a model of a non-donor substituted system.

As said, the introduction of an electron donor red shifts both absorption and emission. Thiolic-subpc presents an absorption maximum at 599 nm, red shifted of 29 nm with respect to the iodo-subpc 3F (570 nm). The introduction of bithiophene further red shifts the absorption to 610 nm, with the appearance of a structured band, probably due to thiophenes-centered transitions (404 and 348 nm). The fluorescence traces show another interesting trend: while the iodo-supc shows basically no Stokes-shift, thiolic-subpc show an emission maximum at 611 nm, with a Stokes-shift of 12 nm, and the thiophenic one a maximum at 631 nm, red shifted of 21 nm with respect to the absorption one. This represents a quite high value, taking into account that subphthalocyanines normally show very low spectral separation (usually 1-10 nm).

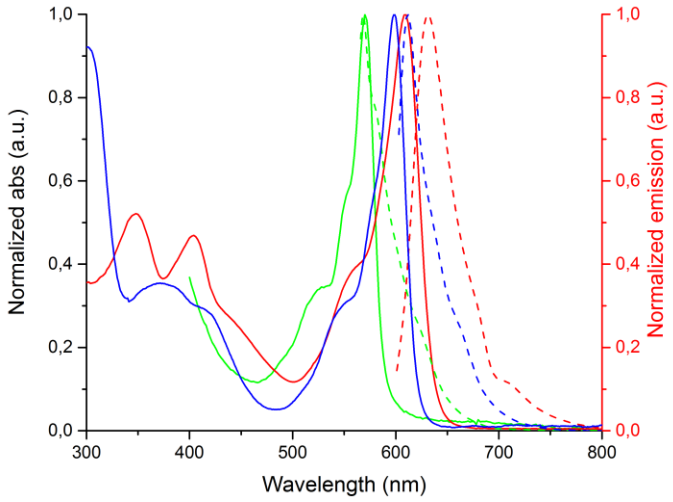

Figure 2.2.19: absorption (solid lines) and emission (dashed lines) of triiodo-subpc (green), thiolic-subpc (blue) and thiophenic subpc (red) in chloroform.

Electrical characterizations to define the band gap are ongoing. The presence of high energy bands in thiophenic-subpc renders the dye able to cover a wide portion of the visible spectrum. This is a positive feature for the implementation of the system in solar cells. Such compound represents a new entry in the subphthalocyanine panorama: the optical properties encourage a deeper analysis of this class of structures, analyzing the band-gap value trend varying systematically the number of thiophenes in a linear fashion or using the subphthalocyanine as branching center for extended π-networks. Trials in this sense are planned.

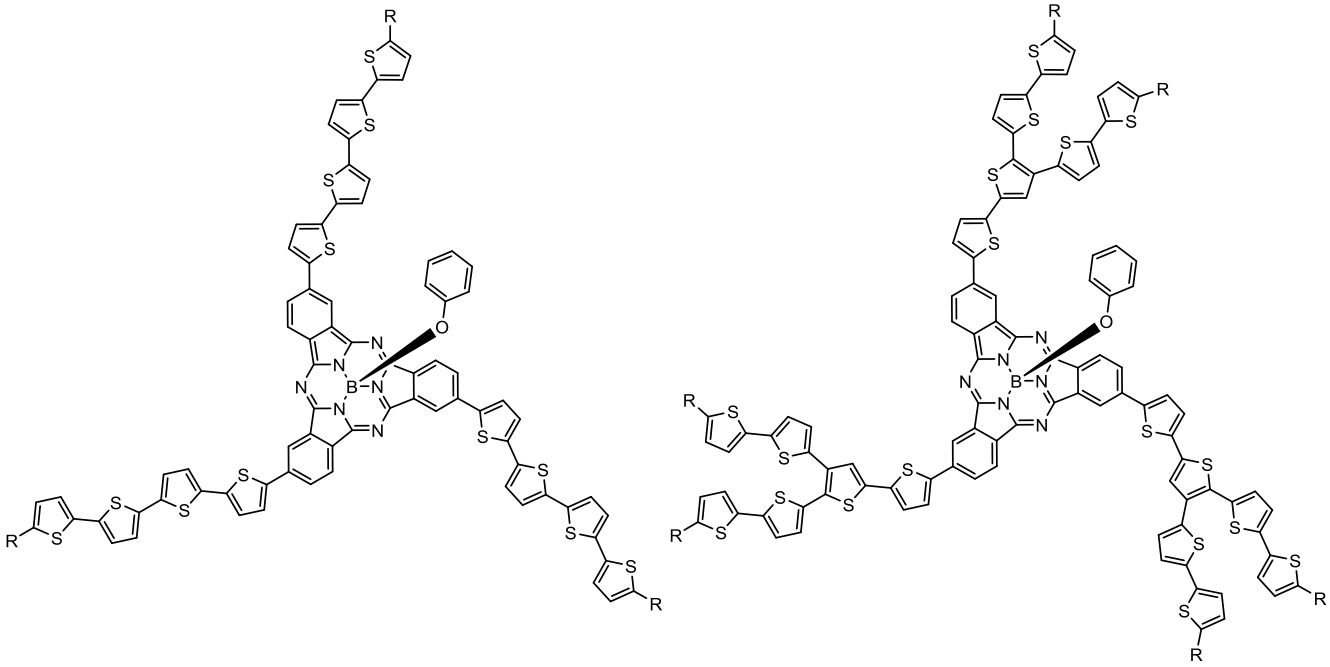

Figure 2.2.20: possible future developments of thiophenic-subpc.

2.3.4 Light emitting materials: Diketopyrrolopyrrolo cyanines.

In the first part of the chapter, the class of boron-containing polymethyne dyes was presented, describing the properties that demonstrated to be useful for NIR-related applications. Moreover, it was introduced the relatively new and not extensively explored class of dyketopyrrolopyrrolo-cyanine. They showed interesting absorption and emission properties, with high molar absorption coefficients and quantum yields, as long as a pretty straightforward synthesis and structural flexibility. As a primary approach to this class of molecules, that was not in the expertise of Beverina's group, the structure synthesized was the one bearing a pyridil-acetonitrile moiety and 3,7-dimethyloctil-phenol as side aromatic group. This choice was taken for two practical reasons: 2-pyridil-acetonitrile is a commercially available and relatively cheap compound and the 3,7-dimethyloctilic chain is a branched alkylic residue that was already tested in the laboratory to impart good solubility to large π-extended squaraines. The complete scheme is reported in scheme 2H.

The branched chain was introduced before the formation of the diketopyrrolopyrrole core by means of a Mitsunobu reaction, coupling 3,7-dimethyloctanol and 4-cyanophenol and using triphenylphosphine and DIAD (diisopropyl azodicarboxylate) as coreagents. Such procedure was chosen because 3,7-dimethyloctilic halogenates are not commercially available while 3,7-dimethyloctanol is a cheap commodity.

In a second step, the cyclization reaction to obtain the diketopyrrolopyrrole-core was carried out following a well-established procedure for the synthesis of such systems. Commercially available sodium tert-pentoxide was used as a base in tert-amylalcohol as solvent. Di-tert-buthyl succinate was employed as dicarbonylic compound instead of the di-isopropyl analogue due to enhanced reactivity of the first.

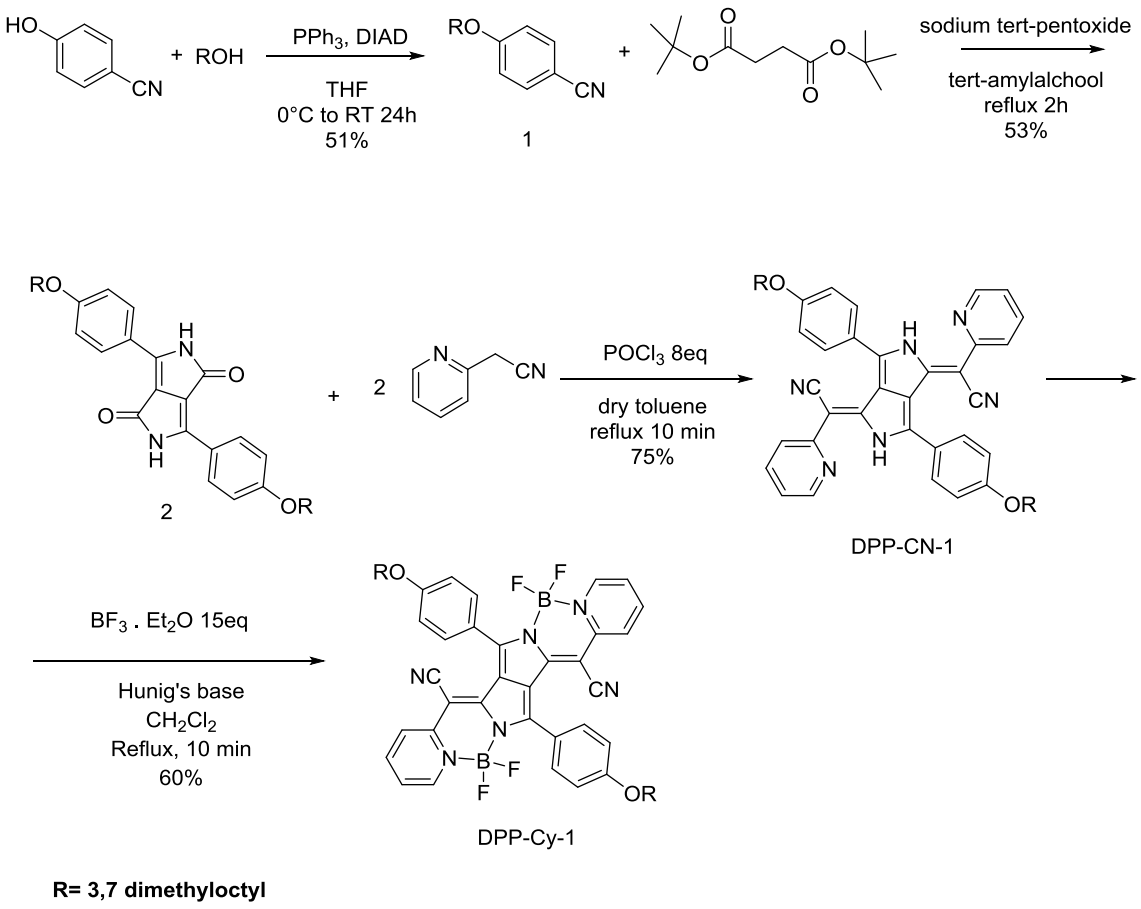

Scheme 2H: synthesis of DPP-Cy-1.

The synthesis of the actual DPP-cyanine backbone was based on the original procedure proposed by Daltrozzo et al. The first step requires the activation of the two lactamic carbonyls of the DPP. To achieve this goal, a large excess of phosphoryl chloride $POCl_3$ is used in refluxing toluene, in the presence of the acetonytrile. The reaction time, counted after the addition of the acid, could seem to be surprisingly short. Actually, exceeding this time leads to massive formation of non-soluble by-products, drastically reducing the yield. This is probably due to the combined effect of temperature and acidic species in the reaction environment that could lead to DPP ring opening by amide hydrolysis. The

result of this reaction is the so-called H-complex of the DPP-cyanine. This definition is due to the fact that the hydrogens on the lactamic nitrogens experience coordinative force from the pyridic nitrogens. This description describes the photopysical behavior of this intermediate: the N-H coordinative bond is not strong enough to efficiently stiffen the structure, resulting in a certain amount of rotational degrees of freedom around the bond in 2 position (of the pyridine). This can provide an efficient non-radiative pathway for the excited state and as a result, the DPP-CN derivatives is not fluorescent (vide infra).

The last step of the reaction is the introduction of the boron centers. It is carried out using $BF_3.Et_2O$ as source of boron and sterically hindered Hünig's base (diisopropyl ethyl amine) to deprotonate the lactames. In a firs trial the reaction was performed in o-dichlorobenzene (b.p. 180°C) giving significant low yield (below 20%). Shifting to refluxing $CHCl_3$ rose the yield to around 60%. A simple workout in water is important to remove all the acidic species that could degrade the product.

The resulting crystalline dark, shiny powder, DPP-Cy-1, results soluble in chlorinated solvents, THF, toluene and acetone. In particular, a test in chloroform was carried out, showing solubility above 20 mg/ml, remarkable value, taking into account that organic thin-film in devices are normally deposed by 5-10 mg/ml solutions. This characteristic made this derivative interesting for organic electronic applications and, for that, a complete characterization was carried out.

The optical characterization was performed, showing the expected behavior of a cyanine-like compound: the absorption bands in solution are narrow and vibrationally resolved. The boron complex shows the principal absorption band at 699 nm, red shifted of 7 nm with respect to the same band of the H-complex, placed at 692 nm.

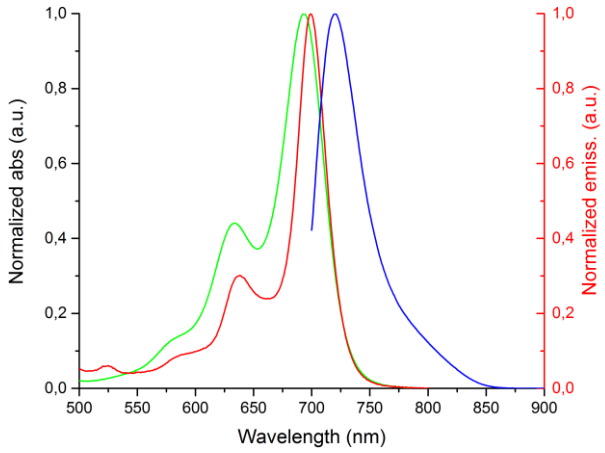

Figure 2.2.21: absorption traces of precursor DPP-CN-1 (green line) and DPP-Cy-1 (red line) and emission of the latter in chloroform.

The fluorescence spectrum shows a maximum peak at 720 nm, red shifted with respect to the absorption maximum of 21 nm. To have an insight of the in-solid features of the compound, a thin film was spin coated on a standard glass microscope slide and both the absorption and emission spectra were recorded. In this case, the absorption band broadens and red shifts to 753 nm and a detectable photoluminescence band appears at 777 nm, with a solid state Stokes-shift of 24 nm.

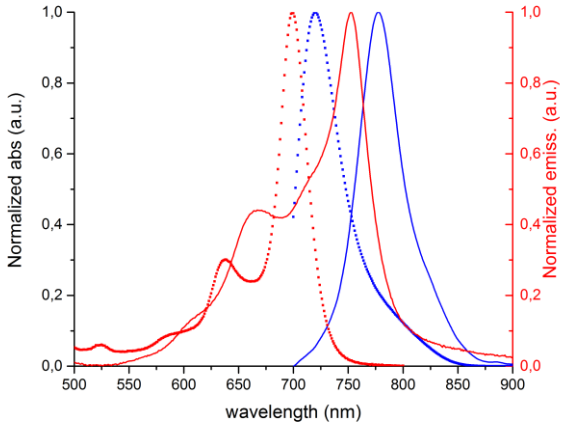

Figure 2.2.22: absorption and emission of DPP-Cy-1 in solution (red line) and thin film spun from $CHCl_3$ (blue line).

To complete the analysis on the different behavior of DPP-Cy1 in solution and in the solid state, the photoluminescence dynamic was recorded. The measure showed a longer lifetime in the solution (6,43 ns) with respect to the thin film (3,45 ns), which is common for this class of compounds.

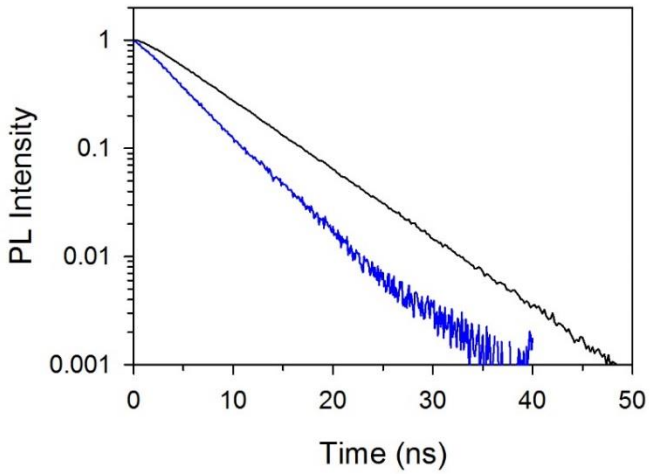

Figure 2.2.23: photoluminescence decay traces in solution (black line) and in solid state (blue line).

in order to estimate the HOMO and LUMO levels, both cyclic voltammetry and differential pulse voltammetry (DPV) traces were recorded. DPP-cy-1 was dissolved in a 2:1 CH_3CN:CH_2Cl_2 solution with 0.1 M $TBAClO_4$ as the supporting electrolyte. Figure 2.2.24a shows a comparison between the CV traces of DPP-Cy-1and its corresponding ligand DPP-CN-1. Unlike the simple ligand, the boron complex DPP-Cy-1 possesses a reversible behavior both in oxidation and in reduction. Furthermore, comparison between the DPV traces (figure 2.2.24b) shows that the introduction of the highly electronegative -BF_2 residue rigidly shifts both the HOMO and the LUMO levels by 0.22 eV, thus leaving the electrochemical gap unchanged.

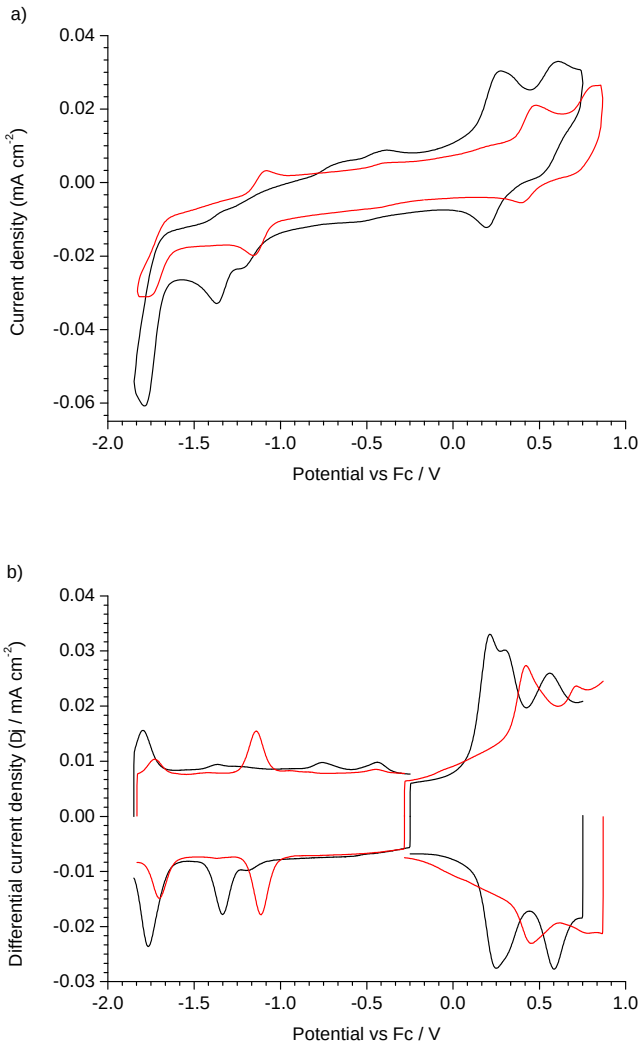

Figure 2.2.24: a) CV traces of DPP-CN-1 (black line) and DPP-Cy-1 (red line). b) DPV traces of the two compounds.

In order to be employed in organic electronic devices, organic structures should demonstrate to possess thermal stability. TGA traces of DPP-Cy-1 in air and under nitrogen were recorded and are reported in figure 2.2.25. The behavior is very similar under both atmospheres with a well-defined weight loss starting at 340 °C. The remarkable thermal stability offers the possibility of using such compound for applications that require thermal evaporation or annealing.

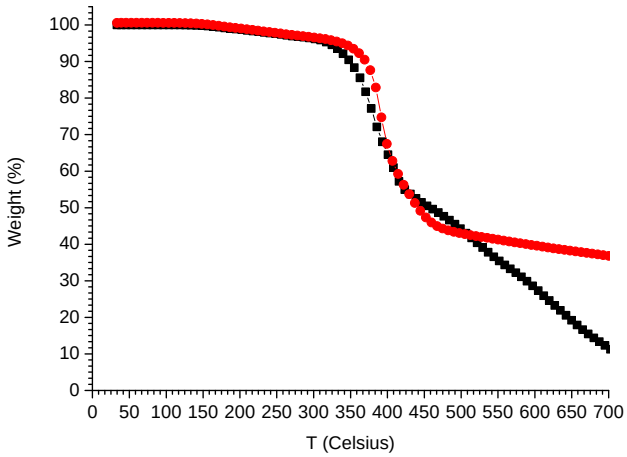

Figure 2.2.25: TGA traces of DPP-Cy-1 recorded in nitrogen (red squares) and air (black squares).

The synthetic flexibility that diketopyrrolopyrrole-cyanines show, allows further manipulations on the conjugated backbone in order to push both the absorption and the emission further in the near infrared. As said in the introduction, it has been demonstrated that the peripheral phenyls are tilted with respect of the DPP plane and do not participate to the conjugation. Every further functionalization on these positions does not affect the spectral properties. The conjugated core can be extended by using different heteroaromatic acetonitriles, with an extended π-system. This strategy was explored with the synthesis of the system DPP-Cy-2, where benzothiazole acetonitrile was used instead of the simple pyridine one (scheme 2l). The target was achieved following the same pathway previously described. The acetonitrile was synthesized as described in the literature[60], by cyclyzation of o-aminothiophenol in the presence of malononitrile in weakly acidic condition at room temperature.

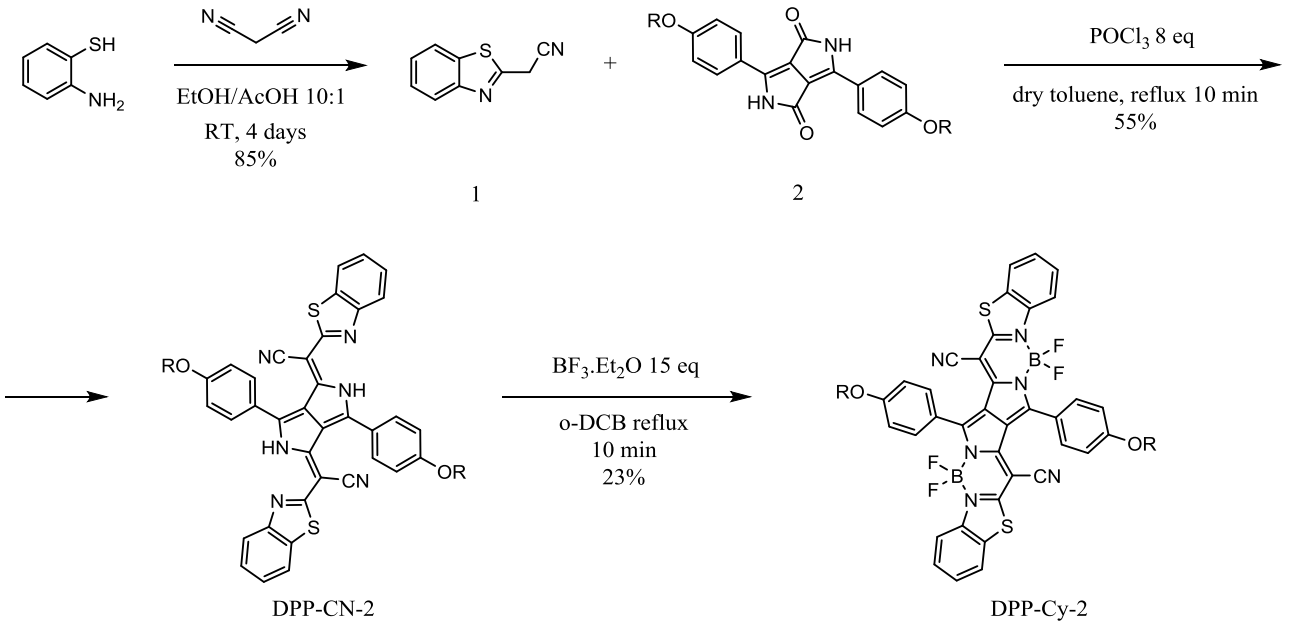

Scheme 2I: synthesis of DPP-Cy-2.

The derivative was employed in the condensation with DPP 2, activated by a strong excess of $POCl_3$. The obtained H-complex, named DPP-CN-2, was then treated with an excess of $BF_3.Et_2O$, using he non-optimized conditions in o-dichlorobenzene at reflux to introduce the boron centers. The final compound was optically characterized both in absorption and in emission. DPP-Cy-2 showed the same absorption pattern of DPP-Cy-1, with a sharp peak red shifted with respect to the ligand. As expected, the introduction of a more extended aromatic moiety greatly shifted the emission toward the NIR, at 728 nm in $CHCl_3$ solution, with a difference of 29 nm with respect to DPP-Cy-1. The photoluminescence spectrum shows the same behavior: the maximum is placed at 734 nm, 14 nm red shifted with respect to DPP-Cy-1. Remarkably, passing from pyridine to

benzothiazole acetonitrile, the Stokes-shift decreases significantly, with a value of 24 nm for DPP-Cy-1 and 6 nm for DPP-Cy-2.

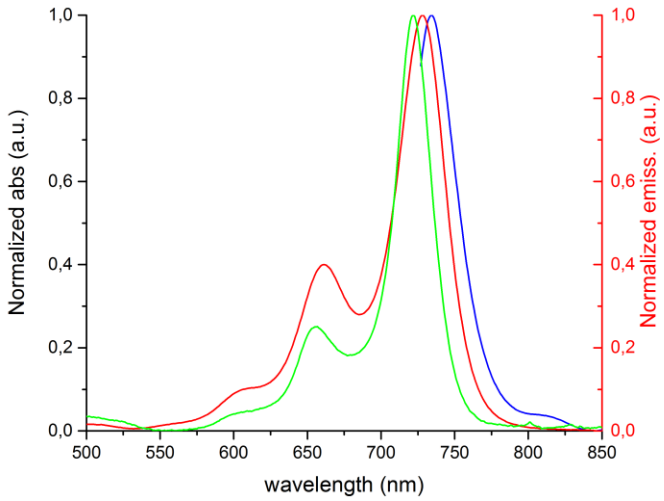

Figure 2.2.26: absorption traces of precursor DPP-CN-2 (green line) and DPP-Cy-1 (red line) and emission of the latter in chloroform.

A solubility test was performed to evaluate the possibility to employ DPP-Cy-2 in solution-processed devices. The derivative showed very low solubility, below 2 mg/ml and no suitable thin-films for optical measurements were obtained. The analysis here reported provided a clear direction in the research: the derivative DPP-Cy-1 shows interesting characteristics in terms of NIR emission and stability. It was chosen as new entry for application in NIR-emitting devices, which will be described in the device section of the thesis.

DPP-Cy-2 confirmed the approach to extend the conjugated core through modification of the heteroaromatic acetonitrile moiety but the scarce solubility makes this derivative not suitable for practical use. A possible strategy to enhance the solubility could be a further manipulation of the benzothiazolic core, inserting, for example, a terbutylic group or a 3,7-dimethyloctiloxy residue.

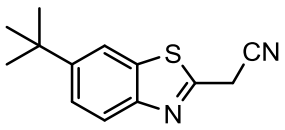

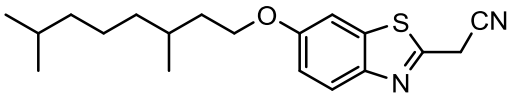

2.3.5 Light emitting materials: Chelates of lanthanides

On the side of light emitting materials, chelates of lanthanides and ancillary ligands have been synthesized and applied. For the ligands, the molecular design started from the consideration that one of the most used co-ligands for lanthanides ions are phenantroline and π-extended phenantrolines. They show remarkable absorption and sensitization properties[46]. Hence, the aim has been to find structures "mimic" of phenantrolines, showing similar binding mode and hindrance, but easier to functionalize, making the tuning of the optical properties easier. For that goal, bis-iminic systems have been chosen and investigated.

The iminic group, also known as Schiff's base (from the Italian chemist Ugo Schiff), is used as nitrogen-based ligands in transition metals complexes, used as catalyzer for many organic syntheses[64]. The nitrogen atom has sp^2 hybridization and the lone pair can give a dative-bond toward the metal. The synthesis of such systems is easily achieved by reaction between a primary amine precursor and the desired aldehyde or ketone.

As the same as acetals formation, this is an equilibrium, and the reverse hydrolysis reaction is always possible. In order to obtain a chelating agent, a bidentate substrate is required. The diketonic precursor acenaphthene quinone has been used for this target. This substrate has been maintained in all the synthesis and various aminic-derivatives have been tried. This kind of products are reported in literature as Ar,Ar-BIAN (bis(aryl)-acenaphthenequinonediimine) compounds[65,66].

The electron-rich zinc complex of 1 has been obtained by the reaction of acenaphthene quinone with p-anisidine in acetic acid. The second reaction step is the cleavage of the zinc complex to give the free Schiff's base, performed using a strong base, K_2CO_3 in

biphasic mixture water/CH_2Cl_2. The free ligand 2 has been obtained following the same procedure. As aminic derivative, 1-aminopyrene has been used, with the goal to have a higher conjugated system, with improved light-harvesting properties, to be compared with the p-anisidine one.

The remarkable characteristic of this kind of synthesis is the exploitation of zinc salt to achieve the desired product. Zn^{2+} has d^{10} electronic configuration. It is a closed shell system and the direct consequence of this, is a large charge-radius ratio and the absence of redox activity of its salts. This property is exploited in this synthesis: Zn^{2+} is used as strong polarizer toward both of carbonyls. A precursor complex with diketone is previously formed in order to reach carbonyls that are more electrophilic. The subsequent nucleophilic attack by amine derivative is, hence, easier. In such synthesis, reaction time plays a key role. Exceed the reaction time of 45 minutes lead the formation of the acetanilide derivative of amine that seem to be the thermodynamic product of the reaction.

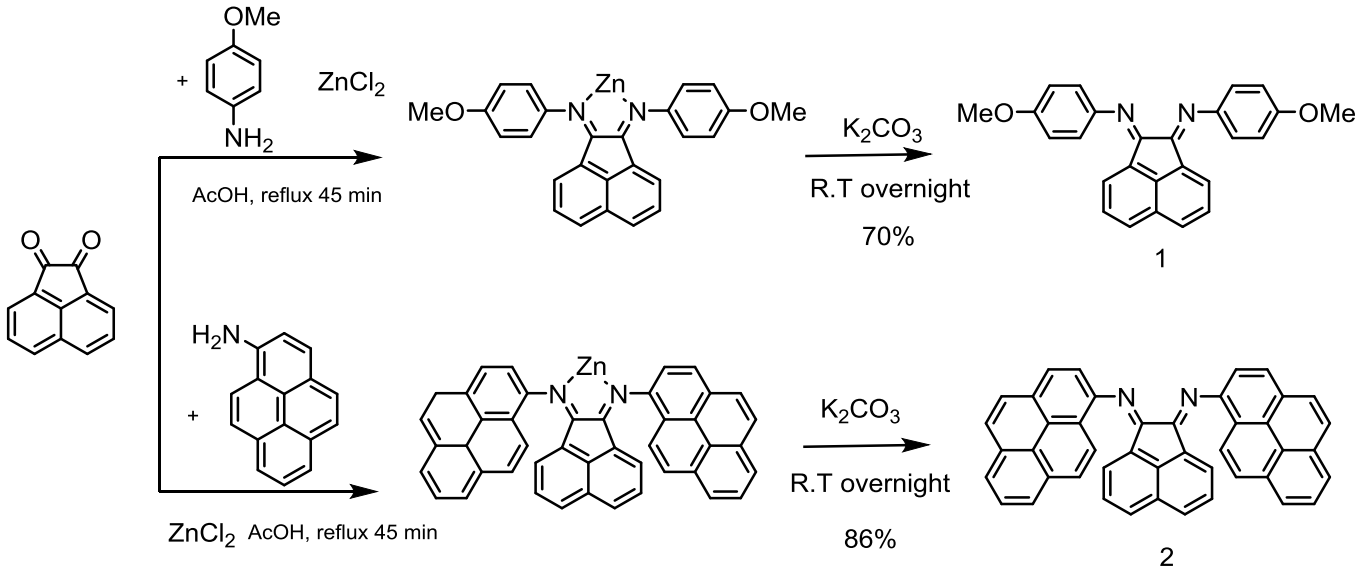

Scheme 2L: two steps synthesis of BIAN derivatives.

The innovative complexes synthesis route (scheme 2M) exploits the formation of lanthanide aquocomplexes (A1, A2,), followed by substitution of the H_2O molecules by the ancillary ligand. This kind of reactions were performed into water/dichloromethane 1:2 bihasic mixture. Thenoyl trifluoroacetone (HTTA) was used as primary ligand, because the conjugated base TTA easily coordinates lanthanide ions[27] and acts as a phase-transfer agent after the deprotonation with NaOH. The amphiphilic behavior is due to the polar diketonate group and the slightly polar thiophenic moiety. Trichlorides of the appropriate lanthanide were used as metal trivalent cations source. Few seconds after salt addition, a copious precipitate of lanthanide hydroxide instantly formed and suspended in the aqueous phase. After two days of vigorous stirring (in order to maximize the contact surface between water and dichloromethane), the hydroxide completely reacts and the complex were isolated by organic phase evaporation.

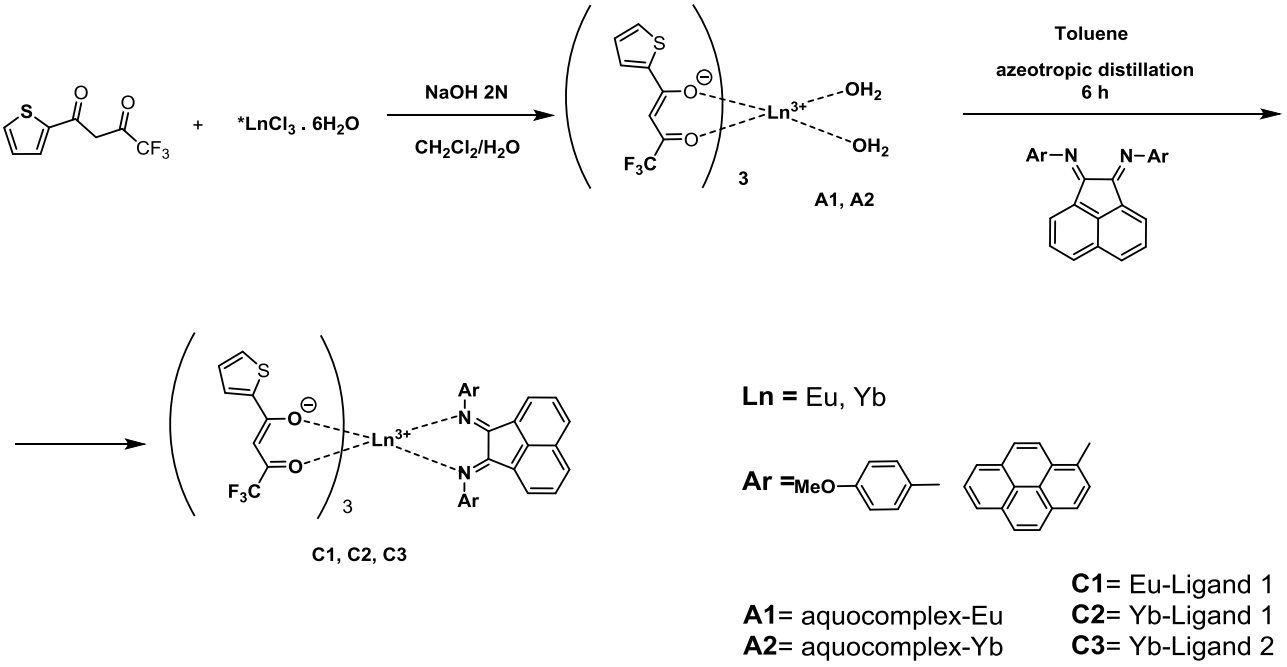

Scheme 2M: synthesis of chelates C1, C 2, C3 via lanthanides aquocomplex.

The second step was the substitution of the H_2O molecules with the double Schiff's base ancillary ligands. These reactions were carried out using dry toluene as solvent in *in-continuum* azeotropic distillatory apparatus to remove water. A treatment with non-coordinative solvents such as n-hexane or petroleum ether is required to purify the final complexes (C1, C2, C3): residuals of non-reacted ligand and toluene are soluble in such solvents.

UV-vis spectroscopy is the routinely tool used in this work to monitor the complexes formation reactions. Upon coordination the band shape changes and a peak at high energy, due to the metal center, appears. The band in the region 400-450 nm is completely due to the presence of the ligand (max at 430 for p-anisidine BIAN and 450 nm for Pyrene-BIAN). Interestingly, the spectra show no significant shift in the ancillary ligand band after complexation, sustaining the evidence of a pure dative coordination mode of the bis-imines and the absence of retro-donation to the ligand.

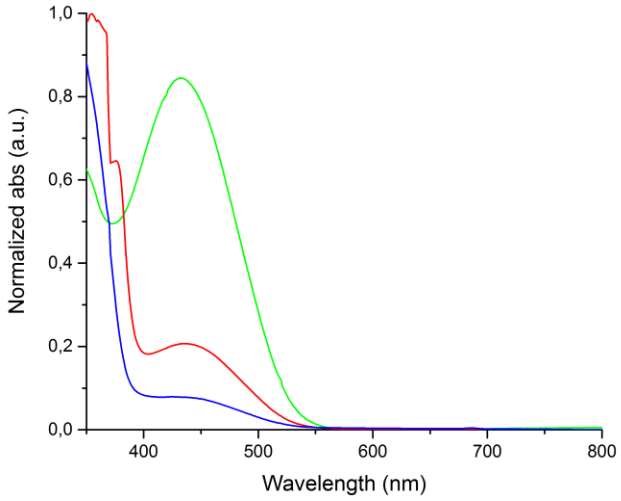

Figure 2.2.27: absorption traces of ligand 1 (green line) and its complexes of europium (C1, red line) and ytterbium (C2, blue line) in chloroform.

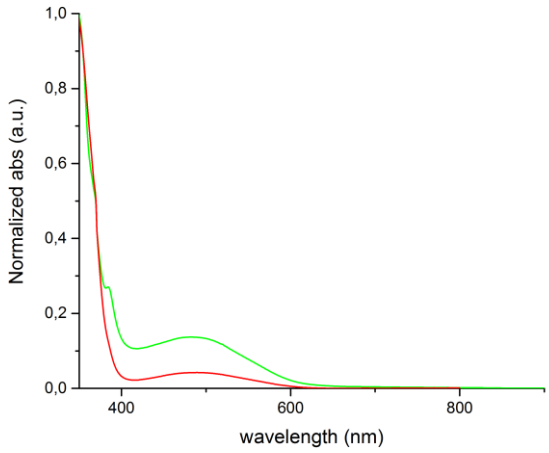

Figure 2.2.28: absorption traces of ligand 2 (green line) and its complex of ytterbium (C3, red line) in chloroform.

FT-IR spectra were recorded to fully characterize the compounds. For sake of clarity, spectra of the complexes are compared with the free ligands ones, highlighting the portion of spectrum between 1900 cm^{-1} and 600 cm^{-1}. It is clear that the complex formation causes the shift of the major part of signals due to the presence of the lanthanide that changes the force constant, hence the frequency of the IR-active normal modes of stretching. Diagnostic signals, for C1 and C2 are present at 1600-1700 cm^{-1} due to C=N- stretching, that probably overlap the C=O stretch of TTA groups. The Eu^{3+} complexes do not show evident bands of C-H stretch (aromatic ring and metoxylic group) that are probably hidden by the noise. In the ligand spectrum, such bands are present but weak. IR spectrum of Yb^{3+} chelate C3 shows the same characteristics of the europium complexes. Complexation causes a shift of the signals and the presence of a broad band at ~1600 cm^{-1} indicate the presence of –C=N- stretching in the complex. Such band is broad for the overlap with the -C=O stretching of diketonate, as expected. For such complex, the -C-H stretching bands between 2700-3000 cm^{-1} are evident, proof of ancillary ligand's presence in the complex.

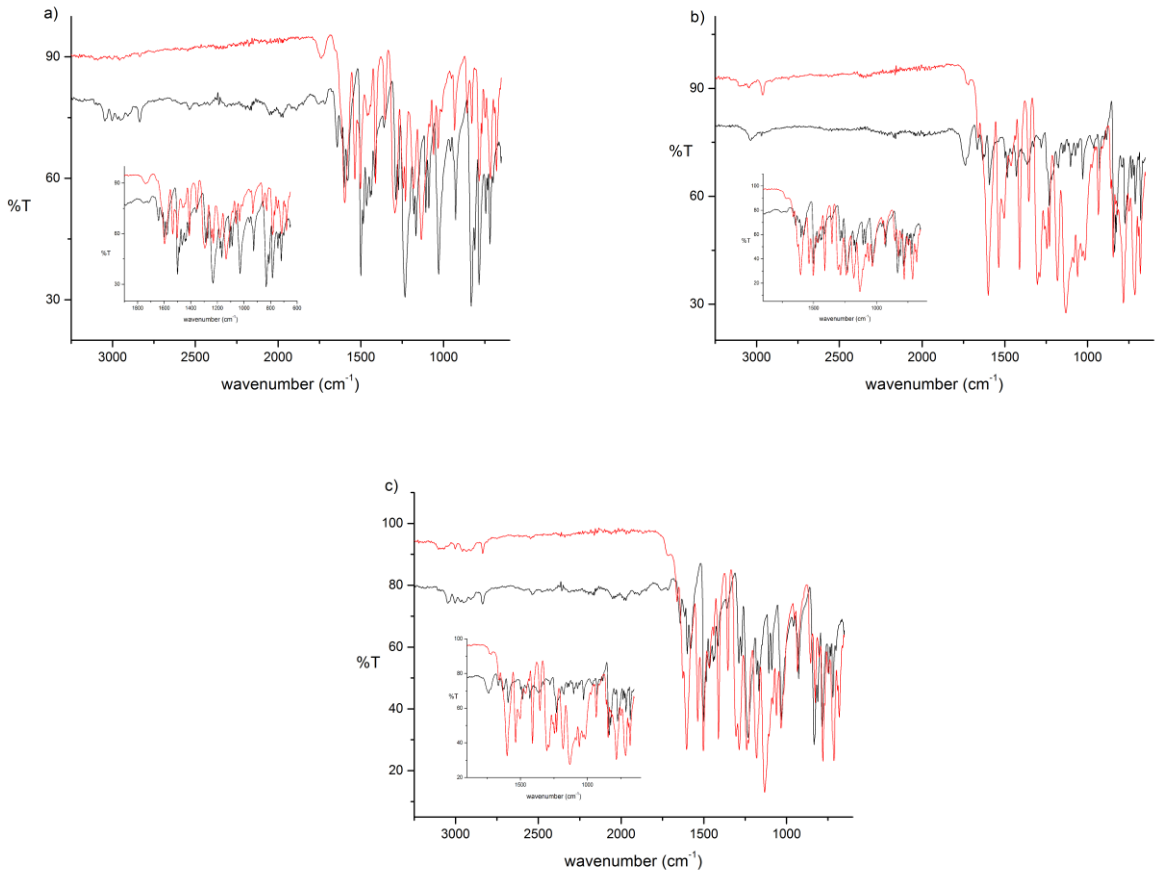

Figure 2.2.29: ATR of ligands (black line) and complexes (red lines). A) C1, b) C2, c) C3. The insets show the fingerprints portion of the spectra

Another interesting observation is that IR traces show no presence of residual water coordinated to the metal or absorbed by the material. This is important for materials emitting in the near infrared: O-H bonds of water absorbing in such region, efficiently quench the fluorescence. Avoiding water is thus important for this kind of luminophores. Taking into account this feature, as well as the good spectral separation of chelates of lanthanides, C1, C2 and C3 were employed as luminescent materials for luminescent solar concentrators. The working principles of these devices and the tests conducted on the materials are reported in the device section.

2.4 Bibliography

1. http://www.marketsandmarkets.com/Market-Reports/colorants-tinting-systems-paints-coatings-market-875.html
2. http://www.pcimag.com/articles/96518-growth-in-key-industries-drives-pigments-and-dyes-market
3. https://ec.europa.eu/programmes/horizon2020/en/what-horizon-2020
4. Katz, Howard E., and Jia Huang. "Thin-film organic electronic devices." Annual Review of Materials Research 39 (2009): 71-92.
5. Jurgen Fabian, Hiroyuki Nakazumi and Masaru Matsuoka, Near-Infrared Absorbing Dyes, Chem. Rev. 1992, 92, 1197-1226
6. Gang Qian and Zhi Yuan Wang, Chem. Asian J. 2010, 5, 1006 – 1029
7. Zhan, Xiaowei, et al. "Rylene and related diimides for organic electronics." Advanced Materials 23.2 (2011): 268-284.
8. Pschirer, Neil G., et al. "Pentarylene-and Hexarylenebis (dicarboximide) s: Near-Infrared-Absorbing Polyaromatic Dyes." Angewandte Chemie International Edition 45.9 (2006): 1401-1404.
9. Bricks, Julia L., et al. "Molecular design of near infrared polymethine dyes: A review." Dyes and Pigments (2015).
10. Wang, Feng, et al. "Luminescent nanomaterials for biological labelling." Nanotechnology 17.1 (2006): R1.
11. Asato, Alfred E., Dana T. Watanabe, and Robert SH Liu. "The use of prochiral centers for demonstrating asymmetric stacking in aggregates of azulenylazulenium cyanine dyes." Organic letters 2.17 (2000): 2559-2562.
12. Beverina, Luca, and Patrizio Salice. "Squaraine compounds: tailored design and synthesis towards a variety of material science applications." European journal of organic chemistry 2010.7 (2010): 1207-1225.

13. Petermann, Ralf, et al. "Synthesis of new squaraine dyes for optical switches." Dyes and pigments 57.1 (2003): 43-54.
14. Maeda, Takeshi, et al. "Near-infrared absorbing squarylium dyes with linearly extended π-conjugated structure for dye-sensitized solar cell applications." Organic letters 13.22 (2011): 5994-5997.
15. Silvestri, Fabio, et al. "Efficient squaraine-based solution processable bulk-heterojunction solar cells." Journal of the American Chemical Society 130.52 (2008): 17640-17641.
16. Chung, Sung-Jae, et al. "Extended squaraine dyes with large two-photon absorption cross-sections." Journal of the American Chemical Society 128.45 (2006): 14444-14445.
17. Beverina, Luca, et al. "New π-extended water-soluble squaraines as singlet oxygen generators." Organic letters 7.19 (2005): 4257-4260.
18. 14 Pham, Wellington, Ralph Weissleder, and Ching-Hsuan Tung. "A practical approach for the preparation of monofunctional azulenyl squaraine dye." Tetrahedron letters 44.20 (2003): 3975-3978.
19. Beverina, Luca, et al. "Panchromatic squaraine compounds for broad band light harvesting electronic devices." Journal of Materials Chemistry 22.14 (2012): 6704-6710.
20. Wei, Guodan, et al. "Functionalized squaraine donors for nanocrystalline organic photovoltaics." ACS nano 6.1 (2011): 972-978.
21. Nakazumi, Hiroyuki, et al. "Near-infrared luminescent bis-squaraine dyes linked by a thiophene or pyrene spacer for noncovalent protein labeling." Synthetic metals 153.1 (2005): 33-36.
22. Brüning, Christoph, et al. "Macrocyclic cis-Indolenine Squaraine Dyes as Efficient Near Infrared Emitters." The Journal of Physical Chemistry C 119.11 (2015): 6174-6180.
23. Büschel, Michael, et al. "Redox-switchable squaraines with extended conjugation." Organic letters 5.17 (2003): 2975-2978.
24. Ayyappanpillai Ajayaghosh, “Chemistry of Squaraine-Derived Materials: Near-IR Dyes, Low Band Gap Systems, and Cation Sensors.”, Acc. Chem. Res. 2005, 38, 449-459

25. Beverina, Luca, et al. "Panchromatic Cross-Substituted Squaraines for Dye-Sensitized Solar Cell Applications." ChemSusChem 2.7 (2009): 621-624.
26. Frath, Denis, et al. "Luminescent Materials: Locking π-Conjugated and Heterocyclic Ligands with Boron (III)." Angewandte Chemie International Edition 53.9 (2014): 2290-2310.
27. Fischer, Georg M., et al. "Near-infrared dyes and fluorophores based on diketopyrrolopyrroles." Angewandte Chemie International Edition 46.20 (2007): 3750-3753.
28. Lenz, R., and O. Wallquist. "DPP chemistry—continuous innovation." Surface Coatings International Part B: Coatings Transactions 85.1 (2002): 19-26.
29. Hendsbee, Arthur D., et al. "Electron deficient diketopyrrolopyrrole dyes for organic electronics: synthesis by direct arylation, optoelectronic characterization, and charge carrier mobility." Journal of Materials Chemistry A 2.12 (2014): 4198-4207.
30. Kaur, Matinder, and Dong Hoon Choi. "Diketopyrrolopyrrole: brilliant red pigment dye-based fluorescent probes and their applications." Chemical Society Reviews 44.1 (2015): 58-77.
31. Qu, Sanyin, and He Tian. "Diketopyrrolopyrrole (DPP)-based materials for organic photovoltaics." Chemical Communications 48.25 (2012): 3039-3051.
32. Fischer, Georg M., et al. "Pyrrolopyrrole Cyanine Dyes: A New Class of Near-Infrared Dyes and Fluorophores." Chemistry-a European Journal 15.19 (2009): 4857-4864.
33. Gerd Löbbert "Phthalocyanines" in Ullmann's Encyclopedia of Industrial Chemistry, 2002, Wiley-VCH, Weinheim.
34. Claessens, Christian G., et al. "Subphthalocyanines, Subporphyrazines, and Subporphyrins: Singular Nonplanar Aromatic Systems." Chemical reviews 114.4 (2013): 2192-2277.
35. A. Meller, A. Ossko, Monatsh. Chem. 1972, 103, 150 – 155
36. Morse, Graham E., and Timothy P. Bender. "Boron subphthalocyanines as organic electronic materials." ACS applied materials & interfaces 4.10 (2012): 5055-5068.

37. Kobayashi, Nagao, et al. "Synthesis, spectroscopy, and molecular orbital calculations of subazaporphyrins, subphthalocyanines, subnaphthalocyanines, and compounds derived therefrom by ring expansion1." Journal of the American Chemical Society 121.39 (1999): 9096-9110.
38. Morse, Graham E., et al. "Fluorinated phenoxy boron subphthalocyanines in organic light-emitting diodes." ACS Applied Materials & Interfaces 2.7 (2010): 1934-1944.
39. González-Rodríguez, David, et al. "Activating Multistep Charge-Transfer Processes in Fullerene− Subphthalocyanine− Ferrocene Molecular Hybrids as a Function of π− π Orbital Overlap." Journal of the American Chemical Society 132.46 (2010): 16488-16500.
40. Claessens, Christian G., et al. "On the mechanism of boron-subphthalocyanine chloride formation." Journal of Porphyrins and Phthalocyanines 11.03 (2007): 181-188.
41. J. Guilleme, D. Gonzalez-Rodriguez and Tomas Torres, Triflate-Subphthalocyanines: Versatile, Reactive Intermediates for Axial Functionalization at the Boron Atom Angew. Chem. 2011, 123, 3568 –3571.
42. González-Rodríguez, David, et al. "Subphthalocyanines: Tuneable molecular scaffolds for intramolecular electron and energy transfer processes." Journal of the American Chemical Society 126.20 (2004): 6301-6313.
43. N. Kobayashi, J. Chem. Soc., Chem. Commun., 1203-1205, 1991
44. Christian G. Claessens and Toma s Torres, Angew. Chem. Int. Ed. 2002, 41, No. 14
45. Takamitsu Fukuda, Jay R. Stork, Richard J. Potucek, Marilyn M. Olmstead, Bruce C. Noll, Nagao Kobayashi, and William S. Durfee Angew. Chem. Int. Ed. 2002, 41, No. 14
46. Bünzli, Jean-Claude G. "On the design of highly luminescent lanthanide complexes." Coordination Chemistry Reviews 293 (2015): 19-47.
47. Weissman, S. I. "Intramolecular energy transfer the fluorescence of complexes of europium." The Journal of Chemical Physics 10.4 (1942): 214-217.
48. Beverina, Luca, and Alessandro Sanguineti. "Organic Fluorophores for Luminescent Solar Concentrators." Solar Cell Nanotechnology (2013): 317-355.

49. Eliseeva, Svetlana V., and Jean-Claude G. Bünzli. "Lanthanide luminescence for functional materials and bio-sciences." Chemical Society Reviews 39.1 (2010): 189-227.
50. Sanguineti, Alessandro, et al. "NIR emitting ytterbium chelates for colourless luminescent solar concentrators." Physical Chemistry Chemical Physics 14.18 (2012): 6452-6455.
51. Sassi, Mauro, et al. "Open circuit voltage tuning through molecular design in hydrazone end capped donors for bulk heterojunction solar cells." Journal of Materials Chemistry A 1.7 (2013): 2631-2638.
52. Turrisi, Riccardo, et al. "Stokes shift/emission efficiency trade-off in donor–acceptor perylenemonoimides for luminescent solar concentrators." Journal of Materials Chemistry A 3.15 (2015): 8045-8054.
53. Wang, Siyi, et al. "N, N-Di aryl anilinosquaraines and their application to organic photovoltaics." Chemistry of Materials 23.21 (2011): 4789-4798.
54. Chen, Guo, et al. "A Series of Squaraine Dyes: Effects of Side Chain and the Number of Hydroxyl Groups on Material Properties and Photovoltaic Performance." *Chemistry of Materials* 26.3 (2014): 1356-1364.
55. Spencer, Susan, et al. "Controlling J-aggregate formation for increased short-circuit current and power conversion efficiency with a squaraine donor." Progress in Photovoltaics: Research and Applications 22.4 (2014): 488-493.
56. Chen, Guo, et al. "J-aggregation of a squaraine dye and its application in organic photovoltaic cells." Journal of Materials Chemistry C 1.40 (2013): 6547-6552.
57. Beverina, Luca, et al. "Panchromatic Cross-Substituted Squaraines for Dye-Sensitized Solar Cell Applications." ChemSusChem 2.7 (2009): 621-624.
58. Silvestri, Fabio, et al. "A squaraine–phthalocyanine ensemble: towards molecular panchromatic sensitizers in solar cells." Chemical communications 30 (2009): 4500-4502.
59. Claessens, Christian G., et al. "Highly Efficient Synthesis of Chloro-and Phenoxy-Substituted Subphthalocyanines." European Journal of Organic Chemistry 2003.14 (2003): 2547-2551.

60. Galliani, Daniela, et al. "Thermochromic Latent-Pigment-Based Time–Temperature Indicators for Perishable Goods." Advanced Optical Materials 3.9 (2015): 1164-1168.
61. Claessens, Christian G., et al. "Highly Efficient Synthesis of Chloro-and Phenoxy-Substituted Subphthalocyanines." European Journal of Organic Chemistry 2003.14 (2003): 2547-2551.
62. González-Rodríguez, David, et al. "Subphthalocyanines: Tuneable molecular scaffolds for intramolecular electron and energy transfer processes." Journal of the American Chemical Society 126.20 (2004): 6301-6313.
63. Mauldin, Clayton E., et al. "Axial Thiophene− Boron (subphthalocyanine) Dyads and Their Application in Organic Photovoltaics." ACS Applied Materials & Interfaces 2.10 (2010): 2833-2838.
64. Chao, Richard Y., et al. "Preparation and Characterization of Substituted 3-Benzothiazol-2Ylcoumarins." *Journal of the Chinese Chemical Society* 57.2 (2010): 213-221.
65. Cozzi, Pier Giorgio. "Metal–Salen Schiff base complexes in catalysis: practical aspects." Chemical Society Reviews 33.7 (2004): 410-421.
66. Gasperini, Michela, Fabio Ragaini, and Sergio Cenini. "Synthesis of Ar-BIAN Ligands (Ar-BIAN= Bis (aryl) acenaphthenequinonediimine) Having Strong Electron-Withdrawing Substituents on the Aryl Rings and Their Relative Coordination Strength toward Palladium (0) and-(II) Complexes." Organometallics 21.14 (2002): 2950-2957.
67. Gasperini, Michela, et al. "Synthesis of mixed Ar, Ar'-BIAN ligands (Ar, Ar'-BIAN= bis (aryl) acenaphthenequinonediimine). Measurement of the coordination strength of hemilabile ligands with respect to their symmetric counterparts." Dalton Transactions 20 (2004): 3376-3382.

Chapter three: NIR Operating devices

From materials to applications

In the first chapter of this manuscript, an introduction to electronics and on the impact electronics has on our lives has been reported. An overview on the field of organic electronics and its importance in the current cutting-hedge research has been the natural appendix. This third, final chapter focuses on applications of some organic systems synthesized during the doctorate work. The goal of such explorative work is to provide some proof of concept and some new entries in the world of NIR active organic materials. More specifically, a diketopyrrolopyrrole cyanine was tested as NIR-emitter for OLED, the perfluorinated subphthalocyanine dimer as tandem light-harvester/electron acceptor for photodetectors and Eu and Yb complexes as fluorophores for planar solar concentrators. A brief description of each technology and the state-of-the-art of application in the NIR will be provided at each subsection too.

3.1 Organic light emitting diodes

Organic light emitting diodes are light emitting diodes in which the emissive layer is composed by an organic thin film, that emits light as a response to an electric stimulus[1]. In the vast panorama of organic electronic devices, only OLEDs actually broke the barrier of the laboratory and niche scale to reach the mass production. In the past ten years, the demand of screen technology for consumer electronics boomed, and now, high-resolution home television and PC screens are very popular. The market of such systems, and consequently the revenues are impressive. For that reason, OLED market is rapidly growing and evolving, but it is still greatly polarized. The Asia-Pacific region is the biggest producer and consumers of electronics and the largest market for OLEDs. To give an example, by 2004 Samsung, South Korea's largest conglomerate, was the world's largest OLED manufacturer, producing 40% of the OLED displays made in the world. In 2010 had the 98% share of the global AMOLED display market (Active-Matrix OLED, which became world famous for the success of Samsung Galaxy smartphone series, contributing to the popularity of OLED technology). As of 2006, it held more than 600 American patents and more than 2800 international patents, making it the largest owner of AMOLED technology patents[2]. The company is still leading the world of OLED industry, but other players are joining this market, such as Korean LG or Japanese Sony.

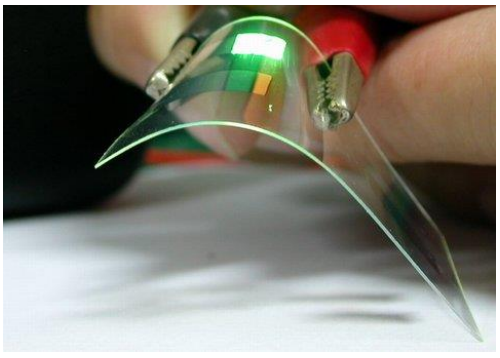

Figure 3.1: like other organic electronics devices OLEDs can be printed on flexible low cost plastics (from Wikipedia).

Going to the structural characteristics of OLEDs, one can recognize a principal building pattern, that can be resumed as:

- Transparent substrate (normally glass)
- Transparent conductive oxide (indium tin oxide, ITO)
- Hole transporting layer
- Emitting layer
- Electron transporting layer
- Metal cathode

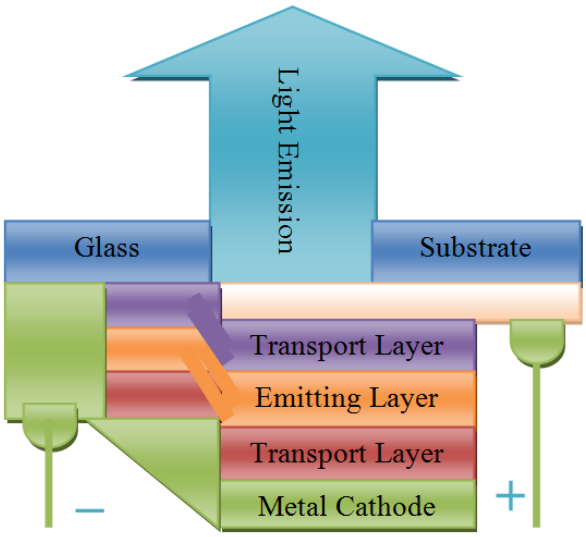

Figure 3.2: general scheme of an OLED. Reprinted from[1].

After the first pioneering work by Tang and Van Slyke[3], a simple organic bilayer structure between two electrodes, the structure of OLEDs greatly evolved. Despite the more complicated structure of the modern OLEDs, the working principles still remain

essentially the same. The core of the device is the organic layer. The organic semiconductor used can be either polymers or small molecules, and their frontier molecular orbitals, HOMO and LUMO, determine the energy gap and, thus the emission wavelength. In the operative conditions, a voltage is applied between the two electrodes (metal cathode and ITO) and a current flows through the device. Electrons and holes that reach the emissive layer are injected respectively into the LUMO and into the HOMO of the organic semiconductor. At this stage, holes and electrons experience a coulombic attractive force resulting in the formation of the so-called exciton, a bound state of an electron and a hole, that for organic small molecules is normally localized on the same molecule. The exciton decays radiatively through recombination, generating radiation that can travel to the transparent electrode and go out from the device. Interlayers can be placed either to the cathode or the anode side, to enhance the charge injection into the emissive layer or to block opposite carriers to the electrodes, preventing recombination losses outside the emissive layer. It is important to mention that in organic semiconductors, the charge transport is assured by electron delocalization in the π-backbone of the molecule and, for this kind of systems, the main conduction mode is by hopping.

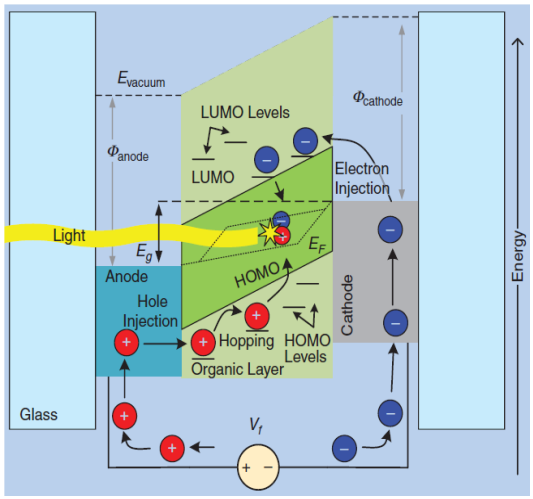

Figure 3.3: scheme of the energy levels and functioning of a simple single layer OLED. Adapted from[3].

Since the OLED market is dominated by screen application and environmental solid state lighting, the organic structures that are commonly employed in this technology are active in the visible range. This originates from the non-trivial consideration that the human eye shows a responsivity only in this wavelength range (it is visible, using a pleonasm). The connection between OLED technology and infrared light is, for that not automatic at a first glance, because the infrared light is not detectable by human eye. The applications of NIR emitting materials, and the devices that implement them, range from biomedicine and biosensing to long range telecommunication and signaling. Unfortunately, NIR emitting materials, especially full-organic are scarcely reviewed[4,5].

From the material point of view, there is a lack of infrared emitting materials, compared to infrared absorbing ones. The major part of the literature on such systems treats complexes of lanthanides[6], complexes of transition metals[7,8], such iridium, or for fully organic systems, cyanines. Completely organic NIR systems have, as important drawbacks, the generally low luminescence quantum yields and a general poor optical purity, derived from the residual emission they show in the visible range.

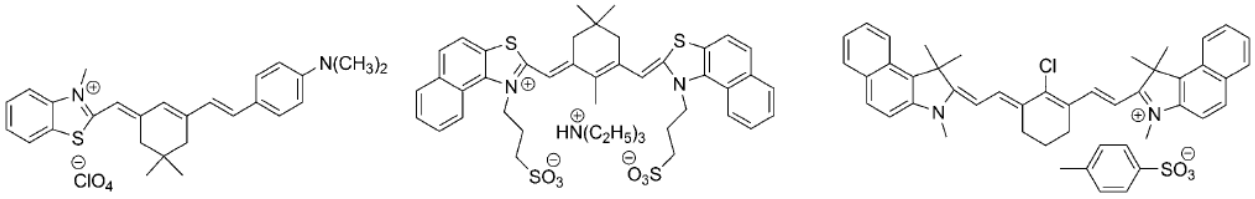

Figure 3.4: structures of three cyanines used for NIR OLEDS. Adapted from[4].

Recently, some fully organic Donor-Acceptor structures, both polymers and small molecules, emerged in the NIR emitting materials for OLEDs panorama[9,10,11]. In these systems, the combination of strong electron-donating and electron-withdrawing substituents at the opposite ends of easily polarizable conjugated moieties is at the basis of the small energy gap, which is placed within the NIR region energy range.

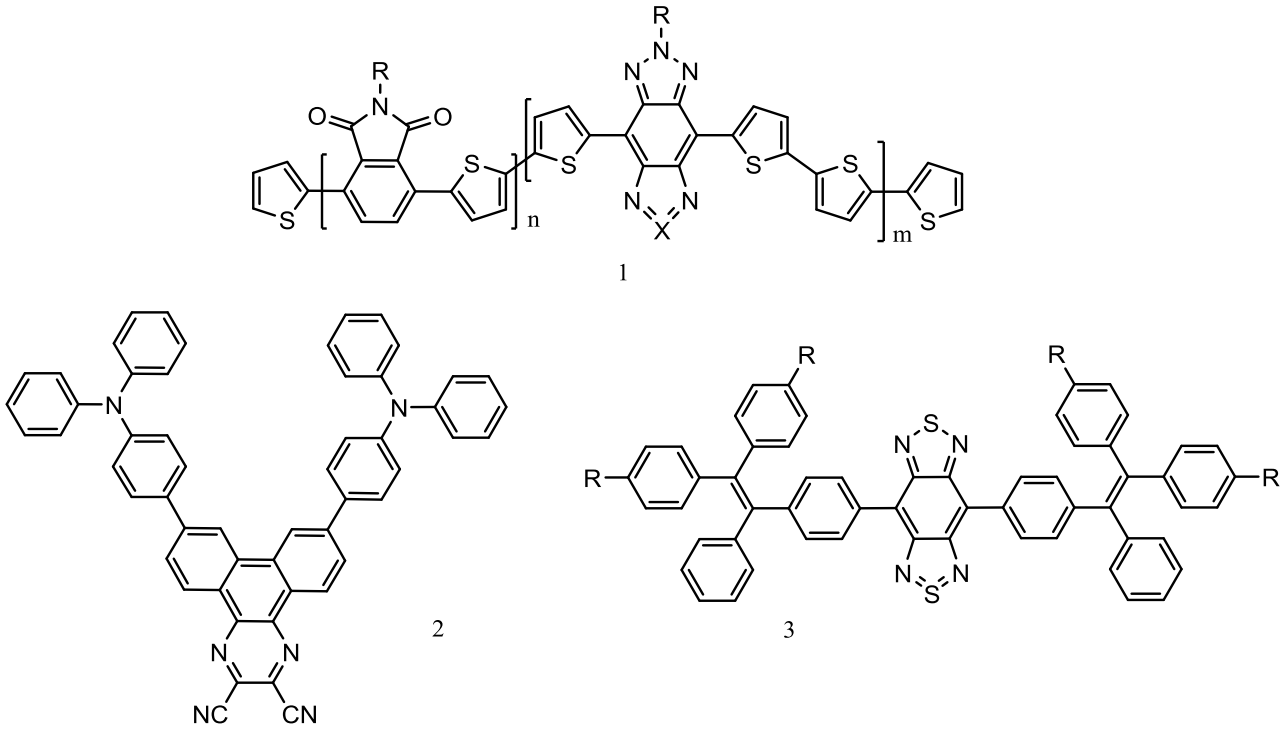

Figure 3.5: examples of structures present in the literature for NIR-OLED applications[9,10,11].

Strong HOMO-LUMO charge transfer transitions usually lead to large spectral separation between the absorption and the emission spectra but also result into low photoluminescence efficiency. The "perfect" molecule for electroluminescence applications should show a trade-off, a balance between a good Stoke-shift (separation

between absorption and emission bands) and a decent photoluminescence quantum yield. In this sense, the best results to date pertain to the class of D-π-A-π-D "butterfly shaped" molecules. They show photoluminescence within the 600-900 nm region reaching a peak EQE exceeding 1.5% in the OLED device[12]. Analogues structure by Wang et al. showed electroluminescence at around 1000 nm, although with low EQE[13,14]. From a pure chemical point of view one can note that almost all the structures used as luminescent materials for NIR-OLEDs (with the exception of the phenantrene-based one from Yao et al.) report as acceptor benzothiadiazole or benzothiazole (or analogues selenazoles) moieties. It is scientifically interesting to investigate new structures showing similar characteristics without the presence of such fragments.

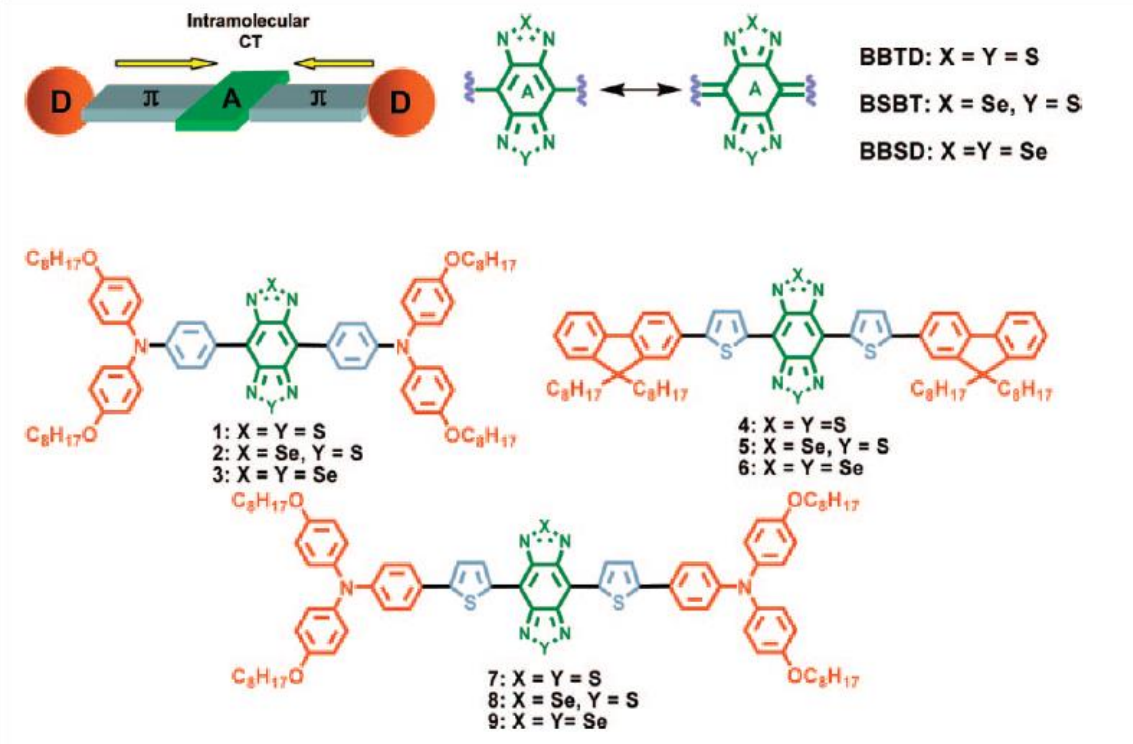

Figure 3.6: structures of different D-π-A-π-D structures reported by Wang et al. On the top a scheme of the charge transfer dynamics and the resonance structure involved are reported. Reprinted from[14].

3.1.2 Results and discussion: NIR-OLEDs based on DPP-Cy

After the synthesis and the characterization of some diketopyrrolo-cyanines, the possible applications of such systems in electronic devices have been evaluated. The good quantum yield in solution and the emission properties preliminary evaluated in thin film lead to the choice of the acetonitrile-pyridine based DPP-Cy as possible luminescent material for solution-processed NIR-OLEDs. A preliminary optimization of the conditions used in the process of fabrication and a more detailed analysis of the performances of the optimized device have been carried out with the collaboration of the laboratory of Dr. Umberto Giovannella at Politecnico di Milano.

For the fabrication of NIR-OLEDs by wet methods, fluorescent or phosphorescent emitters are typically dispersed in an active polymer matrix to increase the film homogeneity and to prevent quenching by intermolecular aggregation. Polyvinylcarbazole has been shown to be a suitable host matrix for NIR Ir(III) complexes[15]. Upon charge injection, excitons are either generated in the host matrix and successively transferred via FRET to the NIR emitter, or they can be generated directly in the emitter through carrier trapping. In either case, efficient NIR emission is achieved. We tested DPPcy potential as a NIR electroluminescent compound working with three different device configurations. In a firs trial the pure compound was tested, showing any result under any experimental condition. Then DPP-Cy blends in PVK were tested, using a simple single layer configuration with ITO/PEDOT:PSS/PVK: DPPcy/Ba/Al structure and a slightly more complex dual layer one having ITO/PEDOT:PSS/PVK/PVK:DPPcy/Ba/Al structure. Apart from the contacts, all layers were deposed by spin coating. The figure 3.7 shows the electroluminescence spectra of PVK-based OLEDs obtained according to the aforementioned structures.

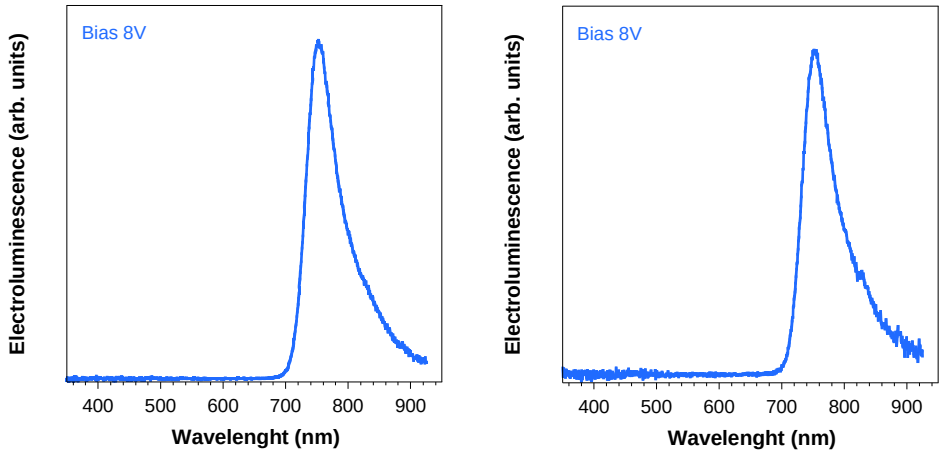

Figure 3.7: Electroluminescence spectra of OLED based on a DPPcy/PVK blend. Left: single layer ITO/PEDOT:PSS/PVK:DPPcy/Ba/Al. Right: dual layer ITO/PEDOT:PSS/PVK/PVK:DPPcy/Ba/Al

In both cases electroluminescence band peaking at 751 nm with a FWHM of 65 nm was observed. Both values very close to the thin film photoluminescence data. In both cases, the efficiencies are low, but the emission demonstrated to be very stable. The figure 3.8 shows that after 271 minutes of continuous working at 6 V applied bias, 80% of the original emission intensity is preserved.

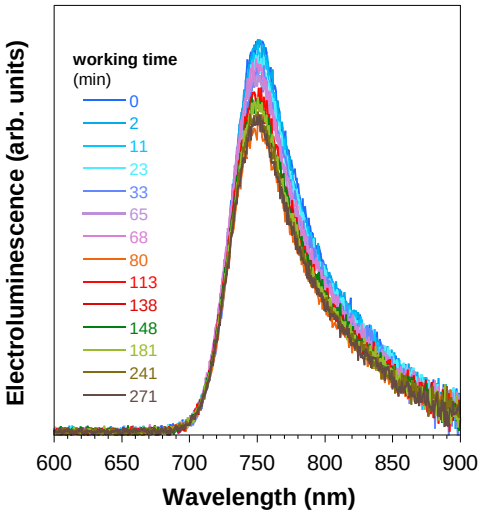

Figure 3.8: lifetime study of the PVK based device biased at 6V and a current of 10 mA/cm².

It is important to note that the HOMO-LUMO levels of poly(9,9-dioctylfluorene-alt-benzothiadiazole, F8BT) are better positioned with respect to the energy levels of DPPcy. This promotes direct exciton formation in the emitters. Furthermore, the hole-transport character of pristine F8BT can be controlled and modified by suitable post-deposition processes, such as thermal annealing above the corresponding glass transition temperature (130 °C), which has been shown to enhance the EQE by enabling bipolar conduction and improving the charge balance in the active layer[16]. After a first explorative trial using PVK as host, the optimization was carried out using F8BT. Different F8BT/DPPcy ratios were tested, from 90:10 w/w to 70:30 w/w, in order to optimize the doping level for higher efficiency.

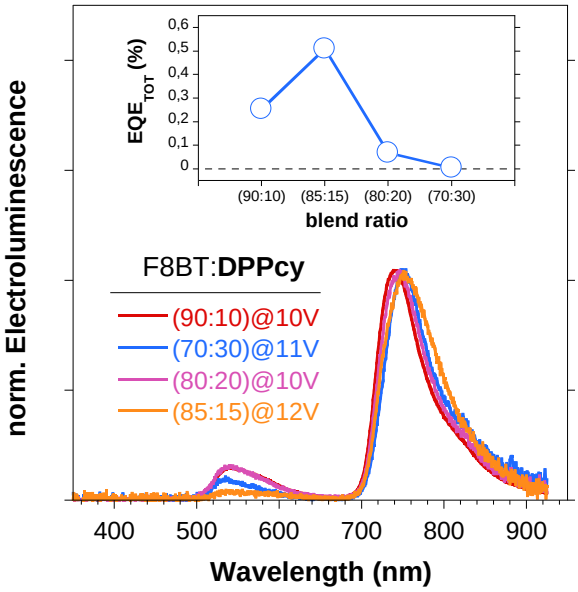

Figure 3.9: Electroluminescence spectra of OLED based on a F8BT:DPPcy blends with different ratios. The inset shows the corresponding EQE values.

Different F8BT/DPPcy ratios were initially tested in order to optimize the doping level in view of film forming ability and optical properties. In figure 3.10, the optical properties of the blend with the F8BT:DPPcy optimized ratio of 85:15 w/w are shown for a 80-90 nm thick film prepared by spin-coating from a 50/50 v/v toluene/chlorobenzene mixture. The blend shows optical features of both F8BT and the DPPcy. Thermal treatment at 130°C for 15 minutes in nitrogen atmosphere led to phase segregation causing a slight blue-shift of the DPPcy absorption spectrum with an increase in intensity of the high energy peak at ~660 nm. Concurrently, the emission peak at ~760 nm broadens and weakens with respect to the F8BT emission at 535 nm. This behavior is ascribed to reduced FRET efficiency from F8BT to DPPcy in the annealed film, in agreement with the formation of phase segregated domains. This scenario is supported by time-resolved measurements of F8BT PL showing slower decay dynamics in the annealed film (~290 ps) with respect to the pristine film (~70 ps).

Atomic force microscopy (AFM) measurements were performed in order to directly monitor the evolution of the surface morphology upon thermal treatment. The comparison between height images measured in semi-contact mode of as-spun and annealed 85:15 F8BT:DPPcy films (Figure 3.10 c, d) evidences increased root mean square roughness from 0.34 nm to 1.46 nm. Thermal annealing induces phase segregation of F8BT- and DPPcy-rich domains, as highlighted by the phase images (inset of figure 3,10 c,d) showing dark and bright nanometer sized domains whose texture is evident in the treated film. Fluorescence microscopy images (Fig.3.10 e, f) further confirm the formation of segregated domains in the treated film, with brighter phase separated domains of F8BT nanostructures in agreement with the reduced FRET to DPPcy. Weaker homogeneous green F8BT emission is observed in the untreated film.

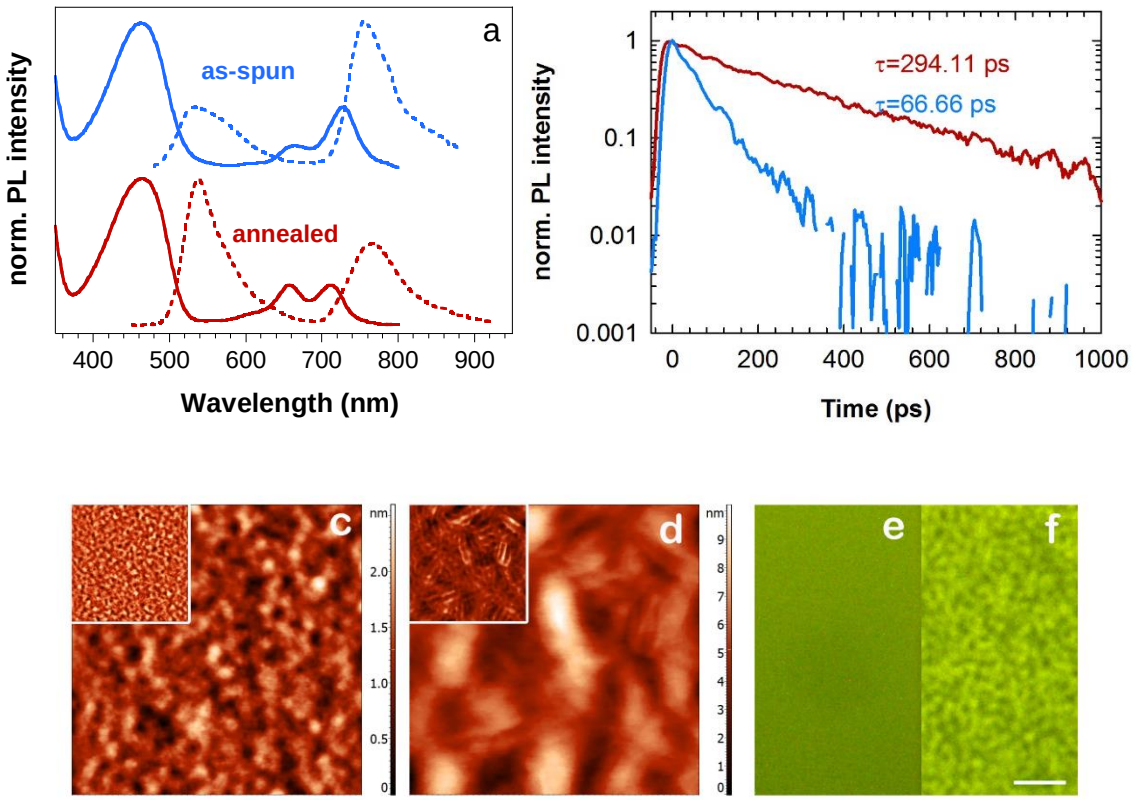

Figure 3.10: (a) Absorption and PL spectra of F8BT:DPPcy (85:15) blended films both as-spun (blue lines) and annealed (red curves) films at 130 °C for 15 minutes in nitrogen. (b) Time decay curves of F8BT PL at 535 nm for pristine (blue) and annealed (red) films (excitation at 405 nm) (b). Height and phase (inset) mode AFM images (1 μm x 1 μm) of as-spun (c) and annealed (d) F8BT:DPPcy films. Fluorescence microscope images of as-spun (e) and annealed (f) F8BT:DPPcy films; the white bar corresponds to 3 μm.

OLED devices were fabricated to experimentally validate the suitability of DPPcy for NIR electroluminescence applications. The architecture used was ITO/PEDOT:PSS/PVK/F8BT:DPPcy/Ba/Al, embedding F8BT:DPPcy films as emissive layer. A thin layer of hole injecting/electron blocking PVK was spin-coated on PEDOT:PSS in order to confine excitons far from the anode and to promote radiative recombination[17].

A remarkable maximum EQE=0.55% at 2 mA/cm^2 and maximum radiant exitance of 200 mW/m^2 were obtained for devices embedding 85:15 F8BT:DPPcy annealed blends (Fig. 3.11).

The EL switches on at 8V and is fully located in the NIR spectral region 700-900 nm with maximum at 753 nm (FWHM of 65 nm). The annealing process, is crucial for achieving the observed LED performance as it leads to a 30-fold enhancement in EQE with respect to devices embedding pristine active layers. NIR-OLEDs with doping ratios ranging from 90:10 w/w to 70:30 w/w show systematically lower efficiency with respect to devices with optimal blending ratio of 85:15 w/w. NIR-OLED manufactured using PVK as host polymer show 10 times lower EQE than those based on F8BT blends.

Beside the EL efficiency, a crucial aspect for practical application of NIR-OLEDs is their device stability under operation. The performances of phosphorescent NIR-OLEDs reported so far were affected by severe efficiency roll-off, which is a strong reduction of the EQE at high current densities. Efficiency roll-off originates from a number of quenching mechanisms including triplet-triplet annihilation, triplet-polaron quenching and electric-field-induced exciton dissociation facilitated by long emission lifetimes and intermolecular aggregation[18]. Remarkably, the DPPcy-based NIR-OLEDs presented exhibit negligible efficiency roll-off with EQE~0.5% for current densities ranging from 0.5 to 50 mA/cm^2, which is comparable to the best reported phosphorescent OLEDs based on Ir(III) complex-emitting in the same spectral region[19].

In order to test the DPPcy stability during continuous device operation, we biased our NIR-OLEDs at constant current density J=10 mA/cm^2 for 60 hours. The inset of Figure 3.11 d shows that the EL intensity remains over 50% its initial value. Such remarkably long lifetime for organic NIR-LEDs derives directly from the inherent stability of DPPcy

and further benefits from the low electrical stress due to well-balanced charge carriers concentration in the thermal treated film.

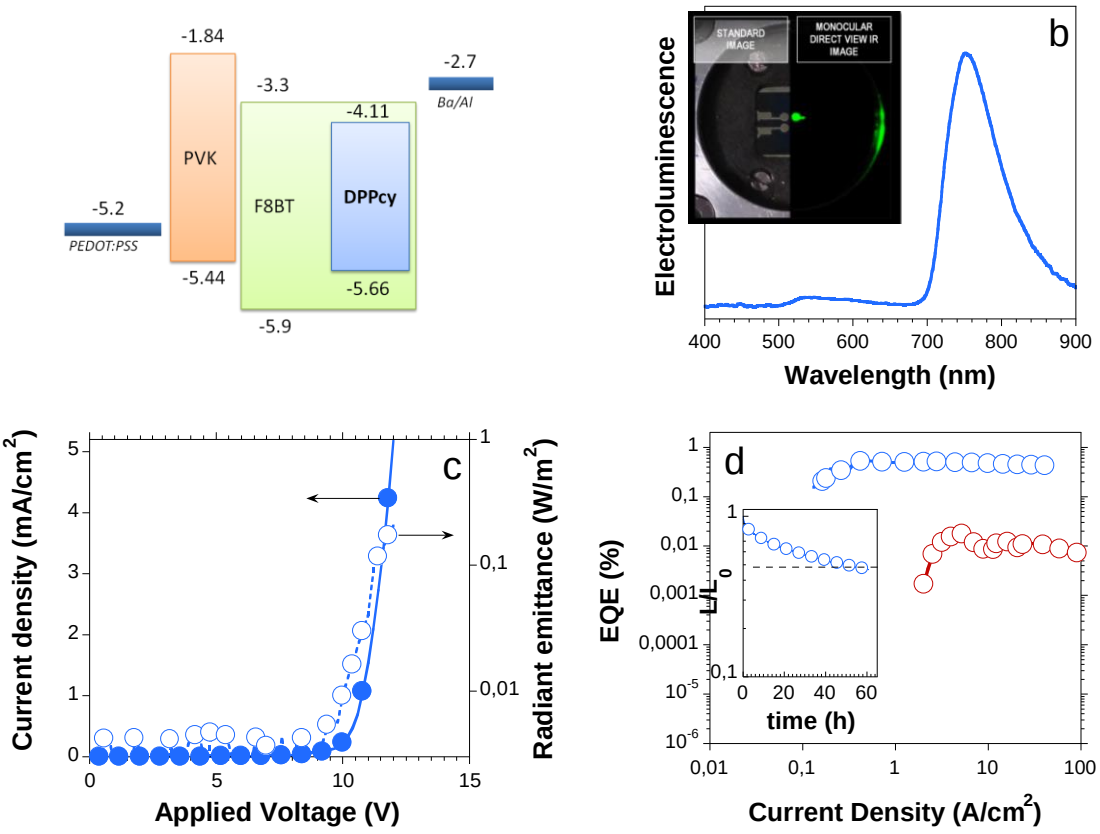

Figure 3.11: (a) Energy level diagram of ITO/PEDOT:PSS/PVK/F8BT:DPPcy(85:15)/Ba/Al device. (b) EL spectrum of annealed device; Inset, NIR emitting OLED picture. (c) representative J-V(bold circles) and Emittance-V (empty circles) curves of annealed device. (d) EQE vs J of as spun (red circles) and annealed device (blue circles); inset, luminance evolution of NIR-OLED driven at 10 mA/cm^2 as a function of device operating time.

3.1.3 Experimental Procedures

Devices preparation. A blend of F8BT:DPPcy in the mass ratio (85:15) was dissolved in toluene 15 mg/mL. Indium tin oxide (ITO; 15 Ω per square) substrates were cleaned by sonication in distilled water, acetone, and isopropyl alcohol. After treatment with nitrogen plasma, a thin film (40 nm) of filtered (nylon 0.45 μm) poly-(3,4-ethylenedioxythiophene)-poly(styrenesulfonic acid) (PEDOT:PSS, Clevios P VP AI 4083, H.C. Starck) used as a hole-injection layer at the anode interface was spin-coated onto the ITO substrate, and then dried under nitrogen atmosphere at 150 °C for 15 minutes. A film of emitting blend was then spin-coated. A thin layer of barium (4 nm) and subsequently a layer of Al (80 nm) were deposited on the top by vacuum ($5x10^{-7}$mbar) thermal evaporation. In the optimized architecture a PVK layer is inserted between PEDOT:PSS and active layer. The device active area was 5.4 mm^2. Devices were fabricated inside a nitrogen-filled dry box with less than 0.1 ppm of both oxygen and water and packaged for the optical characterization

3.1.4 Bibliography

1. Islam, Aminul, et al. "A review on fabrication process of organic light emitting diodes." Informatics, Electronics & Vision (ICIEV), 2013 International Conference on. IEEE, 2013.
2. www.oled-info.com
3. Bender, Vitor C., Tiago B. Marchesan, and J. Marcos Alonso. "Solid-State Lighting: A Concise Review of the State of the Art on LED and OLED Modeling." Industrial Electronics Magazine, IEEE 9.2 (2015): 6-16.
4. Qian, Gang, and Zhi Yuan Wang. "Near-infrared organic compounds and emerging applications." Chemistry, an Asian journal 5.5 (2010): 1006-1029.
5. Ho, Cheuk-Lam, Hua Li, and Wai-Yeung Wong. "Red to near-infrared organometallic phosphorescent dyes for OLED applications." Journal of Organometallic Chemistry 751 (2014): 261-285.
6. Kalyani, N. Thejo, and S. J. Dhoble. "Organic light emitting diodes: Energy saving lighting technology—A review." Renewable and Sustainable Energy Reviews 16.5 (2012): 2696-2723.
7. Borek, C.; Hanson, K.; Djurovich, P. I.; Thompson, M. E.; Aznavour, K.; Bau, R.; Sun, Y.; Forrest, S. R.; Brooks, J.; Michalski, L.; et al. Highly Efficient, Near-Infrared Electrophosphorescence From a Pt–Metalloporphyrin Complex. Angew. Chem. Int. Ed. 2007, 46, 1109–1112.
8. Cheng, C.-H.; Fan, Z.-Q.; Yu, S.-K.; Jiang, W.-H.; Wang, X.; Du, G.-T.; Chang, Y.-C.; Ma, C.-Y. 1.1 Mm Near-Infrared Electrophosphorescence From Organic Light-Emitting Diodes Based on Copper Phthalocyanine. Appl. Phys. Lett. 2006, 88, 213505.
9. Tregnago, G.; Steckler, T. T.; Fenwick, O.; Andersson, M. R.; Cacialli, F. Materials Chemistry C. J. Mater. Chem. C 2015, 3, 2792–2797.
10. Du, Xiaobo, et al. "Efficient non-doped near infrared organic light-emitting devices based on fluorophores with aggregation-induced emission enhancement." Chemistry of Materials 24.11 (2012): 2178-2185.

11. Wang, Shipan, et al. "Highly Efficient Near-Infrared Delayed Fluorescence Organic Light Emitting Diodes Using a Phenanthrene-Based Charge-Transfer Compound." Angewandte Chemie International Edition 54.44 (2015): 13068-13072.
12. Yao, L.; Zhang, S.; Wang, R.; Li, W.; Shen, F.; Yang, B.; Ma, Y. Highly Efficient Near-Infrared Organic Light-Emitting Diode Based on a Butterfly-Shaped Donor-Acceptor Chromophore with Strong Solid-State Fluorescence and a Large Proportion of Radiative Excitons. Angew. Chem. Int. Ed. 2014, 53, 2119–2123.
13. Qian, G.; Zhong, Z.; Luo, M.; Yu, D.; Zhang, Z.; Wang, Z. Y.; Ma, D. Simple and Efficient Near-Infrared Organic Chromophores for Light-Emitting Diodes with Single Electroluminescent Emission Above 1000 Nm. Adv. Mater. 2009, 21, 111–116
14. Qian, Gang, et al. "Band Gap Tunable, Donor− Acceptor− Donor Charge-Transfer Heteroquinoid-Based Chromophores: Near Infrared Photoluminescence and Electroluminescence." Chemistry of Materials 20.19 (2008): 6208-6216.
15. Tao, R.; Qiao, J.; Zhang, G.; Duan, L.; Wang, L.; Qiu, Y. Efficient Near-Infrared-Emitting Cationic Iridium Complexes as Dopants for OLEDs with Small Efficiency Roll-Off. J. Phys. Chem. C 2012, 116, 11658–11664.
16. Van Vooren, A.; Kim, J.-S.; Cornil, J. Intrachain Versus Interchain Electron Transport in Poly(Fluorene-Alt-Benzothiadiazole): a Quantum-Chemical Insight. Chemphyschem 2008, 9, 989–993.
17. Giovanella, U.; Betti, P.; Botta, C.; Destri, S.; Moreau, J.; Pasini, M.; Porzio, W.; Vercelli, B.; Bolognesi, A. All-Conjugated Diblock Copolymer Approach to Improve Single Layer Green Electroluminescent Devices. Chem. Mater. 2011, 23, 810–816.
18. Lamansky, S.; Djurovich, P.; Murphy, D.; Abdel-Razzaq, F.; Lee, H.-E.; Adachi, C.; Burrows, P. E.; Forrest, S. R.; Thompson, M. E. Highly Phosphorescent Bis-Cyclometalated Iridium Complexes: Synthesis, Photophysical Characterization, and Use in Organic Light Emitting Diodes. J. Am. Chem. Soc. 2001, 123, 4304–4312.
19. Xin, L.; Xue, J.; Lei, G.; Qiao, J. Efficient Near-Infrared-Emitting Cationic Iridium Complexes Based on Highly Conjugated Cyclometalated Benzo[G]Phthalazine Derivatives. RSC Adv. 2015, 5, 42354–42361.

3.2 Luminescent Solar Concentrators

In this second section of the third chapter, the application of NIR-luminescent materials in solar concentrators will be presented. The characteristics of the device as well as some of the losses mechanisms that affect them will be briefly reviewed to better understand the approach used in the laboratory work.

Solar concentrating systems are conceptually simple devices able to collect solar light and to focus it on a small area. It is the principle of the so-called Solar Thermal Energy, in which the concentrated power is stored by means of a fluid. The exploitation of the solar irradiance using such systems represents a cheap, abundant and well distributed energy source: to have an idea, the Italian physics Nobel Laureate Carlo Rubbia, in an interview in 2008 stated that a hypothetic mirror of 200 km of side could generate enough power to replace all the oil generated energy[1]. This optimistic vision, although substantially accurate, present some practical difficulties. The lenses and mirrors used in such technology need complex systems of solar trackers to follow the sun and the amount of generated power strongly depends on the weather, since they are not able to use diffuse light. Moreover, the solar plants, although diffused in some countries (i.e. USA, Spain), require large land areas and are not easily implemented in a strongly urbanized region (such as Europe). The last consideration is that large amounts of empty and sunny lands, such deserts and arid regions are concentrated in politically unstable areas, such as north Africa, Sahel region, Middle East and Arab Peninsula, making large scale investments on solar plants virtually impossible (in the time this thesis is written, the mentioned locations are plagued by terroristic groups like ISIS, Al-Shabaab, Boko Haram and by humanitarian bombings from West and Russia).

A different solution is to concentrate the solar power to improve the efficiency of a coupled solar cell and to use luminescent materials to do so. This kind of devices are called Luminescent Solar Concentrators (LSC). They were proposed for the first time in the 70's[2], during the oil crisis that boosted the research on alternative energies. They re-gained popularity in the past 5-10 years, in which the oil price rose again to up to 100$ per barrel (now, in January 2016 it dropped back again to less than 30$ per barrel, with not easily predictable consequences on the research on renewables).

Regardless the geopolitical framework and the oil war underway, LSCs can represent a valid way to improve solar cells efficiency. Structurally, they are slabs of highly transparent plastics or glass in which an optically-active system is dispersed. Such system absorbs the solar radiation and re-emits photons by radiative de-excitation (fluorescence). The slab acts as a waveguide: the emitted photons are trapped into the slab by total internal reflection, that derives from the different refraction index between the host matrix and air. Then the photons travel through the slab to the edges, where a small-area efficient solar cell is positioned. The geometric gain, consisting in the ratio between the larger surface and the edge, can lead to concentration values of several of suns[3,4,5].

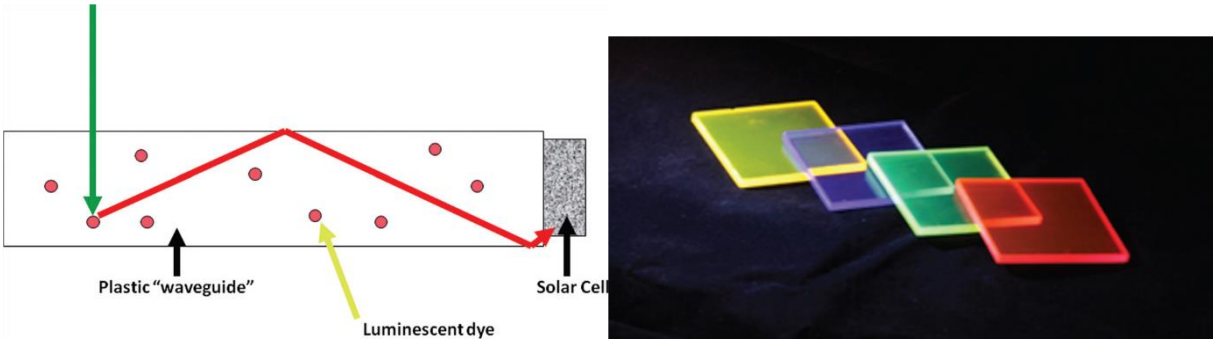

Figure 3.2.1: left, schematic representation of a plastic luminescent solar concentrator and the mechanism involved. Right, real devices under UV illumination. The color only depends on the active material dispersed into the plastic. Reprinted from[3].

The main advantages of such approach to the problem of solar concentration are:

- the exploiting of diffuse light, that is a key feature in environments without direct illumination, such as big urban conglomerates or interiors. The use of diffuse light is also important in regions of the world with intermittent solar power production due to clouds (such as central Europe) or pollution (like Asian megalopolis).
- High concentration ratios, low heating of the devices and tunability of the emission range with respect to the maximum of absorbance of the coupled solar cell.
- Low cost of the materials. Inexpensive plastics such as PMMA is normally used and very low quantity of active material, usually in the range 10^{-4}-10^{-5} M are required.
- Ease of integration in the urban context and production of design objects (the so-called building integration aspect will be discussed at the end of this section).

Like every product of the human intelligence, LSCs present some disadvantages and some losses due to the intrinsic nature of the object. They can be visualized in the following figure and listed below it.

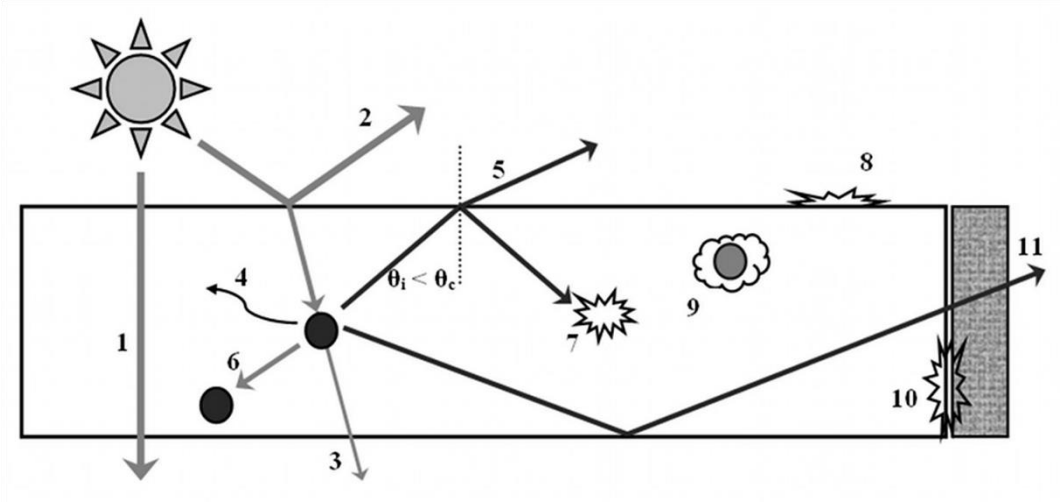

Figure 3.2.2: scheme of the losses mechanisms in an LSC. Reprinted from[4].

1. The incident radiation passes through the slab without being absorbed.
2. The smooth surface of the slab reflects the incoming light.
3. The luminophore absorbs only a fraction of the incoming radiation.
4. The luminescence efficiency of the active species is not unity and some of the energy is dissipated through non-radiative deactivation pathways.
5. The light emitted from the luminophore has not the correct angle ($\theta_i<\theta_c$) to be trapped into the slab and goes out from it from the so-called escape cone.
6. Another luminophore can reabsorb the emitted light.
7. The slab in itself can present some parasitic absorption or scattering due to construction defects.
8. The surface of the slab can scatter the incoming light.
9. The active material, especially with organic systems, can present degradation problems under the operative conditions.
10. Scattering due to inhomogeneity in the slab-cell interface.
11. Efficiency of the solar cell.

The active materials for LSC can be classified in three main families: luminescent quantum dots, organic dyes and chelates of lanthanides. This part of the discussion focuses on this third category. To understand the features of lanthanide-based LSC, a brief introduction on the luminescence behavior of such systems is required. The luminescence properties of lanthanides complexes are well known and extensively reviewed in the literature and widely applied in technological fields such as LEDs, sensors or biological markers[6,7,8]. As reported in the first chapter, the emission properties of lanthanides are determined by the f-f Laporte-forbidden transitions. Moreover, the necessity to sensitize the lanthanides, in order to efficiently harvest the light and enhance the emission. This phenomenon, proposed for the first time by Cosby and

Whan[9], is called *antenna effect*: the incoming light promotes the excitation of the organic ligand to a singlet excited state S1, then the energy is transferred by intersystem crossing (ISC) to the ligand triplet state and finally transferred to the lanthanide center that emits. This energy transfer can be described by the Dexter or Forster formalisms[10,11]. The cascade process can be represented by a simple Jablonski diagram as reported in the following figure:

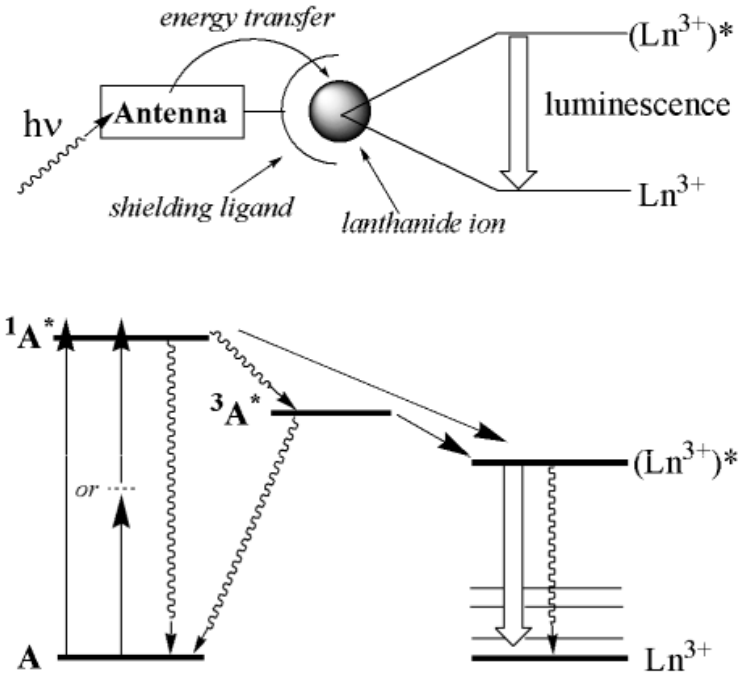

Figure 3.2.3: on the top side a schematized drawing of the antenna effect is reported. Below it, a Jablonski diagram shows the energy transfer processes involved for a generic lanthanide trivalent cation. Reprinted from[8].

The advantages of this approach are evident: the use of an organic ligands absorb the radiation in an efficient way in the UV and visible region, maintaining the emission proper of the lanthanide. Moreover, the emission of the lanthanides usually does not overlap

the absorption of the ligand. The resulting high Stokes-shift of such systems is extremely important for application in LSC. However, it is of great importance to accurately choose the ligand to be employed. It should have an absorption as intense and broad as possible in the region of interest and its energy levels should match the energy levels of the ligand, in particular the triplet state of the ligand should be positioned slightly above the excited state of the lanthanides. This motivations, as long as the research for the correct binding modes make a cautious chemical design fundamental for high performing lanthanide based materials.

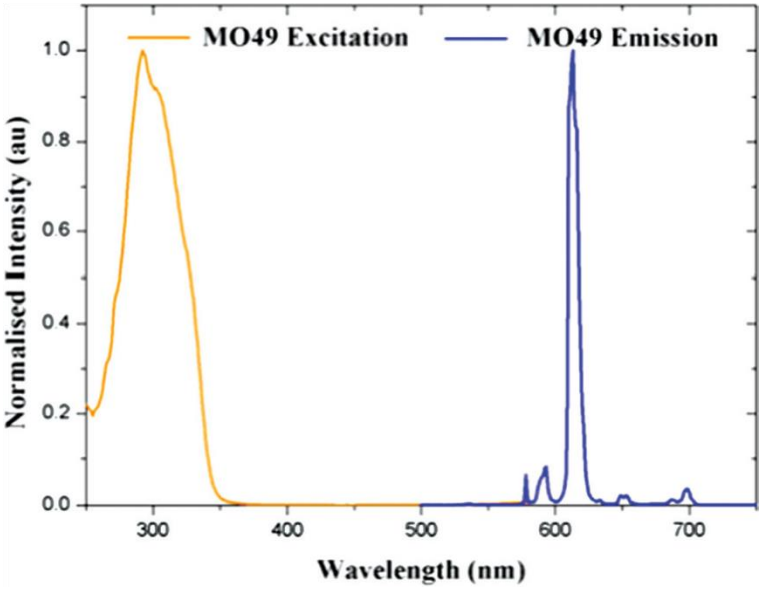

Figure 3.2.4: prototypical absorption and emission behavior of a chelate of lanthanide. In this case Eu3+ is sensitized in the UV and the emission band proper of Eu appears at around 620 nm (red emission). Adapted from[4].

As said, the most important source of efficiency loss is the reabsorption of the emitted radiation by another fluorophore into the slab. This phenomenon is particularly evident for organic dyes, which normally show low Stokes-shift. It has been evidenced in a recent paper by Turrisi et al.[12], that a correct molecular design enlarges the spectral separation

and positively affects the LSC performances. The same paper proposes a method to evaluate the re-absorption losses in LSC devices. The decay of the photoluminescence throughout a slab is measured as a function of the distance between the excitation point and the edge. If there is overlap between the absorption band and the emission one, the signal is attenuated. A further manipulation shows the variation with the distance of a "cumulated" efficiency measured as function of the distance obtained by a linear growth of slab. In an ideal slab (no spectral overlap), only the geometric gain matters and the cumulated efficiency tends to infinite, while for a small Stokes-shift dye it rapidly reaches a plateau. The non-trivial conclusion of such analysis is that Stokes-shift engineering is extremely important for large area panels construction. In, other words, if all the light emitted in the center of the slab, instead of being re-absorbed within a certain distance from the edge, reaches the coupled solar cell, the construction of very large surface devices is possible. Such analysis is important to evaluate the "quality" of the molecular design and it will be applied to chelates of lanthanides in the present work.

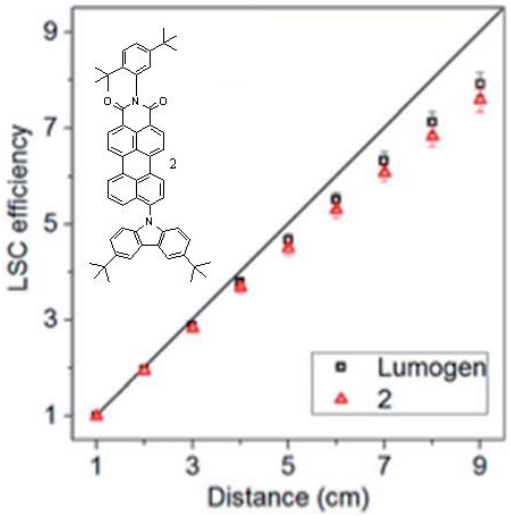

Figure 3.2.5: LSC cumulated efficiency vs the distance from the detector. The triangles represent the Stokes-shift engineered perilene proposed in the paper of Turrisi et al. The results are compared to BASF Lumogen F240 (perylene-3,4,9,11-tetracarboxylic acid bis-(2',6'-diisopropylanilide)). Adapted from reference[12].

3.2.1 Results and Discussion: chelates of Yb^{3+} and Eu^{3+} for LSC

Taking into account all the theoretical aspects enucleated so far, the ligands and the chelates that have been presented in the synthesis chapter, have to match the following requirements to be applied in efficient LSCs:

- ✓ The co-ligands have to absorb in the UV-region or in the first part of the visible. This is important because UV sensitizer can be effectively used as antenna towards lanthanides but making the complex non-colored. This can enable the production of colorless panels that are very attractive for architectural applications, such as smart, energy-producing windows. An absorption tail in the visible is also acceptable for a better energy harvesting but it should not affect the color of the final device in an unpleasant way (the final color intensity is only determined by the ε of the active species, since the concentration is maintained constant).
- ✓ The ancillary ligands have to efficiently chelate the metal ion. The chelation is an effective way to coordinate metals and it results particularly stable, with respect to monodentate ligands binding, essentially for the entropic gain intrinsic in the chelation process (the number of total molecules increases).
- ✓ From the synthetic point of view, the complex synthesis should be straightforward, with high yields, in order to be easily scaled up in an industrial process.
- ✓ The chelates have to present low re-absorption losses, in order to produce panels as extended as possible.
- ✓ Coherently with the goal of this work the complexes have to show sizable luminescence in the red-NIR part of the spectrum. To achieve this, it is important that no C-H or C-O bonds have to be present in the first coordination sphere. This bonds show IR-active overtones that can quench the luminescence. Water, that

efficiently coordinates lanthanides, have to be avoided for the same reason and the absence of it in the first coordination sphere is essential.

- ✓ The chelates, and in general every active molecule for plastic LSC, have to be stable to the polymerization conditions during the production of the slab. As an example, the standard laboratory procedure of polymerization of methyl-methacrylate to obtain PMMA is a radical reaction, initiated by a radical initiator such as AIBN (azabisisobutirronytrile). The actual polymerization is performed at 50-60 °C and followed by curing at 100°C. The fluorophores should not react or degrade with the initiator or with radical species and should be thermally stable at the working temperatures.

The two bidentate, nitrogen-based ancillary ligands presented in the second chapter and their complexes europium and ytterbium (C1, C2, C3) showed characteristics that can match the above mentioned requirements. The UV-Vis spectra showed absorption in the 380-450 nm portion of the spectrum, so in the first part of the visible, with an upper tail in the UV, matching the requirements for a nearly-transparent final device with a good light harvesting. The infrared spectra showed no presence of water. As said, this is an extremely important characteristic for increase the lifetime of the excited state of the ligand and for the energy transfer toward the metal, enhancing the efficiency of the final concentrator device[44,45,46]. In order to test the effectiveness of the compounds as active materials for LSC, PMMA slabs were prepared using the complexes C1, C2, C3. The slabs were prepared performing a pre-polymerization of methyl-methacrylate at 80°C using AIBN as first radical initiator. This process results in a viscous syrup that can be easier poured into the slabs mold, with respect to the pure liquid monomer, avoiding gas bubbles or inhomogeneities. Then the complexes were added along with the secondary

initiator, lauroyl peroxide, and the resulting syrup polymerized at 56 °C during 48 hours. The non-polymerized methylmethacrylate is removed by thermal curing at 95-100 °C. It is extremely important to carefully degas the monomer prior to polymerize it, in order to avoid gas bubbles or a “foggy” aspect of the final device. The complexes demonstrated to be stable to such conditions.

Figure 3.2.6: pictures of the three LSCs over a colored surface. A) C1, b) C2, c) C3.

The pictures in figure 3.2.5 have been taken to have a first visual evaluation of the transparency of the final slab. To appreciate the transparency properties of the produced LSCs, pictures of a colored surface were taken using the devices as a filter. In the case of C1 and C2 chelates, the pale yellow shade due to the ligand does not affect the transparency of the systems and the colors beneath are not significantly modified, in particular in the case of C2. This is a proof of the correct design of the p-anisidine-based ligand: it is capable to absorb a part of visible photons without compromise the optical quality of the final device. Conversely, the reddish shade of C3 based LSC has a stronger impact on colors.

The slabs were characterized in terms of photoluminescence decay and re-absorption losses, in collaboration with the photophysics laboratory of professor Meinardi at University of Milano Bicocca. The same method described in the introduction was used. The evolution of the normalized emission spectrum has been plotted as a function of the distance between the detector placed at the LSC edge and the excitation spot (laser operating @ 405 nm).

The experimental set up is described in the experimental section. The normalization was carried out on the low-energy tail of the spectra, where the re-absorption is always negligible. All the slabs show no significant decreasing in emission intensity moving from the edge to the bulk and the emission spectra overlap almost perfectly (tiny differences are likely due to microscopic defects into the slab or to matrix absorption phenomena, that in the case of red-NIR emitters could appear). To have a better comprehension of the system, the cumulated efficiency plot was taken (as said in the introduction, for a linear growth of the slab, the ideality of the summed efficiencies is a straight line with slope equal to 1, the dashed lines in figure 3.2.6 quadrant c). In the case of the p-anisidine-BIAN chelates the experimental points almost perfectly fit the ideality regime.

For the pyrene-BIAN chelate device there is a more evident decreasing in the PL, nevertheless more than 90% of the initial intensity is maintained. The efficiency values, however, fit very well with the ideality trend. This general behavior is an evidence of the absence of re-absorption processes, due to the extremely high Stoke-Shift proper of rare-earths luminescent chelates.

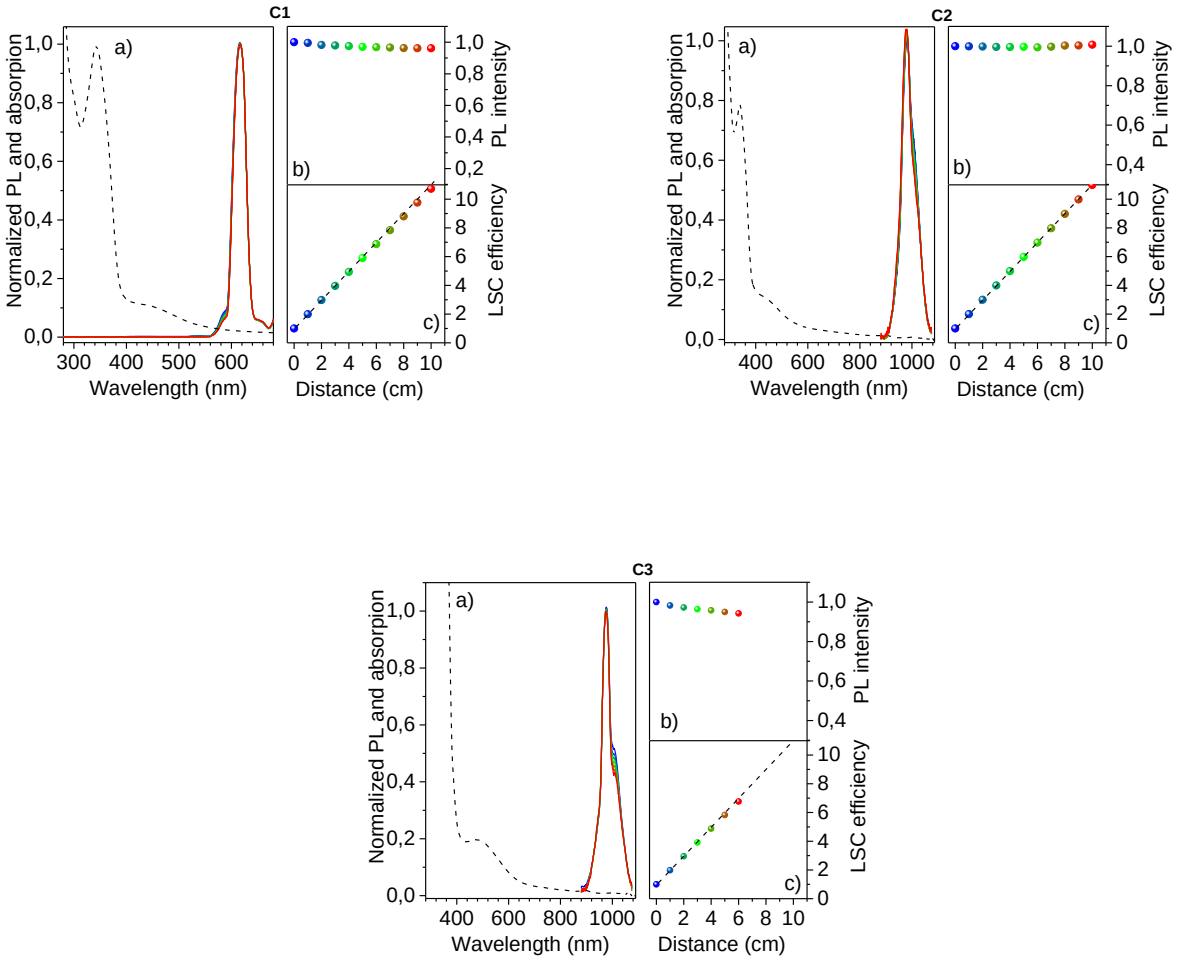

Figure 3.2.7: evaluation of red-NIR luminescence properties of the slabs. In the quadrants labeled "a", the emission spectra at various distances are superimposed to the absorption profile (dotted line). In the second "b" quadrant the normalized photoluminescence intensity is plotted versus the distance, evidencing only a slight decreasing. In the "c" quadrant the cumulated efficiency vs the distance from di edge shows no reabsorption losses while increasing the slab dimensions. For C3 based devices only six points were recorded due to the smaller dimensions of the slab.

3.2.2. Blue and green LSC for building integration.

As an appendix to the discussion on the scientific achievements and the perspectives of luminescent solar concentrator technology, it is worthy to introduce the tests done on two of the fully organic structures synthesized during the doctorate work: the subphthalocyanine dimer (FsubPcDimer), whose synthesis will be discussed in detail in the next section, and DPP-Cy-1. This preliminary characterization was attempted after an examination of the literature on the fluorophores for LSCs. Surprisingly, there is a lack of materials for blue and green LSCs[13]. As a corollary of this statement, such materials, that transmit blue and green light, should absorb in the red-NIR, having an emission in the same range. NIR emission in LSCs is monopolized by lanthanides complexes that normally show ligand absorption in the blue-violet. Organic dyes such as perylenes give panels with colors spanning from orange to red. In the field of *building integration,* the color of LSCs is not a secondary issue. The building integration is the architectural approach aimed to integrate energy producing systems into buildings in a harmonic an aesthetically pleasant way. Taking into account that the European Renewable Energy Framework Directive state that 20% of energy has to come from renewables within 2020 and that, in Europe, the energy consumption of buildings counts for 40% of the total[14], the building integration of solar power generators is crucial. The silicon solar panels on the roofs are sometimes considered foreign elements in the urban context Large fields of solar panels that are nowadays installed in rural areas, subtracting precious soil to agriculture, could be displaced in already anthropic environments. Such problems fuel the research on low-visual and spatial impact solutions[15,16]. LSC technology is aimed to reduce the amount of silicon solar panels required to produce the same amount of energy and it is simple to implement for large areas in urbanized contexts. One can substitute normal windows with energy-generating ones in tall, large-surface buildings

like skyscrapers. Obviously, the color of the light in the interiors, like in an office, is extremely important for health and even for productivity of the workers. Yellow, orange or red light is not indicated in this context, while blue or green window could lead to a more pleasant and relaxing environment. Moreover, one can think to implement blue and green LSC in the automotive context, replacing windshields and windows, in order to generate electricity for the on-board electronics. The color in this case is even more important because it should interfere as less as possible with the surrounding environment colors.

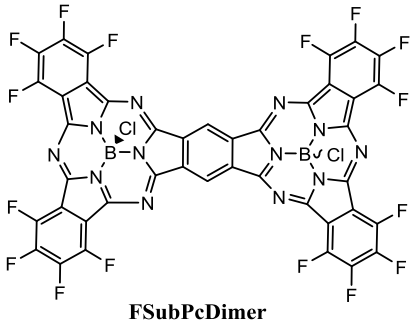

FSubPcDimer

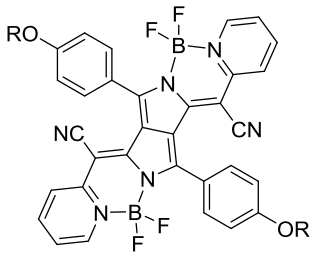

DPP-Cy-1

R= 3,7 dimethyloctyl

Figure 3.2.8: up, rendering of a Tesla Model S in which the windshield is made of an LSC sheet using subpc dimer as fluorophore. Down, rendering of Unicredit Tower in Milan showing the impact of covering the surface with LSCs based on DPP-Cy (left) and subpc dimer (right).

In this framework, two PMMA slabs with a concentration of 10^{-4} M of DPPCy and dimer were prepared and the quantum yields of the slabs measured, giving a value of 26±5% for the DPP-Cy and 24±5% for the subphthlocyanine dimer.

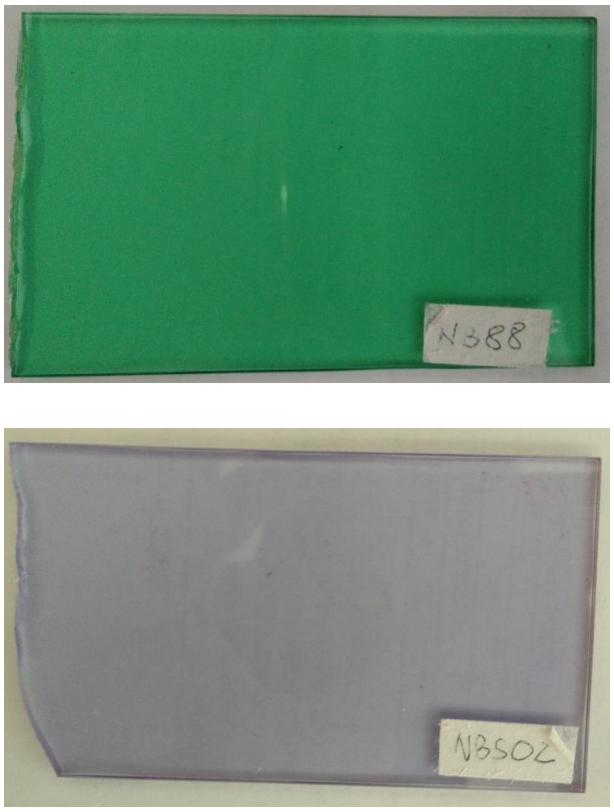

Figure 3.2.8: green and blue LSCs, using respectively DPP-Cy and dimer D1 as florescent materials.

The 3 mm thick slabs were prepared following the same procedure described for lanthanides-based LSCs. A pre-polymerization was carried out using AIBN as initiator and, after addition of the organic dyes and the secondary initiator lauroyl peroxide, polymerization at 56 °C and post-curing at 100°C were performed Both species

demonstrated to be stable to the radical polymerization conditions, with no appreciable change in the optical properties with respect to the molecules in solution.

As reported in the synthesis section, the Dpp-Cy shows a Stokes-shift of about 70 nm while in the dimer the absorption and emission bands are almost superimposed. The expected re-absorption losses should be significant for both systems. An analysis of the photoluminescence decay and of the re-absorption losses have been performed in the same fashion previously described for Ln-based LSCs. As expected, the photoluminescence output decreases in both cases with the distance from the edge and stabilizes at around 40% of the initial value after 6-8 cm. The cumulated efficiency deviates from the ideality after around 2 cm. This behavior can be considered normal for organic dyes than do not present engineered Stokes-shift. It is also interesting to note that the emission peaks tend to red-shift with the increasing distance. This is probably due to the re-absorbed light that is re-emitted again by another fluorophore with a net dissipation of energy.

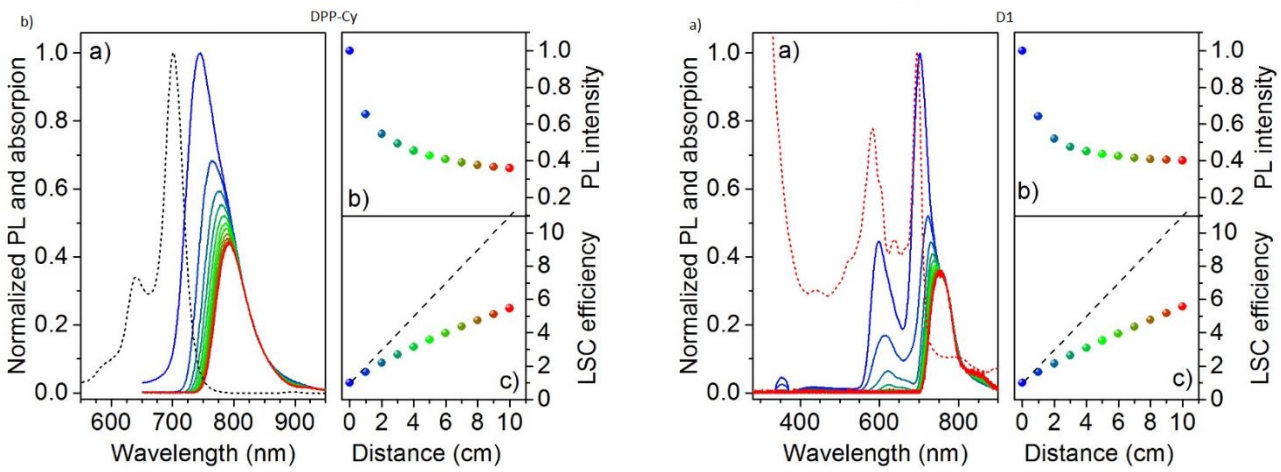

Figure 3.2.9: the graphics report in a) the evolution of the emission spectra with the distance, superimposed to the absorption profile (dotted line), in b) the photoluminescence decay vs the distance to the edge and in c) the cumulated efficiency reported as a sum of efficiencies of 1 cm "slices" of concentrator to evidence the re-absorption

3.2.3 Experimental procedure

Slab preparation. In a typical procedure for the preparation of a 0.1 % slab, 100 mg of AIBN were dissolved in 100 ml of freshly distilled MMA. The solution was placed in a beaker and slowly heated on a hot plate until the temperature of 80 °C was reached. This temperature was maintained for 2 minutes, during which time viscosity increased substantially. The solution was immediately transferred in an ice bath and cooled at 20°C. A solution of rare earth complex (160 mg) in freshly distilled MMA (60 ml) was added along with 150 mg of lauryl peroxide. The viscous syrup thus obtained was poured in a mold of 3 mm thickens and 100 cm^2 area and heated in a water bath at 56°C for 48 h. At the end of this thermal treatment the syrup turns into a solid slab that is further cured at 95°C for 24 h in a oven. After cooling, the slab was separated by the glass mould, cut and polished for optical measurements.

Photoluminescence measurement. The photo physical characterization of the LSCs were performed illuminating a spot of the larger surface of the slab with a titanium-sapphire. The light was guided through an optic fiber, varying the distance to the edge. The laser power output from the edge was measured using a CCD PHIR Nova PD300-3 photodiode. The setup scheme is reported in the figure.

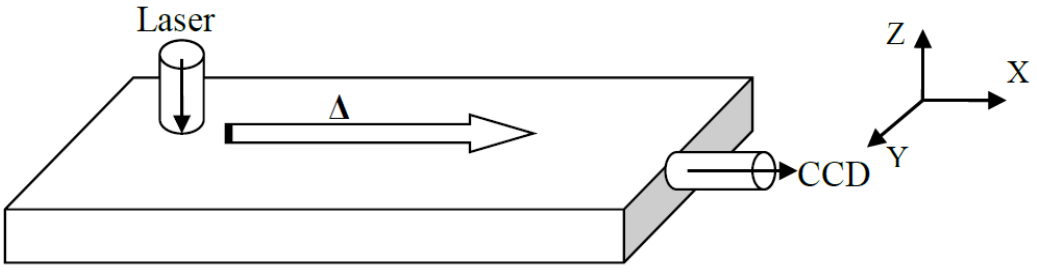

3.2.4 Bibliography

1. http://www.telefree.it/news.php?op=view&id=54374
2. Batchelder, J. S., A. H. Zewai, and T. Cole. "Luminescent solar concentrators. 1: Theory of operation and techniques for performance evaluation." Applied Optics 18.18 (1979): 3090-3110.
3. Debije, Michael G., and Paul PC Verbunt. "Thirty years of luminescent solar concentrator research: solar energy for the built environment." Advanced Energy Materials 2.1 (2012): 12-35.
4. Beverina, Luca, and Alessandro Sanguineti. "Organic Fluorophores for Luminescent Solar Concentrators." Solar Cell Nanotechnology (2013): 317-355.
5. van Sark, Wilfried GJHM, et al. "Luminescent Solar Concentrators-A review of recent results." Optics Express 16.26 (2008): 21773-21792.
6. Binnemans, Koen. "Lanthanide-based luminescent hybrid materials." Chemical reviews 109.9 (2009): 4283-4374.
7. Kalyani, N. Thejo, and S. J. Dhoble. "Organic light emitting diodes: Energy saving lighting technology—A review." Renewable and Sustainable Energy Reviews 16.5 (2012): 2696-2723.
8. Werts, Martinus HV. "Making sense of lanthanide luminescence." Science progress 88.2 (2005): 101-131.
9. Crosby, G. A., R. E. Whan, and R. M. Alire. "Intramolecular energy transfer in rare earth chelates. Role of the triplet state." The journal of chemical physics 34.3 (1961): 743-748.
10. Dexter, D. L. “A theory of sensitized luminescence in solids.” J. Chem. Phys. 1953,21, 836–850.
11. Forster, T. “Excitation transfer and internal conversion.” Chem. Phys. Lett. 1971, 12,422–424
12. Turrisi, Riccardo, et al. "Stokes shift/emission efficiency trade-off in donor–acceptor perylenemonoimides for luminescent solar concentrators." Journal of Materials Chemistry A 3.15 (2015): 8045-8054.
13. Reda, S. M. "Stability and photodegradation of phthalocyanines and hematoporphyrin doped PMMA as solar concentrators." Solar Energy 81.6 (2007): 755-760.
14. Chemisana, Daniel, et al. "Building integration of concentrating systems for solar cooling applications." Applied Thermal Engineering 50.2 (2013): 1472-1479.
15. Kalogirou, Soteris A. "Building integration of solar renewable energy systems towards zero or nearly zero energy buildings." International Journal of Low-Carbon Technologies 10.4 (2015): 379-385.

16. Malara, Francesco, et al. "Smart Windows for Building Integration: A New Architecture for Photovoltachromic Devices." ACS applied materials & interfaces 6.12 (2014): 9290-9297.

3.3 Fullerene-free organic NIR-photodetectors

As a coherent conclusion of the discussion of the possible applications of NIR-operating organic molecules, it can be interesting to introduce the use of such systems in light-harvesting devices. As a broad categorization, light-harvesting organic devices could be divided into two families. The first one are organic solar cells, of the most various nature, that have to absorb the broadest part of the solar spectrum in order to rise the efficiency and to convert the largest part of incoming photons into current. For this goal, the panchromatic dyes presented in the synthesis part of this work could represent valid candidates. Due to the large covering of the solar spectrum, from visible to NIR, they could potentially ensure good efficiencies. The second family is constituted by light-sensing systems, organic photodiodes or phototransistors. As a general description, these devices have the scope to detect a particular wavelength, transducing it into a detectable electric output. As one of the prerequisites for organic molecules intended for light-sensing is a narrow absorption band, cyanine and cyanine-like structures such as squaraines, diketopyrrolopyrrolo-cyanines and subphthalocyanines are suitable materials for this kind of applications. Moreover, light-sensing devices based on organic semiconductors have the already mentioned advantages to have tunable spectral sensitivity from UV to NIR, to be processable at low temperature and to be deposed on a large variety of substrates, from more classic glass to plastic foils. They can be implemented in large area, solution-deposed systems, enabling the fabrication of scanners, imagers, X-ray detectors for biomedical applications and more futuristic plastic fibers based communication systems. In this last section, an ongoing work, focused on the application of a squaraine-subphthalocyanine active layer is presented and the first achievements commented, as well as a brief introduction on the characteristics and the importance of the NIR-detection in modern industry and academia.

3.3.1 Organic photodiodes: an overview

As reported by RP Photonic online encyclopedia, "*photodetectors (or photodiodes) are devices used for the detection of light*[1]." This general definition can be completed with a further consideration; they covert a flux of photons into a flux of charge carriers that is proportional to the intensity of the incident light. As the same of solar cells, photodiodes (or photodetectors) are based on the photoelectric effect that causes the formation of an electron-hole pair upon absorption of a photon. The exciton is split into free charge carriers that can travel through the material towards the electrodes where they are collected, generating a current flow. The main difference with a photovoltaic cell is that, for the latter, the scope is to generate enough power for an external load, while photodiodes have to generate a detectable photocurrent signal.

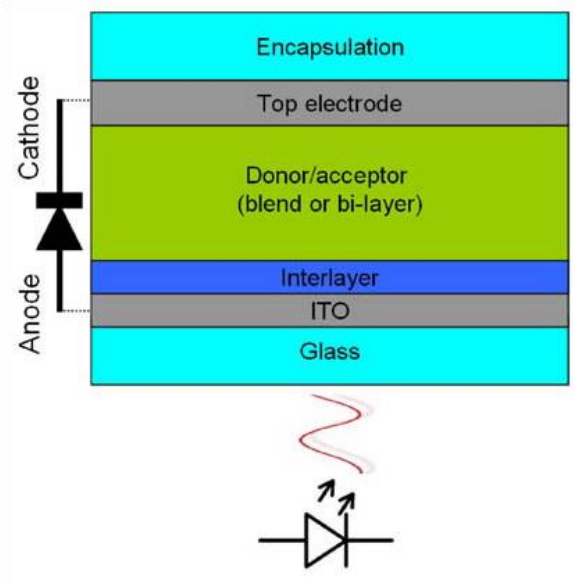

Figure 3.3.1: scheme of a photodetector based on organic semiconductors deposed on a conductive glass substrate. Adapted from[2].

Due to the structure of the present manuscript, it is important to focus on the core of photodetector devices, the active organic layer. It is composed by a donor material and an acceptor one. When a quantum of energy is absorbed by the donor, an electron is promoted from the HOMO to the LUMO level, generating an exciton. If the LUMO level of the acceptor is lower, but close enough to the LUMO of the donor, an electron is transferred to the acceptor (the same process can be described from the hole's side). After the splitting of the exciton, the free carriers can travel through the material driven by the electric field toward the electrodes (usually ITO as anode and a metal such as aluminum, silver or gold as a cathode). The collected charges generate the electric flow that is electronically transduced into a signal.

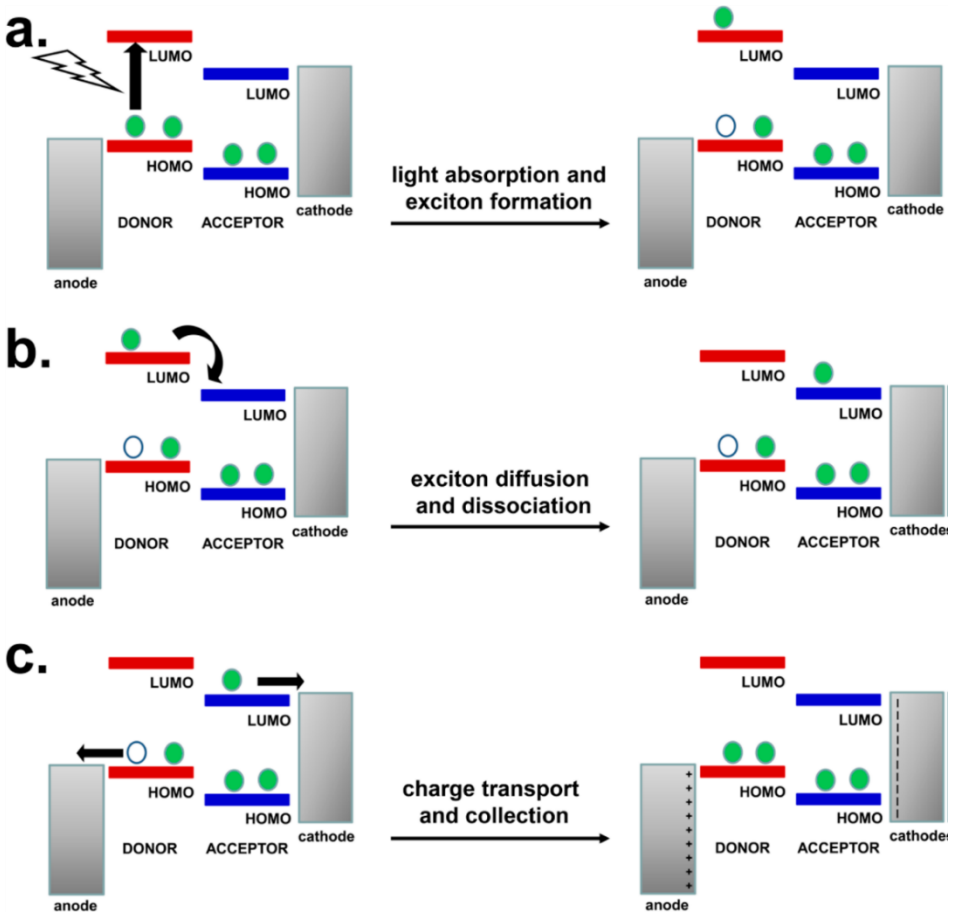

Figure 3.3.2: scheme representing the processes involved in the charge generation upon illumination in a donor-acceptor blend. Reprinted from[3].

Several parasitic processes can affect the final device efficiency, such as charge recombination of electrons and holes into the active layer or traps due to specific fabrication defects. The detailed description of such processes has been extensively reviewed in the dedicate literature[4].

The active layer could be deposed following two main geometries: bilayer geometry and bulk-heterojunction architecture. The first solution is simply described by a planar interface between a thin film of donor material and a layer of acceptor. More interesting for the discussion is the bulk-heterojunction structure (BHJ). In this case the donor and the acceptor are blended together, forming nano- and micro-domains, increasing the interface area between the materials, facilitating the exciton splitting. This solution was firstly reported by Heeger in 1995[5] for photovoltaic devices, paving the way to a highly-impact research field.

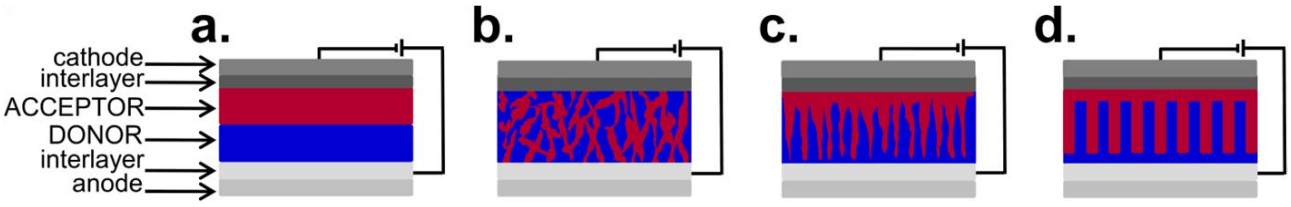

Figure 3.3.3: different junction types between donor and acceptor. a) planar junction, b) bulk heterojunction, c) disordered junction with vertical interdigitation, d) ordered or patterned solar cell. Adapted from[3].

Unless the major part of the literature on BHJ systems is focused on organic solar cells, the basic structure of a photodetector is the same, including the active layer structure (actually an organic solar cell could be considered a large area photodiode). For this reason, all the materials used for solar cells can be virtually applied for light detection.

The main difference is the final goal and the operative conditions (unbiased for solar cells, under external applied voltage for photodetectors). As in solar cells, the class of materials used for light detection are roughly two: polymers and small molecules. While polymer-based devices are a well-established technology and generally show excellent performances, the implementation of small molecules present some advantages:

- Well defined chemical structure that avoid the problems of reproducibility due to the control of polydispersity, or regioregularity.
- High carrier mobility.
- Good control of structure-properties relationship, in terms of conductivity and morphology, and how they affect the performances of the final device.
- Dyes with high molar absorptivity are useful in lowering the thickness of the active material, lowering parasitic resistances and helping the cost reduction of the final product.
- Ease of synthesis and purification, as well as strong tenability of the properties by chemical manipulation.

As mentioned in the first chapter, lowering the band gap is the strategy to move towards polymers and small molecules operating in the NIR[6]. A general overview on the system used to detect NIR light, as well as applications of such technology are presented in the subsequent section.

3.3.2 Near-infrared Light-sensing: applications and materials

Unless it could appear as a niche application, detection of infrared light is extremely important for industrial applications. For everyday uses one can think about remote control or contactless thermometers or infrared cameras. More sophisticated and scientifically fashionable applications include telecommunication, night vision and surveillance systems and chemical or biological sensing. The flexibility that organic materials allow, makes possible the implementation on flexible substrates with spectacular results: a device miming the function of a human eye was published by Xu et al. in 2008, printing a matrix of OPDs on a PET hemisphere[7].

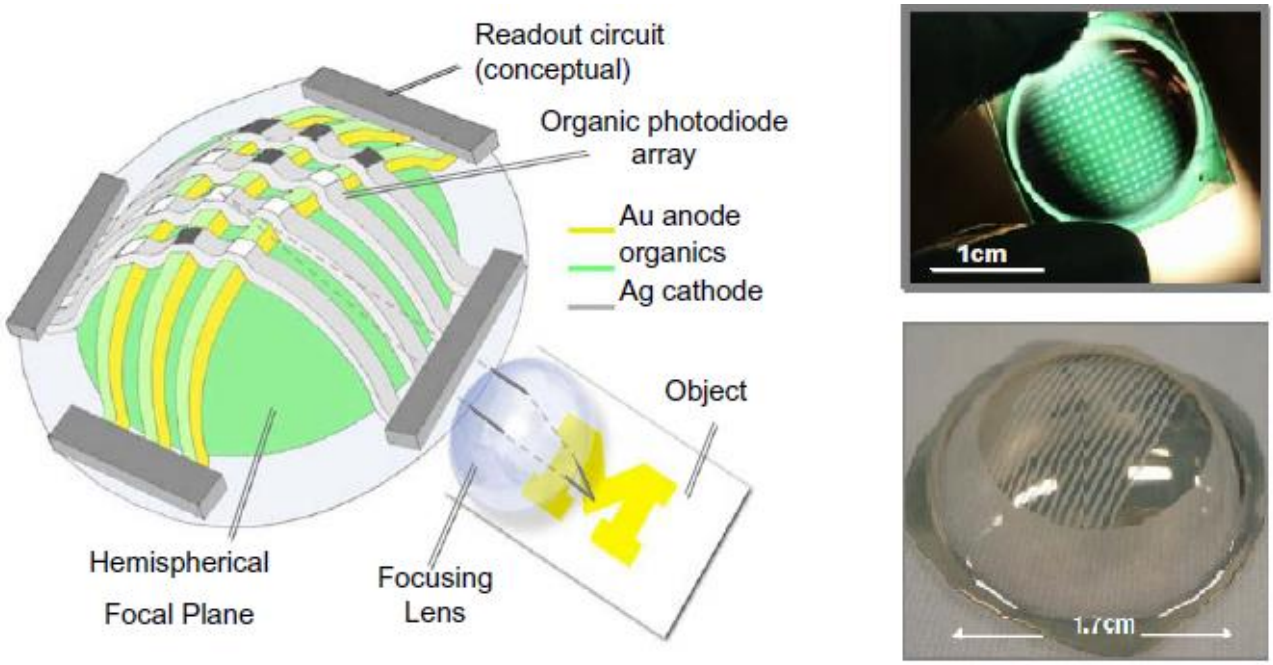

Figure 3.3.4: array of OPD printed on a curve PET surface. This experiment could boost the research towards artificial bio-compatible electro-optic prosthesis. Adapted from[7].

Another industrially interesting application of OPD is in plastic optical fiber-based transceivers (POF). Optical fibers became popular in the past decades for telecommunication, sensors and industrial automation and POF could potentially replace standard silicon-based fibers due to light-weight, ease of fabrication and lower cost. POF-based optical system was proposed by Homori et al. in 2004, integrating an OPD and an OLED with a plastic optical fiber[8]. A spray-coating deposed OPD was fabricated directly at the cutting edge of a POF (Binda et al.[9]), showing the great flexibility of OPD systems.

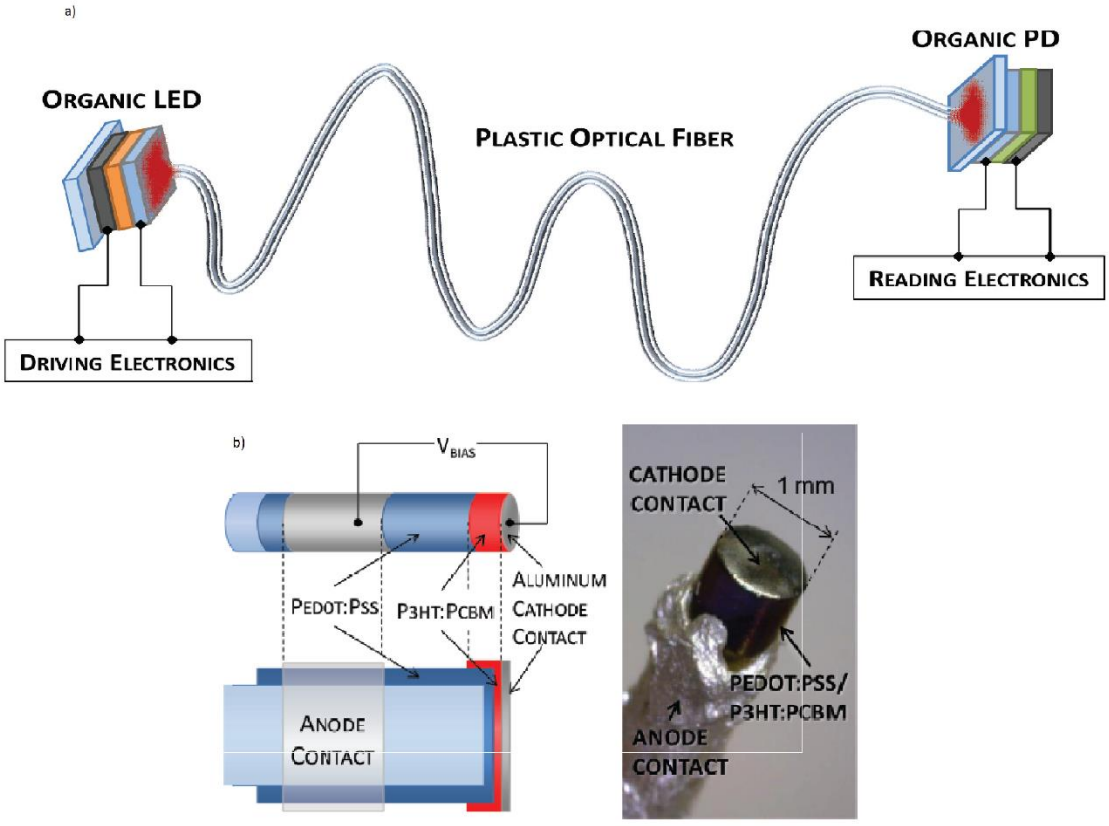

Figure 3.3.5: OPD can be implemented in POFs in order to obtain entirely plastic made, long-distance transceivers. Adapted from[4,9].

Potentially low-cost OPD active in the red-NIR using low-bandgap polymers could be produced by drop-on-demand (DOD) inkjet-printing techniques, as demonstrated by Azzellino et al.[10] in 2013.

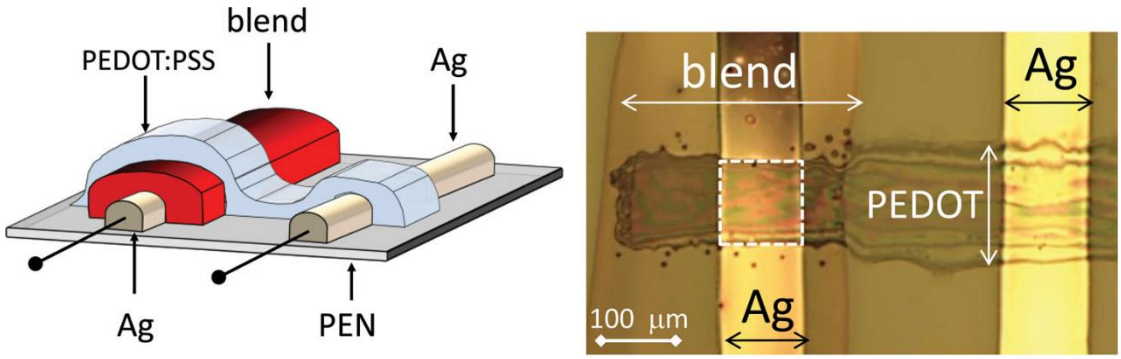

Figure 3.3.6: red-NIR OPD completely printed on a plastic foil. Adapted from [10].

From the materials point of view, the BHJ technology is dominated by the well-established and investigated couple P3HT-$PC_{61}BM$ (poly-3-hexylthiophene/Phenyl-C61-butyric acid methyl ester). As previously described, lowering the band-gap is the strategy to move towards NIR-active compounds and, thus, NIR operating devices. Many NIR-operating polymers for OPDs show the typical D-A-D structure, inherited from the systems used for solar cells. This kind of polymers show band gaps in the range 0.7-1.2 eV, corresponding to absorption bands in the range 700-1400 nm[11-15]. Conversely, only few organic small-molecular structures have been employed for NIR-OPD, despite the very interesting features organic dyes show, in terms of optical properties and levels tunability. Among the most prominent achievements, in is worthy to mention the 2011 work by Binda et al[16]. using a squaraine dye, absorbing at 700 nm and showing high detectivity.

A macrocyclic compound too, a zinc porphyrin, have been used in OPD, showing activity in the region 380-960 nm[17] as well as mixed pyrrolo-thiophene oligomers, presented by Wang et al.[18] in 2014, that showed high specific detectivity at 800 nm. The following table present a selection of structures for NIR-OPD:

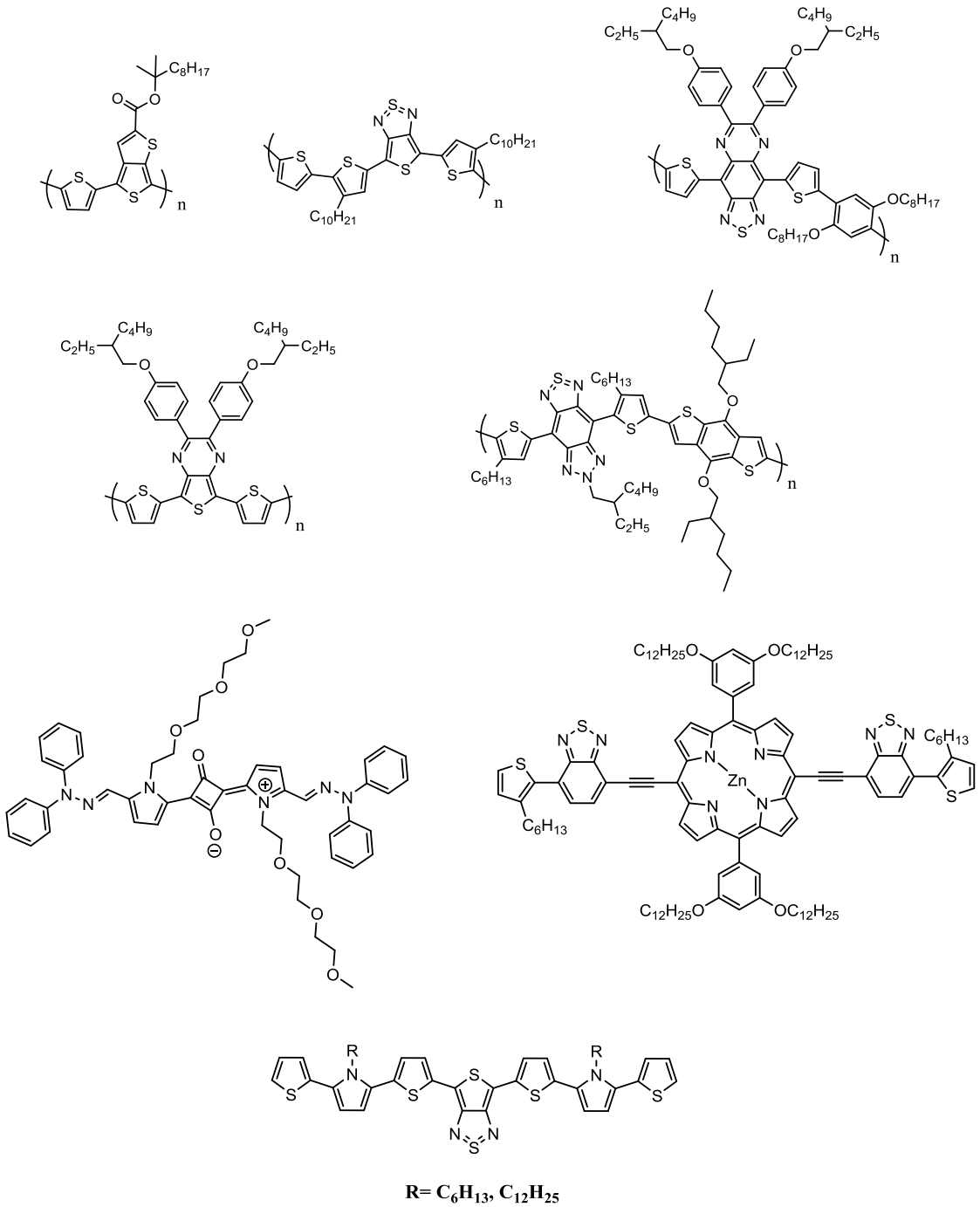

Figure 3.3.7: selection of materials used for NIR light detection.

At this stage, an observation could come to the reader's mind. All the BHJ light-sensing devices described above show variation in the donor material, while the acceptor is always $PC_{61}BM$. Actually, fullerenes derivatives dominate the market of small molecular acceptors for organic photovoltaic, essentially due to the good tendency to accept extra electrons from the donors and the high electron mobility[19].

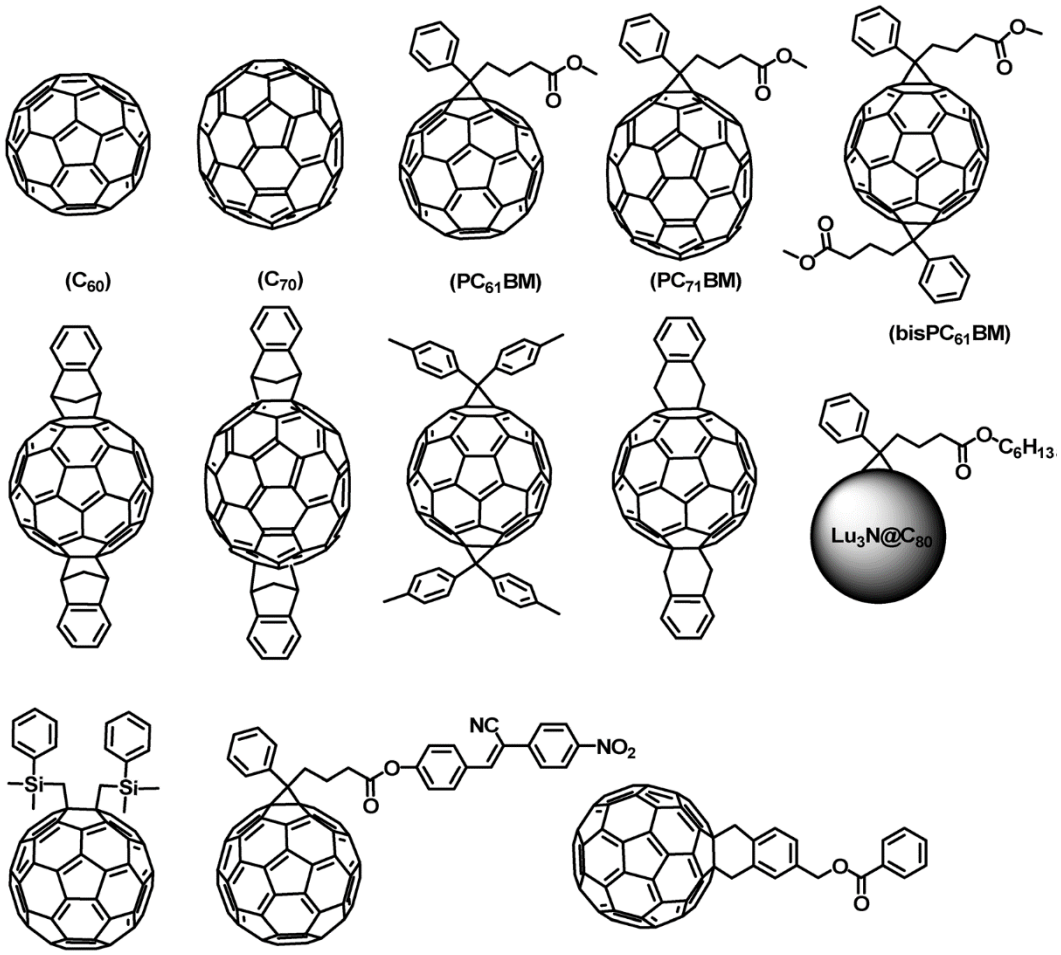

Figure 3.3.8: selection of fullerene-based acceptors. Fullerenes are the most used n-type materials in organic photovoltaics. Adapted from[19].

Although the popularity and the effectiveness of fullerenes, they present some weakness points:

- The high price, especially for C_{71} derivatives, limits the large scale usage (Sigma-Aldrich supplier sells $PC_{61}BM$ and $PC_{71}BM$ at around 2000 and 2600 €/g respectively).
- Limited possibility of chemical manipulation. Basically only Prato and Bingel reactions are used to functionalize fullerenes, limiting the possibilities of tuning the levels and to introduce new features.
- Low molar absorption coefficients.
- Low solubility

In the past years, an entire new field of research arose, aiming at substituting fullerenes as dominant materials in OPV. Fullerene-free devices have been produced, reaching good values of efficiency, exploiting the chemistry of dyes and pigments. Rylene diimides succeeded as high-performance n-materials due to the good photostability, the ease of band gap tuning, the high electron mobility and high electron affinity and the large extinction coefficients. In a recent paper by Sun et al.20, a perylene bisimide dimer was used as an acceptor in BHJ solar cells, reaching an efficiency value exceeding 7%.

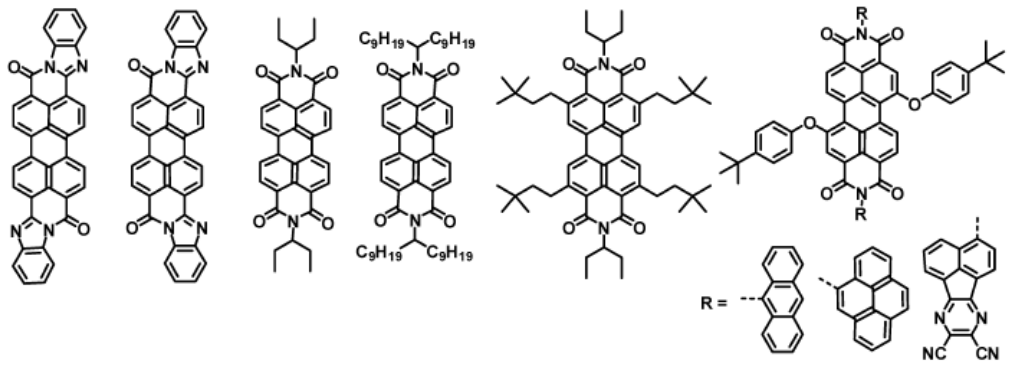

Figure 3.3.9: perylene bisimide acceptors used in OPV. Adapted from[19].

Beside rylene dyes, several other structures showed interesting properties as n-materials. The most used strategy to add fluorine or nitrile groups to the scaffold. In this way, it is possible to turn donors such as acenes, phthalocyanines or oligo-thiophenes into acceptors. DPP and functionalized fluorenes demonstrated electron-transport capability too and a non-exhaustive panel of structures is reported in figure 3.3.10.

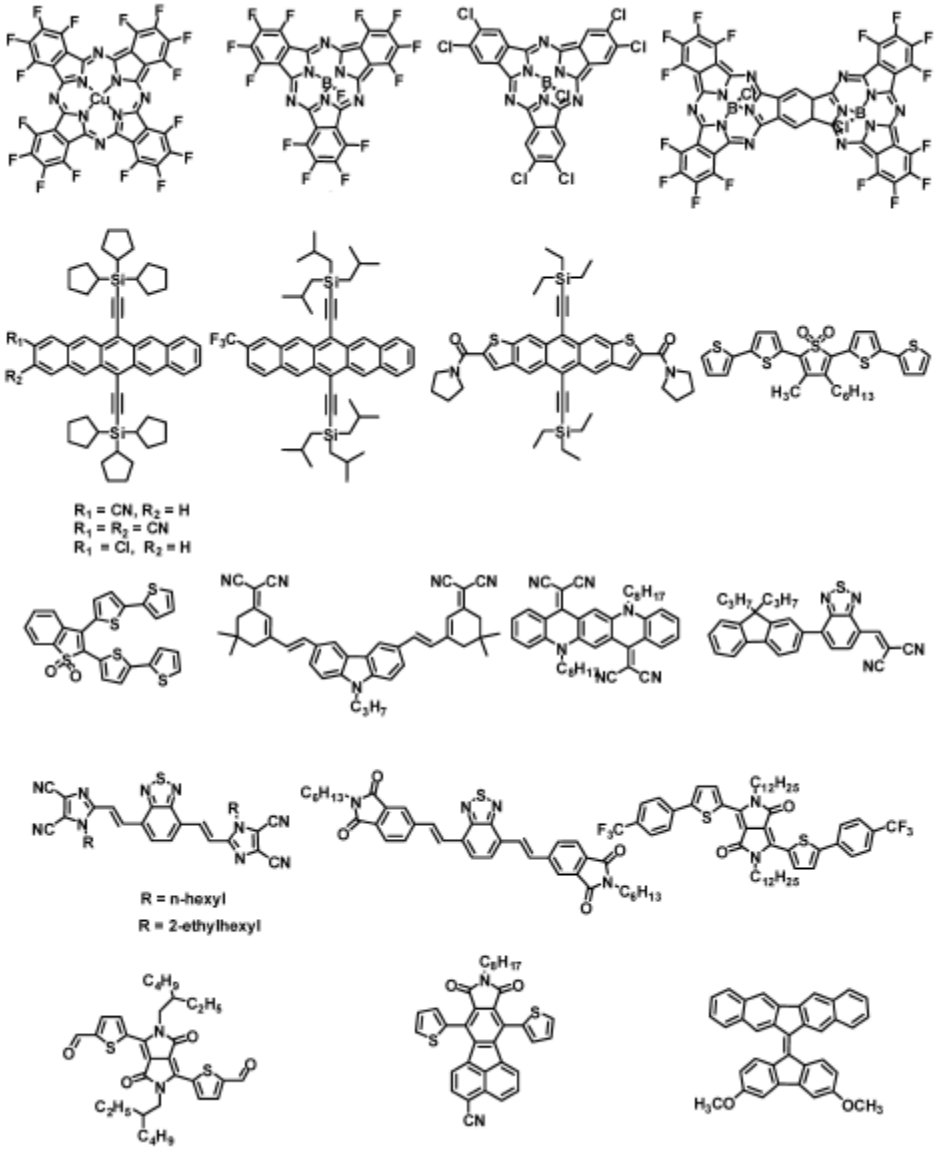

Figure 3.3.10: array of n-type materials for OPV. Adapted from[19].

Even subphthalocyanines, whose chemistry have been described in depth in chapter two, can be employed as n-type materials. In 2014, Torres and co-workers reported the use of hexa-chloro subphthalocyanine as non-fullerene acceptor in planar heterojunction organic solar cell, using a subnaphthalocyanine as donor, with low recombination losses and a claimed efficiency of 6.4%[21]. Subphthalocyanine was also employed as acceptor by Knops et al. in a multi-absorbers configuration with naphthalocyanine, in order to harvest a large portion of light and to improve exciton dissociation by cascade process. The benchmarking reported efficiency was 8.4%[22]. A remarkable efficiency of 4% was reported in 2011, once again by Torres[23], using a perfluorinated dimer of subphthalocyanine as acceptor and non-substituted chloro-subphthalocyanine as donor, in planar heterojunction configuration. The work reported the use of a 1:1 mixture of *syn* and *anti*-isomers that showed the same characteristics of the separated species. The dimer showed good coverage of the solar spectrum, with the Q band at 700 nm, significantly red-shifted with respect to a standard single-core subpc. All the devices reported in this state-of-the-art summary report planar junctions, with layers deposed by thermal evaporation of the organic materials. To the best of the author's knowledge, only one example of solution-deposed BHJ devices have been reported so far. Ebenhoch et al. reported the use of axially substituted hexachloro- and hexafluoro-subphthalocyanine monomer as acceptor in polymer-based solar cells. The highest reported value was 3.5% using PTB7 as donor[24].

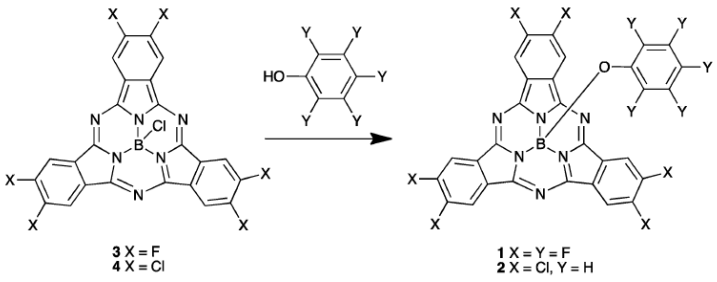

Figure 3.3.11: acceptors used in solution-processed OPV. Reprinted from[24].

Subphthalocyanines have been tested as acceptor materials for organic photodiodes too. Bender and co-workers produced green light sensitive OPD using subphthalocyanine axially substituted with a strong acceptor such as perfluoro phenol. The study reported different Donor-acceptor blends, including a completely subpc-based one (chloro-subpc as donor-perfluorophenol-subpc as acceptor)[25].

Taking into account the results achieved so far in the field of subphthalocyanine as n-type materials, the following section reports an explorative experiment set aimed at proving the suitability of perfluoro-subpc dimer as acceptor in fullerene-free, solution-processed OPD. The material is used in tandem with a squarainie dye as a donor, in order to maximize the light-harvesting. The two compounds absorb in the red-NIR part of the spectrum (around 700 nm), giving the extra-feature of NIR light-sensing to the devices. The work is intended as a proof of concept and an attempt to broaden the knowledge about NIR compounds activity and to enrich the possibilities to apply non-fullerene small molecules.

3.3.3 SubPc dimer as an acceptor for BHJ light-sensing devices

The materials used in this work have been chosen after a careful analysis of the literature. As donor material an hydrazonic end-capped squaraine was used. This compound was previously studied in planar photodetectors, operating in the red-NIR range of the spectrum, based on a bulk-heterojunction of squaraine dyes and $PC_{61}BM$ as active materials. Long-term air stability, good balance between hole and electron mobility and fast response speed were achieved[16]. Structurally, it is a pyrrolic squaraine, in which the pyrrolic nitrogens are alkylated with glycolic chains, in order to enhance the solubility of the dye. This functionalization is carried out directly on 2-formylpyrrole to give compound 1. Condensation with diphenylhydrazine gave the electron-rich compound 2 in good yield. The final condensation with squaric acid was carried out in standard conditions under azeotropic distillation of water in toluene-buthanol mixture.

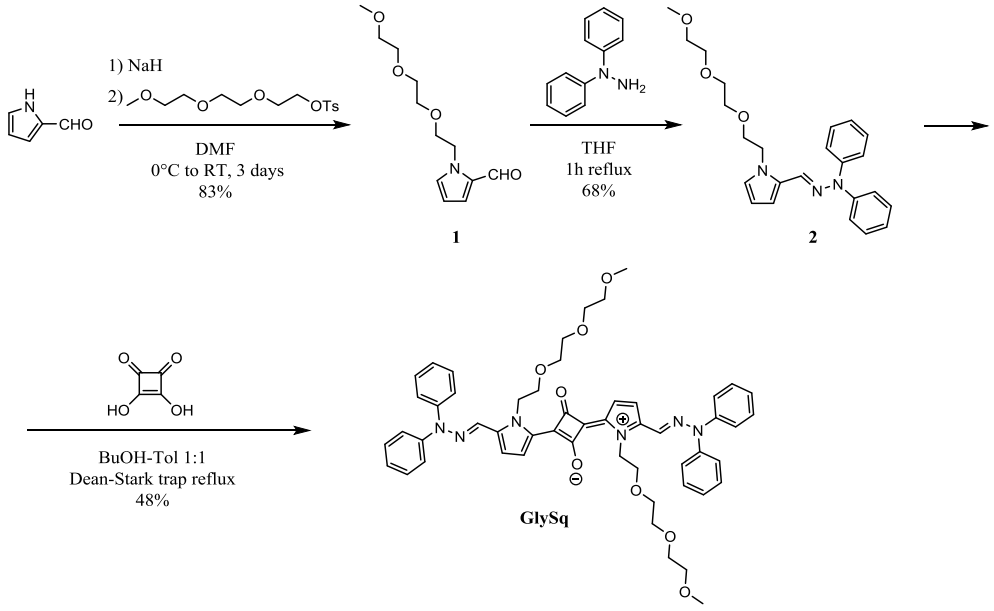

Scheme 3N: synthesis of squaraine donor GlySq.

The synthesis of subphthalocyanine dimer (FSubPcDimer) was carried out adapting the literature procedure[26]. A solid mixture of tetracyanobenzene and tetrafluorophthalonitrile (1:10 ratio) was heated up until melting of the latter. As soon as tetracyanobenzene dissolves, the templating agent was added (BCl_3 1M in p-xylene). After column chromatography the 1:1 mixture on *syn* and *anti*-dimer was separated from the perfluoro-monomer (that is a visible-absorbing crystalline compound, useful as an acceptor too). The dimer was used as a mixture of isomers for all the blends tested.

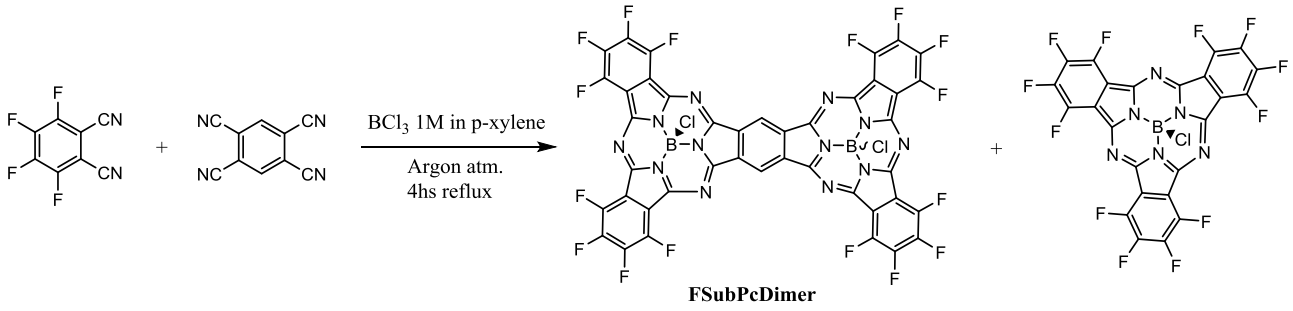

Scheme 3O: synthesis of acceptor FSubPcDimer.

As a first characterization, the properties of thin films were analyzed by UV-Vis. Different blend ratios of dimer and squaraine (1:1, 1:2, 3:1) were deposed by spin-coating on glass-ITO substrates and annealed at 60°C during one hour. The traces show a broadening of the bands that resulted in overlapping. The main band onset is located at around 550 nm and the band's tail extends to about 900 nm, covering a broad portion of the red-NIR region. The spectrum corresponding to the 3:1 dimer/sq ratio show a more structured profile, due to the prevalence of the dimer component. However, the dual absorption of donor and acceptor in the region of interest was highlighted.

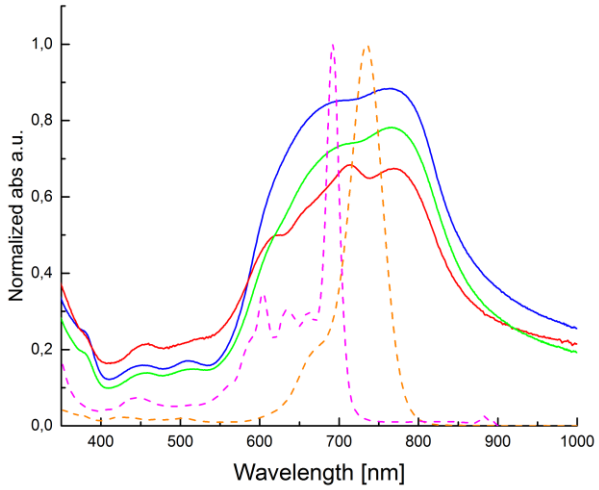

Figure 3.3.12: normalized absorption traces of D-A blend thin films (1:1, green line, 2:1, blue line, 1:3, red line) deposed from chloroform. The dashed lines represent the absorption of dimer (pink line, λmax=701 nm) and squaraine (orange line, λmax=730 nm) in diluted chloroform solution.

The second step made to characterize the materials was to proof the actual capability of FSubpcDimer to act as an acceptor when blended with a donor. This confirmation was achieved by L-ESR (Light Induced Electron Spin Resonance) measurements. This technique can actually give experimental evidences for photoinduced charge separation in a donor-acceptor blend independently from the device architecture. ESR (or EPR) is a resonance technique that identify species bearing unpaired electrons. In this case the species carrying an unpaired electron is the radical anions of the dimer. Upon illumination, the generated excitons that reach the D-A interface can split, resulting in a vacancy on the donor (the squaraine) and an electron on the acceptor, that can be detected[27]. The experiment was carried out on three films: a film of pristine dimer, one of pristine squaraine and one of the 1:1 blend of donor and acceptor. The layers were spun on glass substrates and cooled down to 130 K. All the substrates were illuminated using a xenon lamp at the power of 1 sun and the ESR traces were recorded.

As reported in figure 3.3.13, there is no photogeneration of charges in the pristine films, while in the blend one can recognize the actual detection of an umpaired electron due to the charge transfer from the squaraine to the subphthalocianine dimer.

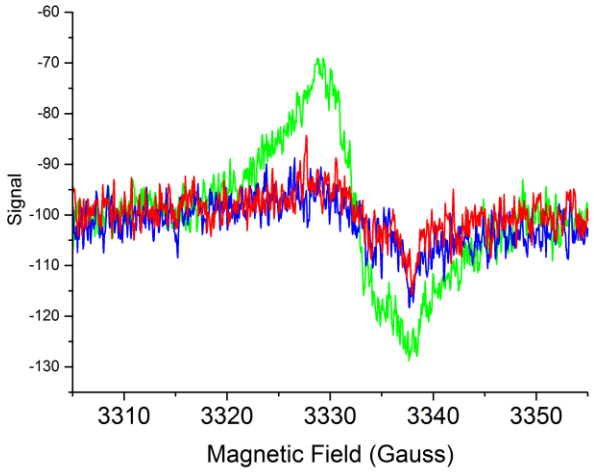

Figure 3.3.13: L-ESR signals of thin films of dimer (blue line), squaraine (red line) and 1:1 blend of D and A (green line).

Once the suitability of the dimer as a n-material in BHJ thin films was confirmed, a set of devices was produced. The OPDs produced had the architecture ITO/PEDOT:PSS/SQ:PCBM/Al. Onto commercially available pre-patterned glass-ITO substrates, a PEDOT:PSS interlayer was deposed by spin coating. Than active layer was deposed by spin coating from chloroform solution. The three D-A ratios (1:1, 1:2, 3:1) were tested to have a general overview on the devices behavior. The final step was the deposition of the cathode by evaporation of aluminum in evaporation chamber. This configuration does not represent an optimization of the conditions but is intended as a preliminary explorative trial and a proof of concept. In particular, PEDOT:PSS is suspected to be not the ideal choice to achieve high performance[28,29,30]. It is an intrinsically acidic material due to the sulfonic residues and this could affect the stability of squaraine dyes.

The EQE profiles of the devices at different voltage were recorded. In the photovoltaic mode, at 0 bias, the EQE of the 1:1 blend is higher than the 1:2 and 3:1. The same behavior is shown when a constant bias of 1 V is applied to the detectors. Increasing the applied voltage to 2 V, the EQE curves tend to be closer to each other and the descrepancy results negligible. This means that, increasing the voltage, the blend composition for these two active materials does not affect the EQE. This behavior is likely due to the good balance in the mobility of the two active materials.

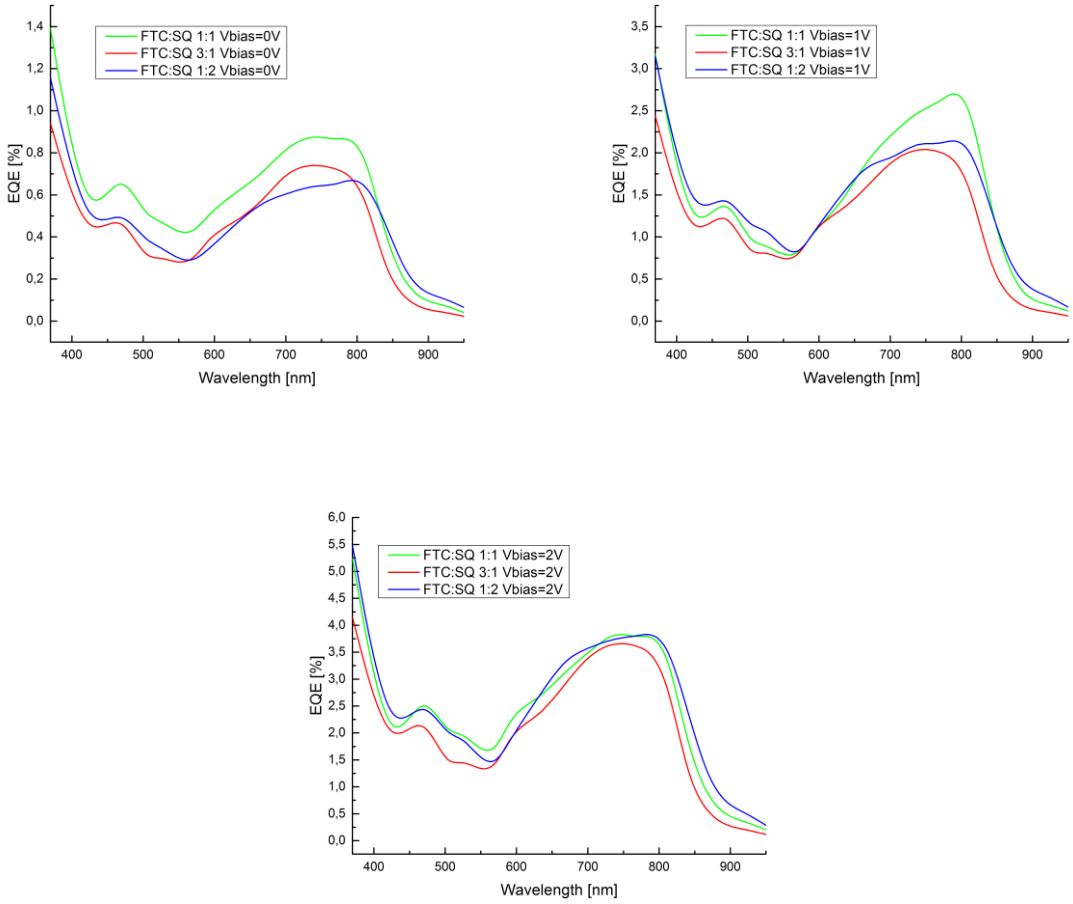

Figure 3.3.14: EQE traces of the devices, based on blends of different ratios, under increasing voltage.

The OPD photocurrent depends on many parameters such as the incident light intensity and the wavelength. In general, for a constant wavelength, the higher is the light intensity the higher is the measured photocurrent because more charge carriers are generated in the semiconductor layer. Equally important to spectral sensitivity is the linear device response on the incident light intensity. The dependence of the photocurrent on illumination intensity at 670 nm is shown in 3.3.15. The photocurrent of the 1:2 blend based diode, biased at 2 V increases linearly with increasing light intensity (r^2=0,999).

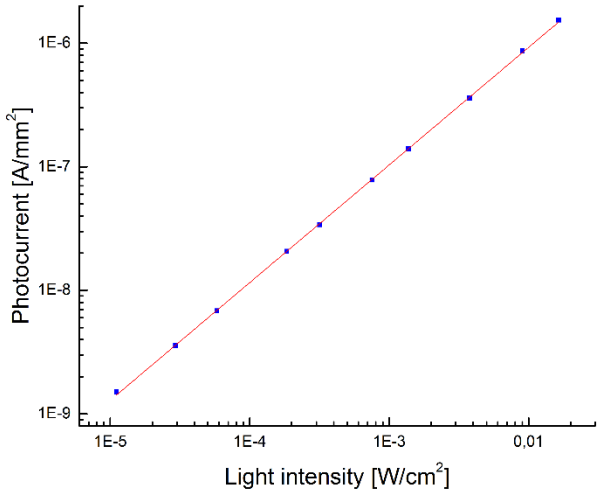

Figure 3.3.15: logarithmic plot of the variation of photocurrent with light intensity.

Further characterizations are ongoing in the moment this thesis is written. In particular, further experiments on devices with different interlayers are planned. Since PEDOT:PSS seems not to be the ideal choice, another device campaign will be carried out in order to verify the effectiveness of MoO_3 as an interlayer.

3.3.4 Experimental procedure

Devices fabrication Photodetectors based on a sandwich-like structure were fabricated on 1 mm thick glass substrates with pre-patterned indium-tin-oxide transparent electrodes. Substrates were cleaned by sonication in bidistilled water, acetone and isopropyl alcohol. Plasma treatment in O_2 was also applied. Poly(3,4-ethylenedioxythiophene) polystyrene sulfonate (PEDOT:PSS, Clevios P VP AI 4083) was then deposited by spin coating at 2000 rpm for 60'', giving a film thickness of approximately 50 nm. The active material solutions were prepared by blending subpc Dimer and GlySQ in different proportions (1:2, 1:1, 2:1, 3:1 by weight) with a concentration of 10 mg/ml in chloroform. All the solutions were stirred overnight and filtered 0.2 µm PTFE before use. Active material deposition was performed by spin coating at 100 rpm for 60 s followed by 1000 rpm for 60 s. Samples fabrication was completed by thermal evaporation in high vacuum (10^{-6} mbar) of a top aluminum electrode defining a device active area of 1 mm^2.

Optical absorbance of the deposited films was recorded in transmission with Jasco V570 UV-vis spectrophotometer. Electrical characterizations were carried on in high vacuum (10^{-5} mbar). External quantum efficiency was measured by impinging on the device with monochromatic light from LED sources in the 370-950 nm range. Light output from each LED was calibrated so that uniform light intensity across the spectrum was applied to the sample. A Siemens BPX-65 silicon detector (1 mm^2 active area) was used as the reference for calibration. The photocurrent of the device in response to the optical stimulus was recorded on an oscilloscope by means of a transimpedance amplifier. Steady state photocurrent value was taken for calculation of the EQE.

3.3.5 Bibliography

1. https://www.rp-photonics.com
2. Arca, Francesco, et al. "Near-infrared organic photodiodes." Quantum Electronics, IEEE Journal of 49.12 (2013): 1016-1025.
3. Guo, Xugang, Antonio Facchetti, and Tobin J. Marks. "Imide-and amide-functionalized polymer semiconductors." Chemical reviews 114.18 (2014): 8943-9021.
4. Baeg, Kang-Jun, et al. "Organic light detectors: photodiodes and phototransistors." Advanced materials 25.31 (2013): 4267-4295.
5. Yu, Gang, et al. "Polymer photovoltiac cells: Enhanced efficiencies via a network of internal donor-acceptor heterojunctions." Science 270.5243 (1995): 1789.
6. Dou, Letian, et al. "Low-Bandgap Near-IR Conjugated Polymers/Molecules for Organic Electronics." Chemical reviews 115.23 (2015): 12633-12665.
7. Xu, Xin, et al. "Direct transfer patterning on three dimensionally deformed surfaces at micrometer resolutions and its application to hemispherical focal plane detector arrays." *Organic Electronics* 9.6 (2008): 1122-1127.
8. Ohmori, Yutaka, et al. "Realization of polymeric optical integrated devices utilizing organic light-emitting diodes and photodetectors fabricated on a polymeric waveguide." Selected Topics in Quantum Electronics, IEEE Journal of 10.1 (2004): 70-78.
9. Binda, Maddalena, et al. "Integration of an Organic photodetector onto a plastic optical fiber by means of spray coating technique." Advanced Materials 25.31 (2013): 4335-4339.
10. Azzellino, G., et al. "Fully Inkjet-Printed Organic Photodetectors with High Quantum Yield." Advanced Materials 25.47 (2013): 6829-6833.
11. Yao, Yan, et al. "Plastic Near-Infrared Photodetectors Utilizing Low Band Gap Polymer." Advanced Materials 19.22 (2007): 3979-3983.

12. Gong, Xiong, et al. "High-detectivity polymer photodetectors with spectral response from 300 nm to 1450 nm." Science 325.5948 (2009): 1665-1667.
13. Perzon, Erik, et al. "A conjugated polymer for near infrared optoelectronic applications." Advanced Materials 19.20 (2007): 3308-3311.
14. Chen, En-Chen, et al. "Polymer infrared photo-detector with high sensitivity up to 1100nm." Synthetic Metals 161.15 (2011): 1618-1622.
15. Hu, Xiaowen, et al. "Solution-processed high-detectivity near-infrared polymer photodetectors fabricated by a novel low-bandgap semiconducting polymer." The Journal of Physical Chemistry C 117.13 (2013): 6537-6543.
16. Binda, M., et al. "High detectivity squaraine-based near infrared photodetector with nA/cm2 dark current." Applied Physics Letters 98.7 (2011): 073303.
17. Li, Lisheng, et al. "Highly responsive organic near-infrared photodetectors based on a porphyrin small molecule." Journal of Materials Chemistry C 2.8 (2014): 1372-1375.
18. Qi, Ji, et al. "Panchromatic small molecules for UV-Vis-NIR photodetectors with high detectivity." Journal of Materials Chemistry C 2.13 (2014): 2431-2438.
19. Lin, Yuze, Yongfang Li, and Xiaowei Zhan. "Small molecule semiconductors for high-efficiency organic photovoltaics." Chemical Society Reviews 41.11 (2012): 4245-4272.
20. Sun, Dan, et al. "Non-fullerene-acceptor-based bulk-heterojunction organic solar cells with efficiency over 7%." Journal of the American Chemical Society 137.34 (2015): 11156-11162.
21. Verreet, Bregt, et al. "Decreased Recombination Through the Use of a Non-Fullerene Acceptor in a 6.4% Efficient Organic Planar Heterojunction Solar Cell." Advanced Energy Materials 4.8 (2014).
22. Cnops, Kjell, et al. "8.4% efficient fullerene-free organic solar cells exploiting long-range exciton energy transfer." Nature communications 5 (2014).
23. Verreet, Bregt, et al. "A 4% efficient organic solar cell using a fluorinated fused subphthalocyanine dimer as an electron acceptor." Advanced Energy Materials 1.4 (2011): 565-568.

24. Ebenhoch, Bernd, et al. "Solution-processed boron subphthalocyanine derivatives as acceptors for organic bulk-heterojunction solar cells." Journal of Materials Chemistry A 3.14 (2015): 7345-7352.
25. Lee, Kwang-Hee, et al. "Green-sensitive organic photodetectors with high sensitivity and spectral selectivity using subphthalocyanine derivatives." ACS applied materials & interfaces 5.24 (2013): 13089-13095.
26. Iglesias, Rodrigo S., et al. "Subphthalocyanine-fused dimers and trimers: synthetic, electrochemical, and theoretical studies." The Journal of organic chemistry 72.8 (2007): 2967-2977.
27. Brück, S., et al. "Structure–property relationship of anilino-squaraines in organic solar cells." Physical Chemistry Chemical Physics 16.3 (2014): 1067-1077.
28. Chen, Guo, et al. "Solution-processed organic photovoltaic cells based on a squaraine dye." Physical Chemistry Chemical Physics 14.42 (2012): 14661-14666.
29. Guan, Zhiqiang, et al. "Power efficiency enhancement of solution-processed small-molecule solar cells based on squaraine via thermal annealing and solvent additive methods." Solar Energy Materials and Solar Cells 109 (2013): 262-269.
30. Yang, Qianqian, et al. "The improved performance of solution-processed SQ: PC 71 BM photovoltaic devices via MoO 3 as the anode modification layer." Applied Surface Science 284 (2013): 849-854.

General conclusions and perspectives

The work presented herein represents an original and improvement of the state-of-the-art of NIR compounds and an occasion to test their potential in real devices. From the synthesis point of view, some new entries in the family of organic functional materials have been achieved. Every category investigated here, squaraines, subphthalocyanines, DPP-cyanines, chelates of lanthanides, could originate an autonomous research branch that could be developed in the laboratory, in order to broaden the expertise. The *trait d'union* is the NIR activity and the band gap tailoring: the different synthetic areas have the same theoretical background and could be coordinated in order to reach the maximum scientific covering along with communication among the areas.

The work demonstrates the feasibility of DPP-cyanines as light-emitters for NIR-OLEDs and LSCs, of chelates of europium and ytterbium in red-NIR LSCs and of subPc dimer as acceptor in BHJ light-sensing devices. The fabrication and characterization of the devices was performed in collaboration with other groups. This represents a valid strategy to set up a scientific network, in order to link together different areas of science that could be not in communication otherwise. The writer's personal opinion is that scientific interchanges are essential in modern science and the stereotype of the scientist in the *turris eburnea* is over. This work represents an attempt to improve the research on NIR materials, keeping in mind this idea.

Chapter four: Experimental Section on the synthesis and characterizations of the materials

4.1 Experimental Procedures

Materials. All chemicals and solvents were purchased from Sigma Adrich, TCI Europe and Alpha Aesar. They were all used as received and not further purified. NMR spectra were recorded with a Bruker AMX 500 Avance operating at 500 MHz or with a BRUKER AC-300 (300 MHz). Melting points were determined using an OPTIMELT MV-160 apparatus and are uncorrected. Chromatographic purifications were performed using Merck 9385 silica gel, pore size 60 Å, (230- 400 mesh). Microwave enhanced reactions were performed in a CEM Discover focused oven.

Spectroscopy. Absorption spectrometry was performed using a Jasco V570 spectrophotometer. FT-IR spectra were recorded on a Perkin Elmer 100-TF Infrared operating in Universal ATR configuration. Fluorescence spectra were recorded using a Jasco FP-6200 spectrofluorimeter.

Electrochemical Measurements. Both organic solvents and electrolyte salts were purchased anhydrous from Sigma Aldrich and stored under Argon atmosphere in a M-Braun glove box (O_2 sensor sensitivity <1ppm). All organic based electrolyte experiments, both depositions and characterizations, were done in the glove box while water based experiments were performed in ambient atmosphere. Electrochemical cell was a three electrodes two compartments glass cylinder flask. Working, counter and reference electrodes were made of Au (0.0314 cm^2 active area) or Glassy Carbon (0.0707 cm^2 active area) pin, Platinum mesh and Ag/AgCl, respectively. A Princeton Applied EG&G PAR2273 potentiostat has been used for electrochemical measurements. Prior to a set of measurements in organic media, the Ag/AgCl pseudo reference electrode was calibrated using a Ferrocene 1mM solution in the corresponding organic electrolyte. Fc^+/Fc couple is +0.69V vs. NHE.

Synthesis of 5-bromo-1-octyl-1H-indole

(1A)

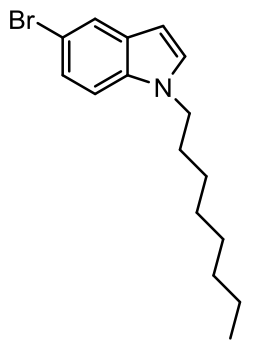

Chemical Formula: $C_{17}H_{24}BrN$

Molecular Weight: 308,26 g mol^{-1}

In a round bottom flask, in nitrogen atmosphere, bromoindole (7.00 g, 35.7 mmol) was dissolved into 60 ml of anhydrous DMF and t-BuOK (4.26 g, 38 mmol) was addt as a solid in small portions through a funnel for powders. The mixture reached 35°C (exothermic reaction) and was allowed to reach room temperature before adding bromooctane (6.98 g, 36 mmol), previously dissolved in 5 ml of DMF. A white solid appeared and the suspension was stirred at room temperature for three hours. The suspension was then poured into 200 ml of water and extracted with hexane (2x100 ml). The organic phases were dried over Na_2SO_4 and evaporated undere reduced pressure, giving a yellow oil (10 g, 32.5 mmol, 91%)

^{1}H NMR (500 MHz, $CDCl_3$): δ= 0.82 (t, J= 6.9 Hz, 3 H), 1.20-1.24 (m, 10 H), 1.76 (t, J=6.9 Hz, 2 H), 4.03 (t, J=7.2 Hz, 2 H), 6.37 (d, J=3 Hz, 1 H), 7.04 (d, J=3 Hz, 1H), 7.17 (s, 1 H), 7.21 (d, J = 1.2 Hz, 1 H), 7.69 (d, J= 1.5 Hz, 1 H).

Synthesis of 5-(1-octyl-1H-indol-5-yl)-5H-dibenzo[b,f]azepine

(2A)

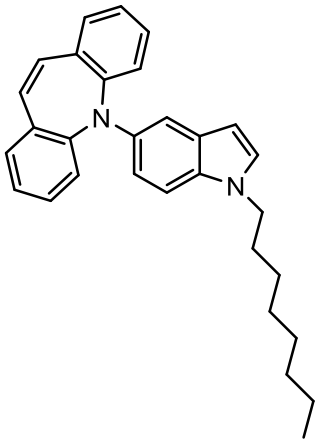

Chemical Formula: $C_{31}H_{34}N_2$

Molecular Weight: 420,60 g mol^{-1}

In a microwave flask, a suspension of azepine (1.55 g, 8.00 mmol), alkylated bromoindole (2.5 g, 8.11 mmol) and t-BuONa (0.77g, 8 mmol) in 40 ml of toluene is degassed and stirred under nitrogen atmosphere. In a second flask, tributyl phosphine (0.7 ml) and Pd(dba)3 were suspended into 5 ml of toluene and stirred for 15 minutes. The catalyst is transferred into the first flask and the mixture was heated in microwave oven at 90°C for 2 hours. After the reaction cooled down, the solvent was removed and the resulting raw mixture was separated by column chromatography (silica gel, DCM/hexane 1:1) and the product recovered as a yellow viscous oil (0.8 g, 1.9 mmol, 24%).

^{1}H NMR (500 MHz, $CDCl_3$): δ= 7.56-7.53 (t, 2H, J=7.43Hz), 7.52-7.49 (t, 2H, J=7.83Hz), 7.39 (t, 2H, J=7.43Hz), 7.11 (d, 1H, J=3.13Hz), 7.02 (d, 1H, J=9Hz), 6.84 (s, 2H), 6.18 (d, 1H, J=1.96Hz), 6.09-6.06 (dd, 1H, J1=2.35Hz, J2=6.65Hz), 3.94 (t, 2H J=7.04Hz), 1.64-1.58 (m, 2H), 1.26-1.09 (m, 10H), 0.81 (t, 3H, J=7.04).

^{13}C NMR (500 MHz, CD_2Cl_2): δ= 143.97, 142.38, 136.55, 130.83, 130.51, 130.35, 129.85, 128.66, 126.91, 109.27, 108,51, 101.79, 99.15, 45.43, 31.17, 29.75, 28.59, 26.33, 26.21, 22.02, 13.87.

Elemental Analysis calculated for $C_{31}H_{34}N_2$ 85,67% C; 7,67% H; 6,66% N. found: 85,51% C; 7,56% H; 6,52% N.

Synthesis of (Z)-2-(5-(5H-dibenzo[b,f]azepin-5-yl)-1-octyl-1H-indol-3-yl)-4-(5-(5H-dibenzo[b,f]azepin-5-yl)-1-octyl-3H-indolium-3-ylidene)-3-oxocyclobut-1-enolate

DBASq

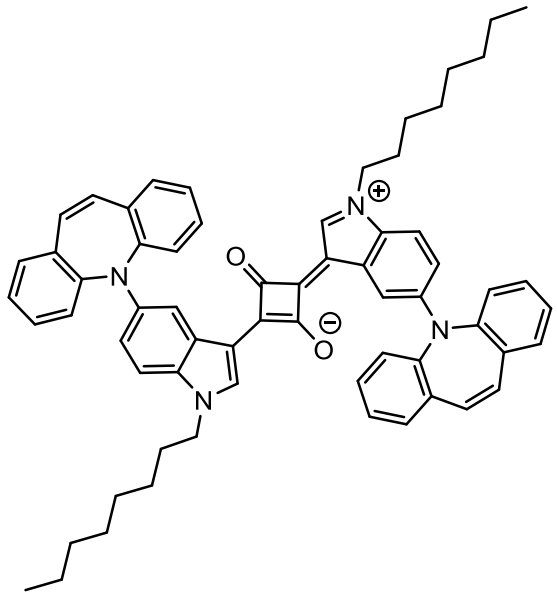

Chemical Formula: $C_{64}H_{62}N_4O_2$

Molecular Weight: 919,23 g mol^{-1}

A suspension of dibenzoazepine derivative (0.8 g, 1.9 mmol) and squaric acid (0.11 g, 0.95 mmol) was refluxed under azeotropic distillation for 3 hours. The reactions turned deep blue and a shiny precipitate formed. The reaction was allowed to cool down to room temperature and the precipitate was filtered off and thoroughly washed with methanol giving the product as a blue powder (0.46 g, 0.5 mmol, 52%).

^{1}H NMR (500 MHz, $CDCl_3$): δ= 8.81 (s, 1H, broad), 7.68-7.62 (m, 5H), 7.56-7.48 (m, 4H), 7.07 (d, 1H, J=9Hz), 6,91 (s, 2H), 6.38-6.35 (dd, 1H, J1=2.35Hz, J2=6.65Hz), 4.15 (t, 2H, J=7.04Hz), 1,93 (t, 2H, J=6,26Hz), 1.41-1.25 (m, 10H), 0.92 (t, 3H, J=7Hz);

^{13}C NMR (500 MHz, CD_2Cl_2): δ= 140.21, 130.67, 130.14, 129.23, 128.69, 127.37, 122.48, 121.80, 117.89, 110.84, 104.13, 47.55, 47.25, 27.91, 27.79, 23.52, 14.98.

Elemental Analysis calculated for $C_{64}H_{62}N_4O_2$ 83,63% C; 6,80% H; 6,10% N. found: 83,67% C; 6,77% H; 6,03% N.

Uv-Vis ($CHCl_3$): λmax= 598 nm, 471 nm, 267 nm.

Emission ($CHCl_3$): λmax= 680 nm, 721 nm, 815 nm.

Synthesis of 1-octyl-1H-indol-2-ol

(1B)

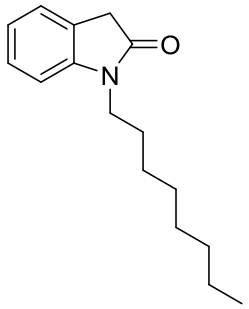

Chemical Formula: $C_{16}H_{23}NO$

Molecular Weight: 245,37 g mol^{-1}

Oxindole (20 g, 150 mmol) and K2CO3 (21.79 g, 158 mmol) were suspended into 100 ml of acetonitrile under nitrogen atmosphere. The mixture is refluxed and octilbromide (52.25 g, 270 mmol) was added through a syringe. The reaction was refluxed for totally 20 hours, then it was allowed to reach room temperature. The base was filtered away and the residual organic phase was evaporated under reduced pressure. The not reacted octilbromide was distilled away at 70°C under reduced pressure. The residual oil was separated by column chromatography (silica gel, hexane/Et_2O 9:1), recovering 1.04 g of O-alkylated and N-alkylated (18.12 g, 73 mmol, 48%).

^{1}H-NMR (500 MHz, $CDCl_3$): δ= 7.27-7.22 (quartet, 2H, J1=7.78Hz, J2=8.15Hz), 7.01 (t, 1H, J=7.41Hz), 6.83 (d,1H, J=7.78Hz), 3.69 (t, 2H, J=7.41Hz), 3.50 (s, 2H), 1.69-1.63 (m, 2H), 1.39-1.15 (m, 10H), 0.89 (t, 3H, J=7.04Hz).

Synthesis of squaraine (Z)-2-(2-hydroxy-1-octyl-1H-indol-3-yl)-4-(2-hydroxy-1-octyl-3H-indolium-3-ylidene)-3-oxocyclobut-1-enolate

(OHindolicSq)

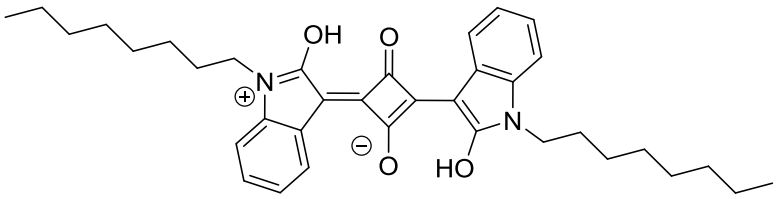

Chemical Formula: $C_{36}H_{44}N_2O_4$

Molecular Weight: 568,76 g mol^{-1}

Alkylated oxyndole (3.00 g, 12.23 mmol) and squaric acid (0.70 g, 6.11 mmol) are suspended into a mixture of toluene/buthanol 1:1 with the addition of 5 ml of H_2SO_4 96% and refluxed under azeotropic distillation of water for 2 days. A precipitate formed and was collected by filtration. After washing with methanol, the product was collected as a purple powder (1.0 g, 0.18 mmol, 30%).

^{1}H NMR (500 MHz, $CDCl_3$): δ= 7.92 (s, 2H, broad), 7.16 (s, 4H, broad), 7.01 (t, 2H, broad), 3.93 (t, 4H, J=7.45Hz), 1.80-1.75 (m, 4H), 1.40-1.22 (m, 20H), 0.88 (t, 6H, J=7.45Hz).

^{13}C NMR (500 MHz, CD_2Cl_2): δ= 182.16, 165.47, 155.07, 137.81, 124.83, 123.80, 122.29, 110.08, 42.19, 32.63, 30.05, 30.00, 29.27, 27.74, 23.47, 14.93.

Elemental Analysis calculated for $C_{36}H_{44}N_2O_4$ 76,02% C; 7,80% H; 4,93% N. found: 76,15% C; 7,83% H; 5,00% N.

Uv-Vis ($CHCl_3$): λmax= 557 nm.

Emission ($CHCl_3$): no detectable emission recorded

X-Ray diffraction

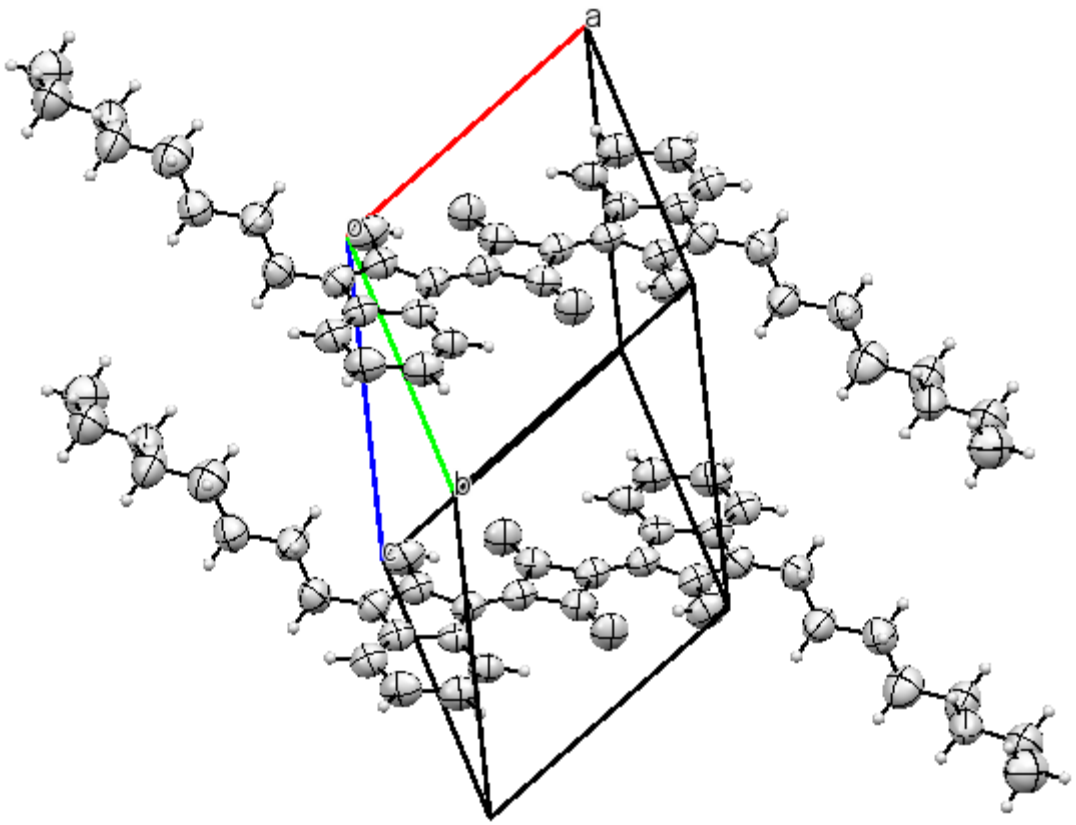

Synthesis of (3,5-dimethoxyphenyl)methanol

(1C)

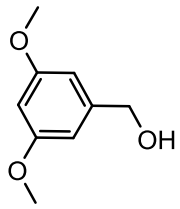

Chemical Formula: $C_9H_{12}O_3$

Molecular Weight: 168,19 g mol^{-1}

NaBH4 was added portion wise as a solid to a solution of3,5-dimetoxy benzaldehyde (10 g, 60 mmol) in MeOH (150 ml). The reaction was kept under stirring overnight at room temperature. It was quenched with 100 ml of water and extracted with AcOEt (200 ml). The organic phase was retro-washed with brine and then dried over Na_2SO_4. After vaporation of the solvent the product was afforded as a white solid (9.9 g, 59 mmol, quantitative).

^{1}H NMR (500MHz, $CDCl_3$): δ= 6.52 (d, 2H, J=2.17Hz), 6.38 (t, 1H, J=2.17Hz), 4.63 (s, 2H), 3.79 (s, 6H).

m.p. 42-45 °C

Synthesis of diethyl 3,5-dimethoxyphenylphosphonate

(2C)

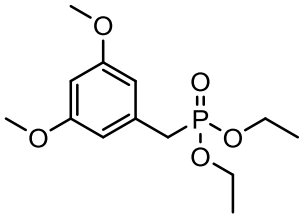

Chemical Formula: $C_{13}H_{21}O_5P$

Molecular Weight: 288,28 g mol-1

To a mixture of 1 (9.9 g, 59 mmol) in triethylphosphite (40 ml) cooled to 0°C with an ice bath, I_2 was added in small portions. The solution was stirred overnight at room temperature. Then the yellow solution was refluxed for three hours until no visible spot of the reagent appeared on TLC plate. The excess of triethilposphite was distilled off under reduced pressure, affording the product as a yellow dense oil (7.3 g, 26.5 mmol, 45%).

^{1}H NMR (500MHz, $CDCl_3$): δ= 6.44 (t, 2H, J=2.17Hz), 6.33 (t, 1H, J=2.17Hz), 4.04-3.97 (m, 4H), 3.75 (s, 6H), 3.09 (s, 1H), 3.04 (s, 1H), 1.24 (t, 6H, J=6.96Hz).

Synthesis of 1-dodecyl-1H-pirrole-2-carbaldehyde

(3C)

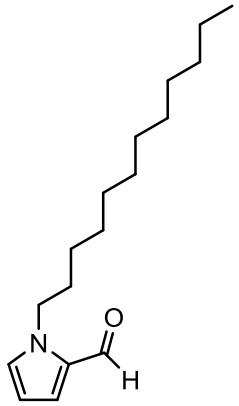

Chemical Formula: $C_{17}H_{29}NO$

Molecular Weight: 263,43 g mol^{-1}

NaH 60% in paraffine (6.61 g, 110 mmol) were placed in a round bottom flask under nitrogen, washed several times with hexane and dissolved in 30 ml of anhydrous DMF after hexane removal. 1-H-pyrrole 2-carbaldehyde (10 g, 105.16 mmol) was dissolved in few ml of DMF under nitrogen and syringed over NaH dropwise. 1-bromododecane (26.79 g, 107.5 mmol) n 20 ml of DMF were then added to the mixture. The reaction was stirred at room temperature for 2 days.

The reaction was quenched with water (400 ml), extracted with Et_2O (400 ml) and the organic phases retro-washed with after (3x300 ml). The combined organic phases were dried over Na_2SO_4 and evaporated giving 25.21 g of raw product that was used in the subsequent step without further purification.

Synthesis of (E)-2-(3,5-dimethoxystyryl)-1-dodecyl-1H-pyrrole

(4C)

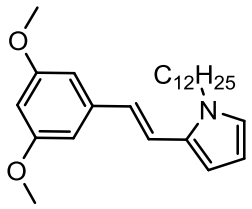

Chemical Formula: $C_{26}H_{39}NO_2$

Molecular Weight: 397,60 g mol^{-1}

To a solution of 1 (1.76 g, 6.4 mmol) and 2 (1.68 g, 6.4 mmol) cooled down at 0°C and under nitrogen, a solution of t-BuOK (1.80 g, 16 mmol) was added dropwise. The solution was then allowed to reach room temperature and stirred overnight. The solvent was evaporated under reduced pressure and the residual solid was taken up with water and extracted with DCM. The organic layer was dried over Na2SO4 and the solvent removed giving a brown oil that was purified by flash chromatography (silica gel, DCM/n-hexane 2:1) giving a yellow dense oil (1 g 2.7 mmol, 42%)

^{1}H NMR (500MHz, $CDCl_3$): δ= 6.93 (d, 1H, J=16Hz), 6.81 (d,1H, J=16Hz), 6.68 (s,1H, broad), 6.61 (d, 2H, J=2.17Hz), 6.49 (d, 1H, J=3.48Hz), 6.37 (t, 1H, J=2.17Hz), 6.16 (d, 1H, J=1.74), 3.95 (t, 2H, J=7Hz), 3.83 (s, 6H), 1.78-1.72 (m, 2H), 1.35-1.21 (m, 20H), 0.89 (t, 3H, J=7Hz).

Synthesis of (E)-2-(5-(3,5-dimethoxystyryl)-1-dodecyl-1H-pyrrol-2-yl)-4-(5-(3,5-dimethoxystyryl)-1-dodecyl-2H-pyrrolium-2-ylidene)-3-oxocyclobut-1-enolate

4MeSq

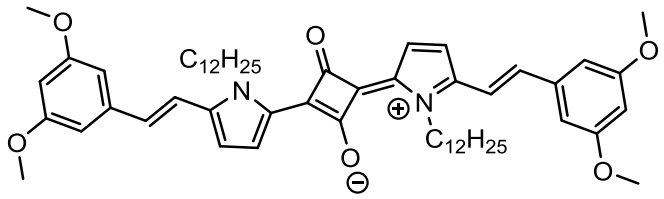

Chemical Formula: $C_{56}H_{76}N_2O_6$

Molecular Weight: 873,23 g mol^{-1}

Compound 4 (0.50 g, 1.26 mmol) and squaric acid (0.071 g, 0.63 mmol) were dissolved into a mixture of Toluene and buthanol 3:1 ratio. The mixture was refluxed and azeotropically distilled using a Dean-Stark trap until the condensation of water stopped. The solvent was evaporated and the residual sticky solid was digested in heptane in ultrasonic bath for 1 h. The solid obtained was filtered off and washed again with heptane on the filtered giving a green metal-like solid (350 mg, 0.4 mmol, 63%).

^{1}H NMR (500MHz, $CDCl_3$): δ= 7.85 (s, 2H), 7.20 (d, 2H, J=16Hz), 7.01 (d, 2H, J=16Hz), 6.88 (d, 2H, J=4.78Hz), 6.67 (d, 4H, 2.17 Hz), 6.46 (t, 2H, broad), 4.81 (m, 4H, broad), 3.84 (s, 12H), 1.78-1.73 (m, 4H, broad), 1.35-1.15 (m, 40H), 0.86 (t, 6H).

^{13}C NMR (500 MHz, CD_2Cl_2): δ= 162.01, 162.00, 146.63, 139.00, 135.90, 116.61, 114.89, 106.05, 102.01, 56.33, 47.64, 33.11, 32.81, 30.50, 30.44, 30.34, 30.24, 27.33, 23.56, 15.00.

Elemental analysis calculated for $C_{56}H_{76}N_2O_6$: C, 77.03%; H, 8.77%; N, 3.21%; found: C, 77.30%; H, 8.54%; N 3.25%.

Uv-Vis ($CHCl_3$): λmax= 679 nm.

Synthesis of (E)-2-(5-(3,5-dihydroxystyryl)-1-dodecyl-1H-pyrrol-2-yl)-4-(5-(3,5-dihydroxystyryl)-1-dodecyl-2H-pyrrolium-2-ylidene)-3-oxocyclobut-1-enolate 4OHSq

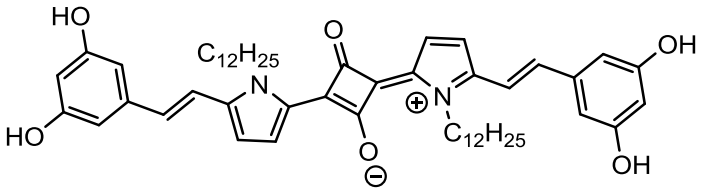

Chemical Formula: $C_{52}H_{68}N_2O_6$

Molecular Weight: 817,12 g mol^{-1}

Protected squaraine 4MeSq (50 mg, 0.06 mmol) was dissolved in 10 ml of DCM in a round bottom flask under nitrogen atmosphere. BBr_3 (1 M in DCM, 1 ml) was added carefully through a syringe and the resulting mixture was refluxed for 7 hs. The reaction was treated with a 10% solution of HCl. After separation, the organic phase was dried over Na_2SO_4, filtered and evaporated giving a blue solid. (51 mg, 0.062 mmol, 54%)

^{1}H NMR (500MHz, $CDCl_3$): δ= 7.80 (s, 2H, broad), 7.43 (d, 2H, J=16Hz), 7.29 (d, 2H, J=16Hz), 7.11 (d, 2H, J=4.35Hz), 6.70 (s, 2H), 6.42 (s, 2H), 4.98 (t, 4H, broad), 1.81-1.76 (m, 4H), 1.46-1.40 (m, 4H), 1.35-1.15 (m, 40H), 0.86 (t, 6H).

Uv-Vis ($CHCl_3$): λmax= 728 nm, 683, 429 nm.

Emission ($CHCl_3$): λmax= 687 nm, 702 nm.

Synthesys of n-heptyl-1,2,2-trimethylindolenine iodide

(1D)

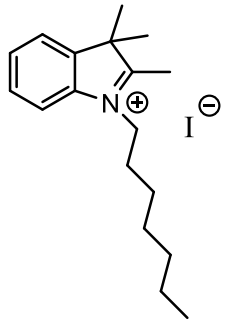

Chemical Formula: $C_{18}H_{28}IN$

Molecular Weight: 385,33 g mol^{-1}

In a microwave tube 1,2,2-trimetilindolenine (1.0 g, 6.2 mmol), iodoheptane (1.4 g, 6.3mmol) and 1 ml of acetone were placed and heated up in a microwave oven at 100°C for 1.5 hs. The crude product of the reaction was diluted with Et_2O (20 ml) and placed overnight in a fridge (4-5°C). The resulting oil is treated in ultrasonic bath until formation of a dark red precipitate that is filtered off and air dried (1.4 g, 3.8 mmol, yield 61%).

^{1}H NMR (500MHz, $CDCl_3$): δ= 7.9 (d, 2H, J=3.28Hz), 7.7 (t, 2H), 4.52 (t, 2H), 1.92 (m, 2H), 1.46 (m, 3H), 1.26 (m, 5H), 0.90 (t, 3H).

Synthesis of (Z)-2-ethylcyano-2-(2-ethoxy-3-hydroxy-4-oxocyclobut-2-enylidene) acetate

(2D)

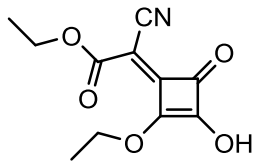

Chemical Formula: $C_{11}H_{11}NO_5$

Molecular Weight: 237,21 g mol-1

In a round bottom flask ethyl cyanoacetare(2.8 g, 29 mmol) and ethyl squarate (5.0 g, 29.4 mmol) were dissolved 50 ml of toluene. Triethylamine (4.2 ml, 30 mmol) was added and the mixture was stirred at room temperature for 48 hs. After removal of the solvent under reduced pressure, the residual oil was treated with 50 ml of water, then 10 ml of 37% HCl were added. A precipitate formed and was filtered off and air dried, giving the product as a scarcely soluble gray solid.

Beverina, Luca, et al. "Panchromatic Cross-Substituted Squaraines for Dye-Sensitized Solar Cell Applications." ChemSusChem 2.7 (2009): 621-624.

Synthesis of EthylesterSq

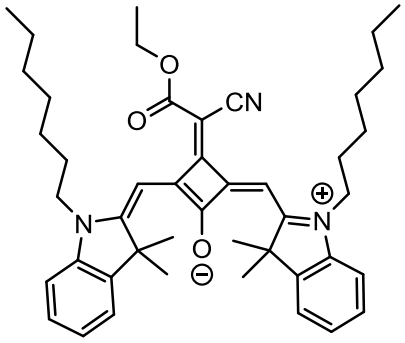

Chemical Formula: $C_{45}H_{57}N_3O_3$

Molecular Weight: 687,97 g mol^{-1}

Indolenine 1 (1.4 g, 3.8 mmol) and squaric ester 2 (0.45 g, 1.9 mmol) were dissolved into 50 ml of a mixture of toluene and buthanol 1:1 ratio. The mixture was refluxed and azeotropically distilled using a Dean-Stark trap until the condensation of water stopped. The solvent was removed and the resulting raw solid was purified by column chromatography (silica gel, AcoEt/DCM 4:1). The less retained spot was further purified by column chromatography (silica gel AcOEt/n-heptane 1:4) affording the pure compound as a green metallic solid (550 mg, 0.8 mmol, 42%)

^{1}H NMR (500 MHz, CD_2Cl_2): δ= 7.54 (s, 1H), 7.34 (d, 2H,J=7.40Hz), 7.31 (t,2H), 7.16 (t,2H), 7.02 (d, 2H, J=7.92Hz), 6.89 (s, 1H), 4.18 (t, 2H), 4.04 (m,4H), 1.80 (m,16H), 1.74 (m,3H), 1.48 (m, 7H), 1.30 (m, 16H), 0.96 (t, 4H), 0.84 (m, 7H).

^{13}C NMR (500 MHz, CD_2Cl_2): δ= 176.2; 172.4; 172.2; 170.2; 169.5; 167.8; 167; 143.7; 143.5; 143.0; 142.9; 129.0;128.9; ;123.5; 123.0; 110.9; 95.0; 90.0; 78.0; 67.5; 64.6; 50.0; 45.1; 32.5; 32; 30;27.6; 25.7; 20.0; 15.0.

Elemental analysis calculated for $C_{45}H_{57}N_3O_3$: C, 78.56%; H, 8.35%; N, 6.11%; found: C, 78.69%, H, 8.33%, N 5.30%.

Uv-Vis ($CHCl_3$): λmax= 688 nm, 413 nm.

Emission ($CHCl_3$): λmax= 710 nm.

Hydrolysis trials

reagent	solvent	equivalents	temperature	time	observations
CF_3COOH	water	1	R.T	overnight	only degradation byproducts
HCl 5%	AcOH	excess	80°C	3 days	only degradation byproducts
TBAOH (1M in H_2O)	CH_3CN	excess	R.T.	15 hs	permanent decoloration of the mixture
TBAOH (1M in MeOH)	CH_3CN	excess	R.T.	15 hs	permanent decoloration of the mixture
KOH 50% in EtOH	EtOH	excess	reflux	2.5 hs	sum of the alcoxyde to the squaraine core

Synthesis of phloroglucynole squaraine

(1E)

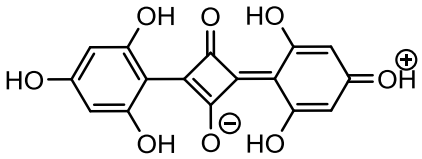

Chemical Formula: $C_{16}H_{10}O_8$

Molecular Weight: 330,25 g mol^{-1}

In a round bottom flask equipped with Dean-Stark apparatus, phloroglucinol (2.00 g, 8 mmol) and squaric acid (0.45 g, 4 mmol) were suspended in a toluene/buthanol 3:1 mixture and refluxed for 3 hours until ending of water evolution. After cooling at room temperature, a shiny precipitate formed. The precipitate was filtered off, washed with MeOH and air dried, giving the titled compound as a deep purple powder (0.80 g 2.4 mmol, 60%)

^{1}H NMR (500 MHz, DMSO-d_6): δ= 5,84 (s, 4H, broad)

Uv-Vis ($CHCl_3$): λmax= 568 nm.

Synthesis of chloro-subphthalocyanine

(2E)

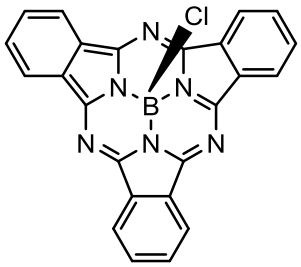

Chemical Formula: $C_{25}H_{12}BClN_6$

Molecular Weight: 430,1 g mol^{-1}

In a round bottom flask under Argon atmosphere, 5 ml of BCl_3 solution 1M in p-xylene were siringed directly onto solid phthalonitrile (2.15 g, 5 mmol). The mmixture was refluxed for 1 hour. The colour changed from yellow to deep purple. After cooling to room temperature, the flask was flushed with a stream of argon, then the solvent was evaporated under reduced pressure and the resulting solid was triturated with methanol. The resulting precipitate was filtered off and washed several times with methanol. The compound was collected as a brow-purple powder (0.140 g, 0.3 mmol, 20%)

^{1}H NMR (500 MHz, $CDCl_3$): δ= 8.75-8.60 (quartet, 6H), 7.90-7.80 (quartet, 6H)

Uv-Vis ($CHCl_3$): λmax= 563 nm, 290 nm.

Synthesis of Subpc-Sq-Subpc ensemble

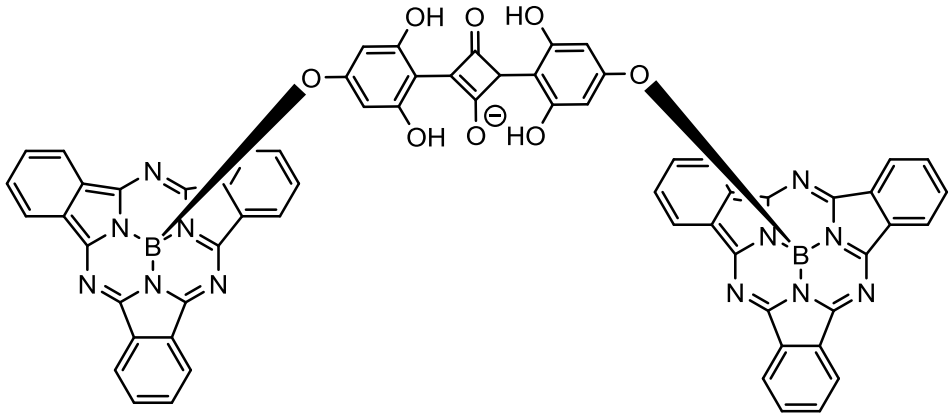

Chemical Formula: $C_{64}H_{32}B_2N_{12}O_8$

Molecular Weight: 1118,27 cm^{-1}

In a round bottom flask under argon atmosphere, squaraine (0.12 g, 0.35 mmol) and subphthalocyanine (0.3 g, 0.7 mmol) were dissolved into 7 ml of o-DCB and refluxed for totally 24 hs. After cooling to room temperature the solvent was evaporated under reduced pressure and the residual solid was purified by coloumn chromatography (silica gel, toluene/THF 9:1). A purple solid was recovered (30 mg, 0.03 mmol, 25%).

MS (MALDI-TOF, matrix DCTB): m/z= 1118,3 $[M]^+$ (calc. 1118,27)

Uv-Vis ($CHCl_3$): λmax= 582 nm, 568, 303 nm.

Emission ($CHCl_3$): λmax= no detectable emission

MALDI and exact mass adapted reports

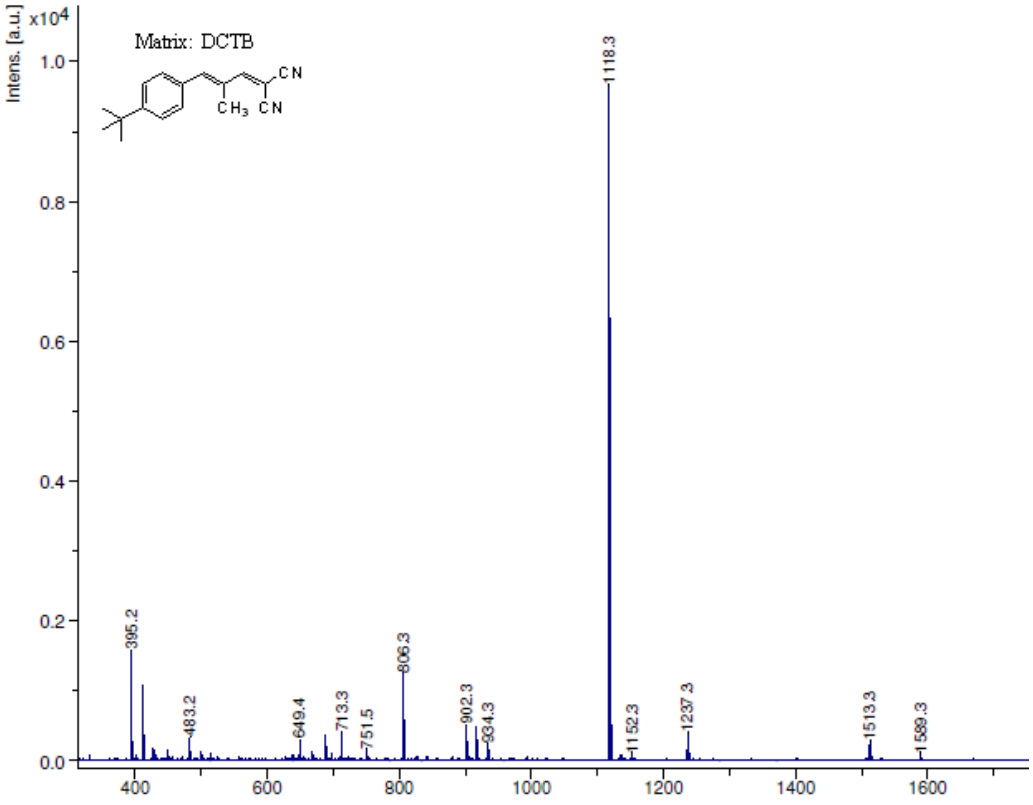

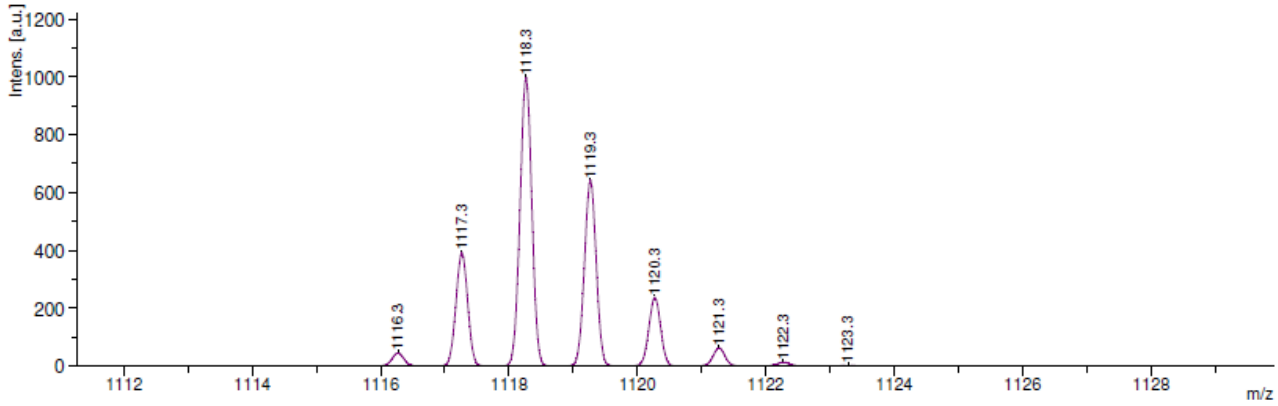

Synthesis of 4,5-dichlorphtalic anhydride

(1F)

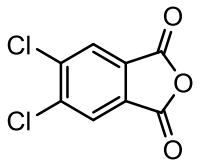

Chemical Formula: $C_8H_2Cl_2O_3$

Molecular Weight: 217,00 g mol^{-1}

A solution of 4,5-dichlorophthalic acid (25 g, 106,4 mmol) in acetic anhydride (45ml) was refluxed for 5 hours using a Dean-Stark trap to remove the aetic acid formed. After cooling to room temperature the remaining acetic acid was eliminated by vacuum distillation. The grey solid obtained was stirred overnight in petroleum ether, obtaining a white solid that was filtered off and thoroughly washed with petroleum ether (22,8 g, 105 mmol, 98%).

^{1}H-NMR (300 MHz, $CDCl_3$): δ= 8.12 (s, 2H)

Mp: 180-102°C

D. Wöhrle, M. Eskes, K. Shigehara, A. Yamada *Synthesis* **1993**, 194.

Synthesis of 4,5-dichloro phthalimide

(2F)

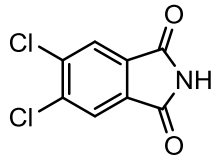

Chemical Formula: $C_8H_3Cl_2NO_2$

Molecular Weight: 216,02 g mol^{-1}

In a round bottom flask 4,5-dichlorophthalic anhydride (22.8 g, 105 mmol) in 35 ml of formamide were heated to reflux for 5 hours. After cooling down to room temperature a pale yellow precipitate formed and it was filtered off and air dried (20.8 g, 96 mmol, 91%).

Mp: 190-193°C

Synthesis of 4,5-dichloro phthalamide

(3F)

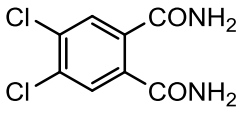

Chemical Formula: $C_8H_6Cl_2N_2O_2$

Molecular Weight: 233,05 g mol^{-1}

4,5-dichlorophthalimide (20.8 g, 96 mmol) was suspended into 250 ml of 33% ammonia solution and stirred for 2 days at room temperature. The white precipitate formed was filtered off and dried in an oven. (20 g, 80.6 mmol 84%)

Mp: 240-242°C

Synthesis of 4,5-dichloro phthalonitrile

(4F)

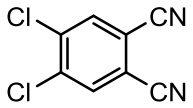

Chemical Formula: $C_8H_2Cl_2N_2$

Molecular Weight: 197,02 g mol^{-1}

In a round bottom flask under nitrogen atmosphere and cooled down to 0°C with an ice bath, freshly distilled $SOCl_2$ (85 ml) was slowly poured over 120 ml of dry DMF and the mixture was stirred for 2 hours. Then 4,5-dichloro phthalamide (20 g, 80.6 mmol) was added as a solid and the resulting suspension was stirred at room temperature overnight. The mixture was poured onto crushed ice until evolution of HCl stopped. The residual raw solid was filtered off, oven dried and recrystallized from MeOH giving the pure compound (10.5 g, 62.8 mmol, 78%).

^{1}H-NMR (300 MHz, $CDCl_3$): δ= 7.94 (s, 2H)

Mp: 180-181°C

Synthesis of 4,5-didodecylthio phthalonitrile

(5F)

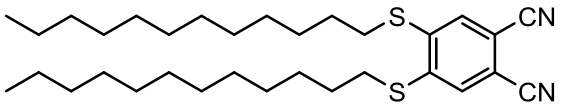

Chemical Formula: $C_{32}H_{52}N_2S_2$

Molecular Weight: 528,90 g mol^{-1}

In a round bottom flask under argon 4,5-dichloro phthalonitrile (2.4 g, 12.2 mmol) and K_2CO_3 (5g, 36.2 mmol) were suspended in 30 ml of dimethylacetamide. A stream of argon was fluxed through the slurry to remove the residual oxygen for about 10 minutes. Dodecylthiol (5.42 g, 26.8 mmol) was added through a syringe and the mixture was heated up to 90°C for 4 hours. After cooling down the mixture was poured over icy water and the precipitate that formed was filtered off and washed several times with cold EtOH. (4.6 g, 8.7 mmol, 71%).

^{1}H-NMR (300 MHz, $CDCl_3$): δ= 7.41 (s, 2H), 3.04-2.99 (t, 4H, J=7.45Hz), 1.80-1.71 (quintet, 4H, J=7.45Hz), 1.57-1.45 (m, 4H), 1.40-1.20 (m, 32H), 0.89 (t, 6H, J=6.80Hz).

Synthesis of thiolic-subphthalocianine

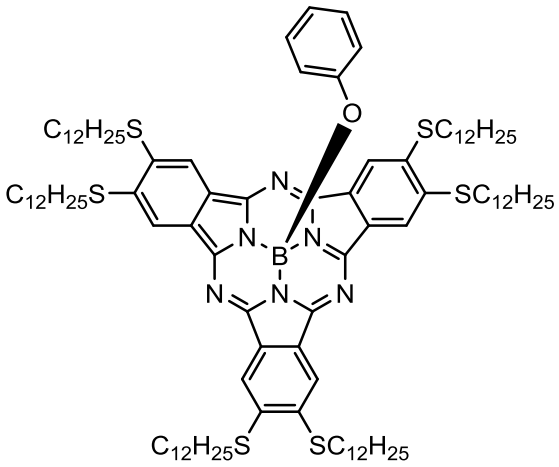

Chemical Formula: $C_{102}H_{161}BN_6OS_6$

Molecular Weight: 1690,62 g mol^{-1}

A 1M solution in p-xylene of BCl_3 (2.5 ml) was syringed over solid dodecylic phthalonitrile (1.3 g, 2.5 mmol) in round bottom flask under argon atmosphere. The mixture was refluxed for 15 minutes, then, after cooling to room temperature, a stream of argon was fluxed to remove all the acidic species. The solvent was evaporated under reduced pressure and the deep purple residual oil was used in the subsequent step.

Under argon atmosphere, the crude product of the previous reaction was suspended in 2 ml of toluene and phenol (0.39 g, 4.1 mmol) was added. The mixture was refluxed for 4 hours. Then, the solvent was evaporated under reduced pressure and the crude product was purified by column chromatography (silica gel, DCM/n-hexane 3:2) giving the pure product as a deep blue extremely viscus oil (0.55 g, 0.33 mmol, 44%).

^{1}H-NMR (300 MHz, $CDCl_3$): δ= 8.60 (s, 6H), 6.81-6.76 (t, 2h, J=7.16Hz), 6.67-6.63 (t, 1H, J=7.16Hz), 5.44 (d, 2H, J=7.16Hz), 3.31-3.20 (m, 12H), 1.92-1.82 (m, 12H), 1.35-1.20 (m, 96H), 0.88 (t, 18H, J=6.40Hz).

^{13}C NMR (300 MHz, CD_2Cl_2): δ= 149.65, 139.48, 137.91, 136.44, 134.30, 134.26, 129.67, 128.02, 127.56, 125.97, 118.62, 32.71, 31.66, 30.91, 28.68, 28.64, 28.62, 28.33, 27.89, 25.89, 21.67, 19.97, 18.15, 13.09.

Elemental Analysis calculated for $C_{102}H_{161}BN_6OS_6$: C, 72.47%; H, 9.60%; N, 4.97%; S, 11.38%; found: C, 72.45%; H, 9.63%; N, 4.93%; S, 10.80%

MS (MALDI-TOF, matrix DCTB): m/z= 1689.0 $[M]^+$ (calc. 1689.11)

Uv-Vis ($CHCl_3$): λmax= 599 nm, 371 nm, 301 nm.

Emission ($CHCl_3$): λmax = 611 nm.

Synthesis of 4-amino phthalonitrile

(1G)

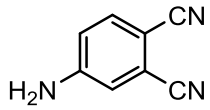

Chemical Formula: $C_8H_5N_3$

Molecular Weight: 143,15 g mol^{-1}

4-nitro phthalonitrile (4.0 g, 23 mmol) was suspended into 90 ml of MeOH and 20 ml of 37% w/w of HCl were added. The mixture was refluxed until dissolution of the nitrile. Iron powder (4.5 g) were added as a solid portionwise and the mixture refluxed for further 1 hour. After cooling to room temperature, the mixture was poured onto crushed ice and the precipitate that formed was filtered away, oven dried and recrystallized fromm toluene, giving the product as ochre needles (2.4 g, 16.8 mmol, 73%)

^{1}H NMR (300 MHz, DMSO-d_6): δ= 7.65 (d, 1H, J=8.67Hz), 7.02 (s, 1H), 6.88 (d, 1H, J=7.91Hz), 6.70 (s, 1H, broad).

J. Griffiths, B. Roozpeikar *J. Chem. Soc., Perkin Trans 1,* **1976**, 42.

Synthesis of 4-iodo phthalonitrile

(2G)

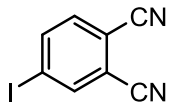

Chemical Formula: $C_8H_3IN_2$

Molecular Weight: 254,03 g mol^{-1}

4-amino phthalonitrile (2.4 g, 16.8 mmol) was suspended into 35 ml of H_2SO_4 2.5 M and the suspension was cooled down to -10°C. $NaNO_2$ (1.34 g, 19.5 mmol) in 5 ml of water was added dropwise. The mixture was stirred for 30 minutes at 0°C. Then a solution of KI (3.25 g, 19.5 mmol) in 5 ml of water was added in one portion. The mixture was stirred for 45 minutes and a brown precipitate formed. The solid was filtered off, dissolved in 50 ml of DCM and washed with a saturated solution of $Na_2S_2O_3$. The separated organic phases were dried over Na_2SO_4 and the solvent evaporated under reduced pressure. The raw yellow solid obtained was purified by column chromatography (silica gel DCM) obtaining a white solid (1.5 g, 5.9 mmol, 36%).

^{1}H NMR (300 MHz, $CDCl_3$): δ= 8.17 (d, 2H, J=1.53Hz), 8.13-8.10 (dd, 1H, J1=1.53, J2=6.58Hz), 7.52 (d, 1H, J=8.11Hz).

M. S. Marcuccio, I. Polina, S. Greenberg, A. B. P. Lever, C. C. Leznoff, B. Tomer *Can. J. Chem.* **1985**, *63*, 3057.

Synthesis of triiodo-subphthalocyanine

(4G)

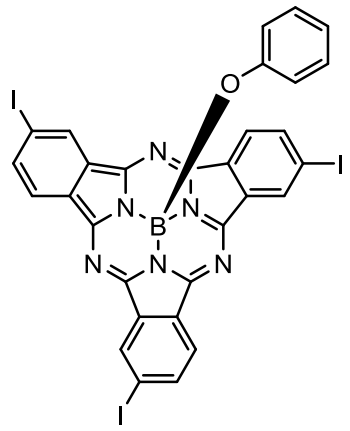

Chemical Formula: $C_{30}H_{14}BI_3N_6O$

Molecular Weight: 866,01 g mol^{-1}

A 1M solution in p-xylene of BCl_3 (2.5 ml) was syringed over solid 4-iodo phthalonitrile (1.5 g, 5.9 mmol) in round bottom flask under argon atmosphere. The mixture was refluxed for 20 minutes, then, after cooling to room temperature, a stream of argon was fluxed to remove all the acidic species. The solvent was evaporated under reduced pressure and the purple residual solid was used in the subsequent step.

Under argon atmosphere, the crude product of the previous reaction was suspended in 5 ml of toluene and phenol (0.47 g, 5 mmol) was added. The mixture was refluxed overnight. Then, the solvent was evaporated under reduced pressure and the crude product was dissolved in DCM and passed through a short silica plug. The pure product was collected as a shiny magenta solid (0.50 g, 0.6 mmol, 30%).

^{1}H NMR (300 MHz, $CDCl_3$): δ= 9.11 (s, 3H), 8.48 (d, 3H, J=8.29Hz), 8.15 (d, 3H, J=8.29Hz), 8.71-8.66 (t, 2H, J=7.16Hz), 6.60-6.55 (t, 1H, J=7.16Hz), 5.29 (d, 2h, J=8.29Hz).

Uv-Vis ($CHCl_3$): λmax= 570 nm

Emission ($CHCl_3$): λmax= 568 nm

Synthesis of 5'-hexyl-bithiophene subphthalocyanine

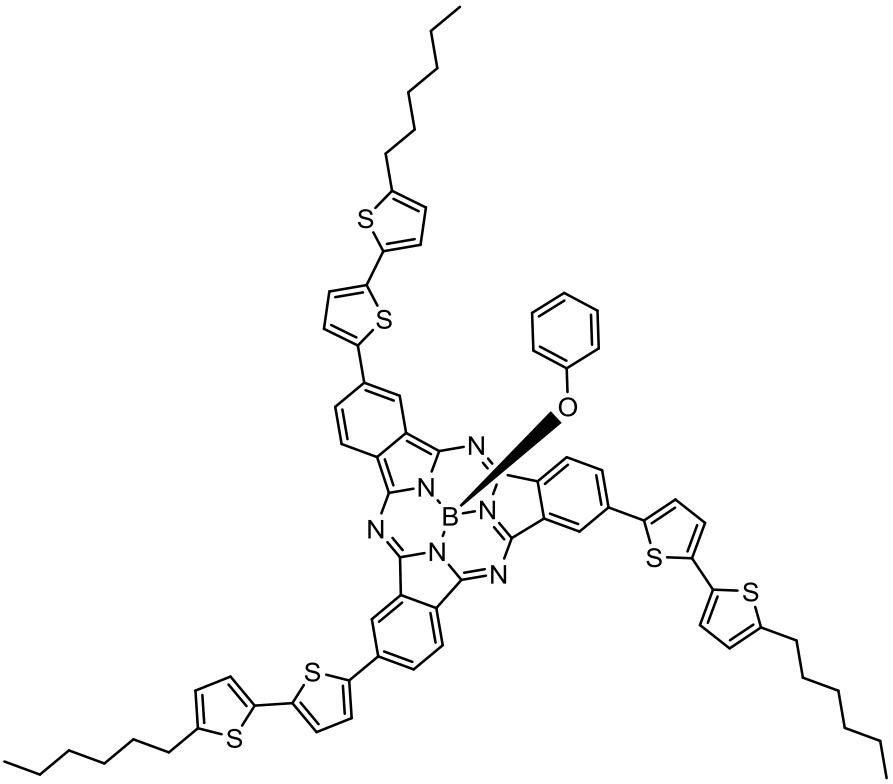

Chemical Formula: $C_{72}H_{65}BN_6OS_6$

Molecular Weight: 1233,52 g mol^{-1}

In a Shlenk tube under argon atmosphere triiodo subphthalocianine (0.170 g, 0.2 mmol), bithiophene derivative (0.250 g, 0.66 mmol) tetrakis palladium (0.034 g, 0.03 mmol) and CsF (0.272 g, 1.8 mmol) were suspended in anhydrous DME and heated up to 90°C for 4 hours.

The mixture turned deep blue. After solvent was removed under reduced pressure, the residual was dissolved into 100 ml of DCM and washed with water (2x100). The reunited organic phases were dried over Na2SO4 and, after solvent removal, the crude solid obtained was purified by column chromatography (silica gel, toluene), collecting the desired compound as a blue solid (50 mg, 0.05 mmol, 25%).

^{1}H NMR (500 MHz, $CDCl_3$): δ= 8.94 (s, 3H), 8.66 (d, 3H, J=8.22Hz), 8.01 (d, 3H, J=8.22Hz), 7.47 (d, 3H, J=3.91Hz), 7.14 (d, 3H, J=3.91Hz), 7.07 (d, 3H, J=3.52Hz), 6.85-6.82 (t, 2H, J=8.22Hz), 6.72 (d, 3H, J=3.52Hz), 6.70-6.67 (t, 1H, J=13.3Hz), 5.56 (d, 2H, J=7.43Hz), 2.84-2.80 (t, 6H, J=7.43Hz), 1.75-1.69 (quintet, 5H, J=7.43Hz), 1.43-1.27 (m, 18H), 0.92 (t, 9H, J=7.04).

^{13}C NMR (500 MHz, CD_2Cl_2): δ= 153.48, 152.10, 151.90, 146.97, 142.38, 139.89, 136.89, 132.72, 130.04, 129.86, 127.80, 126.23, 125.83, 125.05, 124.64, 123.54, 122.48, 120.11, 119.36, 32.46, 31.12, 29.66, 23.47, 14.96.

Elem. Analysis: calculated for $C_{72}H_{65}BN_6OS_6$: C, 70.11%; H, 5.31%; N, 6.81% S, 15.59% found: C, 70.40%; H, 5.00%; N, 6.39%; S, 17.05%.

Uv-Vis ($CHCl_3$): λmax= 610 nm, 404 nm, 348 nm.

Emission ($CHCl_3$): λmax= 631 nm

Synthesis of 4-(3,7-dimethyloctyloxy) benzonitrile

(1H)

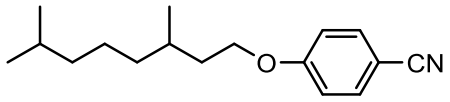

$C_{17}H_{25}NO$

MW: 259,19 g mol^{-1}

4-cyanophenol (125 mmol) and triphenylphosphine (157.35 mmol) were dissolved in THF (200 ml) under nitrogen atmosphere at 0°C. A solution of 3-7-dimethyloctanol (104.9 mmol) in THF (200 ml) were then added and a mixture of DIAD (157.35 mmol) and THF 1:1 in volume was added dropwise over a hour. The reaction was stirred for 24 hours at R.T. The solvent was removed in vacuum and the residue brown oil was dissolved in CH_2Cl_2 (200 ml)and washed with a NaOH solution (5% w/w, 3x 150 ml). A solution of H_2O_2 (10% w/w, 60 ml) was added to the organic layer and the mixture stirred overnight. A solution of NaHSO3 (5% w/w, 100 ml) was then added and the organic phase was separated, the solvent removed, and dried over Na_2SO_4. The oil was triturated with hexane (300 ml) and the white precipitate formed was filtered off. A further purification was carried out with flash chromatography (silica gel, eluent hexane, then 3:1 hexane Et_2O) affording a brown oil that was not further purified and used in the subsequent step (43.8 mmol, 51% yield).

Synthesis of 3,6-bis(4-(3,7-dimethyloctyloxy)phenyl)pyrrolo[3,4-c]pyrrole-1,4(2H,5H)-dione

(2H)

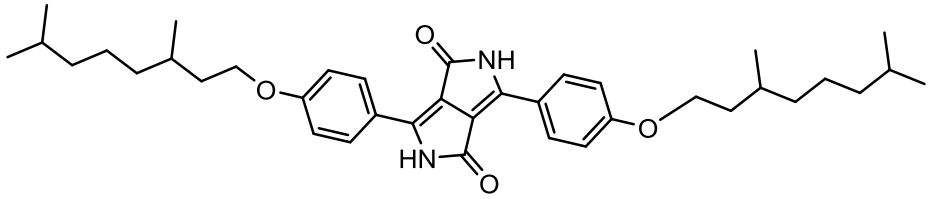

$C_{38}H_{52}N_2O_4$

MW: 600,84 g mol^{-1}

Sodium tert-pentoxide (65 mmol) and 1 (50mmol) were dissolved in tert-amylalcohol (150 ml) and heated at 125°C. A solution of di-tert-butylsuccinate (21.7 mmol) in the same solvent was added dropwise over 1.5 hours, then the reaction was refluxed for 2 hours. The mixture was cooled and isopropanol (20 ml) and water (50 ml) were added. The solid residue was filtered off and washed several times with hot methanol, then it was dried in vacuum at 50°C, giving the product as a red solid (11.5 mmol, 53% yield).

Elemental analysis calculated (%) $C_{38}H_{52}N_2O_4$: C 75.96, H 8.72, N 4.66; found: C 75.90, H 8.68, N 4.33;

Uv-Vis ($CHCl_3$): λmax= 511 nm, 476 nm, 340 nm.

Syntesis of DPP-CN-1

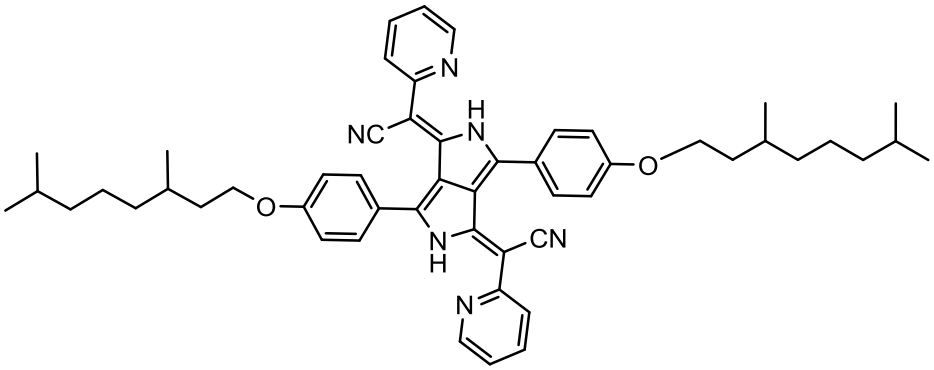

$C_{52}H_{60}N_6O_2$

MW: 801,09 g mol^{-1}

$POCl_3$ (8 eq) was added to a mixture of DPP 2 (1eq) and pyridylacetonitrile (2.5 eq) in absolute toluene (20 ml/eq of DPP) at reflux in a nitrogen atmosphere. The reaction was monitored by TLC. After removal of the toluene and excess of $POCl_3$ by vacuum distillation, the crude product was dissolved in CH_2Cl_2 and neutralized with aqueous $NaHCO_3$ solution. The organic phase was separated and dried with $MgSO_4$. After removing the solvent, the residue was dissolved in acetone in an ultrasonic bath. The remaining solid was separated by filtration and washed several times with acetone giving a metal-like brown powder in 75% yield,

^{1}H NMR (500 MHz, $CDCl_3$): δ= 8.44 (d, J=4.5 Hz, 2H), 7.64 (m, 6H), 7.57 (d, J=8.3 Hz, 2H), 7.08 (d, J=8.7 Hz, 4H), 6.99 (t, J=5.2 Hz, 2H), 4.10 (m, 4H), 1.87 (m, 2H), 1.5-1.7 (m, 8H), 1.35 (m, 7H), 1.15 (m, 7H), 0.97 (d, J=3.4 Hz, 6H), 0.89 (d, J=6.7 Hz, 14H).

^{13}C NMR (125.75 MHz, $CDCl_3$): δ= 162.00, 156.66, 148.15, 146.15, 143.80, 137.68, 132.11, 123.16, 121.88, 121.50, 119.64, 117.25, 114.81, 78.77, 67.40, 40.13, 38.20, 37.04, 30.76, 28.87, 25.56, 23.60, 23.50, 20.58;

Elemental analysis calculated (%) for $C_{52}H_{60}N_6O_2$: C 77.97, H 7.55, N 10.49; found: C 78.20, H 7.70, N 10.54;

Uv-Vis ($CHCl_3$): λmax= 693 nm, 634 nm.

Emission ($CHCl_3$): λmax= no detectable emission signal.

Syntesis of DPP-Cy-1

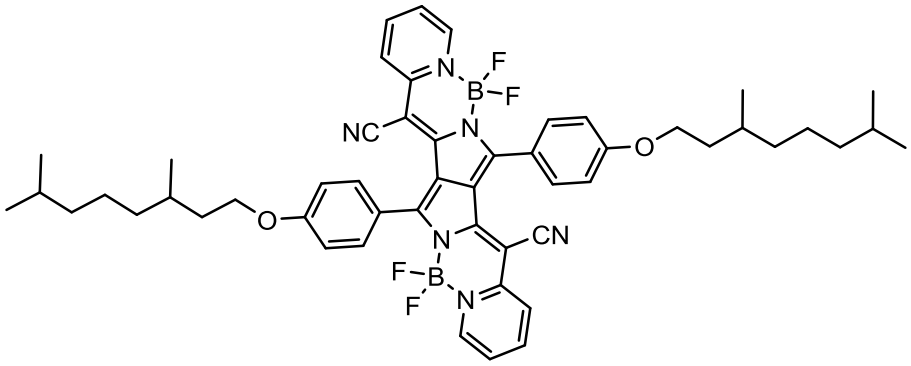

$C_{52}H_{58}B_2F_4N_6O_2$

MW: 896,69 g mol^{-1}

$BF_3.Et_20$ (15 eq) was added to a solution of DPP-CN-1 (1eq) derivative in CH_2Cl_2 (10 ml) at reflux in nitrogen atmosphere. After 10 min, Hünig's base (2.5eq) was added and the mixture refluxed for further for further 10 min. The reaction was stopped and the solvent and $BF_3.Et_20$ excess was removed in vacuum. The crude solid was taken up with water and extracted with CH_2Cl_2. The organic layer was dried over Na_2SO_4, and evaporated after filtration, affording the boron complex as a green metallic solid in 60% yield.

^{1}H NMR (500 MHz, $CDCl_3$): δ= 8.32 (d, J=6.1 Hz, 2H), 7.86 (d d d, J_1=1.3, J_2=1.3, J_3=1.5 Hz 2H), 7.64 (d, J=8.6 Hz, 6H), 7.18 (t, J=6 Hz, 2H), 7.05 (d, J=8.7 Hz, 4H), 4.10 (m, 4H), 1.80-1.90 (m, 2H), 1.50-1.70 (m, 8H), 1.10-1.40 (m, 12H), 0.95 (d, J=6.5 Hz, 6H), 0.85 (d, J=6 Hz, 12H);

^{13}C NMR (125.75 MHz, $CDCl_3$): δ= 162.05, 154.36, 150.05, 146.81, 142.05, 141.58, 133.14, 123.18, 123.13, 122.62, 120.20, 116.87, 114.21, 67.18, 40.14, 38.22, 37.05, 30.75, 30.60, 28.90, 25.57, 23.64, 23.53, 20.62;

^{19}F NMR (376 MHz, $CDCl_3$): δ= 130.95;

Elemental analysis calculated (%) for $C_{52}H_{58}B_2F_4N_6O_2$: C 69.65, H 6.52, N 9.37; found: C 69.48, H 6.54, N 9.17;

Uv-Vis ($CHCl_3$): λmax= 699 nm, 638 nm.

Emission ($CHCl_3$): λmax= 720 nm.

Synthesis of 1,3-benzothiazol-2-ylacetonitrile

(1l)

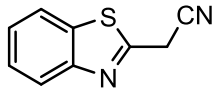

Chemical Formula: $C_9H_6N_2S$

Molecular Weight: 174,22 g mol^{-1}

A mixture of o-aminothiophenol (2 g, 16 mmol) and malononitrile (1.06 g, 16 mmol) was stirred in absolute ethanol (15 ml) and glacial AcOH (1,5 ml) at RT for 4 days, the precipitate was filtered off and carefully air dried to give a yellow powder: yellow powder (2.0 g, 11.4 mmol, 71%);

m.p.: 100–101 °C.

Chao, Richard Y., et al. "Preparation and Characterization of Substituted 3-Benzothiazol-2-Ylcoumarins." *Journal of the Chinese Chemical Society* 57.2 (2010): 213-221.

Synthesis of DPP-CN-2

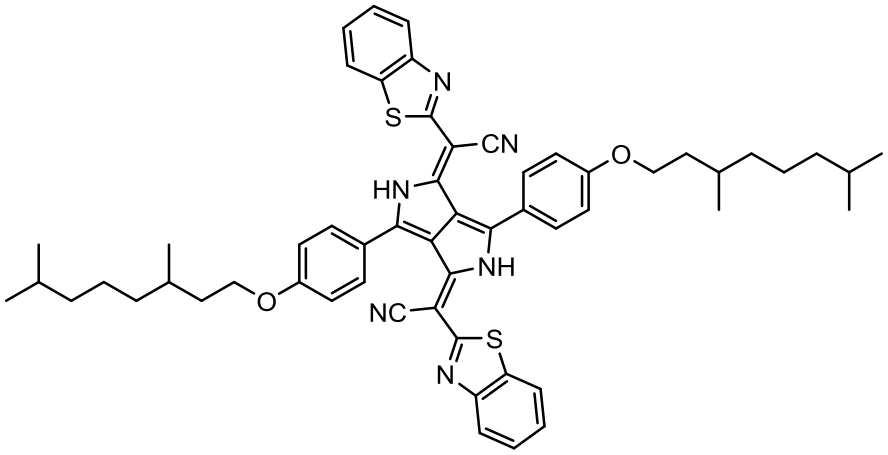

Chemical Formula: $C_{56}H_{60}N_6O_2S_2$

Molecular Weight: 913,26 g mol^{-1}

$POCl_3$ (8eq) was added to a mixture of DPP 2 (1eq) and 1,3-benzothiazol-2-ylacetonitrile 3 (2.5 eq) in toluene (20 ml/eq of DPP) at reflux in a nitrogen atmosphere. The reaction was monitored by TLC. After removal of the solvent and excess of $POCl_3$ by vacuum distillation, the crude product was dissolved in CH_2Cl_2 and neutralized with aqueous $NaHCO_3$ solution. The organic phase was separated and dried with $MgSO_4$. After removing the solvent, the residue was dissolved in acetone in an ultrasonic bath. The remaining solid was separated by filtration and washed several times with acetone giving a metal-like brown powder, 55% yield.

^{1}H NMR (500 MHz, $CDCl_3$): δ= 7.81 (d, J=8.1 Hz, 2H), 7.73 (t, J= 8.9 Hz, 6H), 7.47 (t, J=8Hz, 2H), 7.29 (t, J=7.3 Hz, 2H), 7.14 (d, J=8.7 Hz, 4H), 4.13 (m, 4H), 1.90 (m, 4H), 1.20-1.80 (m, tot. 38 H), 1.00 (d, J=6.5 Hz, 6H), 0.89 (d, J=6.7 Hz, 14H);

^{13}C NMR (125.75 MHz, $CDCl_3$): δ= 167.19, 162.88, 154.32, 146.11, 145.20, 134.20, 132.45, 127.30, 125.20, 122.19, 122.05, 122.00, 115.27, 67.59, 40.14, 38.20, 37.01, 30.78, 30.56, 28.88, 25.57, 23.61, 23.50, 20.58;

Elemental analysis calculated (%) for $C_{56}H_{60}N_6O_2S_2$: C 73.65, H 6.62, N 9.20, S 7.02; found: C 73.61, H 6.91, N 8.92, S 7.30;

Uv-Vis ($CHCl_3$): λmax= 722 nm, 657 nm.

Emission ($CHCl_3$): λmax= no detectable emission signal.

Synthesis of DPP-Cy-2

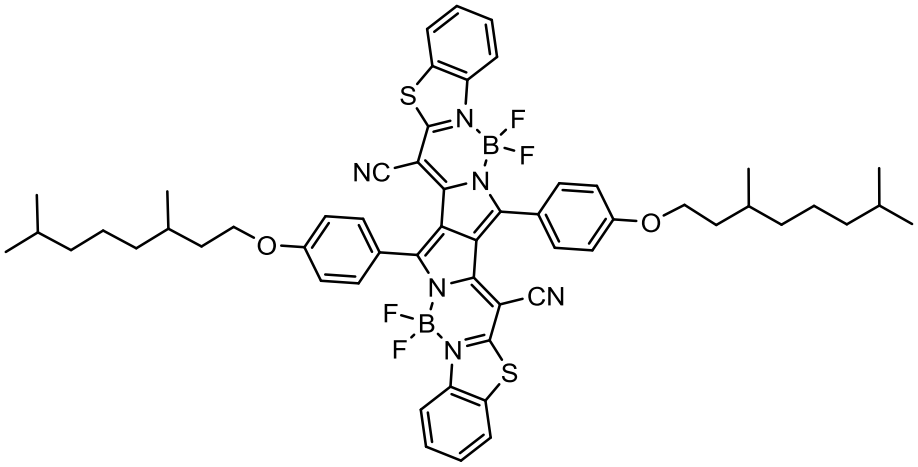

Chemical Formula: $C_{56}H_{58}B_2F_4N_6O_2S_2$

Molecular Weight: 1008,85 g mol^{-1}

$BF_3.Et_20$ (15eq) was added to a solution of DPP-CN-2 (1eq) derivative in ortho-dichlorobenzene (10 ml) at reflux in nitrogen atmosphere. After 10 min, Hünig's base (2.5eq) was added and the mixture refluxed for further for further 10 min. The reaction was stopped and the solvent and $BF_3.Et_20$ excess was removed in vacuum. The crude solid was suspended in MeOH, digested in ultrasonic bath and separated by filtration. Column chromatography (silica gel, CH_2Cl_2) afforded the boron complex as a green metal-like solid in 23% yield.

^{1}H NMR (500 MHz, $CDCl_3$): δ= 8.00 (d, J=8.3 Hz, 2H), 7.75 (d, J=8.0 Hz, 2H), 7.70 (d, J=8.5 Hz, 4H), 7.48 (t, J=7.5 Hz, 2H), 7.41 (t, J=7.7, 2H), 7.08 (d, J=8.7, 4H), 4.10 (m, 4H), 1.9 (m, 2H), 1.60-1.70 (m, 2H), 1.2-1.4 (m, 8H), 1.00 (d, J=6.5, 6H), 0.90 (d, J=6.6, 12H);

^{13}C NMR (125.75 MHz, $CDCl_3$): δ= 167.05, 162.63, 157.98, 147.40, 144.66, 133.29, 129.39, 129.19, 127.06, 122.93, 122.80, 122.53, 119.80, 115.66, 114.60, 76.54, 67.32, 40.15, 38.23, 37.02, 30.79, 30.57, 28.90, 25.56, 23.64, 23.51, 20.61;

^{19}F NMR (376 MHz, $CDCl_3$): δ= 130.95;

Elemental analysis calculated (%) for $C_{56}H_{58}B_2F_4N_6O_2S_2$: C 66.24, H 5.69, N 8.45, S 7.20; found: C 66.67, H 5.79, N 7.53, S 6.36;

Uv-Vis ($CHCl_3$): λmax= 728 nm, 661 nm, 614 nm.

Emission ($CHCl_3$): λmax= 734 nm.

Synthesis of (N,N'E,N,N'E)-N,N'-(acenaphthylene-1,2-diylidene)bis(4-methoxybenzenamine)

(1L)

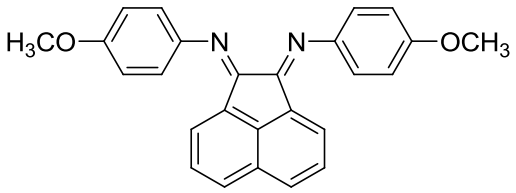

Chemical Formula: $C_{26}H_{20}N_2O_2$

Molecular Weight: 392.45 g mol^{-1}

In a round bottom flask, acenaphthenequinone (5 g, 27 mmol) and dry $ZnCl_2$(7.5 g, 55 mmol) were suspended in 80 ml of glacial acetic acid. The flask was heated at about 50-60 °C and p-anisidine (7.40 g, 60 mmol) was then added. Then the mixture was refluxed for 45 min. and then hot-filtered. An orange precipitate was recovered and washed with AcOH (100 ml) and Et_2O (100 ml). The solid was air dried giving the zinc complex of the ligand.

In the second step, the zinc complex was suspended in CH_2Cl_2 (200 ml) and a solution of K_2CO_3 (100 g in 100 ml) was added. The mixture was stirred at R.T. overnight. After separation, organic phase was washed with water, dried over Na_2SO_4 and evaporated under reduced pressure, giving an orange powder. The compound was recrystallized from ethanol, giving red needles (7.5 g, 19 mmol, yield 70%).

^{1}H NMR (500MHz, $CDCl_3$) δ= 7.91 (d, 2H), 7.42 (t, 2H), 7.15 (d, 4H), 7.09 (d, 2H), 7.02 (d, 4H), 3.58 (s, 6H).

Uv-Vis ($CHCl_3$): λmax= 433 nm, 320 nm.

Synthesis of (E)-N-((E)-2-(3a2,10-dihydropyren-1-ylimino)acenaphthylen-1(2H)-ylidene)pyren-1-amine

(2L)

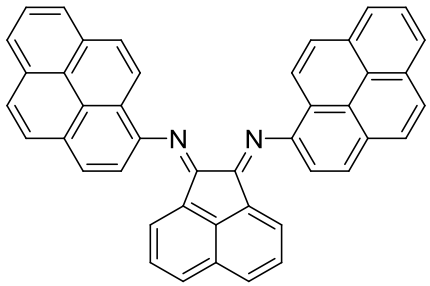

Chemical Formula: $C_{44}H_{24}N_2$

Molecular Weight: 580.68 g mol^{-1}

In a round bottom flask, (0.125 g, 0.7 mmol) and dry $ZnCl_2$(0.2 g, 1.4 mmol) were suspended in 10 ml of glacial acetic acid. The flask was heated to about 50-60 °C and 1-aminopyrene (0.33, 1.4 mmol) was then added. The mixture was refluxed for 45 min. and then hot-filtered. A black precipitate was recovered and washed with AcOH (20 ml) and Et2O (20 ml). The solid was air dried giving the zinc complex of the ligand as a dark powder.

In the second step, the zinc complex was suspended in CH_2Cl_2 (10 ml) and a solution of K_2CO_3 (10 g in 10 ml) was added. The mixture was stirred at R.T. overnight. After separation, organic phase was washed with water, dried over Na_2SO_4 and evaporated under reduced pressure, giving a black powder. The compound was recrystallized from ethanol (0.350 g, 0.6 mmol, yield 86%).

^{1}H NMR (500MHz, $CDCl_3$) δ= 6.47 (d, 2H), 7.06 (t, 2H), 7.72 (d, 2H), 7.92 (d, 2H), 8.02 (t, 2H) 8.09 (q, 4H), 8.16 (d, 4H), 8.21 (d, 2H), 8.33 (d, 2H), 8.40 (d, 2H).

^{13}C NMR (125.77 MHz, $CDCl_3$) δ 116.0, 120.5, 123.1, 123.8, 124.8, 124.9, 125.2, 125.7, 125.8, 126.2, 126.3, 127.2, 127.5, 127.7, 128.6, 128.8, 129.1,142.0,146.0,162.5.

Elem. Analysis: calculated for $C_{44}H_{24}N_2 \cdot C_2H_6O$: C, 88.15%, H, 4.82%, N, 4.47%; found: C, 88.06%; H, 4.25%; N, 4.28%.

m.p.: 189 °C dec.

Uv-Vis ($CHCl_3$): λmax= 482 nm, 349 nm.

Synthesis of Eu^{3+} chelate of thenoyl trifluoromethyl acetylacetonate aquocomplex.

(A1M)

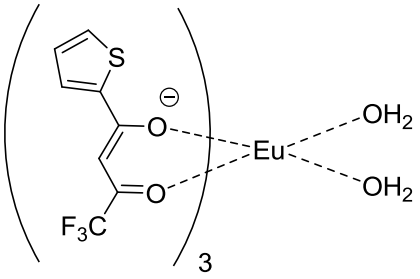

Chemical Formula: $C_{24}H_{16}F_9O_8S_3Eu$

Molecular Weight: 851.53 g mol^{-1}

The ligand (2 g, 9 mmol) was dissolved into 150 ml of a 1:2 biphasic mixture of H_2O and CH_2Cl_2 and NaOH 2N (4.5 ml) was added. The aqueous phase gets yellow. Europium(III) (0.824 g, 2.25 mmol) salt was dissolved into 5 ml of deionized H_2O and added. A white precipitate instantly formed. The mixture was vigorous stirred for two days until the precipitate was gone. Then, organic phase was separated, dried over Na_2SO_4 and evaporated under reduced pressure to give a white powder that was recognized as the aquocomplex of the desired product by elemental analysis and used without further purification. (1.5 g, 1.8 mmol, yield: 78%)

Elemental Analysis calculated for $C_{24}H_{16}EuF_9O_8S_3$: C, 33.85%; H, 1.89%; N, 0.00%; found: C, 33.84%; H, 1.70%; N, 0.00%

Synthesis of Eu^{3+} chelate of thenoyl trifluoromethyl acetylacetonate substitute with (N,N'E,N,N'E)-N,N'-(acenaphthylene-1,2-diylidene)bis(4-methoxybenzenamine).

(C1M)

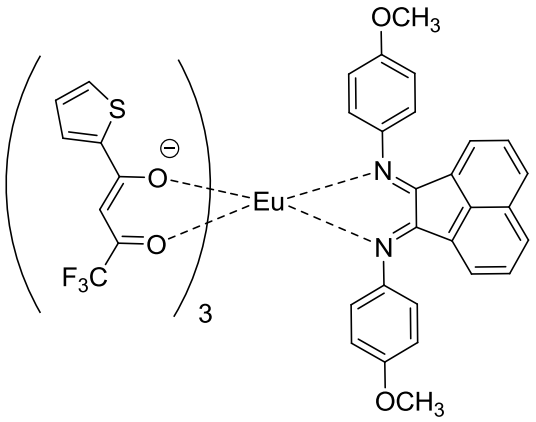

Chemical Formula: $C_{50}H_{32}F_9N_2O_8S_3Eu$

Molecular Weight: 1214 g mol^{-1}

Europium aquocomplex (0.350 g, 0.4 mmol) and Shiff's base 1 (0.157 g, 0.4 mmol) were dissolved in 20 ml of toluene and refluxed in a Dean-Stark trap for 6 hours. Solvent was evaporated under reduced pressure, giving a red oil, that was washed with hexane and dried carefully in vacuum, giving a red vitreous solid (0.282 g, 2.3 mmol, yield 58%)

Elemental Analysis calculated for $C_{50}H_{32}F_9N_2O_8S_3Yb$: C, 49.72%; H, 2.67%; N, 2.32%. found: C, 50.22%; H, 3.20%; N, 2.37%.

Uv-Vis ($CHCl_3$): λmax= 435 nm (ligand).

Synthesis of Yb^{3+} chelate of thenoyl trifluoromethyl acetylacetonate aquocomplex.

(A2M)

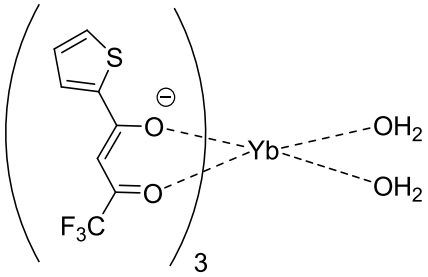

Chemical Formula: $C_{24}H_{16}YbF_9O_8S_3$

Molecular Weight: 872.60 g mol^{-1}

Thenoyltrifluoroacetone (3 g, 13.5 mmol) was dissolved into a 1:2 biphasic mixture of H_2O (75ml) and CH_2Cl_2 and NaOH 2N (6.75 ml) was added. The aqueous phase turns yellow. Ytterbium(III) chloride (0.94 g, 3.5 mmol) was dissolved in 5 ml of H_2O and added. A white precipitate instantly formed. The mixture was vigorous stirred for two days until the precipitate was gone. Then, organic phase was separated, dried over Na_2SO_4 and evaporated under reduced pressure to give a pale yellow gummy solid. (1.9 g, 2.1 mmol, yield 62%)

Elemental Analysis calculated for $C_{24}H_{16}YbF_9O_8S_3$: C, 33.03%; H, 1.85%; N, 0.00%; found: C, 33.03%; H, 1.71%; N, 0.00%

Synthesis of Yb3+ chelate of thenoyl trifluoromethyl acetylacetonate substitute with (N,N'E,N,N'E)-N,N'-(acenaphthylene-1,2-diylidene)bis(4-methoxybenzenamine).

(C2M)

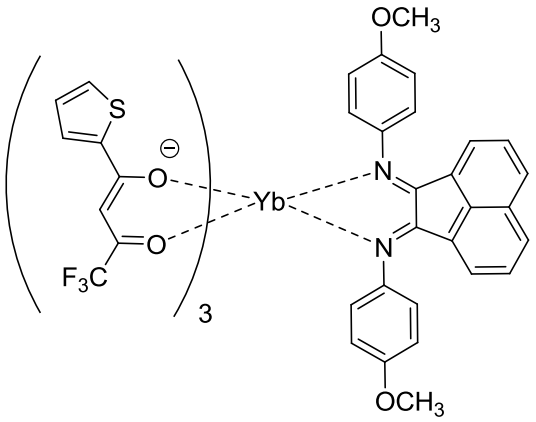

Chemical Formula: $C_{50}H_{32}F_9N_2O_8S_3Yb$

Molecular Weight: 1229.02 g mol^{-1}

Ytterbium aquocomplex (0.350 g, 0.4 mmol) and Shiff's base (0.157 g, 0.4 mmol) were dissolved in 20 ml of toluene and refluxed in Dean-Stark trap for 6 hours. The solvent was evaporated under reduced pressure, giving a red-orange oil, that was washed with hexane and dried carefully in vacuum, giving a dark orange dense oil (0.050 g, 0.04 mmol yield: 10%)

Elemental Analysis calculated for $C_{50}H_{32}F_9N_2O_8S_3Yb$: C, 48.86%; H, 2.62%; N, 2.28%; found: C, 49.03%; H, 3.08%; N, 2.13%.

Uv-Vis ($CHCl_3$): λmax= 424 nm (ligand).

Synthesis of Yb3+ chelate of thenoyl trifluoromethyl acetylacetonate substitute with (E)-N-((E)-2-(3a2,10-dihydropyren-1-ylimino)acenaphthylen-1(2H)-ylidene)pyren-1-amine

(C3M)

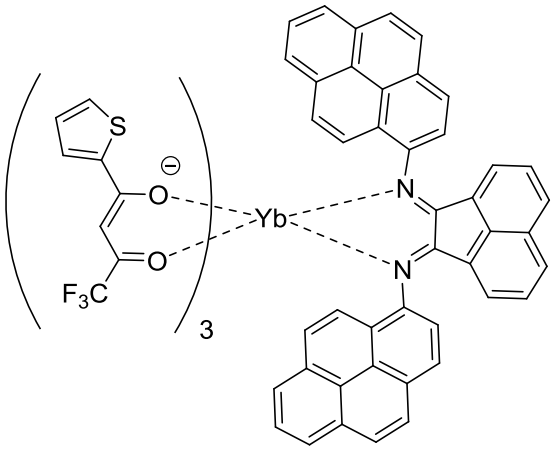

Chemical Formula: $C_{68}H_{36}F_9N_2O_6S_3Yb$

Molecular Weight: 1419.26 g mol^{-1}

Ytterbium aquocomplex (0.350 g, 0.28 mmol) and Shiff's base (0.112 g, 0.28 mmol) were dissolved in 20 ml of toluene and refluxed in Dean-Stark trap for 6 hours. The solvent was evaporated under reduced pressure, giving a red oil, that was washed with hexane and dried carefully in vacuum, giving a dark red dense oil (0.050g, 0.04 mmol, yield: 13 %).

Elemental Analysis calculated for $C_{68}H_{36}F_9N_2O_6S_3Yb$: C, 57.63%; H, 2.56%; N, 1.98%; found: C, 57.09%; H, 3.03%; N, 1.55%.

Uv-Vis ($CHCl_3$): λmax= 490 nm (ligand).

Synthesis of FSubPc Dimer

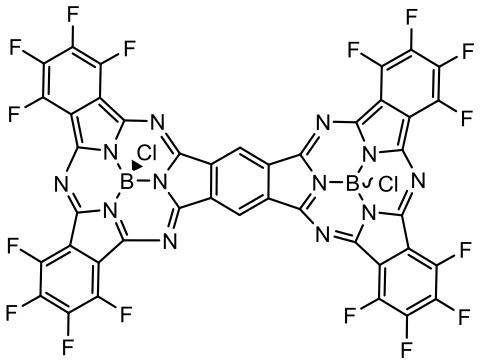

Chemical Formula: $C_{42}H_2B_2Cl_2F_{16}N_{12}$

Molecular Weight: 1071.06 g mol^{-1}

Tetrafluorophthalonitrile (561 mg, 2.81 mmol) and 1,2,4,5-benzenetetracarbonitrile (50 mg, 0.28 mmol) were heated up under Ar atmosphere until tertrafluorophthalonitrile melting. As soon as a clear solution appeared, BCl_3 (10.1 mL 1 M solution in p-xylene) was added dropwise to the mixture, under magnetic stirring. The reaction was refluxed for 4 hs. After cooling down to room temperature, it was flushed with argon to remove the acidic species. The resulting dark-purple slurry was then evaporated under vacuum. SubPc monomer was separated from dimers by column chromatography on silica gel using dichloromethane/hexane (3:2) as eluent. No trimers were recovered. The mixture of 1:1 syn-anti dimers was not further separated and it was washed with hexane to give a blue-purple powder (30 mg, 0,03 mmol, 10%).

^{1}H NMR (300 MHz, $CDCl_3$) δ= 10.46 ppm (s);

Uv-Vis ($CHCl_3$): λmax= 692 nm, 662 nm, 636 nm, 605 nm, 320nm .

Emission ($CHCl_3$): λmax= 700nm

Synthesis of 1-(3,6,9-trioxadecyl)-pyrrole-2-carbaldehyde

(1N)

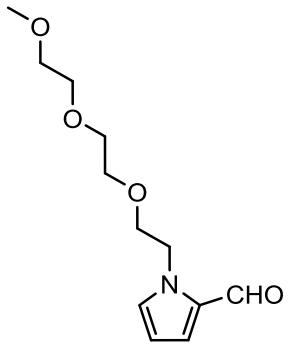

Chemical Formula: $C_{12}H_{19}NO_4$

Molecular weight: 241,29 g mol^{-1}

A solution of pyrrole-2-carbaldehyde (10.00 g, 105.15 mmol) in anhydrous DMF (100 ml) was added dropwise under nitrogen atmosphere and at 0°C to a suspension of NaH (4.40 g of a 60 % mineral oil suspension, 110.00 mmol). The resulting white suspension was stirred for 30 min. A solution of 3,6,9-trioxadecyl-4- toluenesulfonate2 (44.75 g, 106.00 mmol) in anhydrous DMF (50 ml) was added dropwise and the reaction mixture was stirred at ambient temperature over a week end. The mixture was poured into 500 ml of icy brine to give a brown suspension that was washed with hexane (100 ml) and extracted with AcOEt (4 x 200 ml). The combined organic phase was washed with brine (4 x 200 ml), dried over Na2SO4 and evaporated to give a yellow, viscous oil that was further purified by chromatography (SiO2, AcOEt) yielding the pure product as a light yellow oil (21.00 g, 66.0 mmol, 83.0 %).

^{1}H NMR (500MHz, $CDCl_3$) δ= 9.51 (1H, s), 7.07 (1H, m, broad), 6.94 (1H, m, broad), 6.21 (1H, m, broad), 4.50 (2H, t, J=6.1 Hz), 3.75 (2H, t, J=6.1 Hz), 3.52-3.55 (8H, m), 3.37 (3H, s).

Elemental Analysis Calcd for $C_{12}H_{19}NO_4$: C, 59.73; H, 7.94; N, 5.81; Found: C, 59.38; H, 7.91; N, 6.23.

2-(*N*,*N*-diphenylhydrazonomethyl)-1-(3,6,9-trioxadecyl)-pyrrole

(2N)

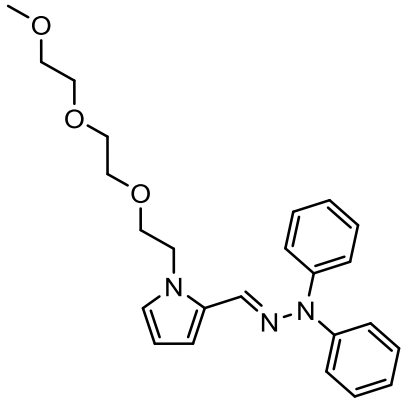

Chemical Formula: $C_{24}H_{29}N_3O_3$

Molecular weight: 407,51 g mol^{-1}

A mixture of *N*,*N*diphenylhydrazine hydrochloride (1.24 g, 5.60 mmol) and aldehyde **5b** (1.35 g, 5.60 mmol) was suspended in degassed THF (50 ml) and refluxed under nitrogen atmosphere for 1h. The color turned gradually from yellow to black. The suspension was cooled and the solvent evaporated to give a dark oil that was taken up with a AcOEt and filtered through a pad of Florisil. Evaporation of the solvent gave the product as a brown oil that was used directly without further purification (1.56 g, 3.80 mmol, 68.0 %).

^{1}H NMR (500 MHz, DMSO-d_6) δ= 7.44 (4H, t, J = 7.9 Hz), 7.18 (2H, t, J = 7.3 Hz), 7.14 (1H, s), 7.09 (4H, d, J = 7.7 Hz), 6.92 (1H, m, broad), 6.19 (1H, m, broad), 6.02 (2H, t, J = 3.3 Hz), 4.49 (2H, t, J = 6.1 Hz), 3.77 (2H, t, J = 6.1 Hz), 3.52-3.55 (8H, m), 3.23 (3H, s).

^{13}C NMR (500MHz, acetoned_6) δ= 145.9, 132.7, 131.7, 129.9, 128.4, 126.0, 124.2, 115.7, 109.7, 73.7, 72.5, 72.3, 72.1, 59.8, 50.2.

Preparation of GlySq.

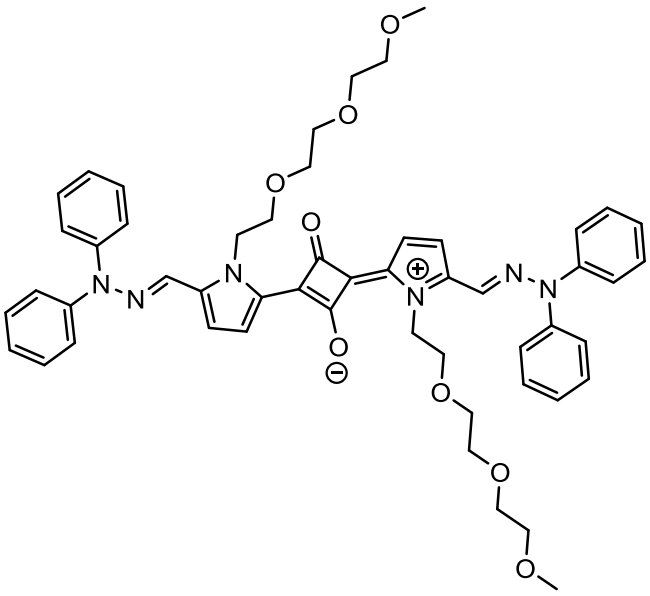

Chemical Formula: $C_{52}H_{58}N_6O_8$

Molecular weight: 895,07 g mol^{-1}

A suspension of squaric acid (0.140 g, 1.22 mmol) and hydrazone (1.000 g, 2.45 mmol) in a 1:1 BuOH/toluene mixture (120 ml) was refluxed in a Dean-Stark apparatus for 3 h. The solvent was removed and the deep green oily residue was washed with water (50 ml) and dissolved in boiling isopropanol (60 ml). The solvent evaporation afforded a golden, shiny solid that was taken up with Et_2O and filtered at reduced pressure. (0.530 g, 0.59 mmol, 48.6 %).

^{1}H NMR (500MHz, DMSO-d_6) δ= 7.62 (2H, d, J = 4.6 Hz), 7.52 (8H, t, J = 7.8 Hz), 7.31 (4H, t, J = 7.4 Hz), 7.26 (2H, s), 7.23 (8H, d, J = 7.8 Hz), 7.06 (2H, d, J = 4.6 Hz), 4.79 (4H, t, J = 4.8 Hz), 3.61 (4H, t, J = 5.2 Hz), 3.43-3.31 (16H, m), 3.15 (6H, s).

^{13}CNMR (DMSO-*d*6) 166.8, 166.7, 144.5, 141.9, 130.1, 130.0, 125.6, 125.0, 122.6, 122.1, 116.0, 71.1, 70.5, 69.8, 69.7, 69.5, 57.9, 46.7.

Elemental Analysis Calc. for $C_{52}H_{56}N_6O_8$: C, 69.94; H, 6.32; N, 9.41; Found: C, 70.18; H, 6.45; N, 9.32.

M.p. 127-130 °C.

Uv-Vis ($CHCl_3$): λmax= 728 nm.

Acknowledgements

I would like to thank my supervisor Prof. Luca Beverina, who gave me the possibility to work in his group, giving me strong support and good advices throughout these three years. I would like to thank all my colleagues, Dr. Mauro Sassi, Giorgio Patriarca, Riccardo Turrisi, Alessandro Sanguineti, Luca Mascheroni, Paolo Brazzo, Sara Mattiello, Daniela Galliani, Federico Tosi, Alessandro Sanzone, Massimiliano Mauri, Ivano Longo, Federica Tosques, Myles Rooney, Anna Ramunni (I apologize if someone is missing, but it's 4:23 am when I'm writing this). I would like to thank Prof. Tomas Torres and Prof. Marivi Martinez for the support they gave me during my time in Madrid. I am grateful to all my colleagues that made my stay in Spain unforgettable. I thank also Prof. Jurgen Parisi and Prof. Manuela Schiek for the occasion they gave me to work within their group in Oldenburg. Finally, I would like to thank my friends and my family that gave me continuous support, even in my hardest times. Thank you all.